Dinesh Shrestha

Modelling of a generalized thermal conductivity for granular multiphase geomaterial design purposes

Schriftenreihe des Lehrstuhls
Geomechanik und Geotechnik
Christian-Albrechts-Universität zu Kiel

6

Schriftenreihe des Lehrstuhls Geomechanik und Geotechnik
Christian-Albrechts-Universität zu Kiel
Heft 6

ISSN 2365-7162

Herausgeber:

Lehrstuhl für Geomechanik und Geotechnik

Christian-Albrechts-Universität zu Kiel

Prof. Dr.-Ing. habil. Frank Wuttke

Ludewig-Meyn-Straße 10

24118 Kiel

Telefon: ++49 – (0)431 – 880 2857

Telefax: ++49 – (0)431 – 880 7606

Internet: www.geotechnics.ifg.uni-kiel.de

Bezugsadresse:

Christian-Albrechts-Universität zu Kiel
Lehrstuhl für Geomechanik und Geotechnik

Modelling of a generalized thermal conductivity for granular multiphase geomaterial design purposes

DISSERTATION

in fulfillment of the requirements for the degree
"Dr.-Ing."
of the Facutly of Mathematics and Natural Sciences
at Kiel University

submitted by
Dinesh Shrestha

Kiel, 2022

First referee: Prof. Dr.-Ing. habil. Frank Wuttke
Kiel University

Second referee: Prof. Dr. John S. McCartney
University of California San Diego

Date of the oral examination: 22.12.2021
Approved for publication: 03.03.2022

The Dean

Declaration of Authorship

I, Dinesh Shrestha, declare that the content and design of this thesis titled, "Modelling of a generalized thermal conductivity for granular multiphase geomaterial design purposes" apart from my supervisor's guidance is my work and only using the sources listed. I confirm that:

- This thesis has not been submitted either partially or wholly as part of a doctoral degree to any other examining body, and it has not been published or submitted for publication.
- The thesis has been prepared in accordance to the Rules of Good Scientific Practice of the German Research Foundation.
- An academic degree of mine has never been withdrawn.

Kiel, 16.10.2021

Dinesh Shrestha

Vorwort des Herausgebers

Die vorliegende Promotionsschrift von Herrn Dr.-Ing. Dinesh Shrestha ist dem Forschungs- und Arbeitsgebiet „Bodenmechanik“ und der „Energie-Geotechnik“ zuzuordnen. Die in der Arbeit zugrundeliegende Problemstellung hatte sich in der Bearbeitung von offenen Fragen auf dem Gebiet der Energie-Geotechnik und den darin zu bestimmenden physikalischen Bodenparametern in poröser Medien ergeben. Die Zielstellung der Promotionsarbeit liegt in der Entwicklung einer Methodik zur Vereinheitlichung in Modellierung der Wärmeleitfähigkeit in granularen Bodenmaterialien unter unterschiedlichen Materialzuständen, wie Sättigung oder Porosität. Neben einer umfangreichen experimentellen Versuchsdurchführung, wurde eine große Anzahl von unterschiedlichen physikalisch basierten Modellen analysiert. Zur Verallgemeinerung der unterschiedlichen Zustände und Bodentypen erfolgte letztlich der Übergang zur Entwicklung eines lernfähigen Modells basierend auf künstlichen neuronalen Netzen. Nach einer entsprechenden Trainingsphase des Modells auf Grundlage der experimentellen Daten, konnte das Modell sehr genau die experimentellen Ergebnisse wiedergeben und für weitere Prognosen genutzt werden. Perspektivisch kann das Modell mit weiteren Bodentypen bzw. Zustandsdaten ergänzt werden, so dass eine umfassende Abbildung der sättigungsabhängigen Wärmeleitfähigkeit beliebiger Materialien erfolgen kann. Für die vorgestellte Herangehensweise ist das Modell ein numerisches ‚Black-Box‘ Modell, welches leider keinen Einblick in die physikalischen Zusammenhänge erlaubt, aber die bisherig zu Verfügung stehende semi-empirischen, physikalischen und numerischen Modelle im Hinblick auf die Verallgemeinerung von Zuständen deutlich erweitert. Neben der numerischen Methodenentwicklung erfolgte eine ausführliche Validierung anhand unterschiedlicher Geomaterialien und Randbedingungen.

Die Dissertationsschrift beinhaltet die konsequente Weiterentwicklung und Kopplung von bisherigen Ansätzen und Modellen zur Bestimmung der effektiven Wärmeleitfähigkeit in ungesättigten Böden. In zahlreichen Validierungsstudien wurde durch verschiedene experimentelle Analysen die Leistungsfähigkeit und hohe Prognosefähigkeit der entwickelten Methode in der Dissertationsschrift dokumentiert. Mit der Entwicklung der neuen Methodik zur Bestimmung effektiver thermischer Leitfähigkeiten basierend auf künstlichen neuronalen Netzen ist ein sehr kraftvolles, weiterhin lernfähiges Werkzeug entstanden, um zukünftige Bauvorhaben in der Energie-Geotechnik effektiv unterstützen zu können.

Kiel, im Dezember 2021 Frank Wuttke

Acknowledgements

I would like to express my acknowledgment to all the people who have contributed to this thesis directly or indirectly for their unconditional support, guidance and encouragement throughout my work.

First and foremost, I would like to express my deep gratitude and sincere appreciation to my advisor, Prof. Dr.-Ing. Frank Wuttke, for his continuous support, motivation and meticulous guidance throughout my work of candidature. Without his support and encouragement, it would not have been possible to complete this doctoral research. I would like to thank Prof. Dr. John S. McCartney for his agreement to be my second advisor and member of the examination committee, and for his fruitful comments and recommendations. I would like to cordially thank other members of the examination committee, Prof. Dr. Christian Winter, Prof. Dr. Sebastian Bauer and Prof. Dr. Stephan Wulfinghoff.

My deepest gratitude also goes to all my past and present colleagues and member of the Department of Geomechanics and Geotechnics of Kiel University for their unconditional support, motivation and friendship during my journey of research. Special thanks go to Dr.-Ing Henok Hailemariam, Mr. Binod Kafle and Dr.-Ing Zarghaam Rizvi for their valuable assistance and scientific discussions during my research work.

Last but not least, I would like to thank all my family members and friends, especially my parents, my wife Mita, my son Rubin and my daughter Sanskriti for their endless love, patient and continuous support throughout my journey. I would like to dedicate this thesis to my beloved parents and lovely wife.

Dinesh Shrestha

Abstract

Soil thermal conductivity has an important role in geo-energy applications such as high-voltage buried power cables, oil and gas pipelines, nuclear waste disposal facilities, shallow geo-energy storage systems and ground source heat pumps and heat transfer modelling. Especially, the efficiencies and performances of high-voltage buried power cables are strongly influenced by the thermal conductivity of the soil in which they are placed. Most soils have a very low thermal conductivity at lower saturation (especially in a dry state) as compared to that in a saturated condition. Due to a reduction in thermal conductivity, the cable fails or breakdowns since heat is produced faster than it is dissipated away. Therefore, it is essential to improve the soil thermal conductivity in the dry state as well as lower saturation levels for the optimum performance and safe operation of the cable. On the other hand, energy piles used as ground heat exchangers also lose their efficiency up to 40% in a dry condition as compared to that in a fully saturated condition. The efficiency loss as a result of soil desaturation needs to be addressed by improving the thermal conductivity of backfill soils, especially at the lower saturation level.

As the heat transfer in granular media is dominated by grain to grain contact conductance, the improvement in thermal conductivity could be achieved by enhancing the quality of the contacts and increasing the number of contacts among the grains. In this thesis, we investigate the effect of the fillers, mineralogy and particle gradation on the thermal conductivity of sand as an innovative improvement method. Porosity and saturation are other dominating factors besides these. An extensive laboratory study is performed to develop geomaterials with higher dry thermal conductivity by modifying particle size distribution into fuller curve gradation and adding fine particles in an appropriate ratio as fillers. The experimental results clearly show a significant improvement in the thermal conductivity at dry and lower saturation degrees and a considerable improvement in the case of full saturation. An improvement of (20-180) % in thermal conductivity of modified geomaterials for the full range of saturation whereas (25-230) % is observed in the dry state.

An artificial neural network as a novel approach is proposed to predict thermal conductivity of geomaterials for the dry and full range of saturation since the existing theoretical and semi-empirical prediction models don't show a good agreement with the measured thermal conductivity. Two ANN models, individual and generalised models are proposed. The feed-forward network with a Back-propagation algorithm is chosen to train the model, whilst a cross-validation technique is used as stopping criteria to develop the ANN models. Both proposed individual and generalised ANN models show a good agreement with the measured thermal conductivity values. Additionally, a result of a thermal simulation for a single cable clearly shows a large improvement in heat dissipation for modified soil as compared to original sand.

Zusammenfassung

Die Wärmeleitfähigkeit des Bodens spielt eine wichtige Rolle bei Geoenergieanwendungen wie erdverlegten Hochspannungskabeln, Öl- und Gaspipelines, oberflächennahen Geoenergiespeichern und Erdwärmepumpen sowie bei der Modellierung der Wärmeübertragung. Insbesondere die Effizienz und Leistung von erdverlegten Hochspannungskabeln wird stark von der Wärmeleitfähigkeit des Bodens beeinflusst, in dem sie verlegt werden. Die meisten Böden haben eine sehr niedrige Wärmeleitfähigkeit bei niedrigerer Sättigung (insbesondere im trockenen Zustand) im Vergleich zu einem gesättigten Zustand. Durch die Verringerung der Wärmeleitfähigkeit kommt es zum Ausfall des Kabels, da die Wärme schneller produziert als abgeführt wird. Daher ist es für eine optimale Leistung und einen sicheren Betrieb des Kabels unerlässlich, die Wärmeleitfähigkeit des Bodens im trockenen und niedrigerer Sättigung Zustanden zu verbessern. Andererseits verlieren Energiepfähle, die als Erdwärmetauscher eingesetzt werden, im trockenen Zustand bis zu 40 % ihrer Effizienz im Vergleich zu einem vollständig gesättigten Zustand. Der Effizienzverlust infolge der Entsättigung des Bodens muss durch die Verbesserung der Wärmeleitfähigkeit der Aufschütungsböden, insbesondere im unteren Sättigungsbereich, behoben werden.

Da die Wärmeübertragung in körnigen Medien von der Kontaktleitfähigkeit zwischen den Körnern dominiert wird, könnte die Verbesserung der Wärmeleitfähigkeit durch eine Verbesserung der Qualität der Kontakte und eine Erhöhung der Anzahl der Kontakte erreicht werden. In dieser Arbeit untersuchen wir die Auswirkungen von Füllstoffen, Mineralogie und Partikelabstufung auf die Wärmeleitfähigkeit als innovative Verbesserungsmethode. Es wird eine umfangreiche Laborstudie durchgeführt, um Verfüllböden mit einer höheren trockenen Wärmeleitfähigkeit zu entwickeln, indem die Partikelgrößenverteilung in eine Fuller Kurvenabstufung modifiziert und feine Partikel in einem geeigneten Verhältnis als Füllstoffe hinzugefügt werden. Die experimentellen Ergebnisse zeigen deutlich eine signifikante Verbesserung der Wärmeleitfähigkeit im trockenen Zustand und bei niedrigeren Sättigungsgraden sowie eine beträchtliche Verbesserung im vollständigen Sättigung. Die Wärmeleitfähigkeit der modifizierten Geomaterialien verbessert sich bei voller Sättigung um (20-180)%, während sie im trockenen Zustand um (25-230)% steigt.

Ein Künstliches Neuronales Netz (KNN) als neuartiger Ansatz wird vorgeschlagen, um die Wärmeleitfähigkeit von Geomaterialien für den vollständigen Sättigungsbereich voherzusagen, da die bestehenden theoretishcen und semiempirishcen Vorhersagemodelle keine gute Übereinstimmung mit der gemessenen Wärmeleitfähigkeit aufweisen. Es werden individuelle und generalisierte KNN-Modelle vorgeschlagen. Das Feed-Forward-Netz mit einem Back-Propagation-Algorithmus wird zum Trainieren des Modells gewählt, während eine Kreuzvalidierungstechnik als Abbruchkriterium für die Entwicklung der KNN-Modelle verwendet wird. Sowohl entwickelte individuelle als auch generalisierte KNN-Modelle zeigen eine gute Übereinstimmung mit den gemessenen Wärmeleitfähigkeitswerten. Darüber hinaus zeigt das Simulationsergebnis für ein einzelnes Kabel eine deutliche Verbesserung der Wärmeableitung für modifizierte Geomaterialien im Vergleich zu sand.

Contents

Abstract **v**

Contents **vii**

List of Figures **xi**

List of Tables **xv**

List of Abbreviations **xvi**

List of Symbols **xviii**

1 Introduction **1**
1.1 Background and motivation 1
1.2 Objective 5
1.3 Organization of Dissertation 6

2 State of the art **8**
2.1 Introduction 8
2.2 Thermal properties of soil 8
2.3 Heat transfer in soil 9
2.3.1 Conduction 10
2.3.2 Convection 11
2.3.3 Radiation 11
2.3.4 Heat transfer equation 11
2.4 Factors affecting soil thermal conductivity 12
2.4.1 Effect of dry density and saturation on thermal conductivity 13
2.4.2 Effect of soil composition and texture on thermal conductivity 15
2.4.3 Effect of structure on thermal conductivity 17
2.4.4 Effect of mineralogy on thermal conductivity 18
2.4.5 Effect of other factors on thermal conductivity 19
2.5 Measurement of thermal conductivity 20
2.5.1 Steady-state method 20
2.5.2 Transient state method 21
2.6 Existing thermal conductivity models 22
2.6.1 Theoretical prediction models 22
2.6.2 Semi/empirical prediction models 25

2.6.3 Numerical models . . . 31
2.6.4 Artificial Neural Network (ANN) models . . . 32
2.7 Material design under consideration of thermal conductivity . . . 33
2.7.1 Importance of thermal conductivity on underground high voltage power cables . . . 33
2.7.2 Materials used to bury underground cables . . . 35
2.8 Factors consideration enhancing thermal conductivity . . . 37
2.9 Summary . . . 39

3 State and structure of Artificial Neural Network 40
3.1 Introduction . . . 40
3.2 Background . . . 40
3.3 Architecture of ANN . . . 44
3.3.1 Transfer function . . . 46
3.3.2 Types of network . . . 48
3.4 Training of the ANN model . . . 50
3.4.1 Types of Training . . . 52
Supervised training . . . 52
Unsupervised training . . . 52
Reinforced training . . . 52
3.4.2 ANN Parameters . . . 52
Learning rate . . . 52
Momentum . . . 53
Input noise . . . 53
Training and testing tolerances . . . 53
3.4.3 Data Selection . . . 53
Data division . . . 54
Data pre-processing . . . 56
3.4.4 Determination of ANN architecture . . . 56
3.4.5 Learning algorithms (rules) . . . 58
3.4.6 Delta rule & Generalized delta rule . . . 60
3.4.7 Weight update method . . . 61
3.4.8 Back-propagation Algorithm . . . 62
3.4.9 Cost function . . . 64
3.4.10 Stopping Criteria . . . 64
3.4.11 Selection of ANN model . . . 65
3.5 Deep Learning . . . 66
3.6 Application of ANN . . . 67
3.7 Advantages and disadvantages of ANNs . . . 68
3.7.1 Advantages . . . 68
3.7.2 Disadvantages . . . 69
3.8 Summary . . . 69

4 Design of granular materials with enhanced thermal conductivity 70
4.1 Introduction . . . 70
4.2 Materials used . . . 70
4.2.1 Analysed materials . . . 70
4.2.2 Design of materials . . . 72
4.3 Equipment used . . . 74
4.4 Experimental procedure . . . 75
4.5 XRD analysis . . . 79
4.6 SEM image analysis . . . 79
4.7 Mechanical tests . . . 80
4.8 Summary . . . 82

5 Experimental material design analysis and discussions 83
5.1 Introduction . . . 83
5.2 Thermal conductivity measurement results . . . 83
5.2.1 Effect of porosity on thermal conductivity in dry state . . . 83
5.2.2 Effect of fine contents on thermal conductivity . . . 88
5.2.3 Effect of saturation on thermal conductivity . . . 88
5.2.4 Effect of dry density and saturation on thermal conductivity . . . 91
5.2.5 Effect of mineralogy on thermal conductivity . . . 92
5.3 Improvement in thermal conductivity . . . 94
5.3.1 Dry state . . . 94
5.3.2 Moist state . . . 97
5.4 Relation between proctor density, water content and thermal conductivity . . . 98
5.5 Comparison of experimental results with prediction models . . . 100
5.5.1 Two phase prediction models . . . 101
5.5.2 Theoretical and empirical prediction models over full range of saturation 103
5.6 Mechanical test results . . . 106
5.7 Summary . . . 107

6 Development of new conductivity models for granular materials by using ANNs 108
6.1 Introduction . . . 108
6.2 ANNs model setup . . . 108
6.3 Data division and pre-processing . . . 110
6.4 Determination of ANN model Architecture . . . 111
6.4.1 ANN architecture for dry materials . . . 111
6.4.2 ANN architecture for moist materials . . . 112
6.5 Stop criteria . . . 114
6.6 Model optimization (Training) . . . 114
6.6.1 For dry materials . . . 115
6.6.2 For moist materials . . . 115
6.6.3 Comparison of experimental and predicted thermal conductivity using selected ANN models . . . 116

6.7 Validation of developed ANN models . . . 118
6.7.1 For dry materials . . . 119
6.7.2 For moist materials . . . 120
6.8 Performance assessment of proposed ANN models . . . 124
6.8.1 For dry ANN models . . . 125
6.8.2 For moist ANN models . . . 128
6.9 Summary . . . 133

7 Applications of new materials design for embedded cables 134
7.1 Introduction . . . 134
7.2 Background . . . 134
7.3 2D Simulation . . . 135
7.3.1 Model setup . . . 135
7.3.2 Results and discussions . . . 136
7.4 Summary . . . 138

8 Conclusions and Recommendations 139
8.1 Conclusions . . . 139
8.2 Recommendations for future work . . . 141

A ANN models' performance indices 143
A.1 Performances indices of different ANN models for Training, Validation & Testing data . . . 143
A.2 Performances indices of different ANN models for new experimental data . . . 143

Bibliography 153

List of Figures

2.1 Region of influencing heat transfer mechanisms with respect to degree of saturation and soil grain size, after Farouki (1981). 9
2.2 Primary particle-level heat transfer process in granular materials, after Yun and Santamarina (2007). 10
2.3 Thermal conductivity of sandy and clayey soils against dry density at constant water content, after Farouki (1981). 14
2.4 Thermal conductivity as function of volumetric water content for coarse-textured (soil-1,2) and fine-textured (soil-5,8) soils, after Lu et al. (2007). 16
2.5 Grain-size distribution of different soils, after Adams and Baljet (1968). 17
2.6 Thermal resistivity (reciprocal of thermal conductivity) of different types of soil, after Adams and Baljet (1968) (arrows represent critical moisture content). 17
2.7 A schematic structure of porous media, after Côté and Konrad (2009). 18
2.8 Thermal conductivity (λ) vs porosity (n) of dry soils using theoretical models. 24
2.9 Thermal conductivity (λ) vs porosity (n) of dry soils using semi-empirical models. 28
2.10 Schematic diagram of underground power cable. 34
2.11 Effect of thermal conductivity on cable ampacity of underground power cable, after Sandiford (1981). 35
2.12 Effect of thermal conductivity on cable life of underground power cable, after Karahn and Kalenderli (2011). 35
2.13 Effect of moisture on thermal conductivity of backfill materials, after Sandiford (1981)(FTB: Fluidized thermal backfill). 37

3.1 Structure of single neuron in brain. 45
3.2 Structure of single layer feed- forward ANN model. 45
3.3 Linear activation function, range (-∞,∞). 47
3.4 Threshold activation function, range (0,1). 47
3.5 Log-sigmoid activation function, range (0,1). 48
3.6 tanh-sigmoid activation function, range (-1,1). 48
3.7 A typical single-layer feedforward ANN architecture. 49
3.8 A typical multi-layer feedforward ANN architecture. 50
3.9 A typical Recurrent network architecture. 50
3.10 Linear regeression model (a) Vs. ANN models representing linear regression model (b). 51
3.11 Behaviour of MSE with overtraining in Crossvalidation technique. 54

3.12 Cross validation technique process. 55
3.13 A Perceptron learning rule. 59
3.14 A single-layer network. 60
3.15 Weight update method: SGD (left), Batch (middle), Mini Batch (right), after Kim (2017). 62
3.16 Back-propagation network. 63
3.17 ReLU activation function, range (0,∞). 67

4.1 Analysed materials. 71
4.2 Analysed fine materials. 72
4.3 SiC. 72
4.4 Particle size distribution. 73
4.5 KD2 Pro device with TR1 needle. 75
4.6 Schematic diagram of the sample cylinder 76
4.7 The schematic diagram of sample saturation process (Shrestha et al., 2019). . . 78
4.8 XRD analysis of sand A (a), sand B (b) and sand C (c) 80
4.9 XRD analysis of stone-dust. 81
4.10 XRD analysis of kieselghur. 81

5.1 Thermal conductivity as function of porosity in dry state for original sands and modified sands with bentonite. 84
5.2 SEM images obtained for the modified 4mmF of sand A: (a) bentonite filling the pore space between the sand grains and (b) bentonite filling the gaps within the grain. 85
5.3 Thermal conductivity as function of porosity in dry state for original sands and modified sands with stonedust. 86
5.4 Thermal conductivity as fuction of porosity in dry state for original sand and modified fuller sand with SiC. 88
5.5 Thermal conductivity at different fine contents in dry state. 89
5.6 Thermal conductivity as function of degree of saturation for modified and original sand A (a) and sand B (b) with stonedust. 90
5.7 SEM images obtained for the modified 2mmF of sand A: (a) stone dust filling the cracks in grain and (b) stone dust filling the pore space between the sand grains. 91
5.8 Thermal conductivity as function of dry density at different saturation of degree for (a) sand A and (b) sand B. 93
5.9 Thermal conductivity as function of porosity for original sands and modified fuller sands with stonedust. 94
5.10 Thermal conductivity as function of porosity for modified fuller sands with and without SiC. 94
5.11 Thermal conductivity vs degree of saturation for modified fuller sands A and B with stonedust. 95

5.12 Improvement in thermal conductivity vs. porosity for modified fuller sands with bentonite. 96
5.13 Improvement in thermal conductivity vs. porosity for modified fuller sands with stonedust. 97
5.14 Improvement in thermal conductivity as function of degree of saturation for modified fuller sands A and B with stonedust. 99
5.15 Dry density (a) and thermal conductivity (b) at various water content for modified fuller sands and original sand A with stonedust. 100
5.16 Comparison of experimental results with theoretical models. 102
5.17 Comparison of experimental results with semi-empirical models. 103
5.18 Comparision of experimental results with semi-empirical models for (a)sand-A, (b)2mmF, (c)4mmF & (d)8mmF. 104
5.19 Comparision of experimental results with semi-empirical models for (a)sand-B, (b)2mmF, (c)4mmF & (d)8mmF. 105
5.20 Vertical stress vs strain for for modified fuller sands with stonedust and original sand A (a) and sand B (b). 106

6.1 Flow chart of ANN models calculation procedure. 110
6.2 Comparison of measured and predicted thermal conductivity using ANN-F models: (a) ANNF6L and (b) ANNF7L. 116
6.3 Comparison of measured and predicted thermal conductivity using ANN-S models: (a) ANNS9L and (b) ANNS20L. 117
6.4 Comparison of measured and predicted thermal conductivity using ANN-G models: (a) ANNG6L and (b) ANNG9L. 117
6.5 Comparison of measured and predicted thermal conductivity using ANNs-F models: (a) ANNs-F7L and (b) ANNs-F9L. 118
6.6 Comparison of measured and predicted thermal conductivity using ANNs-S models: (a) ANNs-S6L and (b) ANNs-S9L. 118
6.7 Comparison of measured and predicted thermal conductivity using ANNs-G models: (a) ANNs-G6L and (b) ANNs-G8L. 119
6.8 Comparison of measured and predicted thermal conductivity using individual models: (a)selected ANN-F and (b)selected ANN-S for independent data. 121
6.9 Comparison of measured and predicted thermal conductivity using generalized model, ANN-G for independent data. 122
6.10 Comparison of measured and predicted thermal conductivity using individual models: (a)selected ANN-F and (b)selected ANN-S for independent data. 122
6.11 Comparison of measured and predicted thermal conductivity using generalized model, ANN-G for independent data. 123
6.12 Comparison of measured and predicted thermal conductivity using individual models: (a)selected ANNs-F and (b)selected ANNs-S for independent data. 123
6.13 Comparison of measured and predicted thermal conductivity using generalized model, ANNs-G for independent data 124

6.14 Comparison of measured and predicted thermal conductivity using individual models: (a)selected ANNs-F and (b)selected ANNs-S for independent data. 124
6.15 Comparison of measured and predicted thermal conductivity using generalised models ANNs-G for (a) modified fuller sand (SandB_4mmF) and (b) sand-A. 125
6.16 Comparison of proposed ANN models and empirical models with measured thermal conductivity value (a)ANN-F & ANN-S (b) ANN-G. 126
6.17 Comparison of proposed ANN models and empirical models with measured thermal conductivity value (a)ANN-F & ANN-S (b) ANN-G. 127
6.18 Comparison of proposed individual ANN models and semi-empirical models with measured thermal conductivity values for (a) modified fuller sand (SandB_4mmF) and (b) sand-A. 129
6.19 Comparison of proposed generalised ANN models and semi-empirical models with measured thermal conductivity values for (a) modified fuller sand (SandB_4mmF) and (b) sand-A. 130
6.20 Comparison of proposed ANN models and empirical models with measured thermal conductivity value for (a)sand (b) modified fuller sand. 131

7.1 Geometry of model setup with mesh generation, after Shrestha et al. (2016). . 135
7.2 Temperature distribution around the underground cable with sand (left) and modified sand (right) at (a)24 hrs (b) 72 hrs (c) 120 hrs, after Shrestha et al. (2016). 136
7.3 Temperature versus time at two observation points for original and modified sand, after Shrestha et al. (2016). 137

List of Tables

2.1 Thermal conductivity of some rock-forming minerals (Côté and Konrad, 2005b). 39

4.1 Sand properties. 71
4.2 Design of Fuller curve gradation. 74

5.1 Odometer parameters for modified fuller and original sands. 107

6.1 Boundaries of the input & output paremeter for ANN models. 112
6.2 Data division for different ANN models. 113
6.3 Artificial Neural Network Paramters. 113
6.4 Performance indices for different ANN models obtained for new experimental data in dry as well as in moist case. 120
6.5 Performance indices of proposed ANN models and prediction models in predicting thermal conductivity of modified fuller and original sands in dry and moist case. 132

7.1 Thermal properties of simulated geometry. 137

A.1 Performance indices for different ANN-F models. 144
A.2 Performance indices for different ANN-S models. 145
A.3 Performance indices for different ANN-G models. 146
A.4 Performance indices for different ANNs-F models. 147
A.5 Performance indices for different ANNs-S models. 148
A.6 Performance indices for different ANNs-G models. 149
A.7 Performance indices for different ANN-F models obtained for new experimental data. 150
A.8 Performance indices for different ANN-S models obtained for new experimental data. 150
A.9 Performance indices for different ANN-G models obtained for new experimental data. 150
A.10 Performance indices for different ANNs-F models obtained for independent data. 151
A.11 Performance indices for different ANNs-S models obtained for new experimental data. 151
A.12 Performance indices for different ANNs-G models obtained for new experimental data. 152

List of Abbreviations

ADALINE	**ADA**ptive **LINE**ar
AI	**A**rtificial **I**ntellignence
ANN	**A**rtificial **N**eural **N**etwork
ANN-F	**A**rtificial **N**eural **N**etwork **F**uller (sand)
ANN-S	**A**rtificial **N**eural **N**etwork **S**and
ANN-G	**A**rtificial **N**eural **N**etwork **G**eneralized
ASMOD	**A**daptive **S**pline **M**odelling (of) **O**bservation **D**ata
ASTM	**A**merican **S**ociety (for) **T**esting (and) **M**aterials
BEM	**B**oundary **E**lement **M**ethod
BP	**B**ack **P**ropagation
CPT	**C**one **P**enetration **T**est
CLSM	**C**ontrol **L**ow **S**trenght **M**aterials
CNN	**C**onvolutional **N**eural **N**etwork
D	**D**imensional
DIN	**D**eutsches **I**nstitue (für) **N**ormung
DEM	**D**iscrete **E**lement **M**ethod
FDM	**F**uid **D**ynamics **M**ethod
FFN	**F**eed **F**orward **N**etwork
FEM	**F**inti **E**lement **M**ethod
FTB	**F**luidized **T**hermal **b**ackfill
FR	**F**raction **R**atio
GA	**G**enetic **A**lgorithm
GHP	**G**uarded **H**ot **P**late
GM	**G**eometric **M**ean
HS-L	**H**ashin (and) **S**htrikman **L**ower (bound)
HS-U	**H**ashin (and) **S**htrikman **U**pper (bound)
I	**I**mprovement
IEEE	**I**nstitute (of) **E**ngineering (and) **E**lectronics **E**ngineers
LEM	**L**attice **E**lement **M**ethod
LMS	**L**east **M**ean **S**quare
LSTM	**L**ong **S**hort **T**erm **M**emory (network)
MAE	**M**ean **A**bsolute **E**rror
MLFFN	**M**ulti **L**ayer **F**eed **F**orward **N**etwork
MLP	**M**ulti **L**ayer **P**erceptron
MSE	**M**ean **S**qured **E**rror

OP	bservation **P**oint
PEs	**P**rocessing **E**lements
RBF	**R**adial **B**asis **F**unction
ReLU	**Re**ctified **L**inear **U**nit
RNN	**R**ecurrent **N**eural **N**etwork
SEM	**S**canning **E**lectron **M**icroscopy
SGD	**S**tochastic **G**radient **D**escent
SiC	**Si**licon **C**arbide
SLFFN	**S**ingle **L**ayer **F**eed **F**orward **N**etwork
SLP	**S**ingle **L**ayer **P**erceptron
SOM	**S**elf **O**rganizing **M**ap
SPT	**S**tandard **P**enetration **T**est
TDR	**T**ime **D**omain **R**eflectometry
TR	**TR**ansient
THM	**T**hermo **H**ydro **M**echanical
VF	**V**olume(tric) **F**raction
XRD	**X** **R**ay **D**iffraction

List of Symbols

a	parameter of Balland & Arp (2005) model	-
a_l&b_l	empirical parameters of Lu et al. (2007) model	-
A	cross sectional area of medium	m^2
b_c&c_c	empirical parameters of Chen (2008) model	-
b	bias of ANN structure	-
C	heat capacity of medium	$J K^{-1}$
c	mass specific heat of medium	$J kg^{-1} K^{-1}$
C	constant of Johansen (1975) model	-
C_s	heat capacity of soil solid	$J K^{-1}$
C_w	heat capacity of water	$J K^{-1}$
C_a	heat capacity of air	$J K^{-1}$
C_c, C_u	coefficients of curvature and uniformity of medium	-
d	diameter of grain or particle	mm
d_m	mean grain diameter	mm
d_N	known output in training	-
D	maximum grain or particle diameter	mm
D_{10}	grain diameter at 10% passing	mm
D_{30}	grain diameter at 30% passing	mm
D_{50}	grain diameter at 50% passing	mm
D_{60}	grain diameter at 60% passing	mm
D_{large}	large grain size diameter	mm
D_{small}	small grain size diameter	mm
e	void ratio of medium	-
e_N	error during training	-
f_c	fine content	-
$Forf$	activation fucntion of ANN structure	-
$g_{a,b,c}$	grain shape coefficients used in De Vries (1963) model	-
G_s	specific gravity	-
K_i	weighting factor used in De Vries (1963) model	-
K_e	Kersten number	-
n	porosity of medium	-
N	Number of training data	-
P	percentage passing through sieve	-
q	heat flux	$W m^{-2}$

q_c	quartz content	-
Q	rate of heat transfer	W ($J\,s^{-1}$)
r	distance between the heater and the sensor of the TR-1 needle	m
S_r	degree of saturation of medium	%
t	time	s
T	temperature	K / °C
v	output of network	-
V_{cf}	volumetric fraction of coarse particles	-
V_q	volumetric fraction of quartz	-
V_{om}	volumetric fraction of organic matter	-
V_{sand}	volumetric fraction of sand	-
w	gravimetric water content of medium	%
W	Weight of ANN structure	-
x	actual input value of data base	-
x_a	volume fraction of air	-
x_q	quartz content or sand content used in Zhang (2017) model	-
x_s	volume fraction of soil solid	-
x_w	volume fraction of water	-
x_{min}	minimum value of data base	-
x_{max}	maximum value of data base	-
x_N	normalized value	-
X	Input of ANN structure	-
Y	Output of ANN structure	-
α	thermal diffusivity of medium	$m^2\,s^{-1}$
α_b&β_b	coordination coefficient of Balland & Arp (2005) model	-
α_l	learning rate	$m^2\,s^{-1}$
α_s	soil texture dependent parameter of Lu et al. (2007) model	-
β	empirical parameter of Côté & Konrad (2009) model	-
β_d	coefficient parameter of Gori & Corasaniti (2004) model	-
χ&η	particle shape effect parameter of Côté & Konrad (2005) model	-
δ	output in network	-
ΔT	change in temperature of medium	K / °C
η_1, η_2	coefficient of pore structure	-
κ	soil texture dependent parameter of Côté & Konrad (2005) model	-
κ_{2P}	structure effect parameter of Côté & Konrad (2009) model	-
λ	thermal conductivity of medium	$W\,m^{-1}\,K^{-1}$
λ_a	thermal conductivity of air	$W\,m^{-1}\,K^{-1}$
λ_d	thermal conductivity of medium in dry condition	$W\,m^{-1}\,K^{-1}$
λ_f	thermal conductivity of fluids	$W\,m^{-1}\,K^{-1}$
λ_k	thermal conductivity of kaolin	$W\,m^{-1}\,K^{-1}$
λ_L	lower bound of thermal conductivity	$W\,m^{-1}\,K^{-1}$
λ_m	measured thermal conductivity	$W\,m^{-1}\,K^{-1}$

λ_{md}	measured thermal conductivity in dry condition	$\mathrm{W\,m^{-1}\,K^{-1}}$
λ_{min}	thermal conductivity of minerals	$\mathrm{W\,m^{-1}\,K^{-1}}$
λ_{o}	thermal conductivity of minerals other than quartz	$\mathrm{W\,m^{-1}\,K^{-1}}$
λ_{om}	thermal conductivity of organic matter	$\mathrm{W\,m^{-1}\,K^{-1}}$
$\lambda_{parallel}$	thermal conductivity in parallel condition	$\mathrm{W\,m^{-1}\,K^{-1}}$
λ_{p}	predicted thermal conductivity	$\mathrm{W\,m^{-1}\,K^{-1}}$
λ_{pd}	predicted thermal conductivity in dry condition	$\mathrm{W\,m^{-1}\,K^{-1}}$
λ_{q}	thermal conductivity of quartz mineral	$\mathrm{W\,m^{-1}\,K^{-1}}$
λ_{s}	thermal conductivity of solids	$\mathrm{W\,m^{-1}\,K^{-1}}$
λ_{sat}	thermal conductivity of medium in saturated condition	$\mathrm{W\,m^{-1}\,K^{-1}}$
λ_{series}	thermal conductivity in series condition	$\mathrm{W\,m^{-1}\,K^{-1}}$
λ_{U}	upper bound of thermal conductivity	$\mathrm{W\,m^{-1}\,K^{-1}}$
λ_{w}	thermal conductivity of water	$\mathrm{W\,m^{-1}\,K^{-1}}$
ρ	density of medium	$\mathrm{kg\,m^{-3}}$
ρ_{d}	dry density of medium	$\mathrm{kg\,m^{-3}}$
ρ_{p}	density of particles	$\mathrm{kg\,m^{-3}}$
ρ_{s}	density of soil solids	$\mathrm{kg\,m^{-3}}$
Δ	change / variation of	
∂	partial derivative	
∇	gradient	

Chapter 1

Introduction

1.1 Background and motivation

Soil thermal properties have an important role in many geoengineering projects including thermal effects, such as high voltage buried power cables, heat exchanger piles, small and large scale ground heat storage, oil and gas pipelines and nuclear waste disposal facilities. A thorough understanding of thermal properties is thus essential to understand the process of heat transfer in soils and to design the thermal facilities. Soil thermal properties mainly consist of thermal conductivity, diffusivity and specific heat capacity. Among them, thermal conductivity is a vital property in heat transfer modelling, geomaterials designing and design of geothermal related earth structures. The performances and efficiencies of these applications depend on the thermal conductivity of soil where they are built. Depending upon the application and desired purpose of such projects, the materials with either low or high thermal conductivity are being used. For example, materials with high thermal conductivity are desirable in the case of high voltage buried power cables, while ground heat energy storage needs materials with moderate thermal conductivity and high heat capacity to hinder heat energy loss.

Over the years, the use of underground power cables has grown significantly across the world with a rapid increase in demand for electric energy and the trend for large infrastructures and vast expansion of metropolitan areas. High voltage underground power cable, alternatives to an overhead power cable, needs proper backfill materials. Since the thermal behaviour of backfill materials affect the design, performance and economics of underground cables, the focus on designing corrective backfill materials has given more attention. The main problem of underground cables is heat, that is generated inside the cable which should be dissipated to surrounding soil. Otherwise, it may lead to cable failure thermally. Heat is generated due to power losses in the conductors, insulation, sheath and other components of the cable system (Sandiford, 1981; Mozan et al., 1997; Afa, 2010). The performance and efficiency of the underground power cable are critically influenced by the thermal conductivity of the medium in which it is placed. In fact, the better the heat dissipation by the medium the lower the maximum temperature reached by the cable, which ultimately limits risks of cable failure. The thermal conductivity of the soil where the cable is embedded usually accounts for more than 50% of the total temperature rise of the cable conductor. Due to the poor thermal conductivity of backfill materials, the cable fails or

breakdowns as heat is produced faster in the cable than it dissipates away. Thus, the thermal conductivity of backfill soil should be, in principle, higher than the surrounding soils. The role of backfill soils is to dissipate the heat into the surrounding soil for the efficient and safe operation of the cable. However, the thermal conductivity is highly moisture dependent and the thermal conductivity decreases most significantly with the soil saturation degree approaching zero (dry state). The reduction in the thermal conductivity largely influences the current capacity of the underground cables (Sandiford, 1981; De León and Anders, 2008) as well as the cable life (Karahn and Kalenderli, 2011). A similar situation is observed in the case of underground energy storage like borehole heat exchangers, underground thermal energy storage, geothermal heat pumps. The efficiency of these applications depends upon the thermal conductivity of the material surrounding the transporting pipes. These applications require 30% - 50% less energy for heating compared with air-to-air pumps with the current grouting materials around the pipes (Sarbu and Sebarchievici, 2014). On the other hand, energy piles used as ground heat exchangers also lose their efficiency up to 40% in a dry condition as compared to that in a fully saturated state (Akrouch et al., 2015; Venuleo et al., 2015). The decreasing efficiency of these applications as a result of soil desaturation needs to be addressed by improving the thermal conductivity of backfill soils, especially at the lower saturation levels. Therefore, the backfill materials or materials used in these applications should be modified prior to use. This could be achieved by introducing the fine fillers, cementing agent and modification of gradation (Drefke et al., 2015; Shrestha et al., 2016; Shrestha et al., 2019).

Soil thermal conductivity is a function of several factors such as soil fabric, porosity (or dry density), water content, mineralogy and temperature (Kersten, 1949; De Vries, 1963; Johansen, 1975; Farouki, 1981; Rao and Singh, 1999; Côté and Konrad, 2005a; Lu et al., 2007; Dong et al., 2015). Heat transfer in granular media is mainly governed by the particle to particle conduction and particle-liquid-particle in presence of the liquid, water (Yun and Santamarina, 2007). The number of contacts per soil volume and quality of inter-particle contacts controls the thermal conduction in granular media. Dong et al. (2015) highlighted that the soil constituent, water content, soil type and particle contacts are the key governing factors, which control the effective thermal conductivity of soil. Most of the soils have a very low thermal conductivity in a dry state as compared to that in wet conditions. It is due to fact that the water bridges formed between soil solid particles improve contact between the particles and the thermal conductivity of water is twenty-five times higher than that of air. Adams and Baljet (1968) analysed the different backfill soils used by utilities for underground power cables and found that the dry thermal conductivity values (0.2-0.5 $W\,m^{-1}\,K^{-1}$) were very lower than moist thermal conductivity for all investigated soils. It is noticed that the typical order of soil thermal conductivity is $\lambda_{air} < \lambda_{drysoil} < \lambda_{water} < \lambda_{sat-soil} < \lambda_{mineral}$ as the thermal conductivity of soil constituents vary over two orders of magnitude like λ_{air} = 0.024 $W\,m^{-1}\,K^{-1}$, λ_{water} = 0.594 $W\,m^{-1}\,K^{-1}$ and $\lambda_{mineral} > 3\ W\,m^{-1}\,K^{-1}$. The thermal conductivity of minerals is considerably very high than that of other soil constituents. The thermal conductivity of dry soils typically ranges from 0.07-0.5 $W\,m^{-1}\,K^{-1}$ (Rao and Singh, 1999; Naidu and Singh, 2004; Cortes et al., 2009), creating a need to develop geomaterials with higher

dry thermal conductivity, which is the first objective of this study.

Improvement in thermal conductivity could be achieved by enhancing the quality of the contacts and increasing the number of contacts among the grains. A bigger size, well-graded grain size distribution, higher solid thermal conductivity, lower porosity, saturation, and effective stress are the factors to enhance the thermal conduction and thus increase the thermal conductivity of soils (Yun and Santamarina, 2007; Nasirian et al., 2015). Keeping these facts in consideration, the grain size distribution of the sand is modified into fuller curve gradations (Fuller and Thomson, 1907), which consists of a wide range of particle arrangements (coarse to fine particles) contributing to lower porosities (or dense mixes) and higher inter-particle contacts. The design mixes are prepared utilizing the concept of fuller curve gradation to achieve lower porosities and adding fine materials as fillers in appropriate proportion to improve the denseness (Shrestha et al., 2016). The fine materials act as thermal bridges between the grains to increase the overall thermal connectivity of the soil solid matrix. The fine materials bentonite and stone-dust are added following the Fuller maximum density optimization scheme. Sand as prime geomaterials is selected because it often uses as backfill material. The experimental results suggest that by lowering the porosity of the system and by adding fillers, the thermal conductivity is significantly enhanced in the dry and partially saturated states.

It is always challenging to predict the soil thermal conductivity since it is dependent of several factors as mentioned above. Many attempts have been made in the past to quantify the effects of various factors on thermal conductivity of different soils and to correlate the thermal conductivity with those factors (De Vries, 1963; Farouki, 1981; Johansen, 1975; Rao and Singh, 1999; Côté and Konrad, 2005a; Lu et al., 2007; Dong et al., 2015). Earlier researchers have put more effort on developing models based on basic geotechnical index properties (De Vries, 1963; Farouki, 1981; Johansen, 1975; Rao and Singh, 1999). Like, Côté and Konrad (2005a) indicated that the effects of grain mineralogy and fabric should be considered while predicting the thermal conductivity of soils. So, basically, three types of approaches such as analytical/theoretical, empirical/semi-empirical and numerical methods have been in use to predict the thermal conductivity of soils. The analytical models are more complex which are adopted from other physical models and involve more calculation parameters. In contrast, empirical models are mostly developed from experimental data regression. These models are, however, more specific to certain boundary conditions and only exhibit satisfactory performance on certain soil types, or they are only applicable to either coarse-grained soils, fine-grained soils or high-quartz soils. Consequently, they are unable to predict the thermal conductivity for artificial or designed geomaterials used for buried power cables or borehole heat exchangers, etc. Many models include some empirical coefficients to describe the impact of some soil properties on the thermal conductivity of unsaturated soils. For example, Côté and Konrad (2005a) and (Lu et al., 2007) proposed different values of κ and α for different soil types. Apart from these models, Dong et al. (2015) proposed the conceptual model based on soil water retention curves (SWRC) which can be further used to develop quantitative thermal conductivity models for unsaturated soils. The numerical approach is accurate but it needs very good knowledge and understanding of the

methods and significant computational power. It can be said that the prediction model that is simple in application, accurate in prediction result and applicable for all types of soil is needed for assessing the thermal conductivity of soils effectively. Therefore, artificial neural networks (ANNs) as a novel approach are proposed in this study to predict the soil thermal conductivity of the sand and modified geomaterials for the dry and full range of saturation.

ANNs have achieved great popularity in the last decade because of an attractive alternative to the previous modelling approaches due to their high parallelism robustness, their inherent ability to extract from the experimental data, the highly non-linear and complex relationships between the variables of the problem without any detailed knowledge of the system (Najjar and Basheer, 1996; Grabarczyk and Furmanski, 2013; Shahin et al., 2002a). Since ANN models have learning capability that physics-based and other constitutive models lack, they have been successfully used in solving many engineering problems. Not only in the field of engineering, it has been also used in various other fields such as science, economics, agriculture, etc (Yoon et al., 1990; Fisha et al., 1995; Denton et al., 1995; Cavalieria et al., 2003). It has been massively used in civil engineering areas including geotechnical engineering, highway engineering, water resources, structural engineering, fluid mechanics, etc (Shahin et al., 2002a; Najjar and Basheer, 1996; Wang and Rahman, 1999; Goh, 1995; Attoh-Okine, 1999; Lee et al., 2001; Shahin et al., 2002b; Baziar and Nilipour, 2003; Kim et al., 2001; Lee, 2003; Holger and Graeme, 1996; Benning et al., 2001; Gontarski et al., 2000; Nejad et al., 2009). Shahin et. al. predicted settlement of shallow foundations on granular soils using ANN and found better prediction than the traditional method (Shahin et al., 2002a; Shahin et al., 2002b). Other researchers predicted the liquefaction potential of soil (Goh, 1995; Wang and Rahman, 1999; Baziar and Nilipour, 2003), the permeability of clay liners (Najjar and Basheer, 1996), pavement performance (Attoh-Okine, 1999), settlements of ground surfaces due to tunnelling (Kim et al., 2001), pile settlement (Nejad et al., 2009), the factor of safety of slope (Jason and Wilson, 2018), concrete strength (Lee, 2003) and forecasting of ocean tide level (Lee and Jeng, 2002; Lee et al., 2002) using ANN. ANN model has been also developed to predict the electrical resistivity of soils (Erzin et al., 2010; Bian et al., 2015; ApalooBara et al., 2019). However, over the last decade, very few studies have been done for predicting the thermal conductivity of soils using ANN (Erzin et al., 2008; Singh et al., 2011; Grabarczyk and Furmanski, 2013; Mishra et al., 2017; Zhang et al., 2020a). Some of the researchers used ANN to predict the thermal conductivity of food, textiles and rocks (Fayala et al., 2008; Sablani et al., 2002; Singh et al., 2007; Scott et al., 2007; Sablani and Rahman, 2003). Grabarczyk and Furmanski (2013) successfully applied ANN modelling for the prediction of thermal conductivity of dry granular media. Based on the ANN approach, the unified thermal conductivity model was developed to determine the relationship between the thermal conductivity of soils and its influence factors including dry density, porosity, saturation degree, quartz content, sand content and clay content (Zhang et al., 2020a). Erzin et al. (2008) reported that the thermal resistivity of different types of soils obtained from ANN models was found to be superior while comparing with those computed from the empirical thermal conductivity models. Singh et al. (2011) developed ANN models with

different combinations of training functions and activation functions and found that the effective thermal conductivity of moist porous materials predicted by ANN models had very good agreement with the available experimental data.

In this study, two separate ANN models (individual and generalised) are proposed to predict the thermal conductivity of newly developed geomaterials, which will be used as a backfill to bury high voltage power cables, for dry and moist states. In order to achieve this goal, the design and training of the networks are performed using the Matlab programming environment (version R2019a) with Neural Networks Toolbox. The data used in developing the models are obtained from the experimental work as well as from the literature survey. The thermal conductivity of original and modified soils is measured in the laboratory at room temperature by varying different parameters namely porosity, water content, quartz content, particle gradation. There are two measurement techniques namely: the transient method and the steady-state method to determine the thermal conductivity of the soils in the laboratory. Since the transient method is fast and convenient as compared to the steady-state method, the transient method is selected in this study. A thermal needle probe (KD2 pro device) is used to measure the thermal conductivity of all designed geomaterials in dry as well as in the moist state. The parameters mentioned earlier are fed into the ANN models as input variables to determine the relationships between input variables and thermal conductivity as output. Several configurations of ANN models were trained and tested while developing the optimal ANN model. ANN models are composed of multilayers with the Feed-forward network structure while the Back-Propagation algorithm is used for training. The Back-propagation algorithm is usually implemented using the Levenberg-Marquardt method, which combines the gradient descent method and the Gaus-Newton optimization method (Levenberg, 1944; Marquardt, 1963). The cross-validation technique(Stone, 1974), which has been successfully employed by several researchers (Erzin et al., 2008; Erzin et al., 2010; Zhang et al., 2020b) developing ANN models, is used as stopping criteria to stop the training. The optimum number of hidden layers and number of neurons in each hidden layer will be determined by using performance indices such as mean squared error (MSE), the coefficient of determination (R), and mean absolute error (MAE) as a measure of prediction accuracy. The predicted values of thermal conductivity obtained from optimal ANN models for independently measured data are compared with the values calculated from existing soil thermal conductivity prediction models. The ANN models show satisfactory results over the prediction models.

Furthermore, thermal simulation is performed for a single cable using Finite Element Methods software (Comsol multiphysics) to observe the heat dissipation characteristics around underground high voltage power cable with original and modified backfill materials (developed geomaterials). A result of thermal simulation for a single cable clearly shows a large improvement in heat dissipation for modified soil as compared to original sand.

1.2 Objective

The main objectives of this dissertation are:

- to study and analyse the effect of various factors on thermal conductivity of soils and generalization of existing thermal conductivity models.
- to design thermal backfill geomaterials with higher thermal conductivity, especially at the lower saturation level which is the critical state.
- to study ANN architecture and its application to the engineering field and its development so far.
- to propose a new ANN model as a new tool for predicting the thermal conductivity of designed geomaterials based on different input parameters obtained from the experiment conducted in the lab.
- simulation of High voltage power cables with original sand and developed backfill geomaterials.

In order to achieve these objectives, the dissertation is structured accordingly as shown in the next section.

1.3 Organization of Dissertation

The dissertation consists of seven chapters, of which the contents are summarized as below:

- Chapter 1: introduces the background, motivation and objectives of the thesis.
- Chapter 2: presents a literature review on the heat transfer process in soil, thermal properties of soil, current backfill in use for embedded high voltage power cables, various factors affecting thermal conductivity, discussing the existing prediction models and their development, measurement techniques.
- Chapter 3: presents background, literature review, structure/architecture and provides insight into the artificial neural network along with ANN application to engineering as well as other fields.
- Chapter 4: presents the materials analysis, measurement equipment used and experimental methodology to obtain the desired geomaterials.
- Chapter 5: presents the results and key findings of the study with a focus on material behaviours and thermal conductivity improvement. The results are also compared with prediction models and discussion is made.
- Chapter 6: presents the development of ANN models to predict the thermal conductivity of original and modified sand (developed geomaterials) from the parameters obtained from experimental work.
- Chapter 7: presents finite element simulation of underground high voltage power cables with original sand and developed geomaterials.

- Chapter 8: concludes the thesis by providing a summary of outputs of the study and recommendations for future works.

Chapter 2

State of the art

2.1 Introduction

This chapter deals with a review of heat transfer in soil, thermal properties of soil and various factors influencing on soil thermal properties. It also briefly discusses about the measurement technique and calculation (or prediction) of thermal conductivity and heat transfer in the buried pipe. It reviews the current backfill materials used in the embedded power cables.

2.2 Thermal properties of soil

Soil thermal properties are of great importance in many geo-engineering projects and energy applications such as underground high voltage cables, radioactive waste disposal, ground heat pumps that involve heat transfer in soil. Soil itself is complex in nature because of its composition, structure, heterogeneity and fluid movement in soil. So, the heat transfer in soil is very complicated. Three coupling processes i.e. thermo-hydro-mechanical (THM) processes are developed within the system. A thorough understanding of the thermal behaviour of soil is essential to deal with and solve the problems related to heat transfer in soil.

Soil thermal properties consist of thermal conductivity, specific heat capacity and diffusivity. The thermal conductivity of soil is the rate at which heat transfer through a unit thickness of the medium per unit area per unit temperature difference. It is the ability of soil to conduct heat. A high value of thermal conductivity indicates that the soil can transfer heat in a faster manner while a low value indicates it has high resistance to heat flow. For example, water can transfer heat twenty-five times faster than air. The measurement and calculation of thermal conductivity and factors affecting them will be discussed in next sections 2.5 & 2.4.

Under a steady condition, the temperature at a point doesn't vary with time. If it is changed with time, soil itself is either gaining or losing heat depending on the heat capacity of the element. The heat capacity, C, per unit volume of soil is defined as the heat energy needed to raise the temperature of this unit volume by 1°C. Mathematically, it is a product of the mass specific heat, c ($\mathrm{J\,kg^{-1}\,K^{-1}}$), and the density, ρ ($\mathrm{kg\,m^{-3}}$). The heat capacity of three-phase soil is given by:

$$C = x_s C_s + x_w C_w + x_a C_a \tag{2.1}$$

where x_s, x_w, x_a are volume fractions of the solid, water and air components present in unit soil volume and C_s, C_w, C_a are their respective heat capacities per unit volume.

In an unsteady condition, the thermal behaviour of soil is governed by both thermal conductivity and heat capacity. The ratio of the thermal conductivity and heat capacity is termed as the thermal diffusivity, α ($m^2\,s^{-1}$). A high value of thermal diffusivity means a capability for fast and considerable changes in temperature. Soil may have much greater thermal diffusivity in frozen condition than in unfrozen one because of the higher thermal conductivity of frozen soil and the lower specific heat of the ice as compared with liquid water. Ice has a thermal diffusivity about eight times greater than liquid water.

The thermal conductivity is a very important parameter amongst them when you deal with heat transfer in soils. Heat transfer in soil plays an important role in many types of problems. It will be explained next.

2.3 Heat transfer in soil

Heat as the form of energy transfers from a higher temperature region to slower one. No heat transfer when two regions reach the same temperature. Conduction, convection and radiation are the mechanisms through which heat can be transferred. All mechanisms need temperature differences for heat transfer. Not only the temperature levels, the soil structure and composition also affect the contribution of each possible mechanism to heat transfer. Figure 2.1 shows the region of influencing mechanisms in the field according to soil texture and degree of saturation. The numbers denoted in Figure 2.1 represent 1- thermal redistribution of moisture, 2- vapour diffusion due to moisture gradients, 3- free convection in water, 5- heat radiation.

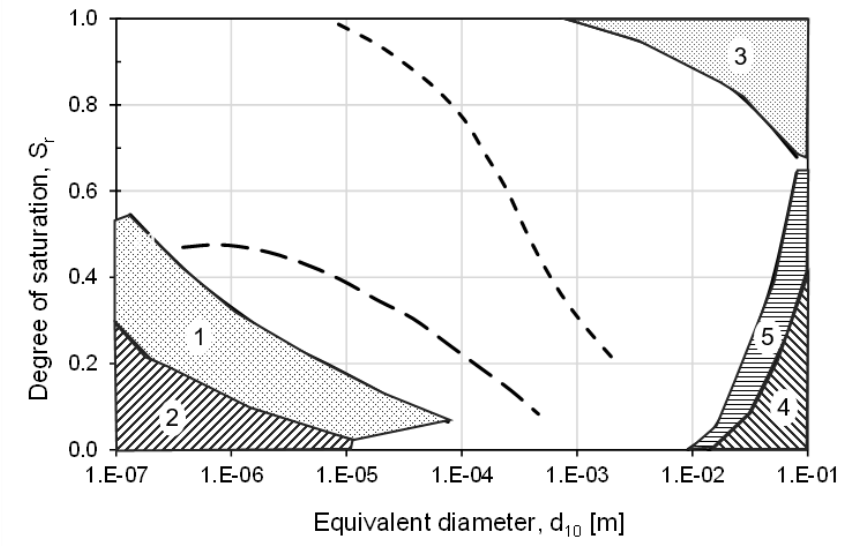

FIGURE 2.1: Region of influencing heat transfer mechanisms with respect to degree of saturation and soil grain size, after Farouki (1981).

Yun and Santamarina (2007) explained particle level heat flow in granular materials as shown in Figure 2.2. The different alphabetical character denotes different mechanism in granular materials. They are as follows:

a. Conduction along the mineral

b. particle-fluid-particle conduction across the fluid near contacts.

c. particle-to-particle conduction across contacts.

d. fluid convection within large pores.

e. particle-fluid conduction

f. conduction along with the pore fluid within the pore space (hydrostatic and advecting pore fluid)

It is evident that heat transfer in soil by conduction is the predominating mechanism. Convection and radiation generally have relatively small or negligible influences but they might have remarkable effects in certain conditions.

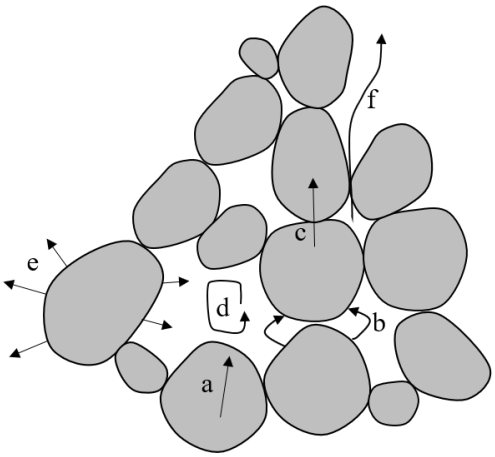

FIGURE 2.2: Primary particle-level heat transfer process in granular materials, after Yun and Santamarina (2007).

2.3.1 Conduction

Conduction is a transfer of energy from more energetic particles to less energetic ones due to interactions between the particles. Conduction occurs in all three soil constituents, i.e. solids (soil grains), liquids (water) and gases (the pore air). It is the primary mode of heat transfer in soils. Heat is conducted in solids in two ways: the lattice vibrational waves induced by the vibrational motions of the molecules and the energy transported through the free flow of electrons in the solid, while in air or water vapour, it is conducted by a process of collision between the molecules and a consequent increase in their mean kinetic energy as heat passes from higher temperature region to lower region. A similar mechanism is partly responsible for heat conduction in liquid water, but energy transfer by breaking and making

hydrogen bonds in water also contributes to heat conduction. The behaviour of liquid water lies between that of gases and solids.

The amount of heat transferred by conduction increases with an increase in soil dry density and degree of saturation. Heat is conducted in soil through all available paths as shown in Figure 2.2. Solid grains to solid grains provide the major path of heat conductive transfer (Yun and Santamarina, 2007). Other paths available are solid grains to fluid-filled pore, particle-fluid-particle and so on. Therefore, in this study, heat conduction is considered.

2.3.2 Convection

Convection is the transfer of energy between a solid surface and the adjacent fluid (liquid or gas) that is in motion. It includes the combined effects of conduction and fluid motion. The faster the fluid motion, the higher the convection. The transfer of heat between the solid surface and the adjacent fluid in the absence of bulk fluid motion is purely conduction. Convection is of two types, forced convection and natural or free convection. If the fluid is forced to flow over the solid surface by external means, it is called forced convection. In contrast, if the fluid flows freely because of buoyancy forces that are induced by density difference due to variation of temperature in the fluid is called free convection. Convection in soils through air or water is usually negligible. It is dominated by conduction and it will be considered in the coarse-grained material where $D_{50} \geq 6$mm (Yun and Santamarina, 2007). Heat transfer due to convection is not considered in this study.

2.3.3 Radiation

Radiation is the transfer of energy in the form of electromagnetic waves or photons due to the changes in the electronic configuration of atoms or molecules. Unlike conduction and convection, it doesn't need the presence of an intervening medium. A body emits radiation because of its temperature. All bodies with the temperature above 0° K emit energy according to Stefan-Boltzmann. The temperature of the radiating body plays the most important factor since the heat flow is proportional to the fourth power of the absolute temperature. In this study, radiation is not considered as it makes a negligible contribution to heat transfer in soils for the temperature below 727°C.

2.3.4 Heat transfer equation

The rate of heat conduction through a medium is dependent of geometry of the medium, thickness and material type of the medium as well as the temperature difference across the medium. The heat flux (q) is the rate of heat transfer (Q) per unit area (A). The area (A) is always normal to the direction of heat flow. According to Fourier's law of heat conduction for one-dimensional heat flow, the heat flux is directly proportional to the temperature gradient in the direction of heat flow and expressed by the following equation:

$$q = -\lambda \nabla T = -\lambda \frac{\Delta T}{\Delta x} \tag{2.2}$$

where q ($W\,m^{-2}$) is the heat flux, λ ($W\,m^{-1}\,K^{-1}$) is the thermal conductivity of the medium, ∇T is the temperature gradient, T (K) is the temperature, x (m) is the medium thickness. Heat flows in the direction of lower temperature and the temperature gradient becomes negative when temperature decreases with increasing x. So, the negative sign ensures that heat flows in the positive x-direction is a positive quantity. For a three-dimensional heat flow, the heat flux is given by:

$$q = -\lambda \left(\frac{\Delta T}{\Delta x} + \frac{\Delta T}{\Delta y} + \frac{\Delta T}{\Delta z} \right) \tag{2.3}$$

Equation for conservation of heat energy results in a general expression for soil heat flow where soil temperature may vary in time and space,

$$\rho c \frac{\partial T}{\partial t} = -\frac{\partial q}{\partial x} \tag{2.4}$$

where ρ is denisty ($kg\,m^{-3}$) of medium, and c ($J\,kg^{-1}\,K^{-1}$) is the specific heat of medium. Combining Equations 2.2 and 2.4 we get:

$$\rho c \frac{\partial T}{\partial t} = \frac{\partial}{\partial x} \left(\lambda \frac{\partial T}{\partial x} \right) = \lambda \left(\frac{\partial^2 T}{\partial x^2} \right) \tag{2.5}$$

In the Equation 2.5, the terms ρc and λ can be replaced by thermal diffusivity, α ($m^2\,s^{-1}$), by definition and the Equation 2.6 becomes heat transfer equation for one dimensional flow.

$$\left(\frac{1}{\alpha} \right) \frac{\partial T}{\partial t} = \frac{\partial^2 T}{\partial x^2} \tag{2.6}$$

For three-dimensional heat flow, the heat transfer equation derived by Fourier in 1822 is given by:

$$\left(\frac{1}{\alpha} \right) \frac{\partial T}{\partial t} = \frac{\partial^2 T}{\partial x^2} + \frac{\partial^2 T}{\partial y^2} + \frac{\partial^2 T}{\partial z^2} \tag{2.7}$$

For the transient state, the temperature changes with time. However, in steady state the temperature doesn't change with the time and the term $\partial T / \partial t$ becomes zero.

2.4 Factors affecting soil thermal conductivity

Soil is mainly composed of three-phases including solid phase, liquid phase and gas phase. In cold regions, ice might present in the soil as a solid phase, but this is not considered in this study because all the works are performed at room temperature (about 20 ± 2^{o}C). Solid grains surround the pore spaces which contain either water or air and both water and air. The solid particles are composed of mineralogy such as quartz, feldspar, etc. That's why the solid phase possesses the best heat conduction and has the highest thermal conductivity as compared to both liquid and gas phases. The soil exit in nature in a certain arrangement of the solid particles. Various changes in soil structure and therefore in porosity or density occur naturally. Soil thermal conductivity is affected by several particle-level and macro-scale

factors such as porosity (or dry density), water content (or saturation), soil composition and texture, soil gradation, cementation, mineralogy, effective stress and temperature (Kersten, 1949; De Vries, 1963; Johansen, 1975; Farouki, 1981; Côté and Konrad, 2005a; Lu et al., 2007; Hailemariam et al., 2015; Dong et al., 2015). The key governing factors that control the thermal conductivity of soils are thermal conductivity of soil constituent (i.e., solids or minerals, liquid and air), soil type, water content and particle contacts (Dong et al., 2015). Other factors also significantly affect the thermal conductivity of the soils.

2.4.1 Effect of dry density and saturation on thermal conductivity

The dry density and saturation which govern the soil thermal conductivity are among the most influential factor . An increase in either dry density or saturation increases thermal conductivity regardless of soil types. A dry density is one of the engineering properties used to represent the degree of denseness of soils. By definition, it is the mass of soil particles per unit volume, while saturation is the amount of moisture contained in the soil. Sometimes porosity instead of dry density may be used to show the variation of thermal conductivity. As the porosity increases, the thermal conductivity of the soils decreases. Many researchers in the past investigated the influences of saturation and dry density on thermal conductivity for different types of soil. It is also important to account for these parameters for the development of prediction models.

An increase in dry density of soil results in an increase in the thermal conductivity due to three factors; more solid grains per unit soil volume, less pore (or void) per unit soil volume and better heat conductive transfer between the grain contacts (Farouki, 1981). Kersten (1949) after numerous tests found that at constant moisture content, the logarithm of the thermal conductivity increased linearly with the dry density (Figure 2.3). The slope of the linear relation for different water contents is approximately the same for given soil. However, the slope is different for different types of soil. It is cleared from Figure 2.3 that the effect of dry density is independent of moisture content. In the case of dry soils, the dry density has a particularly important effect on the thermal conductivity as it implies more solid particles per unit volume and better thermal contacts. Estimating the thermal conductivity of dry soils is more sensible because of variations in dry density and microstructure such as shape differences. Over the last few decades, the prediction models for dry soils has been proposed incorporating microstructure effect, shape factors, soil types and the volumetric fraction of solid and pore (De Vries, 1963; Johansen, 1975; Farouki, 1981; Côté and Konrad, 2005a; Lu et al., 2007). For example, De Vries (1963) model predicted that thermal conductivity of dry soils increases linearly at low densities and the rate of increase becomes more rapid as the soil solids volume fraction increases. Johansen (1975) incorporated microstructure and shape factors while proposing the thermal conductivity of dry soil. The thermal conductivity prediction models for dry soil are discussed briefly in section 2.6.

On the other hand, an increase in dry density for fully saturated soils means that the soil grains replace some of the water in pores. An increase in thermal conductivity is only noticed if the thermal conductivity of a solid is higher than that of water. As clayey and sandy soils have higher thermal conductivity than water (for sand and clay, λ is fifteen and

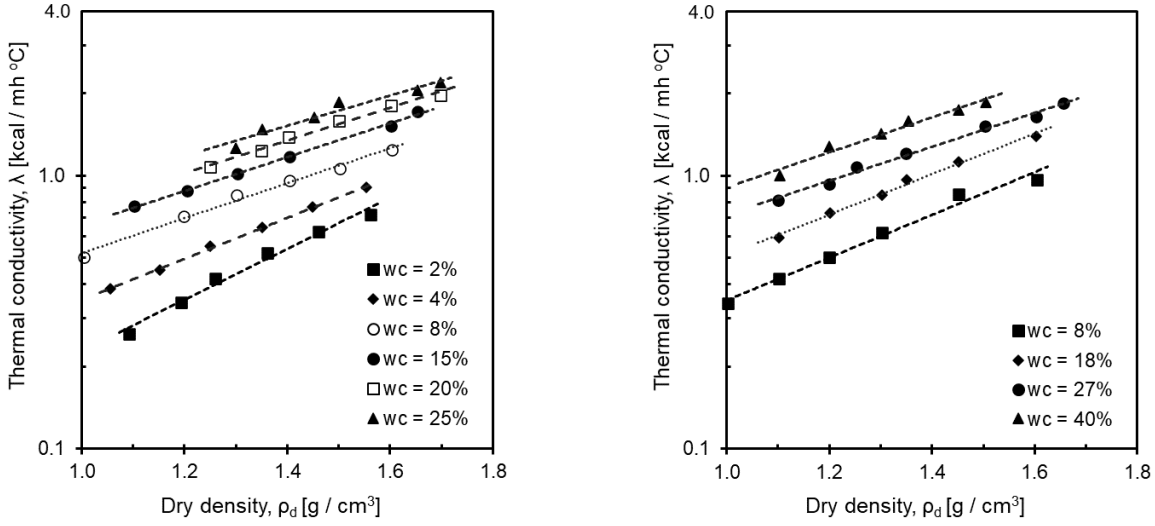

(A) Sandy soils

(B) Clayey soils

FIGURE 2.3: Thermal conductivity of sandy and clayey soils against dry density at constant water content, after Farouki (1981).

four times that of water, respectively), the thermal conductivity of saturated soils increases with an increase in dry density. As sandy soils have a thermal conductivity about fifteen times that of water because of quartz content, the rate of increase in thermal conductivity with dry density is greater than clay soils, but this effect may not be marked. If the soil becomes oversaturated with water (for example ocean sediments), there is a rapid decrease in the thermal conductivity as dry density drops (Farouki, 1981). It is particularly observed if the solid material is quartz which is being replaced by water. In case of organic soils or peat, there will be a slight increase in the thermal conductivity despite doubling or tripling of solid fractions since peat contains much water and thermal conductivity of peat is only about half that of water (Farouki, 1981).

Water as a liquid phase in soil exits in three states: ice, liquid water and water vapour. In this study, we deal with liquid water only. The amount of water in the soils is usually expressed in one of three ways: moisture (or water) content (w), volumetric water content (θ) or degree of saturation (S_r). Water plays a major role in determining the thermal conductivity of soils. The earliest recognition was made by Patten (1909), Bouyoucos (1915) and Beskow (1935). An increase in moisture content leads to an increase in the thermal conductivity because of mainly two factors: a) air is displaced by liquid water which has a thermal conductivity twenty-five times higher than air and b) the presence of a small amount of moisture improves the thermal conduction because of the formation of water bridges at the contact points.

The effect of increasing water content depends on the soil type. It means that the rate of increase in thermal conductivity will be different according to types of the soil. For example, the thermal conductivity increases abruptly with moisture content in sand, while in clay it will increase slowly. As shown in Figure 2.4, there is a high rate of increase in thermal conductivity at the beginning (at lower water contents) due to the formation of water bridges at

the contact points in case of coarse-grained soils. However, the increase in thermal conductivity at lower water content is more gradual in the case of fine-grained soils (Lu et al., 2007). The reason behind the behaviour is that the fine-textured soils have larger surface areas and more water is needed before water bridges are formed between solid particles. In order to understand the effect of water on thermal conductivity, the saturation level (0-100)% is generally divided into three regimes: a) the pendular regime $S_r \leq 0.2$, characteristics by the substantial variation in thermal conductivity with respect to S_r; b) the funicular regime S_r = 0.2-0.7, characterized by the mild conduction changes; c) the capillary regime $S_r \geq 0.7$, characterized by no significant conduction changes. During the pendular regime, the thermal conductivity of soils increases rapidly due to the reasons that the addition of water will inevitably replace a portion of the air from the pore in soils and generate water films and water bridges among soil particles which is beneficial for better thermal conduction as the thermal conductivity of water is relatively higher than that of air (Farouki, 1981; Lu et al., 2007). Further increase in moisture after this regime, will reach the funicular regime. In this regime, the increase in thermal conductivity mainly depends on the replacement of air by water and the soil particles are completely connected with bridges. As a result, the thermal conductivity increases slowly or moderately. Further increase in moisture increases insignificantly thermal conductivity and the maximum thermal conductivity value is reached in the capillary regime. The moisture content corresponding to the state, where changing of the slope of increment of thermal conductivity, is commonly known as critical moisture content, which is shown in Figure 2.6.

The relationship between thermal conductivity and water content has been explored by many researchers over the few decades. Kersten (1949) found that the thermal conductivity is linearly related to the logarithm of water content at a constant dry density. Johansen (1975) introduced Kersten number, soil-type dependent parameter, to develop the relationship between thermal conductivity and degree of saturation from the known values of dry and saturated thermal conductivity. This method is very famous and followed by Côté and Konrad (2005a) and Lu et al. (2007) later. The estimation of thermal conductivity as a function of saturation is explained in section 2.6.

Farouki (1981) found that the effect of water content on the thermal conductivity of some kind of soil is also dependent of hysteresis i.e. whether the soil is in the process of wetting or drying. The thermal conductivity of quartzitic gravel and sand with 8% binder is higher during the drying process than wetting.

2.4.2 Effect of soil composition and texture on thermal conductivity

Soils are broadly classified as coarse-textured and fine-textured soils. Two noticeable effects of texture on thermal conductivity were found by Lu et al. (2007) a) the coarse-textured soils have higher thermal conductivity than the fine-textured soils, b) the increment in thermal conductivity of fine-textured soils increases gradually at lower water contents as compared to coarse-textured soils (Figure 2.4).

The thermal conductivity is affected by grain size distribution and soil type. A well-graded soil has lower thermal resistivity (reciprocal of thermal conductivity) than other

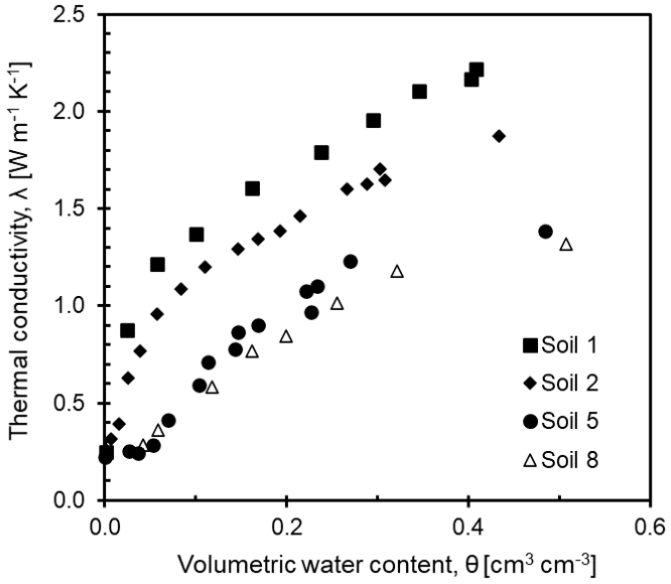

FIGURE 2.4: Thermal conductivity as function of volumetric water content for coarse-textured (soil-1,2) and fine-textured (soil-5,8) soils, after Lu et al. (2007).

gradation (Figures 2.5 & 2.6). The shape and size of the particles also affect the thermal conductivity. With a decrease in particle size, the number of contact points will increase within a soil volume. The thermal resistance of these contact points will be much higher than that of the internal soil particles. Therefore, heat flow through soil becomes more difficult and it results in a decrease in the thermal conductivity of soil. This is the reason that sandy soils have higher thermal conductivity as compared to that of clayed soils as shown in Figure 2.6. Heat transfer through soil particles mainly depends on the contact points, especially in dry soils, because the thermal conductivity of air is extremely lower than that of soil particles. An increase in number of contact points will help to improve the thermal conduction of soils. Moreover, adding binders will improve thermal conduction of the soils because of the generation of more stable soil structure. Larger particles lead to higher thermal conductivity as conductive heat flow is proportional to the particle radius and inversely proportional to the inter-contact distance. The well-graded granular soils with fine particle fractions of 8-10% show good thermal conduction and stability (Adams and Baljet, 1968). The addition of fine grains to uniform sized material fill the voids between the larger grains and thus providing more solid matter per unit volume, which leads to improving the effective thermal conductivity of mixed materials (Shrestha et al., 2016; Shrestha et al., 2019). However, an optimum amount of fine content should be determined prior to use. With a wide range of sizes and continuous grading of grain sizes, a lower porosity or dense packing may be obtained which may have higher thermal conductivity. In addition, soil thermal conductivity is significantly improved if the solid grains are cemented together by clay or other cementing binders.

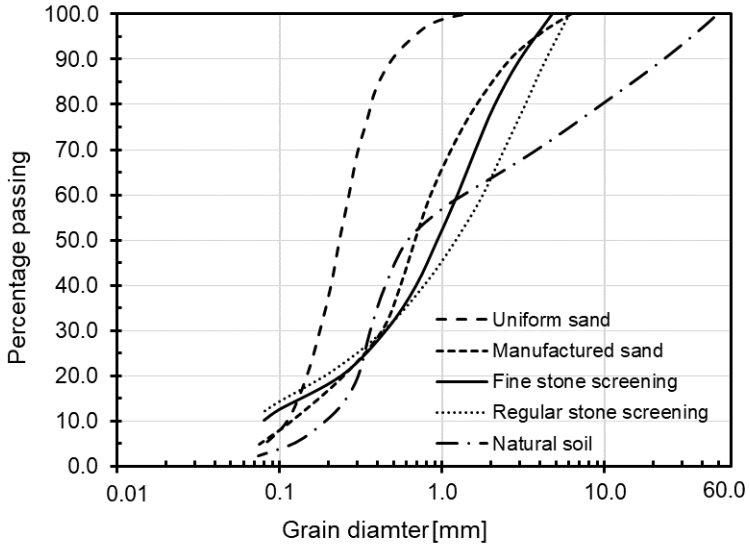

FIGURE 2.5: Grain-size distribution of different soils, after Adams and Baljet (1968).

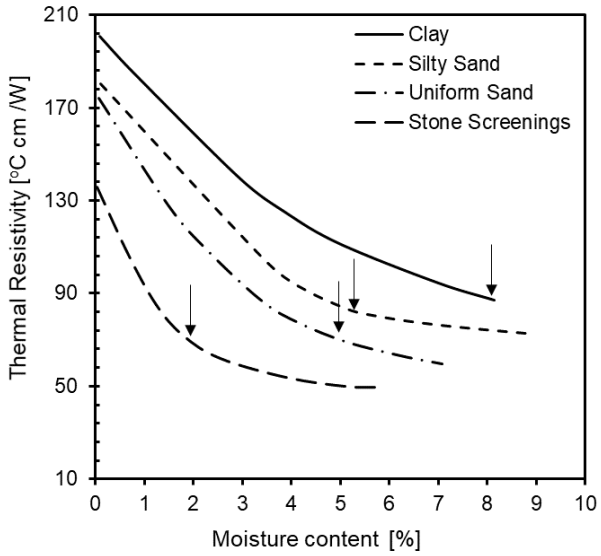

FIGURE 2.6: Thermal resistivity (reciprocal of thermal conductivity) of different types of soil, after Adams and Baljet (1968) (arrows represent critical moisture content).

2.4.3 Effect of structure on thermal conductivity

As explained earlier, heat conduction through two-phase soils depends on the thermal conductivity of each phase and on the structure of the solid matrix. The structure of soils is generally associated with the combined effect of fabric, soil composition and inter-particle forces. The fabric represents to arrangements of particles, particle groups and pore space. The fabric and structure of the soils are affected by the size and shape of particles and the aggregation of particles with or without cementing agents. The cementing agent could be from natural origin (calcites, silicates, etc) or industrial/artificial origin (cement, bitumen, lime).

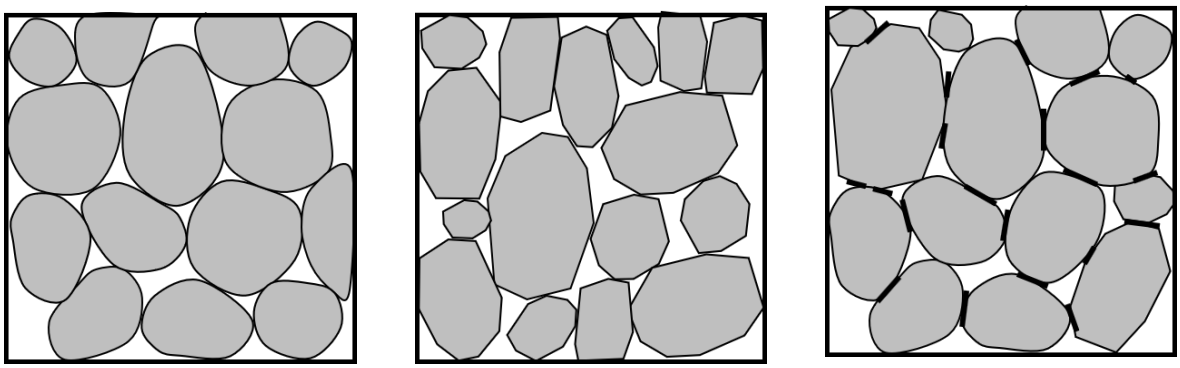

(A) Rounded/sub-rounded particles (B) Angular/sub-angular particles (C) Cemented particles

FIGURE 2.7: A schematic structure of porous media, after Côté and Konrad (2009).

The shape of particles found in natural soil deposits could be rounded and sub-rounded while that obtained from the manufacturing process could be angular and sub-angular. Therefore, the structure can be divided into three categories viz: (a) rounded/sub-rounded particles, (b) angular/sub-angular particles, and (c) cemented particles as shown in Figure 2.7. As solid to solid contact area of angular particles is greater than that of rounded particles, the thermal conductivity of crushed particles (i.e. angular) is higher than that of natural particles (rounded) (Adams and Baljet, 1968; Johansen, 1975; Côté and Konrad, 2005a; Côté and Konrad, 2009). This contact area will increase further in the presence of bounding (cementing) agent. Therefore, the thermal conductivity is generally higher in cemented materials than in other normal materials (Smith, 1942; Woodside and Messmer, 1961; Johansen, 1975). The impact of structure on the effective thermal conductivity of two-phase porous media increases with increasing solid/fluid thermal conductivity ratios (Woodside and Messmer, 1961). Côté and Konrad (2009) demonstrated that the effect of structure increases with decreasing fluid/solid thermal conductivity ratios and the effect is negligible when the ratio is 1/15 (=0.0667) and higher. They proposed the relationship to determine the thermal conductivity of two-phase porous geomaterials accounting structure parameter, which is discussed in next section 2.6. It means the structure effect is more in presence of air instead of water as the fluid/solid thermal conductivity ratios (λ_f/λ_s=0.003) with air is relatively less than that with water (λ_f/λ_s=0.076), taking these values λ_s= 7.7 ($\mathrm{W\,m^{-1}\,K^{-1}}$), λ_a= 0.024 ($\mathrm{W\,m^{-1}\,K^{-1}}$), λ_w= 0.59 ($\mathrm{W\,m^{-1}\,K^{-1}}$). They also observed that there will be no significant effect of particle size and pore-size distribution effects on the effective thermal conductivity of two-phase porous geomaterials.

2.4.4 Effect of mineralogy on thermal conductivity

As explained earlier, the solid phase of soil consists of different minerals like quartz, kaolinite, feldspar, calcite, mica, etc. Therefore, mineralogy has remarkable a influence on the thermal conductivity performance of the solid particles (Côté and Konrad, 2005a; Lu et al., 2007). The quartz is of most important mineral in the soil as it has the thermal conductivity

of 7.69 $W\,m^{-1}\,K^{-1}$, which is the highest among all the soil minerals and the thermal conductivity of other soil minerals do not change considerably (i.e. around 2.0-3.0 $W\,m^{-1}\,K^{-1}$). A soil with high quartz contain possesses a high value of thermal conductivity (Horai and Simmons, 1969). The quartz content controls the thermal conductivity of soil solids. Sand with high quartz content has a higher thermal conductivity then sand with low quartz content. It can be observed from Figure 2.4 that the discrepancy between soil 1 and soil 2 in terms of thermal conductivity is obvious under the same moisture content because soil 1 has a higher percentage of quartz content than soil 2. Johansen (1975) proposed a generalised geometric model to estimate the thermal conductivity of soil solids based on the thermal conductivity of quartz only. Côté and Konrad (2005a) further improved the model by proposing another model which requires thermal conductivity of each mineral contained within the soils. This model is only applicable and accurate than Johansen model when thermal conductivity values of each mineral present in soil are known. The method to calculate the thermal conductivity of soil solids is discussed in section 2.6. However, these prediction models need a volumetric fraction of quartz content. Accurate determination of quartz content in the soil is very difficult and a lack of data for quartz content is another critical issue, hindering the successful application of the existing models. Consequently, the quartz content is assumed to be equal to the mass fraction of sand (Peters-Lidard et al., 1998; Usowicz et al., 2006; Lu et al., 2007). However, this assumption leads to an overestimation of soil thermal conductivity (Tarnawski et al., 2009; Zhang et al., 2017). The quartz content in soils can be experimentally determined by chemical or X-ray diffraction (XRD) methods and to a lesser extent, by petrographic analysis. Chemical methods are generally more precise, but time-consuming, whereas XRD techniques are more rapid but fairly accurate (Hardy, 1992). A new approach was discussed to determine the quartz content using measured thermal conductivity data which are reliable and accurate (Tarnawski et al., 2009). The approach was reverse-modelling of quartz content from thermal conductivity data, assessing the $K_e - S_r$ functions against complete experimental thermal conductivity data.

2.4.5 Effect of other factors on thermal conductivity

The effects of some other factors including temperature, salt content and organic matter on soil thermal conductivity are discussed in this section. The thermal conductivity of soils is considerably varied with temperature since the temperature changes will affect the thermal movement of molecules. Generally, an increase in temperature may accelerate the thermal movement of molecules, which facilitates heat transfer through the materials. Mitchell and Soga (2005) identified that all crystalline minerals in soils show decreasing thermal conductivity with an increase in temperature. In addition, the liquid phase and gas phase have different responses to temperature rise in terms of thermal conduction. Specifically, the thermal conductivity of saturated air increases markedly with an increase in temperature, whereas the thermal conductivity of water increases slightly under the same condition. The net effect is that the thermal conductivity of unsaturated sandy soils increases somewhat with increasing temperature. However, some researchers reported contradictive findings

with the above-mentioned comment. For example, Smits et al. (2013) and Hiraiwa and Kasubuchi (2000) measured thermal conductivity of sandy soils over a wide range of temperatures (5°C–75°C) and found an obvious increment in thermal conductivity with increasing temperature of the tested samples. As explained earlier, the comment on the evolution of thermal conduction of soils with the increasing temperature has not been unified to date, thus, further researches are needed to explore the correlations between thermal conductivity and temperature.

The presence of salt concentration and organic matter in the soils reduces thermal conductivity. An increase in organic matter and salt contents decrease the thermal conductivity of soils (Abu-Hamdeh and Reeder, 2000). However, the concentration of salt also plays a major role on thermal conductivity. Noborio and McInnes (1993) discovered that the apparent thermal conductivity of soils decreases with an increase in salt concentrations ($CaCl_2$, $MgCl_2$, NaCl or Na_2SO_4) from 0,1 mol kg^{-1} to solubility limits. On the other hand, Rooyen and Winterkorn (1959) found that there was no noticeable effect of salt on the thermal conductivity of quartz sand at high solution contents with the concentration of $CaCl_2$ up to 0.18 mol kg^{-1} or with NaCl up to 0.34 mol kg^{-1}. Globus and Rozenshtok (1989) concluded that the quartz sand saturated with 0.25 mol kg^{-1} solution of KOH has lower thermal conductivity than that of quartz sand with water.

2.5 Measurement of thermal conductivity

In order to measure the thermal conductivity of the soils, two methods are mainly existed; steady-state and transient method (Mitchell and Kao, 1978; Farouki, 1981) .

2.5.1 Steady-state method

Steady-state method includes the application of one-directional heat flow across a sample and the observation of temperature gradient across the sample when a steady-state condition is reached (Mitchell and Kao, 1978; Farouki, 1981; Low et al., 2013; Hailemariam et al., 2016c). It follows Fourier's law to calculate the thermal conductivity of the sample. This method will be more reliable and accurate if the temperature of the sample doesn't vary with time (McGuinness et al., 2014; Hailemariam et al., 2016c). The only limitation of the method is that it requires a very good setup of equipment and considerable time to reach steady-state condition. Moisture migration is another problem in the case of unsaturated soil due to the considerable time and the relatively high-temperature difference needed to reach the steady state. As a result, the resulting thermal conductivity would be lower than the value corresponding to the average moisture content (De Vries, 1963). This method is further divided into absolute and comparative methods (Alrtimi, 2008). In the absolute steady-state method, the power and temperature distribution across the sample is determined directly from the input power and temperature parameters. Guarded hot plate (GHP) test, unguarded hot plate test, cylindrical arrangement, in-situ sphere test and heat meter test are examples of

the absolute steady-state method. The GHP test is generally considered as accurate. However, it is quite time consuming and suitable for laboratory use. In situ, sphere test and heat meter test are used to measure the thermal conductivity of soil in situ.

On the other hand, the comparative method uses a series of reference materials of known thermal conductivity aligned in series with the sample (Momose et al., 2008; McGuinness et al., 2014; Hailemariam et al., 2016c). The divided bar apparatus and the guarded comparative longitudinal heat flow are examples of this method. Most recently, an advanced steady-state device was also developed to measure the vertical stress, thermal conductivity, coefficient of thermal expansion, deformation and other hydro-mechanical properties simultaneously (Stegner et al., 2011; Sass and Stegner, 2012; Hailemariam et al., 2016b). This device based on the principle of the divided bar apparatus has been successfully used to measure the thermal conductivity of porous media, unconsolidated rocks, and bedding materials (Stegner et al., 2011; Sass and Stegner, 2012; Hailemariam et al., 2016c; Hailemariam et al., 2016b) without matric suction controlled. Later, the device was modified to measure the thermal conductivity with matric suction controlled (Hailemariam and Wuttke, 2018).

2.5.2 Transient state method

Transient method is faster and more versatile than the steady-state method and can be easily performed. This method involves the application of heat to the sample and recording the temperature changes over time and later uses these data to determine the thermal conductivity of the sample by using an analytical solution to the thermal diffusivity equation (Mitchell and Kao, 1978; Farouki, 1981; Low et al., 2013). A thermal probe (single or dual) , hot wire method and transient plane source method are examples of the transient method. A needle probe (single or dual probes) method is one of the most common and convenient methods for measuring the thermal conductivity of soils in the laboratory or situ. This method has been widely used for the past centuries and successfully used in many research (Farouki, 1981; Lu et al., 2007). A needle consists of a heater producing thermal energy at a constant rate and a thermocouple recording the temperature changes over time. The rate of temperature changes of the probe depends on the thermal conductivity of the surrounding medium, where it is inserted. Due to short measurement time and lower temperature difference, moisture migration will not take place in the unsaturated state (Farouki, 1981). The theory of the probe method is based on an infinite line heat source placed in a semi-infinite, homogeneous and isotropic medium.

According to Fourier's law, the heat equation for one dimensional flow in the x direction is given by:

$$\frac{\partial T}{\partial t} = \alpha \frac{\partial^2 T}{\partial x^2} \tag{2.8}$$

where T is temperature at time t. For cylindrical configuration, the equation 2.7 becomes

$$\frac{\partial T}{\partial t} = \alpha \left(\frac{\partial^2 T}{\partial r^2} + \frac{1}{r} \frac{\partial T}{\partial r} \right) \tag{2.9}$$

where r is the radial distance from the line source. Assuming heat is produced from t=0 at constant rate of thermal energy, q, per unit length of probe, the solution to above equation gives the temperature change, ΔT, of the medium as below:

$$\Delta T = \frac{q}{4\pi\lambda}\left[-Ei\left(-\frac{r^2}{4\alpha t}\right)\right] \tag{2.10}$$

where Ei is an exponential integral, and λ is the thermal conductivity of the medium. For a large value of time, the exponential integral will be approximately a logarithm function. The temperature changes become proportional to the logarithm of time at constant k with space and time. A plot of temperature rise against the logarithm of time gives the straight line and the slope gives thermal conductivity of the medium according to equation 2.10.

$$\lambda = \frac{q}{4\pi\left(T_2 - T_1\right)}\ln\left(\frac{t_2}{t_1}\right) \tag{2.11}$$

In the probe, the device gives directly the thermal conductivity value by recording temperature rise over time.

2.6 Existing thermal conductivity models

Since the measurement of thermal conductivity in the laboratory or situ is time-consuming and difficult, several researchers have proposed different predictive models predicting thermal conductivity based on several parameters such as porosity, water content, mineralogy, particle gradation, etc. which are easily obtainable from the measurement. Accurate prediction of soil thermal conductivity is very crucial to the design of geo-energy applications such as nuclear disposal sites, energy piles, borehole thermal energy storage, ground source heat pumps, etc. These models are further classified as theoretical or analytical, semi/empirical and numerical models. The theoretical models are developed based on approximate models wherein the actual soil structure is simplified in such a way as to permit a mathematical analysis. On the other hand, the empirical models are developed directly from empirical fits to the experimental data to establish the relationship between soil thermal conductivity and influencing factors.

2.6.1 Theoretical prediction models

Many theoretical prediction models have been developed, basically based on the volumetric fractions of soil constituent phases as well as the fabric of the medium in the past (Farouki, 1981; Yun and Santamarina, 2007; Abuel-Naga et al., 2008).

Some theoretical models like series and parallel are considered as boundary models and especially used for the two-phase state. The series (Equation 2.13) model represents the lower boundary while the parallel model (Equation 2.12) represents the upper boundary of theoretical models. These equations are based on volumetric fraction and thermal conductivity of soil constituents. In the equations, the volumetric fractions are represented by porosity (n), which is the ratio of the pore to soil volume.

$$\lambda_{parallel} = n\lambda_f + (1-n)\,\lambda_s \tag{2.12}$$

$$\frac{1}{\lambda_{series}} = \frac{n}{\lambda_f} + \frac{(1-n)}{\lambda_s} \tag{2.13}$$

where, λ_f ($\mathrm{W\,m^{-1}\,K^{-1}}$) is the thermal conductivity of fluid (for water, $\lambda_w = 0.594\,\mathrm{W\,m^{-1}\,K^{-1}}$ and for air, λ_a = 0.024 $\mathrm{W\,m^{-1}\,K^{-1}}$ at 20^{o}C), λ_s ($\mathrm{W\,m^{-1}\,K^{-1}}$) is the thermal conductivity of solid particles. Series heat flow is dominant at high λ_s/λ_f ratios, whereas parallel flow is dominant at low λ_s/λ_f (Farouki, 1981). These two boundaries are also called Wiener bounds and are independent of the pore structure of the porous medium. Equations 2.13 and 2.12 corresponds to lower and upper Wiener bounds.

An average of series and parallel heat flow models is obtained by taking the geometric mean (GM) (Farouki, 1981). The GM equation has been widely used for predicting the thermal conductivity of various types of soils. This model is also adopted to predict the saturated thermal conductivity and the thermal conductivity of soil solid particles. The GM equation is given by:

$$\lambda = \lambda_f^n \lambda_s^{(1-n)} \tag{2.14}$$

In case of three-phase soil, i.e. solid, liquid and air, the geometric mean method is expressed as:

$$\lambda = \lambda_s^{1-n} \lambda_w^{S_r n} \lambda_a^{(1-S_r)n} \tag{2.15}$$

Maxwell (1954) developed the electrical conductivity models for a mixture of uniform spheres dispersed at random in a continuous fluid, which can be used to calculate the thermal conductivity of two-phase soils. It is famously known as Maxwell equation, given by:

$$\lambda = \lambda_s \left[\frac{\lambda_f + 2\lambda_s + 2n\left(\lambda_f - \lambda_s\right)}{\lambda_f + 2\lambda_s - n\left(\lambda_f - \lambda_s\right)} \right] \tag{2.16}$$

Hashin and Shtrikman (1962) also proposed narrow boundary equations for the upper and lower bounds of thermal conductivity. The upper HS-U and lower HS-L equations are given below:

$$\lambda_U = \lambda_s + \frac{n}{\frac{1}{\left(\lambda_f - \lambda_s\right)} + \frac{(1-n)}{3\lambda_s}} \tag{2.17}$$

$$\lambda_L = \lambda_f + \frac{n}{\frac{(1-n)}{\left(\lambda_s - \lambda_f\right)} + \frac{n}{3\lambda_f}} \tag{2.18}$$

The equations (2.12 - 2.18) unless as stated can be used for both dry soils and saturated soils with corresponding thermal conductivity of air and water, respectively. The pore is filled by water in case of saturated soils, while it is filled by air in case of dry soils.

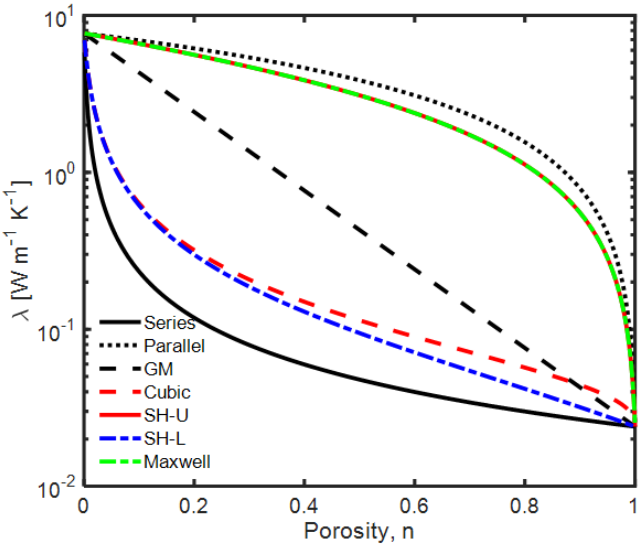

FIGURE 2.8: Thermal conductivity (λ) vs porosity (n) of dry soils using theoretical models.

De Vries (1963) expressed that soil solid particles were uniformly distributed in continuous pore fluid in soils and proposed a soil thermal conductivity model (Equation 2.19) for two-phase soil according to the Maxwell equation.

$$\lambda = \frac{\sum_{i=0}^{N} K_i x_i \lambda_i}{\sum_{i=0}^{N} K_i x_i} \tag{2.19}$$

where, x_i is the volume fraction of each constituent, λ_i is the thermal conductivity of each constituent and K_i is the weighting factor, depend on the shape and orientation of the granules of soil constituent and on the ratio of the conductivities of the constituents, which is given by:

$$K_i = \frac{1}{3} \sum_{a,b,c} \left[1 + \left(\frac{\lambda_i}{\lambda_o} - 1 \right) g_a \right]^{-1}; \quad g_a + g_b + g_c = 1 \tag{2.20}$$

where, g_a, g_b, g_c are the grain shape coefficients and usually taken as $1/3$ for spherical soil particles.

Gori and Corasaniti (2004) developed the cubic cell model to predict the effective thermal conductivity of dry soils.

$$\lambda_d = \left[\frac{(\beta_d - 1)}{\lambda_a \beta_d} + \frac{\beta_d}{\lambda_a \left[(\beta_d)^2 - 1 \right] + \lambda_s} \right]^{-1}; \quad \beta_d = \left[\frac{1}{1-n} \right]^{1/3} \tag{2.21}$$

Yun and Santamarina (2007) also proposed the volume fraction (VF) model (Equation 2.22) and the log-model (Equation 2.23) to estimate the effective thermal conductivity of the dry soils. Both models are based on fitting parameters.

$$\lambda_d = \left[n \lambda_a^s + (1-n) \lambda_s^s \right]^{1/s}; \quad s = -0.25 \tag{2.22}$$

$$\lambda_d = -a \ln(n) + p; \quad a = -0.291 \mathrm{W\,m^{-1}\,K^{-1}} \& \quad p = 0.026 \mathrm{W\,m^{-1}\,K^{-1}} \tag{2.23}$$

Tong et al. (2009) investigated the thermal conductivity of multiphase porous media and developed a generalized thermal conductivity model considering the effects of water content, porosity, degree of saturation, temperature and pressure based on Wiener bound model. The thermal conductivity equation is given by:

$$\begin{aligned} \lambda = {} & \eta_1(1-n)\lambda_s + (1-\eta_2)\left[1-\eta_1(1-n)\right]^2 \\ & \left[\frac{(1-n)(1-\eta_1)}{\lambda_s} + \frac{nS_r}{\lambda_w} + \frac{n(1-S_r)}{\lambda_a}\right]^{-1} \\ & + \eta_2\left[(1-n)(1-\eta_1)\lambda_s + nS_r\lambda_w + n(1-S_r)\lambda_a\right] \end{aligned} \tag{2.24}$$

where, λ_s, λ_w and λ_a are the thermal conductivities of solid, water and air, respectively, n is the porosity, S_r is the degree of saturation, η_1 is the coefficient describing the pore structure characteristic of mixture of solid and air, $0 < \eta_1(n) < 1$, η_2 is the function of pore structure, degree of saturation and temperature, $0 < \eta_2(n,S_r,T) < 1$.

Haigh (2012) derived a theoretical thermal conductivity model (Equation 2.25) for sands from a three-phase soil contact unit cell. He considered the interaction among soil solid, water and air during heat conduction in his model.

$$\begin{aligned} \frac{\lambda}{\lambda_s} = {} & 2(1+\xi)^2 \\ & \left\{\frac{\alpha_w}{(1-\alpha_w)^2}\ln\left[\frac{(1+\xi)+(\alpha_w-1)x}{\xi+\alpha_w}\right] + \frac{\alpha_a}{(1-\alpha_a)^2}\ln\left[\frac{(1+\xi)}{(1+\xi)+(\alpha_a-1)x}\right]\right\} \\ & + \frac{2(1+\xi)}{(1-\alpha_w)(1-\alpha_a)}\left[(\alpha_w-\alpha_a)x - (1-\alpha_a)\alpha_w\right] \end{aligned} \tag{2.25}$$

$$x = \left(\frac{1+\xi}{2}\right)\left(1+\cos\theta-\sqrt{3}\sin\theta\right); \quad \xi = \frac{2e-1}{3} \tag{2.26}$$

$$\cos 3\theta = \frac{2(1+3\xi)(1-S_r) - (1+\xi)^3}{(1+\xi)^3} \tag{2.27}$$

where, λ_s is the thermal conductivity of solid, $\alpha_w = \lambda_w/\lambda_s$ & $\alpha_a = \lambda_a/\lambda_s$, λ_a and λ_w are thermal conductivities of air and water, ξ and x are the coefficients related to the thickness of water film and degree of saturation (S_r), and e is the void ratio.

2.6.2 Semi/empirical prediction models

Semi-empirical models predict more accurately than theoretical models because of the inclusion of soil fabric and gradation but are usually applicable for limited types of soil under certain given conditions. These models predict the thermal conductivity of the soils based

on water content or saturation, porosity or dry density, mineral contents, grain-size distribution, particle shape and size (Kersten, 1949; De Vries, 1963; Johansen, 1975; Farouki, 1981; Rao and Singh, 1999; Côté and Konrad, 2005a; Lu et al., 2007). The models are developed based on empirical fits to experimental data of natural soils.

For example, Kersten (1949) proposed an empirical relationship between thermal conductivity and moisture content and dry density based on a large number of laboratory measurements. For silt-clay soils,

$$\lambda = 0.1442\,[0.9 \log w - 0.2]\,10^{0.6243\rho_d} \tag{2.28}$$

where, λ ($\mathrm{W\,m^{-1}\,K^{-1}}$) is the thermal conductivity of soil, w (%) is water content, and ρ_d ($\mathrm{g\,cm^{-3}}$) is the dry density. For sandy soils,

$$\lambda = 0.1442\,[0.7 \log w + 0.4]\,10^{0.6243\rho_d} \tag{2.29}$$

The proposed equations for silt-clay and sandy soils are valid only with $w \geq 7\%$ and $w \geq 1\%$, respectively. Rao and Singh (1999) improved the Kersten equation by introducing empirical parameters to fit experimental data for different types of soil based on particle size distribution. They established a relationship between thermal resistivity instead of thermal conductivity and moisture content and dry density for clay type to sandy soils and then the thermal conductivity model was derived according to the reciprocal correlation between thermal conductivity and thermal resistivity. The proposed equation is valid only for silt and clay with $w \geq 10\%$ and for sand $w \geq 1\%$ and predicts resistivity values with an absolute difference of 10-15 % from experimental data. These models, which are developed mostly for fine-grained soils and sands, are generally not suitable for the predicting thermal conductivity of dry soils. Later, Naidu and Singh (2004) suggested one more empirical equation for dry soils depending on dry density and soil type (i.e. silt and clays only). The proposed relationship is only applied for fine-grained soils, not for coarse-grained soil.

Johansen (1975) proposed a concept of normalized conductivity as Kersten number to predict the thermal conductivity of soils in unsaturated condition using logarithm function of saturation degree. Because of the logarithm function, the model couldn't predict the thermal conductivity less than 10%. Farouki (1981) observed that the Johansen model was $\pm$25% accurate when compared to the large database on the thermal conductivity of soils.

$$\lambda = (\lambda_{sat} - \lambda_d)\,K_e + \lambda_d \tag{2.30}$$

$$K_e = C \log (S_r) + 1.0 \tag{2.31}$$

where, λ ($\mathrm{W\,m^{-1}\,K^{-1}}$) is the thermal conductivity of soil, λ_{sat} ($\mathrm{W\,m^{-1}\,K^{-1}}$) is the thermal conductivity of saturated soil, λ_d ($\mathrm{W\,m^{-1}\,K^{-1}}$) is the thermal conductivity of dry soils, K_e is the Kersten number which is a dimensionless parameter, C is a constant parameter depending on the soil types (C=0.7 & 1.0 for coarse and fine-grained soils, respectively), S_r is the degree of saturation (in fraction).

For the dry soils, Johansen (1975) suggested semi-empirical equations to predict the thermal conductivity based on dry density and solid density of the soils. He noted that the dry density or porosity (i.e. microstructure) was a major factor in determining the thermal conductivity of dry soils. The solid particle conductivity has less effect as compared to the microstructure effect. So, he developed two separate equations for dry natural soils and crushed rock materials. For dry natural soils, he proposed the following equation based on Maxwell-Fricke's equation.

$$\lambda_d = \frac{0.135\rho_d + 64.7}{\rho_s - 0.947\rho_d} \tag{2.32}$$

where, ρ_b (kg m^{-3}) is the dry density of soil, ρ_s (kg m^{-3}) is the soil solid density. For dry crushed rock materials, he developed the following equation based on porosity (n) only. He found that the thermal conductivity for crushed rock materials is higher than dry natural soils at the same porosity.

$$\lambda_d = 0.039n^{-2,2} \tag{2.33}$$

As Johansen (1975) found that variations in microstructure had little effect on the thermal conductivity of saturated soils, he used the geometric mean (GM) equation to calculate the thermal conductivity of saturated soil and soil solid based on the volumetric fraction of water and solid, and quartz content and thermal conductivity of quartz, respectively.

$$\lambda_{sat} = \lambda_w^n \lambda_s^{(1-n)} \tag{2.34}$$

$$\lambda_s = \lambda_q^q \lambda_o^{(1-q)} \tag{2.35}$$

where, λ_{sat} (W m^{-1} K^{-1}) is the thermal conductivity of saturated soil, λ_s (W m^{-1} K^{-1}) is the thermal conductivity of soil solid, λ_w (W m^{-1} K^{-1}) is the thermal conductivity of water, λ_q (W m^{-1} K^{-1}) is the thermal conductivity of quartz mineral (λ_q = 7.7 W m^{-1} K^{-1}), n is the porosity, q is the volumetric fraction of quartz content and λ_o is the thermal conductivity of other minerals (λ_o=2.0 W m^{-1} K^{-1} or 3.0 W m^{-1} K^{-1} for soils with q>0.2 or q<0.2, respectively).

Midttomme and Roaldset (1998) investigated the impact of the grain size on thermal conductivity of quartz sands and silts and proposed an empirical relationship between the thermal conductivity of solid and mean grain size of samples based on thermal test results of saturated quartz sands.

$$\lambda_s = 0.215 \log(d_m) + 1.93 \tag{2.36}$$

where, λ_s (W m^{-1} K^{-1}) is the thermal conductivity of solid and d_m (μm) is the mean grain size of samples. He found that the influence of the grain sizes was more for the finer and less for the coarse material.

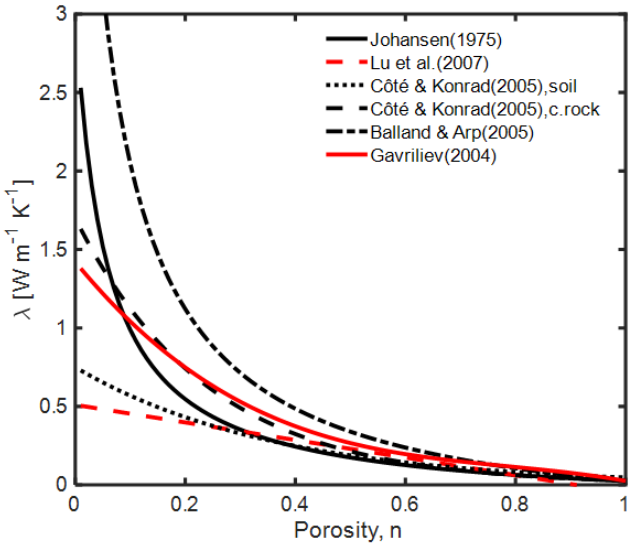

FIGURE 2.9: Thermal conductivity (λ) vs porosity (n) of dry soils using semi-empirical models.

Gavriliev (2004) proposed a purely empirical equation for predicting the thermal conductivity of dry mineral soils based on dry density (ρ_d) by fitting experimental data. This equation is only valid for the mineral soils with dry density lower than 2.0 g cm^{-3}.

$$\lambda_d = 0.025 + 0.238\rho_d - 0.193\rho_d^2 + 0.114\rho_d^3 \tag{2.37}$$

Côté and Konrad (2005a) used the concept of normalized thermal conductivity, first proposed by Johansen (1975), to predict the thermal conductivity of unsaturated soils, but suggested a new empirical function for the Kersten number eliminating logarithm function and enabling the equation to be used for the full range of saturation.

$$K_e = \frac{\kappa S_r}{1 + (\kappa - 1)\, S_r} \tag{2.38}$$

where, κ is a soil texture dependent parameter with values of 4.60, 3.55, 1.90 and 0.60 for gravel and coarse sands, medium and fine sands, silty & clayey soils, and for organic soils in unfrozen state, respectively, S_r is the degree of saturation. Côté and Konrad (2005a) suggested an empirical relationship for estimating the thermal conductivity of dry soils and construction materials according to soil types and particle shape. He found that the mineral content of solid particles had little effect on the thermal conductivity of dry soils and therefore, developed the equation based on porosity for different types of soils.

$$\lambda_d = \chi 10^{-\eta n} \tag{2.39}$$

where, χ (W m^{-1} K^{-1}) and η are particle shape effect parameters depending on types of materials with values of 1.70 (W m^{-1} K^{-1}) and 1.80 for crushed rock materials, 0.75 (W m^{-1} K^{-1}) and 1.20 for natural mineral soils and 0.30 (W m^{-1} K^{-1}) and 0.87 for organic fibrous soils. For the saturated thermal conductivity, Côté and Konrad used the same GM Equation 2.34.

However, they recommended different equations for the thermal conductivity of soil solid based on the volumetric fraction of different minerals and their respective thermal conductivity.

$$\lambda_s = \prod_j \lambda_{mj}^{x_j}; \quad \sum_j x_j = 1 \tag{2.40}$$

where, λ_m ($\mathrm{W\,m^{-1}\,K^{-1}}$) is the thermal conductivity of rock-forming mineral j and x_j is the volumetric fraction of mineral j. They found that Johansen's Equation 2.35 was quite reliable for fine-grained soils and was particularly useful in the presence of quartz content. However, the new generalized geometric mean method was very useful for rock materials with quartz content lower than 20%.

Zhang et al. (2015) simply modified Côté and Konrad (2005a) model for sands with extremely high quartz content by suggesting new values of κ, χ and η after fitting the experimental data obtained by the Thermo TDR probe method. The respective new values are 6.0, 8.12 $\mathrm{W\,m^{-1}\,K^{-1}}$ and 3.2, which are much greater than those in Côté and Konrad (2005a) owing to the quartz content effect.

Balland and Arp (2005) modified Johansen (1975) model considering the effects of organic matter on thermal conductivity of soil. The proposed Kersten equation based on degree of saturation and volumetric fraction of organic matter and sand with empirical parameters is as follows:

$$K_e = S_r^{0.5\left(1+V_{om}-\alpha_b V_{sand}-V_{cf}\right)} \left[\left(\frac{1}{1+\exp\left(-\beta_b S_r\right)}\right)^3 - \left(\frac{1-S_r}{2}\right)^3\right]^{1-V_{om}} \tag{2.41}$$

where, $\alpha_b$and β_b are coordination coefficients, V_{sand} and V_{cf} are volumetric fractions of sand and coarse particles in the solid phase. They established equations to calculate the thermal conductivity of dry soil based on thermal conductivity of solids, dry density and specific gravity.

$$\lambda_d = \frac{\left(a\lambda_s - \lambda_a\right)\rho_d + \lambda_a \rho_p}{\rho_p - \left(1-a\right)\rho_d} \tag{2.42}$$

where, λ_s ($\mathrm{W\,m^{-1}\,K^{-1}}$) and λ_a ($\mathrm{W\,m^{-1}\,K^{-1}}$) are thermal conductivities of solid and air, respectively, ρ_d ($\mathrm{kg\,m^{-3}}$) is dry density of the soil, ρ_p ($\mathrm{kg\,m^{-3}}$) is particle density, and a is dimensionless parameter with a = 0.053. Balland and Arp (2005) used the same GM Equation 2.34, proposed by Johansen (1975), to calculate the thermal conductivity of saturated soils, but proposed another equation incorporating volumetric fraction and thermal conductivity of organic matter in addition to quartz and other minerals to calculate the thermal conductivity of solid.

$$\lambda_s = \lambda_{om}^{V_{om}} \lambda_q^{V^q} \lambda_{min}^{\left(1-V_{om}-V_q\right)} \tag{2.43}$$

where, λ_{om} ($\mathrm{W\,m^{-1}\,K^{-1}}$), λ_q($\mathrm{W\,m^{-1}\,K^{-1}}$), λ_{min}($\mathrm{W\,m^{-1}\,K^{-1}}$) are thermal conductivities of organic matter, quartz and other minerals, respectively, V_{om} and V^q are volumetric fraction

of organic matter and quartz content in the solid phase.

Lu et al. (2007) proposed another Kersten number equation different from Johansen (1975) and Côté and Konrad (2005a) based on soil texture and shape. Lu et al. (2007) found that their new model provided better prediction than Côté and Konrad model in the unsaturated state, especially for the fine-textured soils at lower saturation degree.

$$K_e = \exp\left\{\alpha_s \left[1 - S_r^{(\alpha_s - 1.33)}\right]\right\} \tag{2.44}$$

where, α_s is a soil texture dependent parameter with values of 0.96 and 0.27 for coarse-textured and fine-textured soils, respectively, and 1.33 is a shape parameter. Lu et al. (2007) suggested a simple linear equation to predict the thermal conductivity of the dry soils based on the porosity, which is valid only between porosities of 0.2 and 0.6.

$$\lambda_d = -a_l n + b_l \tag{2.45}$$

where, a_l and b_l are empirical parameters with values of 0.56 and 0.51, respectively. Lu et al. (2007) used the same Equations 2.34 and 2.35 , proposed by Johansen (1975), to predict the saturated thermal conductivity (λ_{sat}) and soil solid thermal conductivity (λ_s).

Chen (2008) developed an empirical model for quartz sand based on experimental thermal conductivity data obtained in the laboratory using the thermal probe method. He found that the porosity (n) of tested sand is linearly varied with the logarithm of measured thermal conductivity and the slope of the linear trend was affected by the degree of saturation (S_r). He included some empirical parameters to fit experimental data and presented the equation as below.

$$\lambda = \lambda_{sat} \left[(1 - b_c)\, S_r + b_c\right]^{c_c n} \tag{2.46}$$

where, b_c and c_c are empirical parameters withb_c = 0.0022 and c_c = 0.78 for quartz sands, λ_{sat} (W m^{-1} K^{-1}) is the thermal conductivity of saturated sand, which is calculated using Equation 2.34, proposed by Johansen (1975).

Côté and Konrad (2009) assessed the impact of structure on thermal conductivity of two-phase porous geomaterials that include natural soils, natural rock, crushed rock, cement rock, etc. They proposed the semi-empirical equation 2.47 to determine the thermal conductivity of two-phase porous geomaterials considering the structure effect parameter, which is denoted by κ_{2P}.

$$\lambda = \frac{\left(\kappa_{2P}\lambda_s - \lambda_f\right)(1 - n) + \lambda_f}{1 + (\kappa_{2P} - 1) - (1 - n)} \tag{2.47}$$

where, λ_f & λ_s are thermal conductivity of fluid and solid, respectively and n is porosity. They established simplified a relationship (Equation 2.48) between κ_{2P} and fluid/solid thermal conductivity ratios by incorporating empirical parameter, β, which is dependent of λ_f/λ_s ratio. The values of β are 0.46 for all materials when $\lambda_f/\lambda_s > 1/15$ and 0.81, 0.54 & 0.34 for round/sub-rounded, angular/sub-angular, & cemented materials when $\lambda_f/\lambda_s \leq$

1/15. It is observed that the structure effect increases with decreasing λ_f/λ_s ratio and no structure effect on the thermal conductivity appears when $\lambda_f/\lambda_s > 1/15$.

$$\kappa_{2P} = 0.29 \left(\frac{\lambda_f}{\lambda_s}\right)^{\beta} \tag{2.48}$$

Zhang et al. (2017) expressed that the existing prediction models couldn't predict thermal conductivity for a wide range of soil types due to the gaps in measured thermal conductivities between any two tested natural soils. They proposed a generalized soil thermal conductivity model based on extensive laboratory experiments on sand, kaolin clay and sand-kaolin clay mixtures using new Thermo-time domain reflectometry (TDR) probe. They also used the concept of normalized thermal conductivity, first proposed by Johansen (1975), to estimate soil thermal conductivity in the unsaturated state based on the degree of saturation and quartz content. They simply modified Kersten Equation 2.38, proposed by Côté and Konrad (2005a), based on quartz content, rather than empirical soil texture dependent parameter (κ).

$$\kappa = 2.168 * 10^{-5} * \exp\left(\frac{x_q}{7.903}\right) + 1.252 \tag{2.49}$$

$$K_e = \frac{\left[2.168 * 10^{-5} * \exp\left(\frac{x_q}{7.903}\right) + 1.252\right] S_r}{1 + \left[2.168 * 10^{-5} * \exp\left(\frac{x_q}{7.903}\right) + 0.252\right] S_r} \tag{2.50}$$

where, x_q (%) is the quartz or sand content. In this model, the sand content is assumed to be identical to quartz content. The thermal conductivity of dry soils (Equation 2.39), proposed by Côté and Konrad (2005a), is further formulated based on quartz content, which is expressed as follows:

$$\lambda_d = \left[1.216 * 10^{-6} * \exp\left(\frac{x_q}{6.599}\right) + 3.034\right] 10^{\left[-0.003 * \exp\left(\frac{x_q}{16.452}\right) - 1.840\right] n} \tag{2.51}$$

For saturated soils, the equation 2.34 is recalculated based on quartz content as follows:

$$\lambda_{sat} = \lambda_w^n \left(\lambda_q^{x_q/100} \lambda_k^{1-x_q/100}\right)^{(1-n)} \tag{2.52}$$

where λ_q (W m^{-1} K^{-1}) & λ_k (W m^{-1} K^{-1}) are thermal conductivities of quartz and kaolin with assumed values of 7.5 W m^{-1} K^{-1} & 2.9 W m^{-1} K^{-1}, respectively. The limitation of this model is that it may not provide very satisfactory results when quartz content is much less than sand content for a given type of soil.

2.6.3 Numerical models

The third approach to predict the thermal conductivity of the soil is numerical models which include particle shape, particle distribution and orientation in space as well as material property (anisotropy) apart from other soil properties. Finite element method (FEM), boundary element method (BEM), fluid dynamics method (FDM), discrete element method (DEM) and more recently lattice element method (LEM) are the techniques to calculate the effective

thermal conductivity of the soils and other granular materials based on different systems and configurations.

FEM has been used for particle and fibre filled composites (Kumlutas and Tavman, 2006), polymer composites (Xu et al., 2006), the effect of the filler concentrations (Karkir et al., 2011) to study thermal conduction in granular matter. In this method, each individual grain discretize into small particle counts. However, it is challenging to model heat transfer in granular material with a large number of particles due to an excessively large scale finite element model resulting from the discretization of each particle. BEM method was also applied to predict the effective thermal conductivity of packed beds and it was found that the model showed a relatively high accuracy than others (Zhou et al., 2007). DEM is a particle-based method in which the microstructure is modelled with regular arrays of simple shapes like spheres, cubes or cylinders. For example, Feng et al. (2008) developed a new mathematical algorithm in conjunction with the DEM approach, which contains many spherical particles of different sizes, to simulate the heat conduction process in 2D space and then derived the formula to calculate thermal conductivity. Shamy et al. (2013) also used the DEM technique to study the effect of shear-induced anisotropy on soil thermal conductivity. Choo et al. (2012) studied the evolution of stress-related thermal conductivity of soil in DEM modelling. The oversimplification of particle representation as isothermal spheres/disks loses the mathematical rigour but is computationally efficient. Therefore, the knowledge of shape, size, distribution and conductance of each particle is required to model heat transfer in granular materials, which is sometimes difficult and cumbersome as the packing of the granular matter is very complex with wide ranges of size and shape, distribution and thermal properties. In order to make this complexity into a simplified way, the LEM is developed to predict the effective thermal conductivity of the sands and modified backfill materials (Rizvi et al., 2018; Shrestha et al., 2019). In this method, 2D and 3D simulations are conducted to analyse and identify the differences resulting from model simplification. The effective thermal conductivity is determined considering the volume and shape of each constituting portion.

2.6.4 Artificial Neural Network (ANN) models

The theoretical or analytical models are more complex which are developed from other physical models wherein the actual soil structure is simplified in such a way as to permit a mathematical analysis and include more calculation parameters. In contrast, the empirical models are developed directly from experimental data regression in order to establish a relationship between soil thermal conductivity and influencing factors. These models are, however, more specific to certain boundary conditions and only exhibit satisfactory performance on certain soil types, or they are only applicable to either coarse-grained soils, fine-grained soils or high-quartz soils. Consequently, they are unable to predict the thermal conductivity for special designed and artificial materials. Many models include some empirical coefficients to describe the impact of some soil properties on the thermal conductivity of unsaturated soils. For example, Côté and Konrad (2005a) and (Lu et al., 2007) proposed different values of κ and α for different soil types. The numerical approach is accurate but

it needs very good knowledge and understanding of the methods and significant computational power. It can be said that the prediction model that is simple in application, accurate in prediction result and applicable for all types of soil is needed for assessing the thermal conductivity of soils effectively. Therefore, the fourth approach could be artificial neural networks (ANNs) as a novel tool that is developed to estimate the thermal conductivity of the soils and artificial or designed materials in dry as well as in moist case. ANN is briefly explained in Chapter 3.

2.7 Material design under consideration of thermal conductivity

The material design is a very important aspect in the case of thermal related facilities, especially in the underground high voltage power cables, which is explained next.

2.7.1 Importance of thermal conductivity on underground high voltage power cables

The performance and efficiency of underground high voltage cable depend on the thermal conductivity of the medium where it is placed. The knowledge of heat transfer in cable and soils is also required to develop the backfill materials which is used to bury the cables.

High voltage buried power cable which is alternatives to overhead power cable, needs a proper burial. Otherwise, improper installations often can lead to cable failure due to heat generated from the cable, though the underground cables are designed for a 30 years life. The cables are designed to achieve a certain temperature at the full load requirement such that no deterioration occurs to the cable insulation. For example, polymeric cables may be allowed to rise to 90°C while oil/paper insulated cables to 85°C (Sandiford, 1981). Exceeding these temperatures can lead to insulation failure and breakdowns of cable conductors. Heat is generated in the cable due to many factors such as power losses in the conductors, insulation power losses, sheath losses and other components of the cable system (Sandiford, 1981; Mozan et al., 1997; Afa, 2010). The ability of the backfill soil to transfer the heat determines whether the cables remain cool or overheat. The thermal conductivity of the soil where the cable is embedded usually accounts for more than 50% of the total temperature rise of the cable conductor. Therefore, it is very essential to design the proper backfill materials and to know the thermal behaviour of soil. In order to take away the heat from the cable to the surrounding environment for the safe and efficient operation of the cable, the medium where it is placed should have high thermal conductivity (Drefke et al., 2015). In fact, the better the heat dissipation, the lower the maximum temperature reached by cable, which ultimately protects the cable failure. When the thermal conductivity of the medium is poor, the heat is produced in the cable faster than the heat dissipates away. Therefore, the thermal conductivity of the medium should be, in principle, higher than the surrounding soil in a dry as well as the moist state.

Under unfavourable conditions, a significant migration of moisture away from the immediate vicinity of the cable due to heat flux forms dry zones around the cable in which

the thermal conductivity of soil is reduced to that of its dry state (Adams and Baljet, 1968; Radhakrishna et al., 1980; Gouda, 1986; Anders and Radhakrishna, 1988). The temperature gradient around an embedded cable, which is generated by heat losses, may induce moisture migration away from the immediate vicinity of the cable. Consequently, zones of low moisture content can develop, considerable decreasing the thermal conductivity of the soil to well below that assumed in the design of the cable. The resulting increase in the temperature gradient will cause further drying of the backfill soil and the temperature of the cable may arise to a value far more than its safe operating level, which consequently leads to damage or failure of the cable. The schematic diagram of the underground power cable is shown in Figure 2.10.

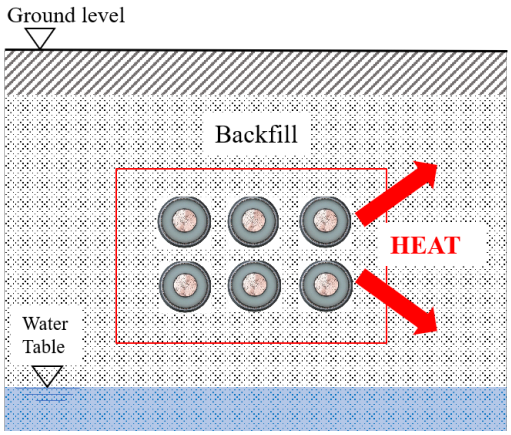

FIGURE 2.10: Schematic diagram of underground power cable.

The reduction in thermal conductivity largely influences the current carrying capacity of the underground cables (Sandiford, 1981; De León and Anders, 2008) as well as cable life (Karahn and Kalenderli, 2011). In Figure 2.11, the current carrying capacity decreases with a decrease in thermal conductivity. The most crucial reduction of current-carrying capacity is noticed when the thermal conductivity is below 2 $W\,m^{-1}\,K^{-1}$. Improving the thermal conductivity of backfill soils results in 10-30 % increase in cable ampacity. The soils only have thermal conductivity above 2 $W\,m^{-1}\,K^{-1}$ when it is in the moist state. It means the partial drying state or complete dry state is very crucial in the design of backfill materials. The cable life is exponentially increased with the increase of thermal conductivity and the cable has a comparatively larger life of 30 years at the soil thermal conductivity of 1 $W\,m^{-1}\,K^{-1}$ as compared to 5 years at 0.8 $W\,m^{-1}\,K^{-1}$ (Figure 2.12). Actually, most soils have a very lower thermal conductivity in dry states as compared to that in a saturated condition. It is due to fact that the water bridge formed between solid particles improves the contact quality by replacing air and water has thermal conductivity about 25 times higher than that of air. Adams and Baljet (1968) analysed different backfill soils used for underground power cables and found that the dry thermal conductivity data (0.2-0.5)$W\,m^{-1}\,K^{-1}$ were extremely lower than moist thermal conductivity. The thermal conductivity of dry soils typically ranges from (0.07-0.5) $W\,m^{-1}\,K^{-1}$ (Rao and Singh, 1999; Naidu and Singh, 2004; Cortes et al., 2009; Waite et al., 2009). Therefore, the thermal conductivity of backfill materials in the dry state is more

crucial for the best performance of underground power cables. This is the reason more attention is particularly given to the dry state while designing the granular backfill materials in this study.

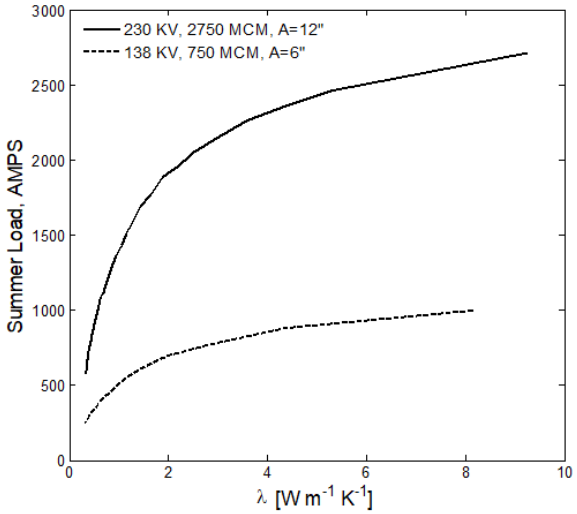

FIGURE 2.11: Effect of thermal conductivity on cable ampacity of underground power cable, after Sandiford (1981).

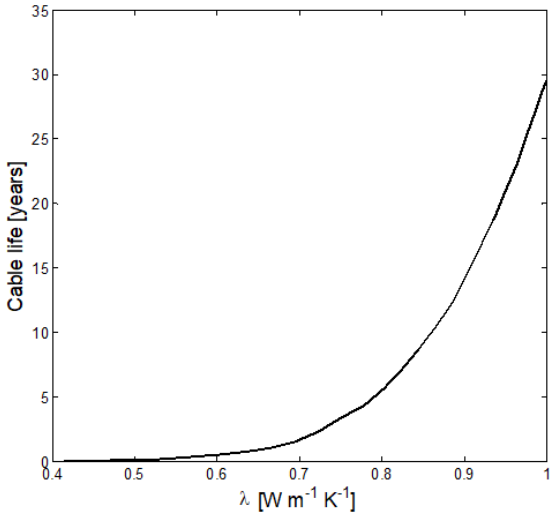

FIGURE 2.12: Effect of thermal conductivity on cable life of underground power cable, after Karahn and Kalenderli (2011).

2.7.2 Materials used to bury underground cables

The backfill material used to bury underground high voltage power cables plays an important role with respect to the ampacity of a cable system. The selected materials, which

are placed systematically to meet the cable guidelines and specifications, are called 'thermal backfill' or 'corrective backfill'. Besides for low-voltage power high cables, the excavated materials are always replaced by thermal backfills. However, in some cases, the excavated/native soils are also used as backfill materials to avoid the additional cost incurred by disposal of these materials in another site. But, these soils are thermally very poor as it dries out easily under high cable loads. In the past, the backfill materials commonly used to bury the underground power cables were natural sand, manufactured sands, or stone screening, etc. depending on its availability. Adams and Baljet (1968) investigated the typical thermal backfills (e.g. uniform sand, manufacture sand, fine stone screening, regular stone screening) used for underground power cables by utilities. They found that well-graded granular materials behaved the best. Limestone screening, a by-product from rock quarries, was particularly found to have better thermal conductivity than other materials (Figure 2.6). They also concluded that the well-graded granular soils with a clay fraction of 8-10 % are considered as good thermal backfills. In current practice, the well-graded sands are also widely used in many places where crushed rock products are not easily available. It is evident that good gradation of particle size and the degree of compaction ensure high thermal conductivity and good thermal stability (Adams and Baljet, 1968). There are some other backfill materials like sand-gravel with cementing materials, sand with some other additives (fly ash, bentonite), liquid soil, weak flowable concrete which have been in practice. In recent years, fluidized thermal backfill (FTB), developed by Radhakrishna (1981) have become more common. It is one of the example of controlled low strength materials (CLSM). It is a slurry backfill composed of natural aggregate, sand, a small amount of cement, water and fluidizer (fly ash, bentonite, or polymer) or metal-based additives (iron ore pellets, hematite powder, magnetite dust, or metal filling steel fibres). The fluidizer and additives help to improve the flow and thermal properties of the backfill. The main advantage of FTB over other granular backfills are FTB doesn't need proper compaction and long-distance haulage which are major tasks in the case of granular materials or stone screening. Over the last couple of years, many commercial products like Thermocrete, Powercrete, Cable-cem are available in the market. These products are expensive though these materials have good thermal performance and stability.

Due to the diffusion of water vapour and the decrease of the capillary suction tension, the excavated soils, as well as sands, tend to dry out partially when critical temperatures are exceeded. This kind of material shows a strong decrease in thermal conductivity when drying out. The effect of moisture migration of some backfill materials on thermal conductivity is shown in Figure 2.13. In Figure 2.13, all the materials have lower thermal conductivity than FTB over the entire range of moisture content. FTB is good backfill material due to high thermal conductivity in both dry and moist states. However, it is not economically feasible and might have a future maintenance problem. Quality control is also needed during mixing and installation to ensure thermal performance.

In order to enable higher current ratings of power cable by avoiding a partial drying out of the cable trench, a wax treatment has been developed to maintain the high thermal conductivity (Mitchell et al., 1981). Waxes were found to be more effective than other additives.

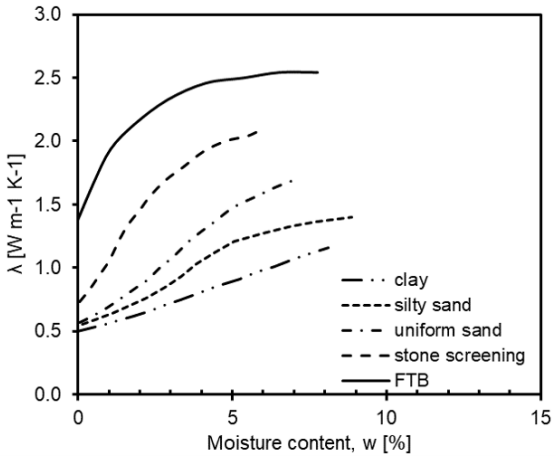

FIGURE 2.13: Effect of moisture on thermal conductivity of backfill materials, after Sandiford (1981)(FTB: Fluidized thermal backfill).

A variety of backfill treatments such as hot-mixed slack wax, cold-mixed emulsified slack wax, and a granulated refined wax was used with crushed limestone screening and silty clay soil.

In this study, without adding cement and applying wax treatment, the thermal conductivity of the granular materials like sand has been improved by just modifying the gradation and adding fine materials. As said earlier, a particular focus is given on dry state as dry sand has a thermal conductivity of about one-tenth that of moist sand. The design of materials is explained in detail in chapter 3. The factors considering to enhance the thermal conductivity of the soils are described next.

2.8 Factors consideration enhancing thermal conductivity

As explained in earlier section 2.4, the thermal conductivity is affected by various factors, which are very crucial parameters to enhance the thermal conductivity of the geo-materials. The factors which can enhance the thermal conductivity are particle shape and size, distribution, mineralogy, packing density or porosity, moisture content or saturation, cementing agent and applied pressure (Yun and Santamarina, 2007; Nasirian et al., 2015). Researchers have found that the bigger particles, as well as gradation, can increase the thermal conduction due to good contacts between the particles (Adams and Baljet, 1968; Yun and Santamarina, 2007; Nasirian et al., 2015). For example, sand has a bigger size than clay or silty soil, which leads to better heat conduction through the grains to grains and at contact points. The inclusion of larger particles is also effective to improve conduction as conductive heat flow is proportional to the particle radius and inversely proportional to the inter-contact distance. Another factor with relationship to granular materials is their physical shape, whether the material is composed of generally well-rounded particles or generally angular particles or particles which fall more in the angular range rather than the well-rounded range. In well-rounded particles, particles have no or few rough edges and being generally round and smooth in shape while the shape of angular particles is predominantly not rounded and in

fact the particles contain many sharp points or projections at their surface. It has generally been found that granular materials like sand with predominantly angular shaped particles are preferred rather than sand with well-rounded particles since a greater interparticle contact area may be provided with angular particles as compared with rounded particles. Such a greater interparticle contact area allows for greater interparticle thermal heat conduction. Well graded limestone screening, a by-product from rock quarries, was particularly found to have better thermal conductivity than other materials like well-graded sand, uniform sand (Adams and Baljet, 1968). So, the gradation of soil is another important aspect for enhancing thermal conductivity. With a wide size range and a continuous grading of particle sizes, a lower porosity or a denser mix can be obtained. This kind of mix can be determined from the Fuller gradation curves developed by Fuller and Thomson (1907), which is explained in detail in Chapter 3. It results an increase in dry density and the number of contact points per unit volume. This gradation is very popular in producing dense materials in concrete technology. That's why these factors particle shape and size and gradation are interrelated to another factor porosity or dry density, which is the most important factor to be considered. Reducing porosity increase the thermal conductivity of the soils because the heat transfer process was facilitated by an increase in the number of inter-particle physical contact points as porosity reduced. Apart from fuller curve gradation, another is mixing coarse and fine-grained soils in appropriate proportion. Minimum porosity is attained for the mass fraction of fine particles (FR_{mass}= 30-40%) and larger size ratio $FR_d = D_{large}/D_{small}$ (Guyon et al., 1987; Santamarina et al., 2001). Adams and Baljet (1968) found that the well-graded granular soils with fine particles of 8-10 % have higher thermal conductivity than other normal soils. These factors are more sensible in the case of dry soils as the thermal conductivity of air is relatively very small than that of solid soils.

In the case of granular materials as backfill, proper compaction plays a major role to ensure good thermal performance. In order to achieve desired maximum dry density and optimum moisture content, compaction of backfill should be done in a proper way. Another factor is using bonding agents like cement, bentonite, fly ash, etc. A sand or stone screening with a small amount of cement also improve the thermal conductivity of these materials since the solid to solid contact area is increased due to cementing agent. FTB and liquid soil are examples of cemented stabilized sand. As said earlier, a small fraction of clay particles in the sand also improves the thermal conductivity of sand. As an example, the sand at a dry density of about 2 $\mathrm{g\,cm^{-3}}$ without binder has a thermal conductivity of 0.91 $\mathrm{W\,m^{-1}\,K^{-1}}$ while it is 2 $\mathrm{W\,m^{-1}\,K^{-1}}$ with 8% kaolin as a binder for the same moisture content less than about 4% (Farouki, 1981).

The rock-forming minerals with higher solid thermal conductivity are another factor to be considered (Yun and Santamarina, 2007; Nasirian et al., 2015). The quartz mineral has the highest thermal conductivity than other rock-forming minerals. Using geomaterials with high quartz content is another good way to enhance thermal conduction. Sand usually posses high quartz contain than other soils. Therefore, sand or stone screening has been commonly used as backfill materials for embedded high voltage power cables. The details of thermal conductivity of rock-forming minerals are given in Horai and Simmons (1969).

TABLE 2.1: Thermal conductivity of some rock-forming minerals (Côté and Konrad, 2005b).

Mineral	λ **(W m^{-1} K^{-1})**
Quartz	7.69
Dolomite	5.51
Chlorite	5.15
Olivine	4.57
Pyroxene	4.52
Calcite	3.59
Amphibole	3.46
Feldspar	2.25
Mica	2.03
Plagioclase	1.84
Plagioclase (labradorite)	1.53

Some of the important minerals' thermal conductivity are presented in Table 2.1, where quartz has the highest thermal conductivity than other minerals.

The inclusion of water also improves the thermal conductivity of the soil, which is already explained in section 2.4. The critical moisture content is important since the thermal conductivity is reduced abruptly at the water content below this point. Another factor to be considered is avoiding organic matter in the backfill materials since the thermal conductivity of organic matter is relatively very low than that of soil and the presence of organic matter further reduces the effective thermal conductivity of soil.

2.9 Summary

The chapter reviewed the fundamental of heat transfer in soils and buried pipes, thermal properties of soils and factors affecting thermal conductivity. A further discussion on measurement and calculation (or prediction)of thermal conductivity was also presented. Furthermore, factors that need to be considered to improve the thermal conductivity of the soil and materials currently using as backfill materials were discussed.

Chapter 3

State and structure of Artificial Neural Network

3.1 Introduction

This chapter deals with background, literature review, structure and provides insight of artificial neural network. It reviews ANN application to engineering as well as other fields and the importance of ANN. It also provides basic knowledge about ANN architecture, methodology and finally its advantages and limitations.

3.2 Background

As discussed earlier in chapter 2.6, predicting the thermal conductivity of soil and geomaterials is a very difficult and challenging task due to the dependence of thermal conductivity on several factors. In the literature, various analytical, empirical and numerical models have been developed for the estimation of thermal conductivity of the soils. However, most of the available methods discussed in chapter 2.6 simplify the problem by including several assumptions associated with the aforementioned factors that affect the thermal conductivity of soils. Consequently, most of the existing methods fail to consider inherent characteristics of particle behaviour contacts, microstructure, etc. In addition, the numerical models require either the finite element (FE) or discrete element simulations to estimate the thermal conductivity and these simulations are computationally intensive and time-consuming. An alternative simple method that has shown to have some degree of success and is based on the data alone to determine the structure and parameters of the model is needed. The method is known as artificial neural network (ANN), which model complex and non-linear problems where the relationship between the model variables is not known (Hunick 1992). ANN models may be used as an alternative method in engineering analysis and predictions. The main advantage of this method is that it is a powerful tool to solve non-linear multidimensional problems. Another advantage is their ability to handle large and complex systems with many interrelated parameters. They can simply ignore excess data that are of less significance and concentrate instead on the more important inputs. It is comparatively fast and accurate than other available methods.

Over the last few years, artificial neural networks (ANNs) have been applied successfully in various fields of mathematics, engineering, medicine, science, economics, meteorology and many others. It was first introduced by Warren McCulloch and Mathematician Walter Pitts in 1943 by developing simple neural networks using electrical circuits. However, research into the application of ANN to real-world problems has significantly increased since the introduction of the back-propagation (BP) training algorithm for feed-forward (FF) artificial neural network by Rumelhart et al. (1986). Therefore, it is considered a relatively new tool in various fields. Since 1990's, ANNs have been extensively used to solve a wide variety of real-world problems. Not only in the field of engineering and science but it has been also used to solve problems in the economics and business sector. Predicting stock market price (Yoon et al., 1990), classifying discriminant analysis and logistic regression (Fisha et al., 1995), determining the employment status of workers for tax purposes (Denton et al., 1995), estimating production costs in the automotive industry (Cavalieria et al., 2003) are some of the examples of ANN application in the economics and business sector. Not all the contributions of ANN in the various field can be discussed here, however, some significant contributions in the field of engineering are discussed next.

In the case of the field of engineering and science, ANNs have been extensively used to solve many complex engineering problems. This area can be divided into geotechnical engineering, structural engineering, water resources and coastal engineering. In particular, ANNs have been successfully applied to many geotechnical engineering problems like settlement of foundations, pile capacity prediction, slope stability, design of tunnels and underground openings, liquefaction, soil permeability, hydraulic conductivity, soil properties and behaviour, site characteristics, and earth retaining structure. Goh (1995) investigated the feasibility of ANNs to model the complex relationship between the seismic and soil parameters, and the liquefaction potential. He used a simple back propagation neural network algorithm with more input variables and found that the neural network model was more reliable than conventional dynamic stress method. ANN model was developed for the prediction of horizontal ground displacement induced by liquefaction (Wang and Rahman, 1999). They used a large database containing the case histories of lateral spreads observed in eight major earthquakes to develop the ANN model. It was found that the ANN model had a more significant improvement in the estimation of horizontal ground displacement than the traditional multiple linear regression model. Later in 2002, they established an ANN model for the assessment of earthquake-induced liquefaction potential training case-history data (Rahman and Wang, 2002). The results showed that the ANN models are found to be reasonably good prediction model when compared to predicted data with the actual field observation data. Baziar and Nilipour (2003) proposed an ANN model to evaluate the liquefaction potential based on Cone Penetration Test (CPT) data and concluded that the model can find the relation between basic parameters of a multi-factor problem. However, they also recommended that the collection of more CPT data is required to impvrove the proposed ANN model in both generalization and applicability. A computational neural network was developed to predict the permeability of clay liners from known sets of soil properties (Najjar and Basheer, 1996). They highlighted the advantages of computational

neural networks over the regression models. ANN model was successfully proposed to predict the factor of safety of a slope from various slope parameters namely slope angle, pore-water pressure, cohesion, internal friction angle and water content (Jason and Wilson, 2018). They evaluated that the most significant parameters modifying the factor of safety are pore-water pressure and water content from the ANN models results. They found that ANN models were relatively accurate and could be utilized in the development of early warning systems.

Kim et al. (2001) established ANN model for the prediction of ground surface settlements due to tunnelling and found that the capability of making accurate predictions depends entirely on the quality and quantity of data used in training the model. Shahin et al. (2002b) developed an ANN model for the prediction of the settlement of shallow foundations on cohesionless soils. They evaluated the effect of neural network geometry and some internal parameters on the performance of ANN models and the relative importance of the factors influencing settlement by performing a sensitivity analysis. They also compared the performance of the ANN model with some of the most commonly used traditional methods and found that ANN had significant advantages over traditional one that make them a powerful and practical tool for settlement prediction of shallow foundations. Nejad et al. (2009) developed an ANN model to predict the pile settlement based on Standard Penetration Test (SPT) data and compared it with those given by several traditional methods. It is found that the ANN model outperforms the traditional methods and provides accurate pile settlement predictions.

Attoh-Okine (1999) investigated the effect of learning rate and momentum term on back-propagation neural network algorithm, which is developed for the prediction of flexible pavement performance. He used real pavement condition and traffic data and specific architecture. The results indicated that the learning rate of around 0.2 to 0.5 and momentum term of around 0.4 to 0.5 provide better pavement performance prediction as an extremely low learning rate around 0.001 and relatively high momentum term between 0.5 and 0.9 don't provide an satisfactory results for a three-layered network.

In structural engineering, the ANN model has been successfully used for the prediction of structural behaviour of sub-girder system, concrete strength, ultimate shear strength of reinforced concrete (Lee et al., 2001; Lee, 2003; Mansour et al., 2004). Lee et al. (2001) concluded that the ANN model can be successfully used to solve many empirical and uncertainty problems including approximation structural analysis that needs both an acceptable margin of error and fast calculation. Lee (2003) developed ANN model for the prediction of concrete strength that provides in-situ concrete strength. For this, he used multiple ANN architecture and found that the prediction results are well agreed with 90 cases of actual results from cylinderical concrete strength test. Another application of ANN is to successfully predict the ultimate shear strength of reinforced concrete beams with transverse reinforcement within the range of input parameters being investigated (Mansour et al., 2004).

Simulation of an industrial wastewater treatment plant (Gontarski et al., 2000), and prediction of water quality parameters (Holger and Graeme, 1996) are examples of ANN application to the area of water resources engineering. Holger and Graeme (1996) reviewed the

difference between traditional forecast methods, like time series and physically based models and ANN models. They applied the ANN model for forecasting salinity in the River Murray at Murray Bridge, South Australia and concluded that the ANN model was a more useful tool for forecasting salinity in the river despite having difficulty in determining the appropriate model inputs. Later, they improved the model by investigating the relative performance of various training algorithms using feed-forward network model for forecasting salinity (Holger and Graeme, 1999). Zhang and Stephen (1999) found that the ANN model, which forecasts the raw-water quality parameter for the North Saskatchewan River in Canada, is a fast and flexible way to include multiple input and output parameters into one model. Benning et al. (2001) used the ANN model and a conventional numerical method to investigate initial studies for modelling flow fields and concluded that ANN had advantages in fluid fields, such as shortening the computation time. ANN models have been also successfully applied in forecasting tidal level in the ocean using short-term tidal data (Lee and Jeng, 2002; Lee et al., 2002).

Chauhan et al. (2016b) applied seven different machine learning algorithms including ANN to study phase segmentation and analysis of Tomographic Rock Images. It was a classification problem and the problem was solved by using Levenberg-Marquardt backpropagation method and the network was the feed-forward network (FFN). The research showed that the porosity values obtained from seven machine learning techniques are in good agreement with the experimental results. For the ANN, the accuracy was up to 97%. While investigating the performance and accuracy of different machine learning algorithms, the classification performed by ANN was good despite of low accuracy i.e. high MSE error (Chauhan et al., 2016a).

ANNs are also applied for predicting the thermal resistivity of soils from different soil parameters (Erzin et al., 2010; Bian et al., 2015; ApalooBara et al., 2019). Two ANN models namely Multilayer Perceptron (MLP) and Radial Basis Function (RBF) networks were developed to predict soil electrical resistivity from meteorological data (ApalooBara et al., 2019). They found that MLP has the best result compared to the RBF. ANN model was successfully proposed to predict the electrical resistivity of fine-grained soils from three basic soil parameters like water content, porosity and degree of saturation, which were obtained by different laboratory tests (Bian et al., 2015). Erzin et al. (2010) employed ANN models for estimating the soil electrical resistivity based on its soil thermal resistivity and the degree of saturation. It was found that ANN models yield better results as compared to the generalized relationships proposed by the earlier researches.

Regarding the prediction of the thermal conductivity of the soils using ANN, comparatively a very few studies have been done to date (Erzin et al., 2008; Singh et al., 2011; Grabarczyk and Furmanski, 2013; Mishra et al., 2017; Zhang et al., 2020a). In the literature, ANN has been used for predicting the thermal conductivity of heterogeneous materials such as food, textiles and rocks (Fayala et al., 2008; Sablani et al., 2002; Singh et al., 2007; Scott et al., 2007; Sablani and Rahman, 2003). Fayala et al. (2008) developed an ANN model to predict the thermal conductivity of a knitting structure from the input parameters such as porosity, air permeability, yarn conductivity and weight per unit area. ANN modelling has been

successfully applied to the prediction of the thermal conductivity of pistachio (Chayjan et al., 2007), fruits and vegetables (Hussain and Rahman, 1999) and bakery products (Sablani et al., 2002). The thermal conductivity of sedimentary rocks from a set of geophysical Well logs was also predicted using ANN. Grabarczyk and Furmanski (2013) successfully applied ANN modelling to predict the effective thermal conductivity of dry granular media as a function of the ratio of thermal conductivity of solid grains (discontinuous phase) to fluids (either liquid or gas), porosity and coordination number. Based on the ANN approach, the unified thermal conductivity model was developed to determine the relationship between the thermal conductivity of soils and its influence factors including dry density, porosity, saturation degree, quartz content, sand content and clay content (Zhang et al., 2020a). Their ANN models considered the effects of various influence factors on the thermal conductivity of soils in a quantitative and systematic way. Erzin et al. (2008) reported that the thermal resistivity of different types of soils obtained from ANN models was found to be superior while comparing with those computed from the empirical thermal conductivity models. The ANN models were developed based on influencing factors such as types of soils, particle size distribution, dry density and moisture content. Singh et al. (2011) developed ANN models with different combinations of training functions and activation functions based on the volume fraction of filler and the ratio of thermal conductivity of the constituents as input parameters and found that the effective thermal conductivity of moist porous materials predicted by ANN models had very good agreement with the available experimental data.

3.3 Architecture of ANN

An artificial neural network is a form of artificial intelligence (AI), which attempts to simulate the biological structure of the human brain and nervous system. The biological neural network is the mechanism through which the human's nervous system functions, leading complex tasks to be performed instinctively. The central processing unit of the nervous system is called a 'neuron' or 'cell'. The human brain consists of billions of interconnected neurons which transmit information from one to neighbouring neurons. The neurons themselves have no storage capability. These neurons are connected to each other by 'Synapses'. The human brain has around a trillion of Synapses. These connections control the human body and its abilities like identification, thinking, and applying previous experiences to every action. Figure 3.1 shows the relationship of a single neuron of the brain to its four basic elements, known by their biological names: dendrites (Input), soma (Process), axon (Turn input into output) and Synapses (Contact each neuron). The axon is the output path of a neuron that branches out through axon collateral which in turn connect to the dendrites or input paths of neurons through a junction or a gap known as the synapse. In short, ANN attempts to simulate the learning process of the human brain. They operate like a 'black box' model that requires no detailed information about the system. Instead, ANN models learn the relationship between the input parameters and the controlled and uncontrolled variables by studying old data. A biological neuron is so complex that even current supercomputers cannot model a single neuron. Therefore, researchers have simplified neuron

models in designing ANNs. The single neuron of the brain with its elements can be compared with a schematic diagram of single layer feed-forward neural network architecture as shown in Figure 3.2. The basic unit of ANN is simulated from the biological model but is much simpler.

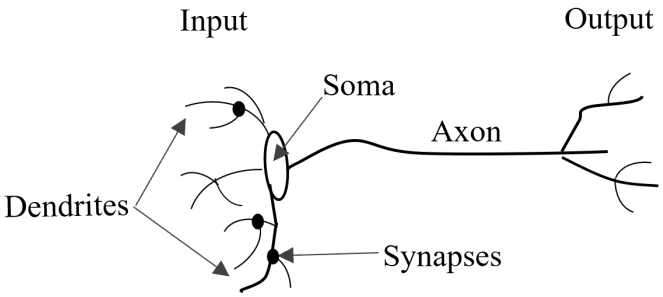

FIGURE 3.1: Structure of single neuron in brain.

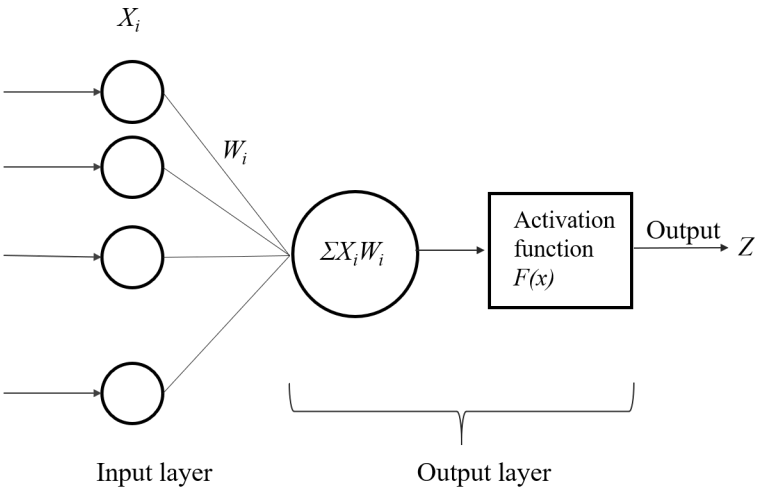

FIGURE 3.2: Structure of single layer feed- forward ANN model.

Similarly, ANN is a computing system made up of highly interconnected processing elements (PEs) which process the information through their dynamic state response to external inputs. These elements are known as 'neurons' or 'nodes' which are usually arranged in layers. ANN consists of basically single or multi-layers neural networks: input and output layers for single layer; input, hidden and output layers for multi-layers. The typical structure of single layer feed-forward network is shown in Figure 3.2, where X_i represents input parameters, and Z is output in the output layer. The purpose of each layer is

- input layer: receives information from an external source, and passes this information to the successive layers (networks) for processing.
- hidden layer(s): are the layers between input and output layers, which are not accessible from the outside of the neural network. It receives information from the input layer and processes the information within the network. Depending on the problem being investigated, the number of hidden layers will be defined.

- output layer: receives processed information from the previous (hidden) layers and transmits the results as output.

A connection medium that connects each neuron in a given layer to all the neurons in the next layer is known as weight (W). This connection can deliver the calculation results to the next layer completely. The input parameters (X) will be processed in neurons to get the outputs (Y) by using the following equation:

$$Y_i = F_i \left(\sum W_i X_i + b_i \right) \tag{3.1}$$

where, W is the weight connecting neurons, b is bias (or threshold value) of neurons, and F is the activation function (or transfer function) of neuron. There are various types of activation functions, such as linear function, threshold (step) function, and sigmoid functions (Haykin, 1999). These activation functions are explained in the next section 3.3.1. The number of neurons in input layer and output layer is decided by several input variables and output, whereas the number of neurons in hidden layers and the number of hidden layers depend on the complexity of the problems and is decided based on trial and error. In Equation 3.1, the inputs are multiplied by their specified connection weight and the product is added to bias and then the activation function is used to generate output. This equation indicates that the information with a greater weight has a greater effect. Finally, the values from the output layer will be compared with known values. When the error (the difference between the output and the known values) is larger than the tolerance level, the weight factors are adjusted through the repeated training until the error is within an acceptable range. In this way, the network learns from input data and use these data to adjust weight in order to capture the relationship between the model input and corresponding outputs. This process is known as the learning rule, which is explained in section 3.4.5. Consequently, ANNs don't require any prior special knowledge about the nature of the relationship between input and output variables, which is one of the advantages of ANN over empirical and analytical methods. ANNs also perform their tasks simultaneously which makes them very fast.

3.3.1 Transfer function

A transfer function, also known as the activation function, convert a summation of the weighted inputs of the neuron to output. It is required in every node of the network and determines the behaviour of the node. The output is set at one of two levels, depending on whether the input is greater or less than some threshold value. Without transfer function, the whole neural network could be linear function and couldn't learn non-linear relationships. The transfer functions at neurons in the hidden layers are often non-linear and provide the non-linearities for the network. It maps any real numbers into a domain normally bounded by 0 to 1 or -1 to 1. There are a variety of these functions. The most commonly used functions are the linear function, the threshold function, the log-sigmoid function and the tanh-sigmoid function. The selection of the transfer function depends on the application. In this study, the tanh-sigmoid and linear function have been used.

The linear transfer function (Figure 3.3) is a simple function that will not alter the output in the network. Hidden layers become ineffective when they have an activation function as linear activation function. It is normally used in the input and output layer. The output range of this function lies between -∞ to ∞ and the equation is given by

$$f(x) = x \tag{3.2}$$

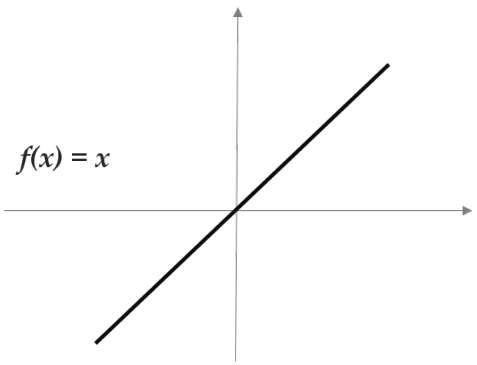

FIGURE 3.3: Linear activation function, range (-∞,∞).

The threshold transfer function computes only 1 and 0 as shown in Figure 3.4. It reflects a sort of "all-or-nothing" ability with a neural network. This activation function was used by a perceptron model, the early ANN model. The function is given by

$$f(x) = \begin{cases} 1, & \text{if} \quad x \geq 0 \\ 0, & \text{if} \quad x < 0 \end{cases} \tag{3.3}$$

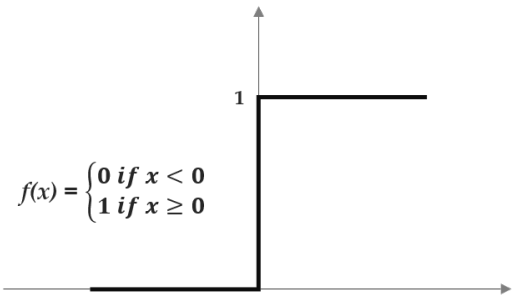

FIGURE 3.4: Threshold activation function, range (0,1).

Sigmoid functions are the most common transfer functions used in ANN models. The sigmoid functions are continuous, real-valued functions whose domains are the reals, whose derivates are always positive and whose range is bounded (Masters, 1993). The shape of the function has little effect on a network although it can have a significant impact on the speed of training (Masters, 1993). These functions can never reach their theoretical limit values and the values that are close to the limits should be considered as reaching those

values. For example, the log-sigmoid function has a limiting value of 0 to 1, a neuron should be considered to be fully activated at values around 0.9 and 0.1. Logistic and hyperbolic tangent(tanh) are examples of sigmoid functions.

Log-sigmoid transfer function converts the sum of weighted input into the output in the range of 0 to 1. It makes a very soft transition as shown in Figure 3.5. It will be given by the following equation.

$$f(x) = \frac{1}{1 + e^{-x}} \tag{3.4}$$

It remains the most commonly applied in ANN models due to ease in computing its derivative: f'(x) = f(x)(1-f(x)).

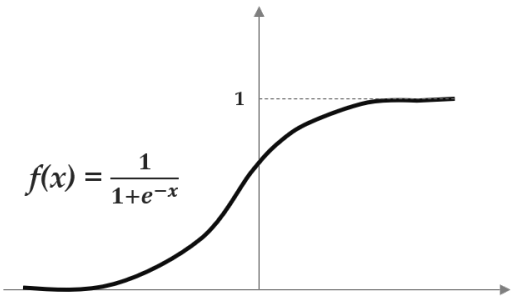

FIGURE 3.5: Log-sigmoid activation function, range (0,1).

Tanh (tangent hyperbolic)-sigmoid transfer function can give a negative output (Figure 3.6). The output of the function lies in the range of (-1,1). The function represents as follows:

$$f(x) = \frac{e^{x} - e^{-x}}{e^{x} + e^{-x}} \tag{3.5}$$

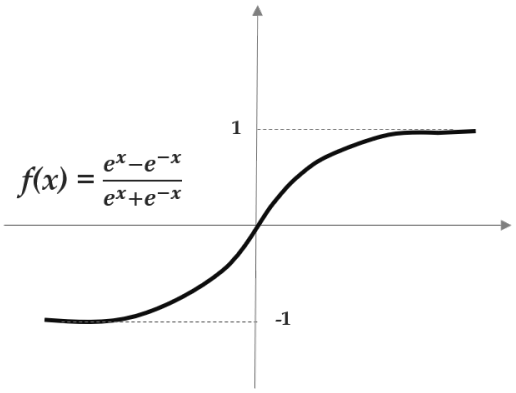

FIGURE 3.6: tanh-sigmoid activation function, range (-1,1).

3.3.2 Types of network

There are generally three fundamentally different classes of networks based on the structure of network: single layer feed-forward, multi-layer feed-forward and recurrent neural network (Haykin, 1999) .

- **Single layer feed-forward network:** The network is called feed-forward because the information is processed from input to output. A single layer feed-forward network (SLFFN) has a single layer of artificial neurons (input layer) and it processes to output layer in the forward direction (Figure 3.7). The main disadvantage of SLFFN is the disability of solving non-linear functions or problems. The complexity of a single layer network is not big enough to solve greater categorization problems. In order to solve these problems, more layers have to be created in the network. This network is commonly referred as a multi-layer feed-forward network.

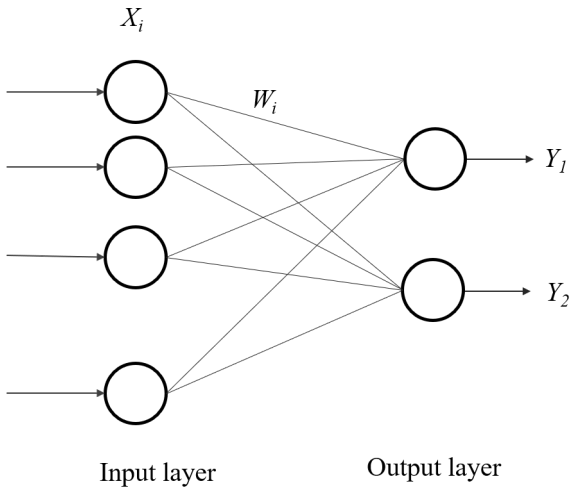

FIGURE 3.7: A typical single-layer feedforward ANN architecture.

- **Multi-layer feed-forward network:** When hidden layers are added to a single layer neural network, it becomes multi-layer feed-forward network (MLFFN). Therefore, it consists of an input layer, hidden layer(s) and output layer. Figure 3.8 shows the typical MLFFN, where Y_i and Y_j are the neurons in hidden layers. This kind of network is mostly used to solve much more difficult and complex problems. The hidden layers allow the network to extract features from the input. The neural network with a single hidden layer is known as a shallow neural network or vanilla neural network, whereas with more than a single layer is known as a deep neural network. This classification came from the historical background of development. The neural network started as a single-layer neural network and evolved to the shallow neural network, later followed by the deep neural network. In the layered network, the information enters the input layer, transmits through the hidden layers, and leaves through the output layer. During the process, the information advances layer by layer. The nodes or neurons on one layer receive the information simultaneously and send the processed information to the next layer at the same time. The number of neurons in input and output layers is decided according to the number of input variables and outputs, respectively. However, the optimum number of the hidden layers and neurons in hidden layers has to be chosen on a trial and error basis because of no standard rules or theories in determining the number of neurons, but sometimes depends on the complexity of the problems. There are some thumb rules which select the number of neurons in the

hidden layers suggested by various ANN researchers which will be elaborated in next section 3.4.3.

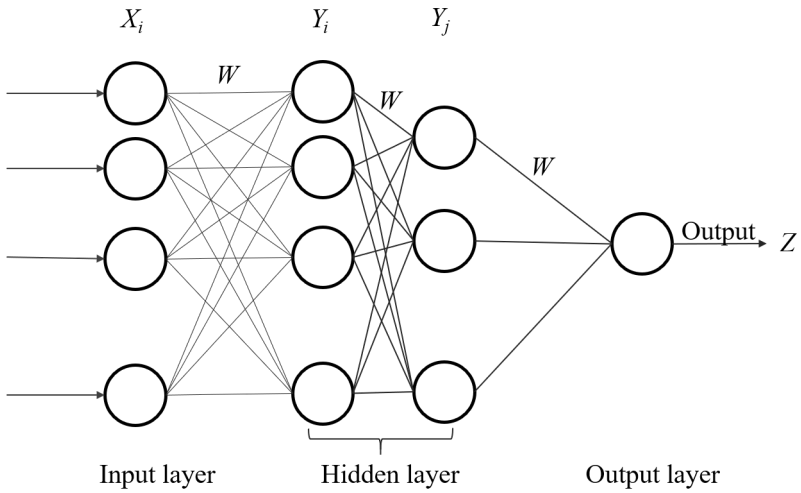

FIGURE 3.8: A typical multi-layer feedforward ANN architecture.

- **Recurrent neural network:** It is similar to the feed-forward neural network, the only difference is that it has at least one feedback loop as shown in Figure 3.9. This feedback connection propagates the outputs of nodes or the network back to the inputs layers or nodes to carry out repeated computations. An input presented in the recurrent network at time 't' will affect the output of the network for future time steps greater than t. Therefore, the RNN has to be operated over time.

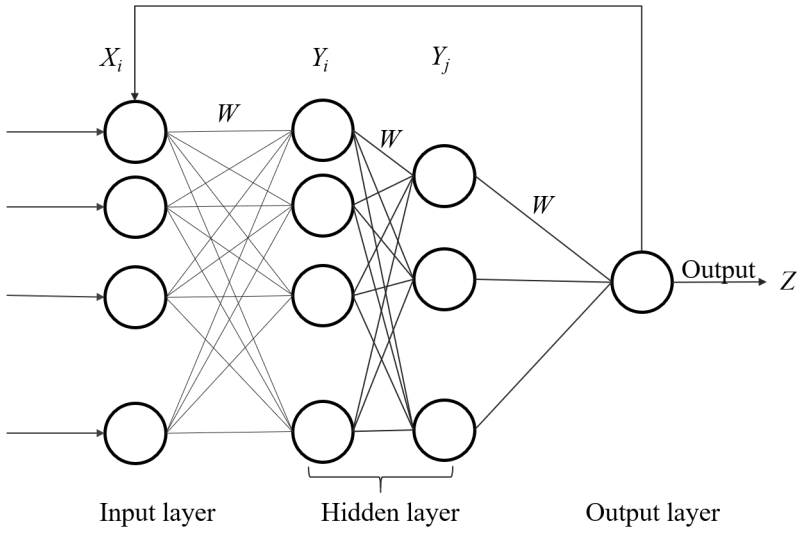

FIGURE 3.9: A typical Recurrent network architecture.

3.4 Training of the ANN model

An ANN has to be configured in a way that the application of a set of inputs produces desired set of outputs. The propagation of information starts from the input layer where the

input parameters are presented. The network adjusts its weight on the basis of the training data set and uses a learning rule to find a set of weights that produce input/output results that has the possible lowest error. This process is called learning or training, which attempts to capture the relationship between the model input variables and the corresponding outputs. The output will be processed using Equation 3.1. The philosophy of ANN modelling is quite similar to conventional statistical models in the way that both try to capture the relationship between the historical set of model inputs and corresponding outputs (Shahin et al., 2001). It is very easy to understand from this example given by Shahin et al. (2001).

Let's assume a set of input variables, x and corresponding output values, y in 2D space, where y = f(x) where 'f' is an unknown function that is needed to find. In a linear regression model, the function 'f' will be obtained by adjusting the slope (m) and intercept (c) of the straight line equation (y = mx + c) (Figure 3.10a) so that the error between the known outputs and outputs obtained from a straight line is minimized. The same principle is used in ANN models. ANNs can set a simple linear regression model by having one input, one output and no hidden layer nodes with a linear activation function such as a single layer network with x, y and w as input, output and weight, respectively (Figure 3.10b). The connection weight 'w' and threshold 'b' in the ANN model are equivalent to the slope (m) and intercept (c) of the linear regression model. ANN adjust the weight using input data in order to minimise an error between the known outputs and outputs predicted by the ANN model.

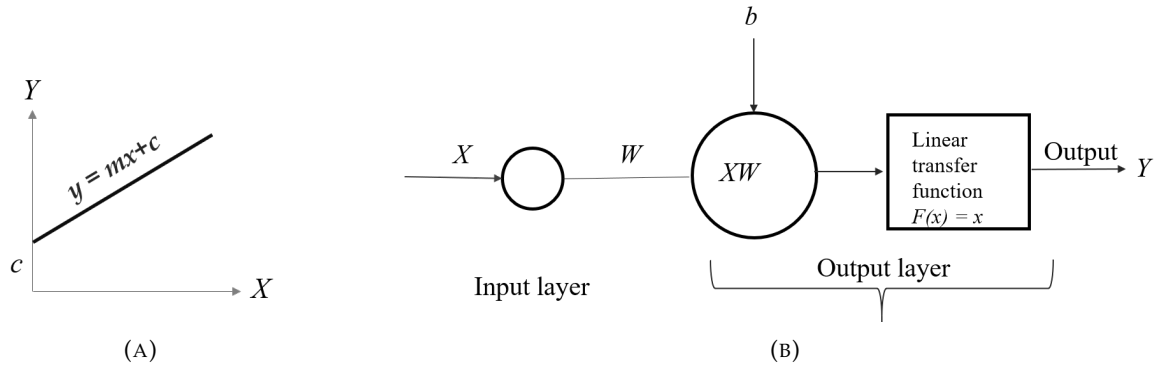

FIGURE 3.10: Linear regeression model (a) Vs. ANN models representing linear regression model (b).

If the relationship between x and y is non-linear, a regression analysis can only be successfully applied if prior knowledge of the nature of the non-linearity is known. In contrast, this prior knowledge of the nature of the non-linearity is not necessary for ANN models as the degree of non-linearity can be easily addressed by changing the transfer function and the number of hidden layer nodes. Thus the ANN models can be used to deal with complex and highly non-linear problems. In addition, ANN models can be upgraded from univariate to multivariate by extending the number of input nodes.

The performance of the trained model will be validated using independent testing set after accomplishing the training step of the model. Once the structure of ANN is designed, it is necessary to adjust the weights and bias values of its neuron. This adjustment process is

known as training and three kinds of training are available, supervised, unsupervised, and reinforcement training.

3.4.1 Types of Training

Supervised training

It is so far the most common type of training in ANNs. Both inputs and outputs are known in supervised training, where the actual output of ANN is compared to the desired output, therefore it attempts that desired solution is known for the training sets. This method also tries to minimise the current errors of all processing elements. Such a global error reduction is created over time by continuously adjusting the input weights until an acceptable network accuracy is reached. Most representative supervised training algorithms use the back-propagation algorithm, which has been used since it was first introduced by Rumelhart et al. (1986). Supervised training has been used in this study.

Unsupervised training

In contrast, the training data of unsupervised training contains only inputs and no correct output data set (i.e. the outputs are unknown). Indeed the underlying structures in the data or correlations between the patterns in the data are investigated and organised into categories. This method is especially useful and applicable when the solutions are not known. It is not as popular as supervised training and has not been used in this study and hence will not be considered further.

Reinforced training

It is a hybrid learning method in which no desired outputs are given to the network, but the network is set if the computed output is going in the correct direction or not. It is not used in this study and hence will not be considered further.

3.4.2 ANN Parameters

Learning rate

Learning functions mostly have some term for a learning rate, which is positive and lies between 0 and 1. It determines how much the weight is changed per time during training. If small values of the learning rate are selected, more time is needed in training an ANN but it tends to decrease the chance of overshooting the optimal solution and thus the results will be more stable. At the same time, they increase the likelihood of becoming stuck at local minima. The training takes less time with a faster learning rate, but the accuracy of the results will be not good. However, several other factors can play a role in determining how long it will take to train a network such as network complexity (size of the network), size of data, network architecture and type of learning rule. The adaptive learning rate varies according to the amount of error being created. The larger the error, the smaller the values

and vice-versa. Therefore, if the ANN is processing towards the optimal solution it will accelerate, while it will decelerate when it is heading away from the optimal solution.

Momentum

Momentum is one of the methods to adjust the weights. The benefits of using this kind of weight adjustment formula are to keep higher stability and faster speeds in the training process of the neural network. The momentum value determines how much of the previous corrective term should be remembered and carried on in the ongoing training. The larger the momentum value, the more emphasis is placed on the current correction term and the less on previous terms. It serves as a smoothing process that 'brakes' the learning process from heading in an undesirable direction.

Input noise

Random noise is used to perturb the error surface of the neural net to jolt it out of local minima. It also helps the ANN to generalize and avoid curve fitting.

Training and testing tolerances

The training tolerance is the amount of accuracy that the network is required to achieve during its learning stage on the training data set. The testing tolerance is the accuracy that will determine the predictive result of the ANN on the test data set.

3.4.3 Data Selection

ANN models have to be developed in a systematic way to improve the performance of the model. In order to achieve this, determination of adequate model inputs, data division and pre-processing, set up of network architecture, selection of ANN parameters that control the optimization method, stopping criteria and model validation are major steps.

The selection of data input variables is also an important step to develop the good ANN models. Normally, the input variables that have the most significant influence on the model output will be selected. However, a large number of input variables may increase the network size, resulting in a decrease in processing speed and a reduction in the efficiency of the network. Various techniques have been recommended in the literature to solve this condition. But, this is not the case in this study as there are no more variables and the selection of variables are selected based on prior knowledge. One approach available in the literature can be used to find which input variables have more influence on the model output. The method includes training of many neural networks with different combinations of input variables and selecting the network with the best performance (Goh, 1995; Najjar and Basheer, 1996). Another useful technique is to employ a genetic algorithm (GA) to find the best sets of input variables (NeuralWare, 1997).

Data division

While training the ANN model, the model might tend to memorization rather than generalization because the number of degrees of freedom of the model is large compared with the number of data points used for training (Shahin et al., 2002b). Consequently, a separated validation set is required to ensure that the model can generalize within the range of the training data. That's why it is common practice to divide the available data into groups namely training and validation sets (Twomey and Smith, 1997; Maier and Dandy, 2000) . The training set is used to build a neural network model while an independent validation set to assess the model performance in the deployed environment. However, dividing the data into only two subsets may lead to model overfitting. Overfitting makes multi-layer neural networks begin to memorize training patterns rather than generalization to the new data (Banimahd et al., 2005). In order to overcome this problem, another method for the data division, a cross-validation technique (Stone, 1974) has been used for developing ANN models (Erzin et al., 2008; Zhang et al., 2020b; Shahin et al., 2002b). This is also one of the methods of stopping criterion to decide when to stop the training process (Shahin et al., 2002b). It is the most valuable tool to ensure overfitting does not occur.

In the cross-validation technique, the training data are divided into three sets *viz.* Training set, Testing set and Validation set. The training data is utilized to adjust the weights of networks to reduce error (MSE) and the updating process is monitored by the error of validation data (Figure 3.11). The training will not stop until the error of validation data in the validation set begins to increase, at which point the model generalization is considered to reach its best stage. Finally, the performance of developed networks is evaluated by feeding the testing data into it. The overall process is shown in Figure 3.12. Therefore, the cross-validation technique is used for developing ANN models in this study.

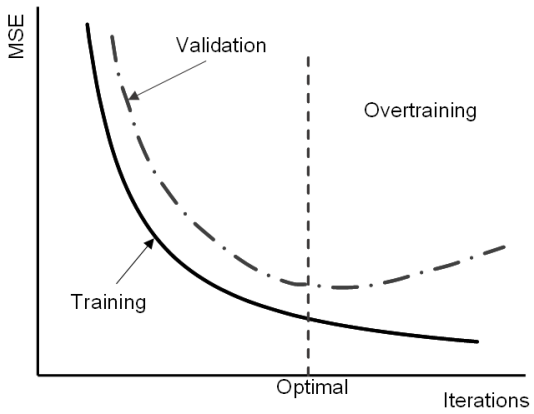

FIGURE 3.11: Behaviour of MSE with overtraining in Crossvalidation technique.

There is no proper way to find the proportion of data to be used for training, testing and validation. Shahin et al. (2004) investigated the impact of the proportion of data to find the optimal proportion of the data used for training, testing and validation and found no clear relationship between the proportion of data and model performance. They recommended

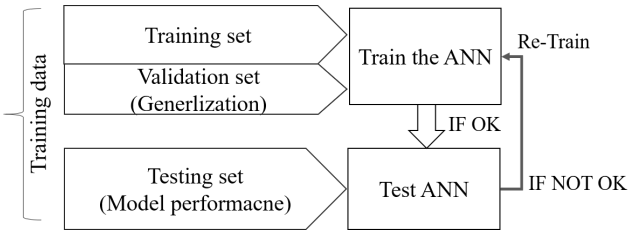

FIGURE 3.12: Cross validation technique process.

using 20% of data as a validation set and the remaining data were divided into 70% for training and 30% for testing which gave the best result. Some of the researchers also used 70:15:15 as training, testing and validation set. This method is acceptable when you have enough data to distribute into three subsets. In many situations, the data available are small enough to distribute data into training, testing and validation. In order to overcome this situation, Masters (1993) proposed the 'leave-k-out' method which involves holding back a small fraction of the data for validation and using the remaining data for training. After training, the performance of the trained model has to be evaluated with a validation set. Then, a different small subset of data is held back and the network is trained and tested again. This process is repeated many times with different subsets until an optimal model can be achieved from the use of all available data.

In the majority of ANN applications in geotechnical engineering, the data are distributed into their subsets on an arbitrary basis. However, recent researches show that the way the data are distributed may have a significant influence on the results obtained (Tokar and Johnson, 1999). Since ANNs have difficulty extrapolating beyond the range of the data used for calibration, all of the patterns that are contained in the available data need to be included in the calibration set in order to develop the best ANN model. As an example, if the available data contain extreme data points that were excluded from the calibration data set, the model cannot be expected to perform well, as the validation data will test the model's extrapolation ability and not its interpolation ability. If all of the patterns that are contained in the available data are contained in the calibration set, the toughest evaluation of the generalization ability of the model is if all the patterns (and not just a subset) are contained in the validation data. In addition, if the cross-validation technique is used as the stopping criterion, the results obtained using the testing set have to be representative of those obtained using the training set, as the testing set is used to decide when to stop training i.e. which model architecture or learning rate is optimal. Consequently, the statistical properties (e.g. mean and standard deviation) of the various data subsets (e.g. training, testing and validation) need to be similar to ensure that each subset represents the same statistical population (Masters, 1993). If this is not the case, it may be difficult to judge the validity of ANN models (Maier and Dandy, 2000).

Many researchers have used the 'ad-hoc' method to ensure that the data used for calibration and validation have the same statistical properties (Braddock et al., 1998; Tokar and Johnson, 1999; Ray and Klindworth, 2000). Masters (1993) also strongly confirms the above strategy of data division. Masters (1993) used a genetic algorithm (GA) to minimize the

difference between the means and standard deviations of the data in the training, testing and validation sets. While this approach ensures that the statistical properties of the various data subsets are similar, there is still a need to choose which proportion of the data to use for training, testing and validation. In order to solve this, a self-organizing map (SOM) was used to cluster high dimensional input and output data in two-dimensional space and divided the available data so that values from each cluster are represented in the various data subsets (Kocjancic and Zupan, 2000; Bowden et al., 2002). This method ensures that data in the different subsets are representative of each other and has the additional advantage that there is no need to decide what percentage of the data to use for training, testing and validation. The major drawback of this method is that there are no guidelines for determining the optimum size and shape of the SOM, which can significantly impact the results obtained, as the underlying assumption of the approach is that the data points in one cluster provide the same information in high-dimensional space. However, if the SOM is too small, there may be significant intra-cluster variation. Conversely, if the map is too large, too many clusters may contain single data points, making it difficult to choose representative subsets. To overcome the problem of determining the optimum size of clusters associated with using SOMs, a data division approach that utilizes a 'fuzzy clustering' technique was proposed so that data division can be carried out in a systematic manner (Shahin et al., 2004).

Data pre-processing

Once the available data have been divided into their subsets (i.e. training, testing and validation), it is important to pre-process the data in a suitable form before they are applied to the ANN as data pre-processing is necessary to make sure all variables receive equal attention during the training process (Maier and Dandy, 2000). Moreover, data pre-processing usually, accelerate the learning process. Pre-processing can be in various forms such as data scaling, normalization and transformation (Masters, 1993). Scaling the output data is essential, as they have to be commensurate with the limits of the transfer functions used in the output layer (For example, output data between –1.0 to 1.0 for the tanh-sigmoid transfer function and 0.0 to 1.0 for the log-sigmoid transfer function). Scaling the input data is not necessary but it is almost always recommended. In some cases, the input data need to be normally distributed in order to obtain optimal results. Normalization is done to ensure that there is no effect of input units and get equal attention during the training process.

3.4.4 Determination of ANN architecture

Determining the network architecture is one of the most important and difficult tasks in ANN model development, which involves the selection of the optimum number of layers and the number of nodes in each of these. There is no unified approach or standard rule or theories for the determination of an optimal ANN architecture. It is generally achieved by fixing the number of layers and choosing the number of nodes in each layer on a trial and error basis. It has been shown that one hidden layer is sufficient to approximate any continuous function provided that sufficient connection weights are given. (HechtNielsen, 1989)

showed that a single hidden layer of neurons using a sigmoid activation function is sufficient to model any solution surface of practical interest. On the contrary, some researches noted that there are many solution surfaces that are extremely difficult to model using a sigmoidal network using one hidden layer and recommended that the use of more than one hidden layer provides the flexibility needed to model complex functions in many situations (Flood and Kartam, 1994; Chester, 1990). According to Chester (1990), the first hidden layer is used to extract the local features of the input patterns while the second hidden layer is useful to extract the global features of the training patterns. However, Masters (1993) stated that using more than one hidden layer often slows the training process dramatically and increases the chance of getting trapped in local minima.

The number of nodes in the input and output layers is decided by the number of model inputs and outputs, respectively. As said earlier, there is no direct and precise way of determining the best number of nodes in each hidden layer. A trial-and-error procedure, which is generally used in geotechnical engineering to determine the number of hidden layers and neurons in each hidden layer can be used. The neural networks with a large number of free parameters (connection weights) are more subject to overfitting and poor generalization (Masters, 1993). Consequently, keeping the number of hidden nodes to a minimum is always better which provides satisfactory performance because of following reasons:

- It reduces the computational time needed for training;
- It helps the network achieve better generalization performance;
- It helps avoid the problem of overfitting and
- It allows the trained network to be analyzed more easily.

For single hidden layer networks, there are a number of rules-of-thumb to obtain the best number of neurons in the hidden layer.

- First approach is to assume the number of hidden nodes to be 75 % of the number of input units (Salchenberger et al., 1992).
- Second approach suggests that the number of hidden nodes should be between the average and the sum of the nodes in the input and output layers (Berke and Hajela, 1991).
- A third approach is to fix an upper bound and work back from this bound. It was suggested that the upper limit of the number of hidden nodes may be taken as (2I+1) in a single hidden layer network, where I is the number of inputs (HechtNielsen, 1989; Azoff, 1994).
- The best approach was to start with a small number of nodes and to slightly increase the number until no significant improvement in model performance is achieved (Nawari et al., 1999).

For networks with two hidden layers, the network topology or architecture with the geometric pyramid shape can be used (Nawari et al., 1999; Shih, 1994). The notion behind this method is that the number of nodes in each layer follows a geometric progression of a pyramid shape, in which the number of nodes decreases from the input layer towards the output layer. It means the network should have the greatest number of neurons in the initial layers and fewer in the later layers. The number of neurons in each layer should be a number from mid-way between previous and succeeding layers to twice the number of the preceding layer. For example, a network with 12 neurons in its previous layer and 3 neurons in the succeeding layer should have 6 to 24 neurons in the intermediate layer.

Another way of determining the optimal number of hidden neurons is to relate the number of hidden nodes to the number of available training data. This method can result in good model generalization and avoid over-fitting. Researchers suggested a number of thumb rules to related the training data to the number of connection weights. For example, the required minimum ratio of the number of training data to a number of connection weights should be 2 and the minimum ratio of the optimum training data to the number of connection weights should be 4 (Masters, 1993). Other researchers recommended that this ratio should be 10 (Hush and Horne, 1993) and at least 30 to avoid overfitting (Amari et al., 1993). No specific ratios were found by either researcher. It could depend on the complexity of the problems.

There are some other approaches available in the literature to determine automatically the optimal configuration of network architecture. The adaptive method of architecture determination (Ghaboussi and Sidarta, 1998), Bayesian approaches (Kingston et al., 2008), Pruning (Karnin, 1993), adaptive spline modelling of observation data (ASMOD) (Kavli, 1993), Cascade-Correlation (Fahlman and Lebiere, 1990) are some available automatic methods for determining optimal network architecture.

However, most of the researchers argued that there is no way to determine a good network topology from just the number of inputs and outputs. Starting with a small number of hidden neurons and then increase gradually only if the ANNs don't seem to 'learn' is the best way to create the network. Previous studies also recommend one or two hidden layers are enough for solving most of the civil engineering problems (Habibagahi and Bamdad, 2003; Zhang et al., 2020b; Erzin et al., 2008; Erzin et al., 2010).

3.4.5 Learning algorithms (rules)

The process of determining the neural network model is called the learning rule. In another word, the systematic approach to modify or adjust the weights according to the given information is called the learning rule. The learning algorithm determines how the weights are adjusted normally depending on the size of the error in the network output to the desired output. The aim of the learning algorithm is to minimize this error to an acceptable value. Although a variety of learning algorithms (rules) are available in the literature, the two most important and useful learning rules have been discussed in this section viz. (1) Delta rule and Generalized delta rule, (2) Back-propagation (BP) algorithm. Both rules use supervised

training and work iteratively to update their weights. By far, the back-propagation algorithm is the most popular learning algorithm for multi-layer networks, while the delta rule is generally used for single-layer networks.

Before starting Delta rule and Back-propagation algorithm, let's briefly discuss Perceptron algorithm, invented by Frank Rossenbalt in 1958. It is supervised learning for binary classification applications. A single layer perceptron (SLP) can only be used to implement linearly separable functions. It consists of a single layer neural network with one output node. It is composed of nonlinear artificial neurons, which uses threshold transfer function. Because of the thresfold function, the output results as 0 or 1. Figure 3.13 shows the perceptron with one neuron and threshold activation function.

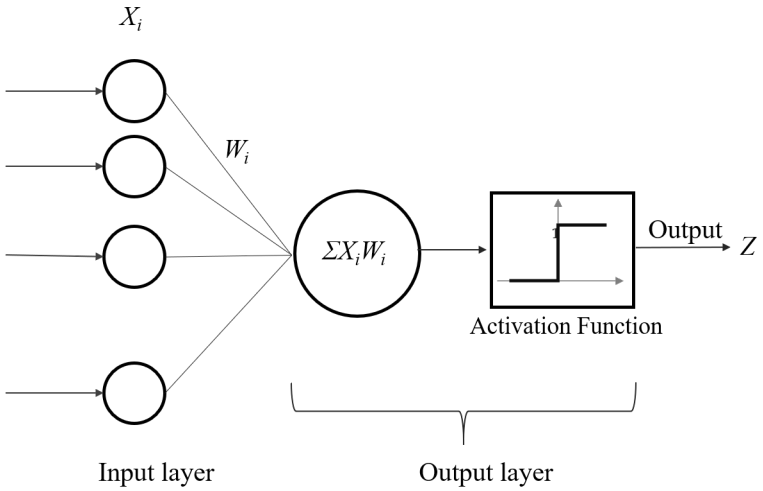

FIGURE 3.13: A Perceptron learning rule.

Steps to be followed in this rule:

1. Assign initially the weight with random values.
2. Calculate the output 'Y' using equation 3.1 and determine the error 'e_n' from the known output 'd_n' using the following equation.

$$e_n = d_n - Y_n \tag{3.6}$$

   where n is the iteration number.

3. Adjust the weight to reduce the error using equation 3.7 below, where α_l is the learning rate.

$$W_{n+1} = W_n + \alpha_l e_n X_n \tag{3.7}$$

4. Perform steps 2-3 for all training data.

3.4.6 Delta rule & Generalized delta rule

Delta rule is one of the most commonly used learning rule methods for the single-layer neural network. This rule updates the weights in a way that minimize the mean squared error of the network. So, the rule is also known as Least Mean Square (LMS) Learning rule. The delta rule is also called as Adaline rule as well as Widrow-Hoff rule as the LMS algorithm was first proposed by Widrow and Hoff in 1960 when they introduced the ADALINE (Adaptive Linear). It is superior to Rosenblatt's perceptron learning algorithm in terms of speed but it also could not be used on multi-layer networks. In this rule, the threshold activation function is replaced by a linear activation function. Kim (2017) explained training process of delta rule and generalized delta rule with Matlab examples in a simple way. The steps of the learning rules are briefly explained next to understand the learning process clearly.

Steps to be followed during the training process for the single-layer network (Figure 3.14) using delta rule:

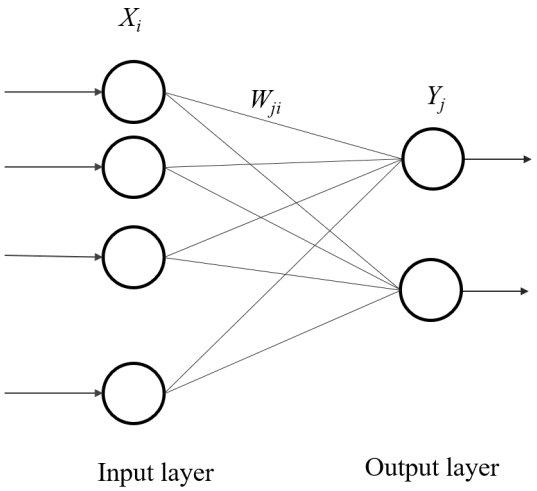

FIGURE 3.14: A single-layer network.

1. Assign initially the weights with random values.
2. Calculate the output using equation 3.1 and determine the error using the following equation, where d_j is known-output.

$$e_j = d_j - Y_j \tag{3.8}$$

3. Determine the weight updates using the equation below, where α_l is the learning rate ($0<\alpha_l \leq 1$).

$$\Delta W_{ji} = \alpha_l e_j X_i \tag{3.9}$$

4. Update and adjust the weights using the following equation,

$$W_{ji+1} = W_{ji} + \Delta W_{ji} \tag{3.10}$$

5. Repeat steps 2-4 for all training data.
6. Repeat steps 2-5, which is called epoch until the error reaches within an acceptable range.

This rule is also called gradient descent method. The modified version of the Delta rule is known as the generalized delta rule. This rule uses sigmoid function instead of linear function as an activation function. All the steps described in the delta rule are also applied in this rule except calculating the weight update (ΔW_{ji}). The weight update is calculated as follows:

$$\Delta W_{ji} = \alpha_l \delta_j X_i; \quad \delta_j = f'(v_j) e_j = f(v_j)\left(1 - f(v_j)\right) e_j; \quad v_j = \sum W_j X_j + b_j \tag{3.11}$$

If this rule uses linear activation function, f(x)=x, it becomes the delta rule as $\delta_j = e_j$ since f'(x) = 1. Using new weight update, Equation 3.10 becomes for the sigmoid function as:

$$W_{ji+1} = W_{ji} + \alpha_l f(v_j)\left(1 - f(v_j)\right) e_j X_i \tag{3.12}$$

This is the learning rule for the generalized delta rule.

3.4.7 Weight update method

There are three different methods to calculate the **weight update** (Kim, 2017). They are:

- **Stochastic Gradient Descent (SGD)**: In this method, the weight is adjusted 'n' times if the network has the same 'n' training data. All the previous delta rules are based on the SGD approach. Equation 3.11 is used to calculate the weight updates for corresponding training data.
- **Batch**: Each weight update is calculated for all errors of the training data and the average of weight updates is used for updating the weights using the equation 3.13. This method uses all of the training data and updates only one time. It spends a significant amount of time training the data.

  $$\Delta W_{ji} = \frac{1}{N} \sum_{k=1}^{N} \Delta W_{ji}(k) \tag{3.13}$$

  where $\Delta W_{ji}(k)$ is the weight update for k training data and N is the total number of the training data.
- **Mini Batch**: It is actually a combination of SGD and batch methods. The training data are distributed in the batch and weight is adjusted by using the average weight update of each batch. Finally, these weights are adjusted again for the number of batches since the batches are considered as training data in the SGD method. The benefit of this method is to get the speed from the SGD and stability from the batch. This is the reason, Deep learning often uses this method.

All these three methods are more clear to understand from Figure 3.15.

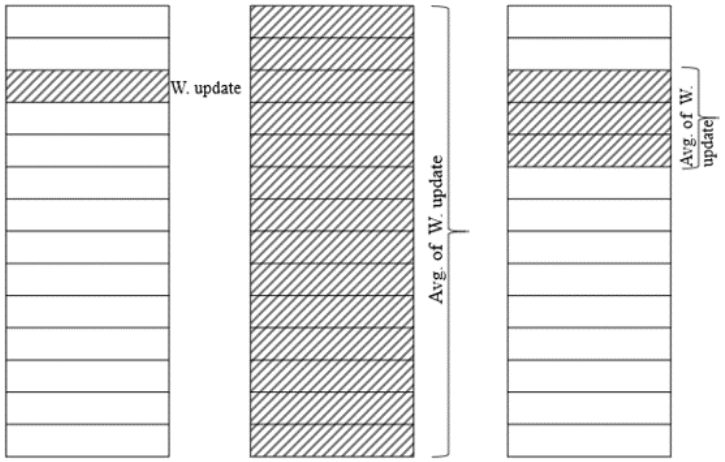

FIGURE 3.15: Weight update method: SGD (left), Batch (middle), Mini Batch (right), after Kim (2017).

3.4.8 Back-propagation Algorithm

The most popular and powerful training algorithms in the neural network are back-propagation (BP) algorithm, which is applied to train a multilayer feed-forward network. It is part of a supervised neural network. It was first proposed by Rumelhart et al. (1986) in 1986. This algorithm is usually implemented using the Levenberg-Marquardt method, which combines the gradient descent method and the Gaus-Newton optimization method (Levenberg, 1944; Marquardt, 1963).

This algorithm solves the problems and difficulties of the perceptron model that were pointed out by Minsky and Papert (1969) by allowing multi-layer perceptron models to learn. The previous delta rule or generalized delta rule is also ineffective for the training of the multilayer network. The reason behind this is that there is no defined rule to calculate the error in the hidden layer(s) in the delta rule. The error of output is calculated as the difference between the correct (known) output and the output obtained from the neural network. However, training data doesn't provide correct outputs for the hidden layer nodes, and hence the error can't be calculated using the approach used in the delta rule. Therefore, the back-propagation algorithm is developed as a solution to train the multi-layer feed-forward network. The feed-forward networks trained with the back-propagation algorithm have already been applied successfully to many geotechnical engineering problems (Erzin et al., 2008; Najjar and Basheer, 1996; Grabarczyk and Furmanski, 2013; Zhang et al., 2020b). So, the back-propagation algorithm is used for optimizing the connection weights in this study.

The details of the back-propagation algorithm can be found in many publications (e.g. Fausett (1994) and Kim (2017)). The training data used as inputs are transmitted through the network, layer by layer and a set of outputs is obtained. During this forward pass, the weights of the network are assumed with random values. The transfer function used in the

back-propagation algorithm is the sigmoid function. The obtained outputs are compared with the desired outputs and, as a backward pass; the difference between desired outputs and calculated outputs, i.e error, is used to adjust the weights of the network in order to reduce the level of the error (Figure 3.16). This is an iterative process, which continues until an acceptable level of errors will be obtained. Each time the network processes, the whole set of data (both a forward and a backward pass) is called an epoch. In this way, the network is trained and the error is reduced by every epoch until an acceptable level of error will be achieved. Kim (2017) explained the basic principle and training process of back-propagation in a simple way with Matlab examples. The steps of training process are described next to understand the back-propagation algorithm clearly.

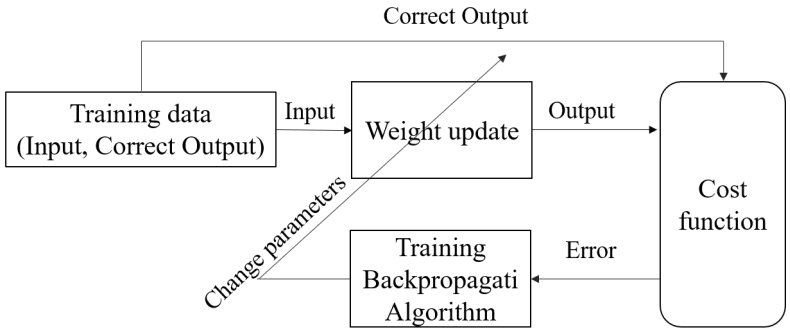

FIGURE 3.16: Back-propagation network.

Steps to be followed during the training process for the multi-layer network using back-propagation algorithm:

1. Assign initially the weights with random values.
2. Calculate the output using equation 3.1 and determine the error and delta using Equations 3.14 & 3.15, where d is correct (known) output.

$$e = d - Y \tag{3.14}$$

$$\delta = f'(v)e; \quad v = \sum W_j X_j + b_j \tag{3.15}$$

3. Propagate the output node delta (δ) backwards and calculate the errors and deltas of immediate next nodes (last hidden layer). 'k' denotes the number of hidden layers. Repeat the process until it reaches the first hidden layer.

$$e^{(k)} = W^T \delta \tag{3.16}$$

$$\delta^{(k)} = f'(v^k) e^{(k)} \tag{3.17}$$

4. Calculate weight updates using the equation below, where α_l is learning rate ($0<\alpha_l \leq 1$).

$$\Delta W_{ji} = \alpha_l \delta_j X_i \tag{3.18}$$

5. Update the weights using this equation,

$$W_{ji+1} = W_{ji} + \Delta W_{ji} \tag{3.19}$$

6. Perform steps 2-5 for all training data.

7. Repeat steps 2-6, which is called epoch until the error reaches an acceptable tolerance range.

In the above steps, apart from step 3, all the steps are similar to the generalized delta rule. Step 3 describes how the output delta propagates backwards to obtain the hidden node delta. Therefore, it is called back-propagation.

3.4.9 Cost function

As said earlier, supervised training of neural networks is a process of adjusting and updating 'weight (W)' to reduce the error of the training data. In this context, the measure of the error of the neural network is the cost function. The greater the error of the neural network, the larger the value of the cost function. It is also known as loss function and objective function. There are two primary types of cost functions for supervised training, given by Equations 3.20 & 3.21 (Kim, 2017).

$$J = \sum_{j=1}^{M} \frac{1}{2} \left(d_j - Y_j\right)^2 \tag{3.20}$$

$$J = \sum_{j=1}^{M} \left\{ -d_j ln(Y_j) - \left(1 - d_j\right) ln \left(1 - Y_j\right) \right\} \tag{3.21}$$

where, Y_j & d_j are output obtained from neural network and correct (known) output, respectively, M is the number of output modes. The first cost function given by Equation 3.20 is the square of the difference between the correct (known) output (d) and calculated output (y) from the neural network. If the calculated output and correct output are the same, the error is zero, while a greater difference between those two values implies higher errors. Hence, the cost function value is proportional to the error. This function is commonly used in the Regressions problem and in this study.

The second cost function is known as the cross-entropy function and is mainly used in classification problems. It uses a combination of sigmoid and softmax transfer functions for the best solution. It yields better performance than the sum of squared error in most cases.

3.4.10 Stopping Criteria

Stopping criteria are used to decide when to stop the training process. They determine whether the model has been optimally or sub-optimally trained (Maier and Dandy, 2000).

Many approaches like Bayesian Information Criterion, Akaike's Information Criterion and Final Prediction Error can be used to determine when to stop training. Training can be basically stopped in three ways *viz.* (a) after the presentation of a fixed number of training records, (b) when the training error reaches a sufficiently small value or less than the desired value, and (c) when no or slight changes in the training error occur. However, the above examples of stopping criteria may lead to the model stopping prematurely or overtraining. As mentioned earlier, the cross-validation technique developed by Stone (1974) is an approach that can be used to overcome such problems. Many researchers have successfully used this approach (Erzin et al., 2008; Erzin et al., 2010; Zhang et al., 2020b; Shrestha and Wuttke, 2020). It is considered to be the most valuable tool to make sure that overfitting does not occur . Amari et al. (1993) recommended that there are clear benefits in using cross-validation when limited data are available, which is the case for many real-life case studies. As mentioned earlier, the cross-validation technique requires that the data shall be divided into three sets *viz.* training, testing and validation. The training set is used to adjust the connection weights, while the validation set measures the ability of the model to generalize, and the performance of the model is checked at many stages of the training process using the testing set. The training process is stopped when the error of the validation set starts to increase. The testing set is finally fed into the networks to assess model performance, once training has been accomplished. The aim of the cross-validation method is to ensure that the model has the capability to generalize within the limits set by the training data in a robust fashion, rather than simply memorizing the input-output relationships which are contained in the training data (Shahin et al., 2002b). Unlike cross-validation, other methods like Bayesian Information Criterion, Akaike's Information Criterion and Final Prediction Error require the data be divided into only two sets i.e. training set and independent validation set. A training set is used to construct the model, whereas an independent validation set is used to test the validity of the model in the deployed environment. The basic aim of these stopping criteria is that model performance should balance model complexity with the amount of training data and model error.

3.4.11 Selection of ANN model

For the selection of best performing ANN model, three performances parameters such as Mean Square Error (MSE), Mean Absolute Error (MAE) and R (coefficient of determination) are calculated for each model. These parameters were used to compare network usefulness in the prediction of thermal conductivity after training. These parameters are computed for all training, validation and testing data. The first one was the Mean Squared Error (MSE). It is defined as the arithmetic mean of the squared differences between the outcome (predicted values) and the measured values. The smaller the value of this parameter the more accurate the network to predict the thermal conductivity of soils. It describes the absolute difference between measured and prediction values. The second one was R which describes the linear regression line between predicted values from the ANN model. When R is equal to 1, the accurate relationship is obtained, while when it is close to 0, no clear relationship is obtained. It may also be understood as the tangent of the linear function that approximates

the correlation between the outcome and measured values. The third one was a mean absolute error (MAE). The MSE is the most popular measure of error for statistical analysis and it has the advantage that the large errors get more attention than small errors (HechtNielsen, 1989). In contrast, MAE eliminates the emphasis given to large errors. The RMSE and MAE are desirable when the data evaluated are smooth or continuous (Twomey and Smith, 1997). The mathematical expressions of these parameters are given below.

$$R = \sqrt{1 - \frac{\sum_1^n \left[\lambda_m - \lambda_p\right]^2}{\sum_1^n \left[\lambda_m - \lambda_{mean}\right]^2}} \tag{3.22}$$

$$MSE = \frac{1}{n}\sum_1^n \left[\lambda_m - \lambda_p\right]^2 \tag{3.23}$$

$$MAE = \frac{1}{n}\sum_1^n \left[\lambda_m - \lambda_p\right] \tag{3.24}$$

where λ_m ($\mathrm{W\,m^{-1}\,K^{-1}}$) is the measured thermal conductivity, λ_p ($\mathrm{W\,m^{-1}\,K^{-1}}$) is the predicted thermal conductivity, λ_{mean} is the mean value of measured thermal conductivity and n is the number of measurements.

3.5 Deep Learning

A neural network with more than a single hidden layer is known as a deep neural network. In other words, the deep neural network is a multilayer network with two or more hidden layers. The problem of training the deep neural network (multilayered network) was solved when a back-propagation algorithm was introduced in 1986. However, the back-propagation training with additional hidden layers often yielded poor performance. Many methods have been attempted to solve the problems, including the addition of nodes in the hidden layer and addition of hidden layers. However, none of them worked because the deep neural network was not properly trained. There are three primary difficulties in the training process of deep neural networks using the Back-propagation algorithm (Kim, 2017). They are

- Vanishing gradient
- Overfitting
- Computation load

Deep learning is introduced, which provides the solution to the above problems. It is a simple feed-forward neural network with the addition of new types of networks *viz.* Convolutional Neural Network (CNN), Recurrent Neural Network (RNN), Long Short-Term Memory Network (LSTM), etc. It is used in supervised, unsupervised and reinforcement learning models. The training is usually done by optimizing a cost function using some form of gradient descent.

In vanishing gradient, output errors cannot reach the first hidden layer and hence the 'weights' can't be adjusted. Therefore, the hidden layer close to the input cannot be trained properly. In order to solve the problem, Rectified Linear Unit (ReLU) function as an activation function has to be employed in the network (Kim, 2017). In addition to this, the cross entropy-driven learning rules can be employed to improve the performance of the deep neural network (Kim, 2017). The use of the advanced gradient descent method, which is a numerical approach that better achieves optimal value, is also beneficial to overcome this problem.

$$f(x) = \begin{cases} 0, & \text{if} \quad x \leq 0 \\ x, & \text{if} \quad x > 0 \end{cases} \tag{3.25}$$

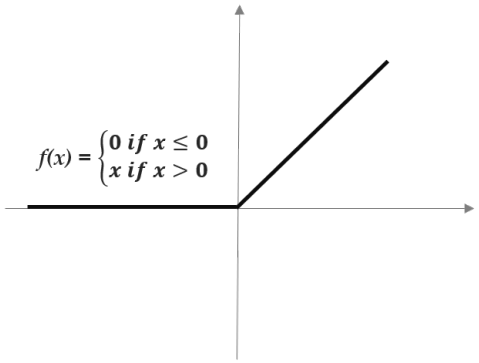

FIGURE 3.17: ReLU activation function, range (0,∞).

Increasing the number of hidden layers and neurons will not solve the complex non-linear problems, rather it leads to complicated network model because of more weights. A complicated model is more vulnerable to overfitting. Dropout or regularization is the solution to overfitting (Kim, 2017). The adequate percentage of Dropout is approximate 50% and 25% for hidden and input layers, respectively. Another method is regularization which simplifies the neural network's architecture as much as possible and hence reduces the possibility of overfitting. Mathematically, adding the sum of the weights to the cost function is referred as regularization.

The complicated model also requires a longer time for training the network. The more computation the Neural network performs, the longer the training takes. High-performance hardware such as GPU and an algorithm such as batch normalization are required to solve this problem (Kim, 2017).

3.6 Application of ANN

ANN has different types of application. The two most common types of application are classification and prediction or regression. Both classification and regression are part of supervised learning which means they both have input and correct ouput. The main difference

is the type of correct outputs; classification needs classes, while the prediction needs values. Others are data association and data filtering. Brief driscription are given below:

- Prediction: is one of the applications of supervised learning. It is also known as regression which doesn't determine the class. Instead, it basically predicts output using input data. It is mostly used in the engineering field to predict the output based on several input values. The BP algorithm is most commonly used for solving engineering problems which uses a multi-layer architecture. In the current study, the ANN models have been developed to generalize the thermal conductivity based on this category.
- Classification: is also the application of supervised learning. It uses input data to determine the class. It focuses on finding the classes to which the data belongs. Some of the examples are pattern recognition, face or image recognition and spam mail filtering service.
- Data association: It simulates the classification, while also recognising data that contains errors.
- Data Filtering: This method analysis input data and makes them smooth for the output such as taking the noise out of telephone signals.

3.7 Advantages and disadvantages of ANNs

3.7.1 Advantages

ANNs are easy to construct and can deal very well with a large amount of data. The main advantage of the artificial neural network is that it can handle complex tasks with many parameters and solve non-linear multidimensional problems. They can simply ignore excess data that are of less significance and concentrate instead on the more important inputs. Instead of complex rules and mathematical formulations, ANNS are able to learn the key information patterns within a multidimensional information domain. Further, they have the capability to successfully classify objects, even with the distribution of objects with noisy parameters. They work well for problems where there are no known rules. They are adaptive in nature. ANN can be handled with ease and it requires less human intervention than does a traditional analysis. One doesn't need to be competent in the mathematical background and computational analysis. ANN software packages are also relatively easier to use than the typical statistical packages. Researchers can successfully use ANNS software without requiring a full understanding of the learning algorithms, which makes them more accessible to a wider variety of researches. That's why it is becoming popular in every field.

It is comparatively fast and accurate than other available methods. It provides several advantages over more conventional computing techniques. For most traditional mathematical models, the lack of physical understanding is usually supplemented by either simplifying the problem or incorporating several assumptions into the models. Consequently, many mathematical models fail to simulate the complex behaviour of most practical and engineering problems. In contrast, ANNs are a data-driven approach in which the model can

learn input-output relationships with previous data to determine the structure and parameters of the model. In this case, no need to either simplify the problem or incorporate any assumptions. Moreover, ANNs can always be updated to obtain better results by training with newly available data. These factors combine to make ANNs a powerful modelling tool in every field, especially in civil engineering.

The training process of an ANN itself is relatively simple. However, the pre-processing of data including data selection and representation to the ANN and the post-processing of the outputs require an ample amount of work. But, constructing a problem with ANNs is still assumed to be easier than modelling with conventional statistical methods. There are many statisticians who argue that ANNs are nothing more than the special case of statistical models, and thus the rigid restrictions that apply to those models must be applied to ANNs as well. However, there are probably more successful novel applications using ANNs than conventional statistical tools.

3.7.2 Disadvantages

Despite the good performance of ANNs in many situations, they have a number of drawbacks including mainly time-consuming, the limited ability to extract knowledge from the trained network models, inability to extrapolate beyond the range of the data used for model training and dealing with uncertainty.

The main disadvantage of artificial neural networks is that it requires a lot of time, particularly finding a good ANN structure, as well as the pre-processing and post-processing of the data, though ANNs are easy to construct. For example, the training or learning is repeated until the desired output data is reached. Another significant disadvantage is the difficulty of determining how the network is making its decision, i.e. lack of interpretability. It only provides results but does not give any reasonable interpretations between input and output variables. So, the neural network works as a black box. Consequently, it is hard to determine which of the input data are important and useful for the classification as well as prediction, and which are worthless. It has no ability to extrapolate beyond the range of data used for the training model. Whilst this is not unlike other models, it is nevertheless an important limitation of ANNS, as it restricts their applicability and usefulness. Extreme value prediction is particularly concerned in many fields of civil engineering such as flood forecast, liquefaction potential assessment, etc.

There are also limitations with training data. As an example, the ability of ANN to identify indications of an intrusion is entirely dependent on the accurate training of the system. Thus, the training data and methods are critical to effective outcomes. Therefore, qualified training data sets are essential to meet the desired results.

3.8 Summary

In this chapter, the background and development, application to many fields including engineering field, advantage and disadvantage of ANN as well as description and methodology of ANN were explained.

Chapter 4

Design of granular materials with enhanced thermal conductivity

4.1 Introduction

This chapter explains the methodology to improve the thermal conductivity of granular materials. The materials used, measurement technique used and experimental work steps to achieve thermally conductive materials are discussed. The experimental program covered the study of different mix proportions of granular soils, binder, additives to achieve the desired properties.

4.2 Materials used

The selection of materials was based on the knowledge that higher thermal conductivity can be achieved with bigger and round-shaped particles, well-graded soils, minerals with higher thermal conductivity, an appropriate proportion of fine particles and (dense packing), which are discussed in Chapter 2 . It was also kept in mind that utilizing of naturally available materials is also key in the design process so that it will be more economical and practical. In this study, the design mixes were prepared following the concept of fuller curve gradation to achieve lower porosities and adding fine materials as fillers in appropriate proportion to improve denseness. Sand was selected as prime geomaterials because it often uses as backfill materials and Bentonite and stone dust, which are fine materials, were selected as fillers. Another reason to select sand and stone dust was that they had high quartz content than other materials. The quartz content in the materials was experimentally determined by the X-ray diffraction (XRD) method. The most important factor to be considered was to increase the packing density or reduce the porosity as reducing porosity increases the thermal conductivity of the soils, which was fulfilled by Fuller curve gradation.

4.2.1 Analysed materials

Three different sand from different sites with different mineral compositions were selected in this study for the experimental program. They were Sand A from Weimer, Germany, Sand B and Sand C from Kiel, Germany. The physical properties of all the sand are presented in Table 4.1 and the particle size gradation are presented in Figure 4.4. It is noticed from

(A) Sand A (B) Sand B (C) Sand C

FIGURE 4.1: Analysed materials.

TABLE 4.1: Sand properties.

Properties	**Sand-A**	**Sand-B**	**Sand-C**
Specific gravity, G_s	2.65	2.65	2.65
D_{50}	0.65	0.99	0.51
D_{10}	0.28	0.30	0.23
D_{60}	0.80	1.30	0.64
D_{30}	0.41	0.54	0.34
C_u	2.86	4.33	2.78
C_c	0.75	0.75	0.79
Quartz content, q_c	>99	70	80

Figure 4.4 that all three sand were uniform. The specific gravity (or solid density) of all three sand was found to be 2.65. The mineral composition of the sand was determined semi-quantitatively by X-ray diffraction (XRD) analysis. The XRD reports of sand are presented in Figures 4.8a-4.8c. From these reports, it is concluded that Sand A has a higher percentage (i.e. greater than 99%) of quartz. The others two Sands B and C have lower contains of quartz of 70% and 80%, respectively. In Sand B, the other minerals are calcite of 10% and albite of 20% while in Sand C, the other minerals are calcite of 20%. The aim of the selection of sand with different mineralogy is to check the influence of mineralogy on the thermal conductivity of the sand.

The fine materials used in this study were bentonite, stone-dust and kieselghur (Figure 4.2). The bentonite is basically a very fine material with high clay content (basically montomorollite). That's why it has swelling characteristics when in contact with water and it is highly impermeable. The bentonite was used as filler for the thermal modification of the sand in the dry state and the results were published in Shrestha et al. (2016). As a replacement for bentonite, stone-dust was used which is obtained during the crushing of stone or rock from the crusher manufacture company. It is like waste and will be economically viable to use with sand. The XRD of stone-dust was also done and the report is shown in Figure

(A) Bentonite (B) Stonedust (C) Kieselghur

FIGURE 4.2: Analysed fine materials.

4.9. It contains 80% quartz and 20% zeolite. The stone-dust shows no swelling characteristics and water is easily flowable through the sample (Shrestha et al., 2019).

Another material used in this study was Silicon carbide (SiC), which possess a very high thermal conductivity of more than 100 $W\,m^{-1}\,K^{-1}$ when it is in solid form. But, here in this study, it is in the crushed-state and size ranges from (0.5-1) mm. The particle size distribution is shown in Figure 4.4. The thermal conductivity is relatively very low when it is measured in a granular state because of higher porosity and small grains. The reason for using SiC is to check whether it can improve the thermal heat conduction or not.

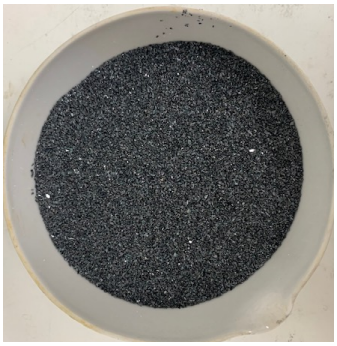

FIGURE 4.3: SiC.

4.2.2 Design of materials

The modification of the original sand was done by changing the original gradation first and then adding fine materials in appropriate proportions. The original gradation of sands was first modified with the Fuller curve gradation using Equation 4.1 proposed by Fuller and Thomson (1907).

$$P_i = (d_i/D)^{0.5} \tag{4.1}$$

where P is percentage passing through sieve i of diameter (d) and D is the maximum particle diameter of the fuller mix. For example, D is 8mm for 8mm fuller curve gradation.

Three different kinds of fuller curve gradation owing maximum size of particles with 8mm, 4mm and 2mm were developed in this study, of which gradations are shown in

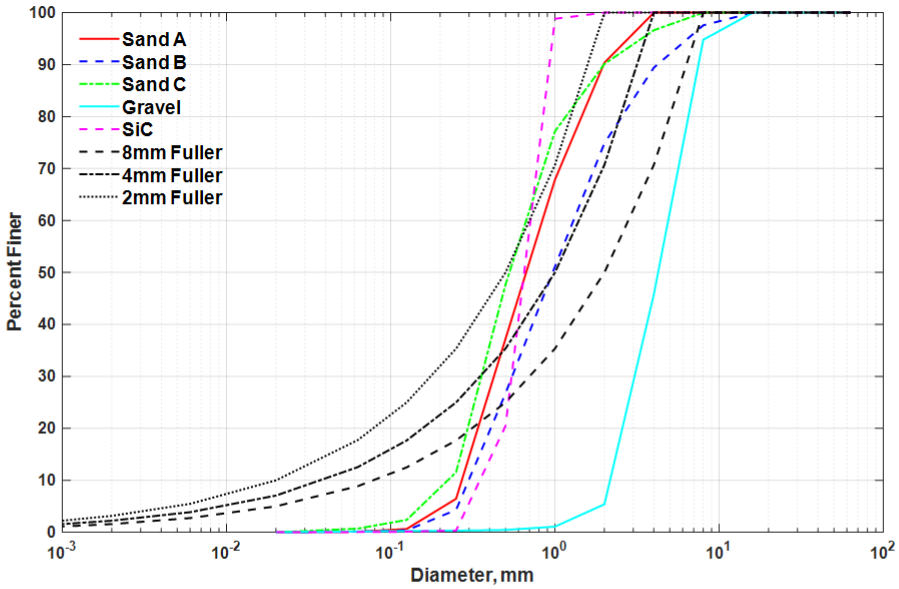

FIGURE 4.4: Particle size distribution.

Figure 4.4. Three gradations owing maximum size of 8mm, 4mm and 2mm are referred as 8mmF, 4mmF and 2mmF, respectively. Thus, sand A and B have 8mmF, 4mmF and 2mmF, whereas sand C has only 4mmF and 2mmF because of lack of the bigger particles in sand C. Gravel-A was used to prepare 8mmF of sand-A as both were from the same query. Thus, altogether eight new mixtures of three sand were prepared, named as sandA_8mmF, sandA_4mmF, sandA_2mmF, sandB_8mmF, sandB_4mmF, sandB_2mmF, sandC_4mmF, and sandC _2mmF. It is very difficult to obtain the fine particles below 125 μm in the desired amount from the sand gradation. In order to solve this problem, the fine materials bentonite and stone-dust were added in appropriate proportion following Fuller curve gradation modification. For 8mmF, 4mmF and 2mmF, the fine particles proportions were 12.5%, 17.68% and 25% by volume, respectively for all three sand. The details in the calculation to prepare fuller gradation of 8mmF, 4mmF and 2mmF using standard sieves (DIN-18123) in the laboratory is presented in Table 4.2. The bentonite was added to all modified sands while the stone-dust was added to only modified sands of sand A and sand B. The added fillers act as inter-granular bridges to enhance the thermal conduction path by improving the quality and quantity of contacts due to an increase in number of contact paths because of large surface area. Hereafter, the developed sand after modification of gradation is called modified fuller sand whereas the sand with original gradation is called original or natural sand.

Apart from fuller curve gradation, the mixture of coarse and fine materials was also prepared with different proportions. For this purpose, sand A was used to mix with fine particles in different proportions. The fine particles used for this purpose were bentonite, stone-dust and kieselghur. The effect of fine content on thermal conductivity can be observed from these tests. Another material SiC was also added to modified fuller sands sandA_8mmF, sandA_4mmF, and sandA_2mmF in 11% by volume in order to know the

TABLE 4.2: Design of Fuller curve gradation.

particle size [mm]	**8mmF [%]**	**4mmF [%]**	**2mmF [%]**
4-8	29.29	0.00	0.00
2-4	20.71	29.29	0.00
1-2	14.64	20.71	29.29
0.5-1	10.36	14.64	20.71
0.25-0.5	7.32	10.36	14.64
0.125-0.25	5.18	7.32	10.36
< 0.125	12.50	17.68	25.00

importance of highly conductive minerals. The dry thermal conductivity of SiC only was also measured in the laboratory and it was found to be between 0.20-0.35 $\mathrm{W\,m^{-1}\,K^{-1}}$ for the dry density of 1.45-1.70 $\mathrm{g\,cm^{-3}}$, which is very low thermal conductivity. This is due to the large void contained in the matrix which is filled by air and the air has a higher resistance to thermal heat conduction because of very low thermal conductivity ($\lambda_{air} = 0.024\ \mathrm{W\,m^{-1}\,K^{-1}}$). Another reason may be that the higher dry density cannot be achieved due to the uniform gradation of SiC. It contains sizes between 0.5-1.0 mm. The thermal conductivity of SiC was found to be more than 7.0 $\mathrm{W\,m^{-1}\,K^{-1}}$ when measured in a wet state.

4.3 Equipment used

In order to measure the thermal conductivity of investigated materials, the transient method was selected due to its fast measurement time and easy handling. The method can be hydro-mechanically controlled as well. The thermal conductivity of studied mixes was measured with a thermal needle probe, Decagon KD2 Pro, based on transient line source measurement technique in compliance to ASTM D 5334 - 08 (2008) and IEEE 442 (1981) standards. Many researchers have successfully used this device to measure the thermal conductivity of different kinds of materials from fine-grained soils to coarse-grained soils, cementing materials and mixed materials (Hailemariam et al., 2017; Hailemariam et al., 2016a). The specifications serve to ensure the best possible process for the most precise measurement results. The KD2 Pro measuring the thermal conductivity of the samples is shown in Figure 4.5. The device has ability to measure thermal conductivity at a constant interval, which can be set manually or with the help of a computer. The number of measurements, as well as waiting time for the first measurement, can be also set in the device. The waiting time is very important to bring the sample and needle temperature to equilibrium. A specification recommends 15 minutes of waiting time before the first measurement. A thermal needle probe, TR-1 (single needle), with a length of 100 mm and a diameter of 2.4 mm was used to measure the thermal conductivity of the samples. The sufficient needle length to diameter ratio ensures that conditions for an infinitely long and infinitely thin heating source are met. The measurement error recorded for all samples was kept well below the 0.015% limit. The KD2 Pro includes

a linear heat source and a temperature measuring element with a resolution of 0.001^{o}C, and computes the thermal conductivity of the analysed materials using the following equations.

$$\lambda = \frac{Q\left(\ln t_2 - \ln t_1\right)}{4\pi\left(\Delta T_2 - \Delta T_1\right)} \tag{4.2}$$

$$\Delta T = \frac{Q}{4\pi\lambda}\left[-Ei\left(-\frac{r^2}{4\alpha t}\right)\right] \tag{4.3}$$

where, λ (W m^{-1} K^{-1} is the thermal conductivity of the sample, Q (W m^{-1}) is the constant rate of application of heat, ΔT (K) is the temperature response of the source over time, t (s) is the amount of time that has passed since the heating has started, Ei is an exponential integral, r (m) is the radial distance from the line source and α (m^2 s^{-1}) is the thermal diffusivity of the sample.

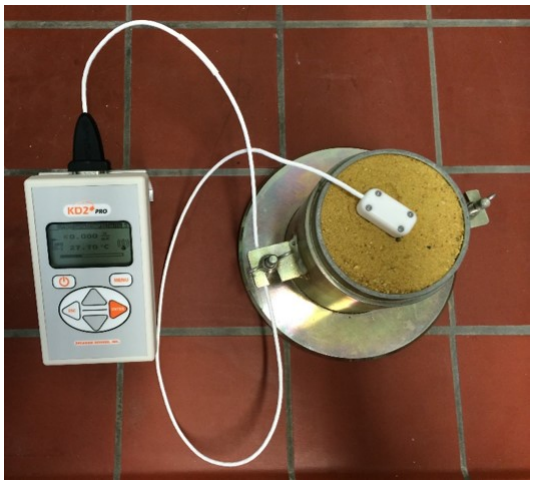

FIGURE 4.5: KD2 Pro device with TR1 needle.

4.4 Experimental procedure

All the samples were prepared in cylindrical mould and the thermal conductivity of these samples was measured using the KD2pro device in the laboratory. A mould used in this study was a cylindrical mould with 5cm in diameter and 14 cm in height. The minimum dimension required for the cylindrical mould according to specifications is shown in Figure 4.6. The height of the mould should be at least 2cm longer than the length of a needle. The needle is supposed to place at the centre of the mould so that it has at least 2.0 cm gap between the needle and the wall of the mould. It ensures no effect from the boundary on the heat distribution of the needle and measurement of thermal conductivity. The samples were prepared with different compaction techniques in a dry state as well as in a moist state. In the dry state, the samples were prepared in the combination of compaction and vibration to vary the dry density and attain maximum dry density in order to see the influence of dry density or porosity on the thermal conductivity of original and modified fuller sands.

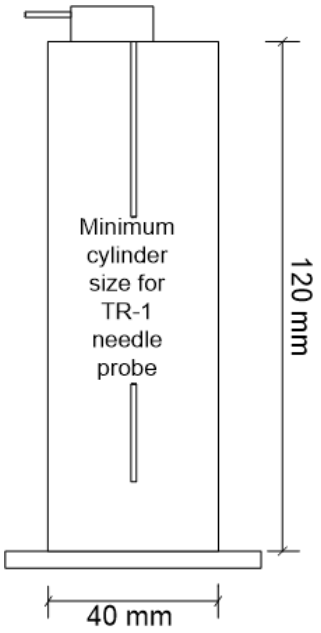

FIGURE 4.6: Schematic diagram of the sample cylinder

On the other hand, two methods are existed to prepare the sample for the measurement of thermal conductivity over different moisture contents. They are listed as below:

- **Single sample method:** The first method is known as the single sample method, where the thermal conductivity and mass of the sample will be monitored and measured continuously at a certain interval as the sample dries from saturation to dry state. It is based on the evaporation method. The sample is prepared in the dry state and then saturated with water by allowing water to flow from bottom to top. The amount of test time depends on the method of drying, boundary conditions, soil type and initial water content. The schematic diagram of the saturation process is presented in Figure 4.7. This method requires filter paper, porous stone, water inlet and outlet. The drying process is a natural air-dry process and finally, the sample is oven-dried to measure final water content. The thermal conductivity is also measured at a dry state. In this method, the needle is kept inside the sample throughout the measurement from saturation to dry state. The method is more accurate as the sample remains undisturbed and the measurement is continuous without taking out the needle. However, it is time-consuming and might have a variation of moisture distribution across the sample. A significant moisture variation across the length of the sample during the thermal conductivity measurement using the vertical probes was observed in the case of coarse-grained soils than fine-grained soils (Woodward et al., 2013; Yao et al., 2014). The moisture variation is a function of the height/depth of the sample. The longer the sample, the higher the moisture variation. The effect can be minimized by reducing the height of the sample. For example, the average volumetric water content and thermal resistivity of the soil specimen are 0.14 $mm^3\,mm^{-3}$ and 36 $°C\,cm\,W^{-1}$ which are the overestimation of the actual volumetric water content (0.11 $mm^3\,mm^{-3}$) and actual thermal resistivity (40 $°C\,cm\,W^{-1}$) along the length of the sensor (Woodward

et al., 2013). The sample length is 20.3 cm, 10 cm longer than the needle length. If the specimen length is reduced from the bottom and the average volumetric water and the average thermal resistivity are recalculated, the recalculated values are 0.12 $mm^3\,mm^{-3}$ and 39.5 $°C\,cm\,W^{-1}$ respectively indicating closer to the actual values. In this study, the sample length is just 2.5cm longer than the needle length (10 cm) and also 2.5 cm wider from the needle in the radial direction. It helps somehow to minimize the moisture variation. However, the study of moisture variation depending on the length of the sample and its effect on the thermal conductivity could be the scope of future work. Woodward et al. (2013) also found that moisture is consistent through a specimen in the case of fine-grained soil. In this study, the modified fuller sand is the mixture of sand and fine materials. Because of these reasons, it can be assumed that there will be less moisture variation and not affecting the effective thermal conductivity of the samples. The measured water content would be average water content along the length of the needle and the needle provides effective thermal conductivity of the specimen.

- **Multiple sample method:** It is the second method to prepare the samples in which the samples are prepared at different water contents and the thermal conductivity and corresponding water content of each sample are measured. The first method is accurate and the sample remains undisturbed i.e. dry density remains constant throughout the test. The needle used in this method is TR1 which is long enough to give the effective thermal conductivity at average water content. The second method is fast as compared to the first method but it is difficult to control the same dry density when every new sample is prepared and the sample remains disturbed which changes the microstructure of the sample completely. Consequently, it gives different thermal conductivity. Therefore, the first method 'single sample method' was chosen in this study to measure the thermal conductivity at various moisture contents.

All the samples prior to use were oven-dried. In order to measure the thermal conductivity of dry samples at various porosity, the sample was prepared in the mould by a combination of compaction and mechanical vibration. The sample was compacted into the mould in four equal layers to achieve the desired porosity using conventional compaction procedures and mechanical vibration was applied when dense packing was needed. It was required to attain the lowest porosity. The mass of the sample was recorded, once the sample preparation was finished. The needle probe (TR1) was then inserted vertically in the sample and the thermal conductivity readings were taken. Thermal needle proble (TR1) is always calibrated prior to use to check the accuracy of the needle. A drill press was sometimes used to ease the insertion of the needle in case of a dense or stiff sample. The measurement of thermal conductivity was done at room temperature and atmospheric pressure conditions and was repeated at least three times for each sample. The longer reading time was selected to minimize errors from contact resistance in granular samples. The minimum interval time kept for each measurement is 30 minutes. The measurement was always started after 15 minutes of needle insertion. In the case of dry samples, the main problem was an error in

measurement due to contact resistance. To avoid this problem, the gel provided by KD2 was also coated around the needle prior to use, which helps to reduce error during the measurement.

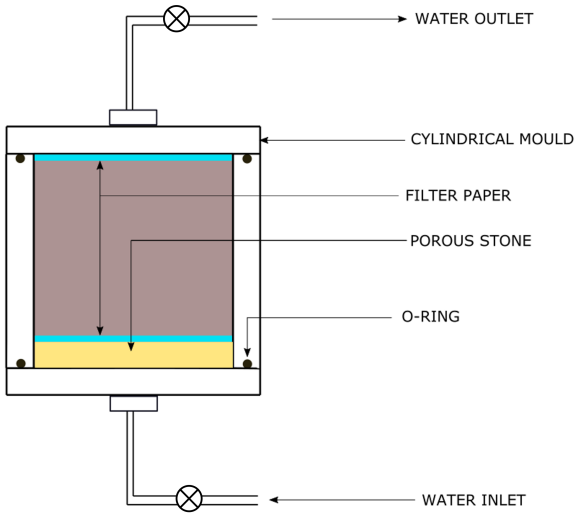

FIGURE 4.7: The schematic diagram of sample saturation process (Shrestha et al., 2019).

In order to measure the thermal conductivity in an unsaturated and saturated state, the 'single sample' method was selected. The sample was first prepared like dry samples and the mass of the samples was recorded. The dry density was kept 2.08 $g\,cm^{-3}$, 2.04 $g\,cm^{-3}$, 1.95 $g\,cm^{-3}$ & 1.71 $g\,cm^{-3}$ for sandA_8mmF, sandA_4mmF, sandA_2mmF and the original sand A, whereas 2.08 $g\,cm^{-3}$, 2.02 $g\,cm^{-3}$, 1.92 $g\,cm^{-3}$ & 1.71 $g\,cm^{-3}$ for sandB_8mmF, sandB_4mmF, sandB_2mmF and sand B, respectively. The sample was enclosed by placing caps at both ends of it, after placing the porous stones and the filter papers at both ends of the sample as shown in Figure 4.7 and then saturated by allowing distilled water to flow from the bottom through a pipe from the tank, elevated at a height of 1m. The sample was assumed to be saturated once the water started to come from the top. The advantage of saturating the sample from the bottom is to remove the entrapped air within the sample. The needle probe was then inserted into the sample vertically at the centre after removing the top cap of the mould after waiting for certain hours. The weight was recorded before and after insertion of the needle to know the mass of water in the sample. The water content was known at the beginning. The attention was given while inserting the needle into the samples and the needle was not taken out until the final measurement. The measurement of thermal conductibility was done as described in the case of dry samples. The only difference is that over a period of time, additional thermal conductivity readings and weightings were recorded, as the sample dried. During the measurement process, the water content was reduced by air drying and finally, the sample was oven-dried at 60 °C to measure final water content. The thermal conductivity of the sample was again measured at a dry state.

Measuring the thermal conductivity at proctor density and various water content is a

very important step while designing the thermal backfill as the backfill materials are compacted in the site using proctor density and optimum water content. Some samples were also prepared with the proctor compaction method to obtain thermal conductivity at maximum dry density and corresponding optimum moisture content. Once these parameters are known, it is very useful for field application. This method was applied to the samples sandA_8mmF, sandA_4mmF, sandA_2mmF, sandB_4mmF, and sandB_2mmF. In the field, the backfill materials are laid using proctor compaction to get desired dry density. So, it is essential to know the corresponding thermal conductivity. The measurement of thermal conductivity was similar to that applied to dry samples.

4.5 XRD analysis

Accurate determination of mineral content in the soil is very essential to estimate the thermal conductivity of soil. It was a quite difficult process in the past. Consequently, the quartz content was assumed to be equal to the mass fraction of sand (Peters-Lidard et al., 1998; Usowicz et al., 2006; Lu et al., 2007). However, this assumption leads toan overestimation of soil thermal conductivity (Tarnawski et al., 2009; Zhang et al., 2017).

The quartz content in soils can be experimentally determined by chemical or X-ray diffraction (XRD) methods and to a lesser extent, by petrographic analysis. Chemical methods are generally more precise, but time-consuming, whereas XRD techniques are more rapid but fairly accurate (Hardy, 1992). Here, the XRD method was used to determine the mineral contents of the analysed materials. The results of the XRD test on three sand, stone-dust and kieselghur are presented in Figures 4.8-4.10. It was concluded from this analysis that sand A had almost all quartz content of more than 99%; sand B had 70% quartz, 10% calcite and 20% albite; sand C had 80% quartz, 10% albite and 10% calcite; and stonde-dust consists of 80% quartz and 20% zeolite. The bentonite and kieselghur consist of mostly montomorillonite.

4.6 SEM image analysis

A Scanning Electron Microscopy (SEM) is a test process that produces a magnified image of a sample for analysis by scanning the surface with an electron beam. The electron beam is scanned in a raster scan pattern, and the beam position is combined with the intensity of the detected signal to generate an image. The method is also known as SEM analysis and SEM microscopy, which is used very effectively in microanalysis and failure analysis of solid inorganic materials. Electron microscopy is conducted at high magnifications, produces high-resolution images and precisely measures very small features and objects. In this study, the new backfill materials sandA_2mmF with bentonite and stone-dust were selected for SEM analysis to see the bonding or connection between the grains and fines of mixed geomaterials which ensures the improvement in thermal conductivity of designed geomaterials.

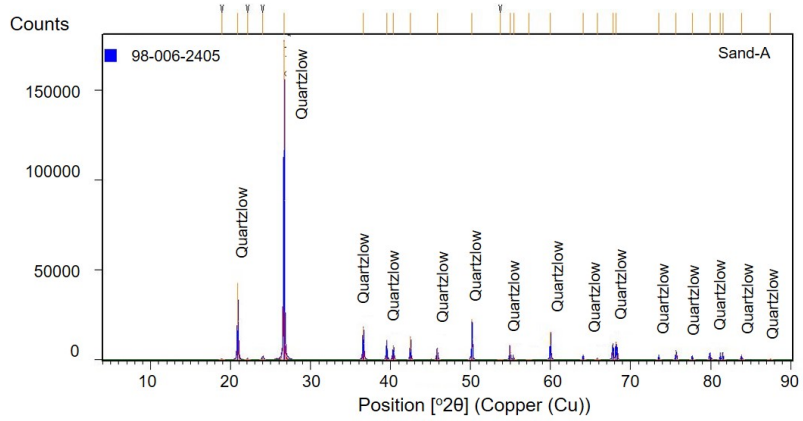

(A)

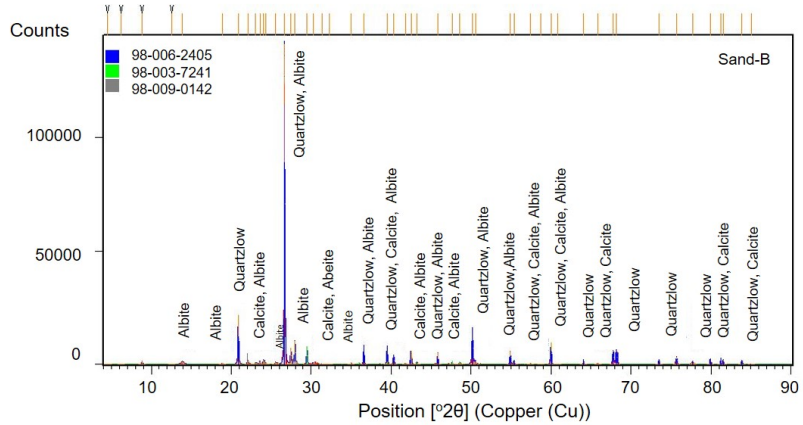

(B)

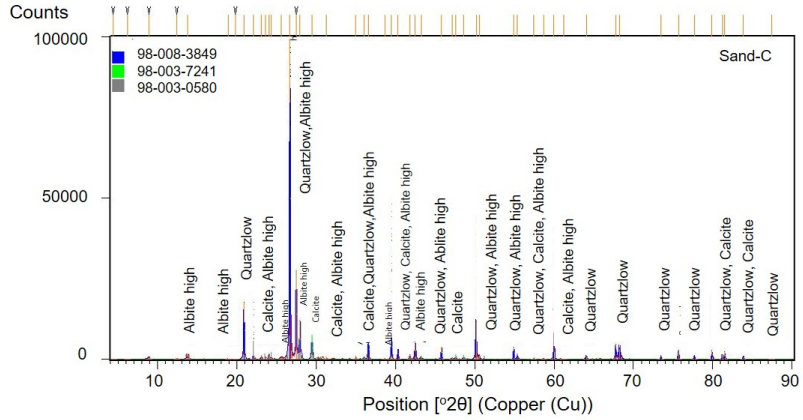

(C)

FIGURE 4.8: XRD analysis of sand A (a), sand B (b) and sand C (c) .

4.7 Mechanical tests

Odometer tests (1D consolidation test) were carried out to investigate the mechanical strength of designed materials by determining odometer parameters such as compressibility index (C_c) , regression index (C_r) and swelling index (C_s) of natural sand and developed materials.

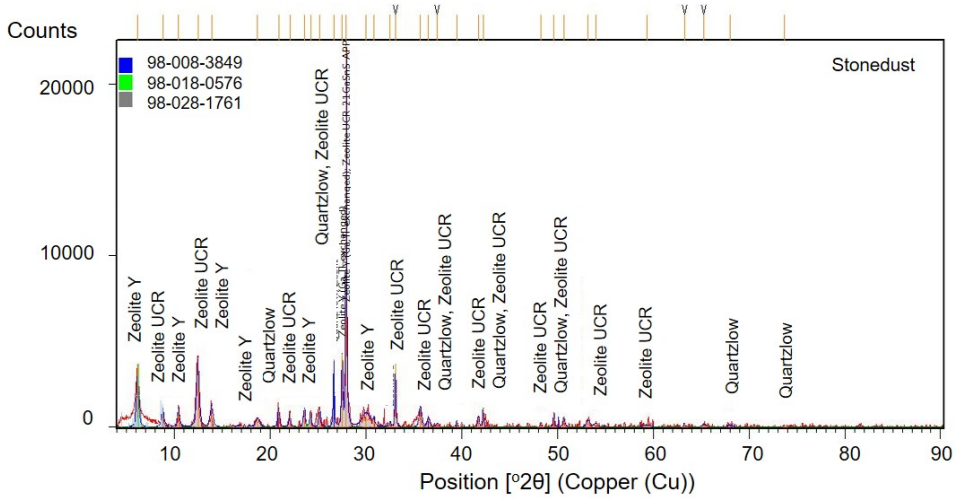

FIGURE 4.9: XRD analysis of stone-dust.

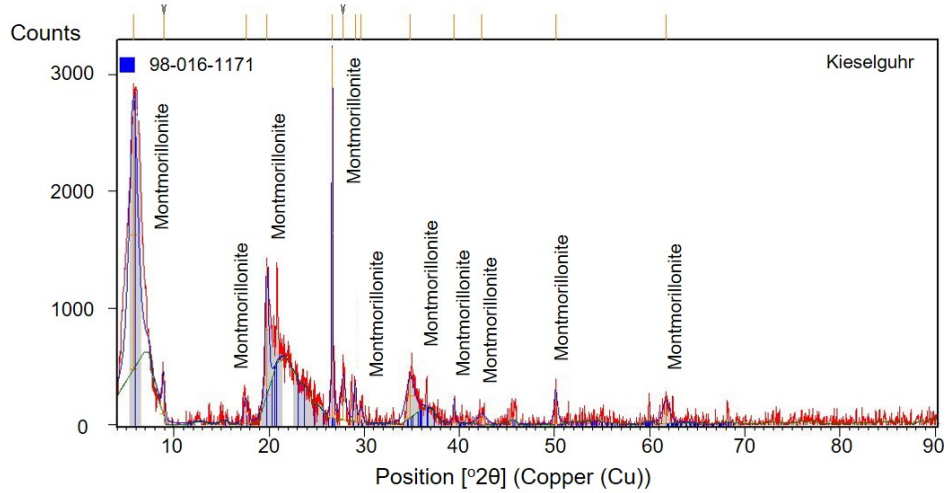

FIGURE 4.10: XRD analysis of kieselghur.

It characterizes the soil stress-strain behaviour during one-dimensional compression. The purpose is to predict how the modified fuller sand deforms in response to a change in effective stress in the field application scenario. Due to the addition of different proportions of fine particles to the modified fuller sand, a reduction in mechanical strength is expected. The test was carried out according to DIN-18135. As it is one-dimensional compression, there is no lateral deformation during loading. When stress is applied to the sample, the soil grains pack together reducing voids and the sample gets deformed. The tests were carried out for the modified fuller sand (with stone-dust) and original sand of A and B. In order to determine odometer parameters, the test was performed with loading, unloading and reloading. The sample was first loaded until 400 kPa starting with 12 kPa and unloaded up to 25 kPa and finally reloaded till 800 kPa. The loading, unloading and reloading are done to determine the compression, swelling, and regression indices, respectively. For each loading step, the sample was left for 24 hours before going for the next loading. The same procedure was applied to the unloading and reloading steps. All the samples were prepared at maximum

dry density and corresponding optimum moisture content.

4.8 Summary

This chapter explained the properties and characteristics of the geomaterials and the design methodology to develop the granular composite geomaterials. Moreover, the measurement technique and steps to be followed to measure the thermal conductivity in a dry and moist state were also explained. The results or outcomes of the experimental work are discussed in next chapter 4.

Chapter 5

Experimental material design analysis and discussions

5.1 Introduction

In this chapter, the outcomes of experimental investigations are presented and discussed in detail. Moreover, a focus on thermal conductivity enhancement is given. Furthermore, the experimental results are compared with existing theoretical and empirical prediction models which are described in section 2.6.

5.2 Thermal conductivity measurement results

5.2.1 Effect of porosity on thermal conductivity in dry state

With bentonite

Figure 5.1 shows thermal conductivity measurement results as a function of porosity in the dry state for original and modified fuller sands with bentonite. As stated earlier in the section 2.4.1, the dry thermal conductivity values of original sands increase in a quasi-linear fashion with decreasing porosity. However, the dry thermal conductivity values of modified fuller sands tend to follow an exponential increase with a decrease in porosity (i.e. increase in dry density). The thermal conductivity data of dry original sand are lower than 0.4 $W\,m^{-1}\,K^{-1}$, range from 0.28-0.39 $W\,m^{-1}\,K^{-1}$ for the porosities between 0.45 and 0.3. As stated earlier in section 2.7, all the granular soils generally have thermal conductivity less than 0.5 $W\,m^{-1}\,K^{-1}$ in the dry state (Rao and Singh, 1999; Naidu and Singh, 2004; Cortes et al., 2009; Waite et al., 2009). For the developed mixes (modified fuller sands) with all three sand A, B, and C, the measured dry thermal conductivity data ranges from 0.4-1.1 $W\,m^{-1}\,K^{-1}$ for porosities between 0.4 and 0.2, which is significantly higher than that of ordinary dry soils. The experimental results clearly state that there is a significant improvement in thermal conductivity for modified fuller sand in dry conditions. It is noted that about two to threefold increment in dry thermal conductivity of modified sands as compared to that of original sand.

It is also observed that the increase in maximum particle size of fuller gradation produces a lower porosity and the lowest porosities of about 0.21 are attained with 8mm fuller

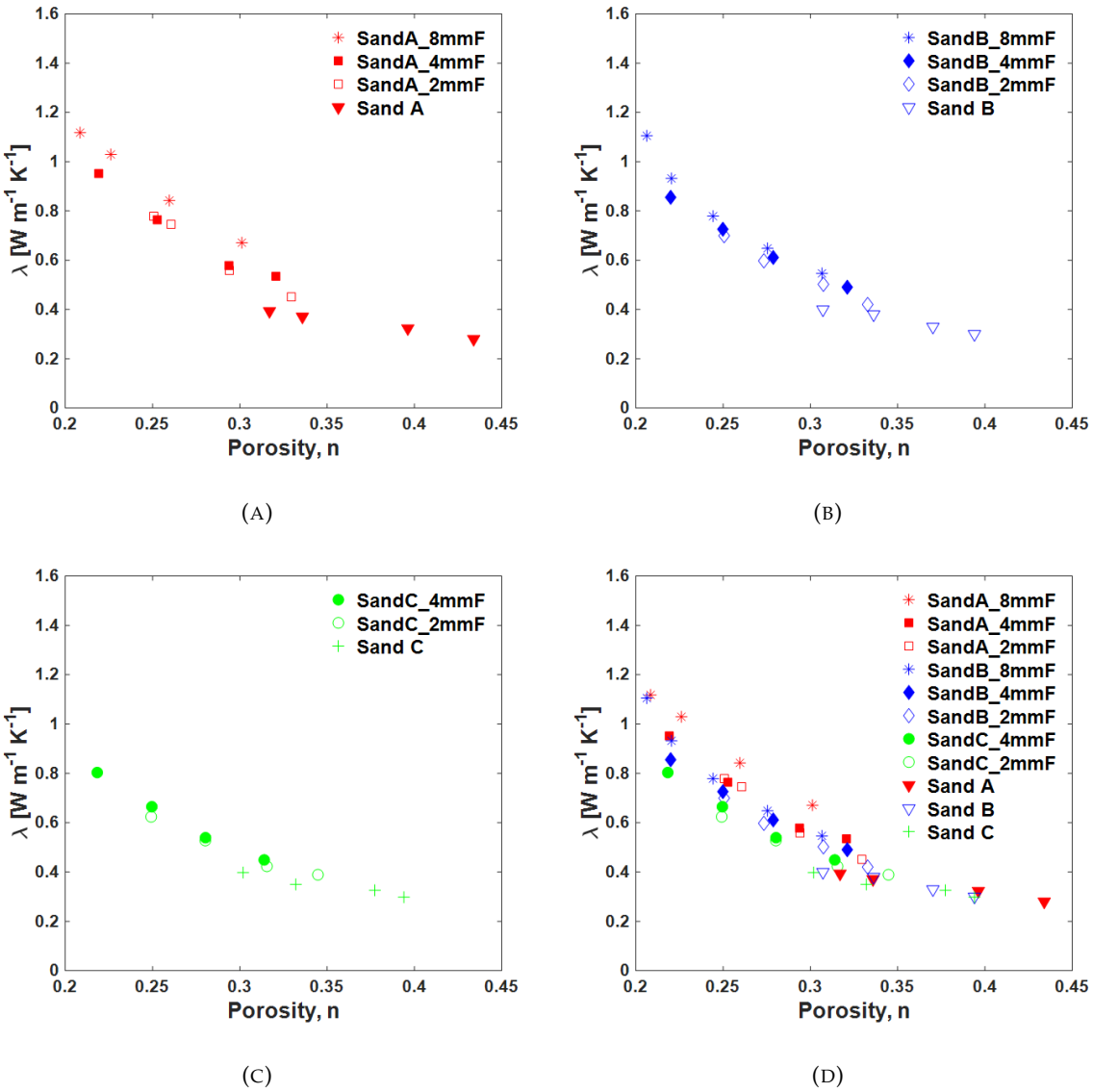

FIGURE 5.1: Thermal conductivity as function of porosity in dry state for original sands and modified sands with bentonite.

gradation of designed mixes. For 4mmF and 2mmF, the lowest porosities are 0.22 and 0.25, respectively for all three sand. Therefore, the dry thermal conductivity values also increase with the increase in maximum particle size of fuller gradation and 8mmF of both sand A and B has the highest thermal conductivity of 1.12 $W\,m^{-1}\,K^{-1}$ and 1.11 $W\,m^{-1}\,K^{-1}$, respectively. However, the dry thermal conductivity values for the same porosity are not remarkably affected by the maximum particle size of fuller gradation. For example, thermal conductivity values are 0.64 $W\,m^{-1}\,K^{-1}$, 0.61 $W\,m^{-1}\,K^{-1}$ and 0.60 $W\,m^{-1}\,K^{-1}$ at a porosity of 0.27 for sandB_8mmF, sandB_4mmF and sandB_2mmF fuller gradations respectively (Figure 5.1b). The porosity is the main factor affecting the dry thermal conductivity of the modified sand and this kind of design mixes helps to produce dense packing and consequently, achieves higher thermal conductivity (Shrestha et al., 2016; Rizvi et al., 2018).

The significant increase in thermal conductivity with a reduction in porosity reflects the

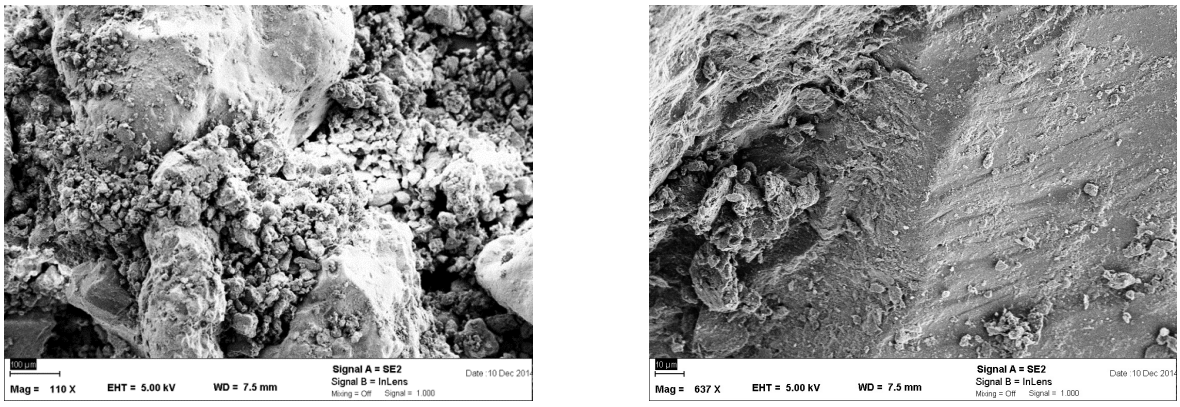

(A) (B)

FIGURE 5.2: SEM images obtained for the modified 4mmF of sand A: (a) bentonite filling the pore space between the sand grains and (b) bentonite filling the gaps within the grain.

increase in the number of contacts per volume and the improvement in heat conduction efficiency. Actually, the number of contacts per volume and contact quality depends on the porosity, particle shape and grain size distributions (Yun and Santamarina, 2007). Because of the fuller graduation and the fine particles filled in the interstitial space that increases the grain to grain conduction path, the thermal conductivity is abruptly increased with decreasing porosity for all modified fuller sands. This phenomenon can be observed through SEM observations. Figure 5.2 represents the SEM images obtained for a modified 4mmF of sand A (sandA_4mmF). In Figure 5.2b, the bentonite filling the gaps of irregularly shaped grains improves the heat conduction path and in Figure 5.2a, the bentonite filled the gap among the grains to bridge the gap by increasing the contact among the grains. In this case, heat is transmitted through much large contact areas rather than through distinct contact points. The advantage of a wide range of particle arrangements in fuller gradation is to attain denser packing and a higher coordination number as the number of contacts per unit volume and inclusion of high conductivity mineral helps to improve the quality of contacts. The fine particles (fillers) act as the bridge at contacts to improve the quality and quantity of interparticle contacts. Hence, the fuller curve gradation with fine particles enhanced the thermal conduction path for granular type soils.

It is also noticed from Figure 5.1d that, the dry thermal conductivity values of modified fuller sands can be arranged in order of sand A > sand B > sand C. For the same fuller gradation mixes, the dry thermal conductivity values of modified sands are different according to the types of sands. The modified sand obtained from sand A has maximum dry thermal conductivity than that of sand B and sand C. For example, 4mmF of sand A, sand B and sand C has the thermal conductivity of about 0.95 $W\,m^{-1}\,K^{-1}$ > 0.86 $W\,m^{-1}\,K^{-1}$ > 0.80 $W\,m^{-1}\,K^{-1}$ at the same porosity of 0.22. This observation might be due to the particle shape and size of the sands since there is no big difference in thermal conductivity despite different quartz contents of the original sands. The quartz content of sands can be ordered in sand A > sand C > sand B. In dry soils, the microstructure is a more influencing parameter than other factors like mineralogy ((Johansen, 1975; Farouki, 1981; Côté and Konrad, 2009)).

The mineralogical effect on thermal conductivity of soils in dry as well as in moist state is discussed in next section 5.2.5.

With stonedust

Figure 5.3 shows the relationship between thermal conductivity and porosity of the original sand and modified fuller sands with stone-dust in the dry state. As shown in Figure 5.3a, the thermal conductivity of modified fuller sand A increases exponentially with a decrease in porosity and attains the maximum thermal conductivity of 1.1 $W\,m^{-1}\,K^{-1}$ for 8mmF modified sand. In the same manner, all the modified fuller sands have significantly higher thermal conductivity than the original sands (Figure 5.3). The measured dry thermal conductivity of modified fuller sands are in the range of from 0.4-1.1 $W\,m^{-1}\,K^{-1}$ for porosities between 0.4 and 0.2.

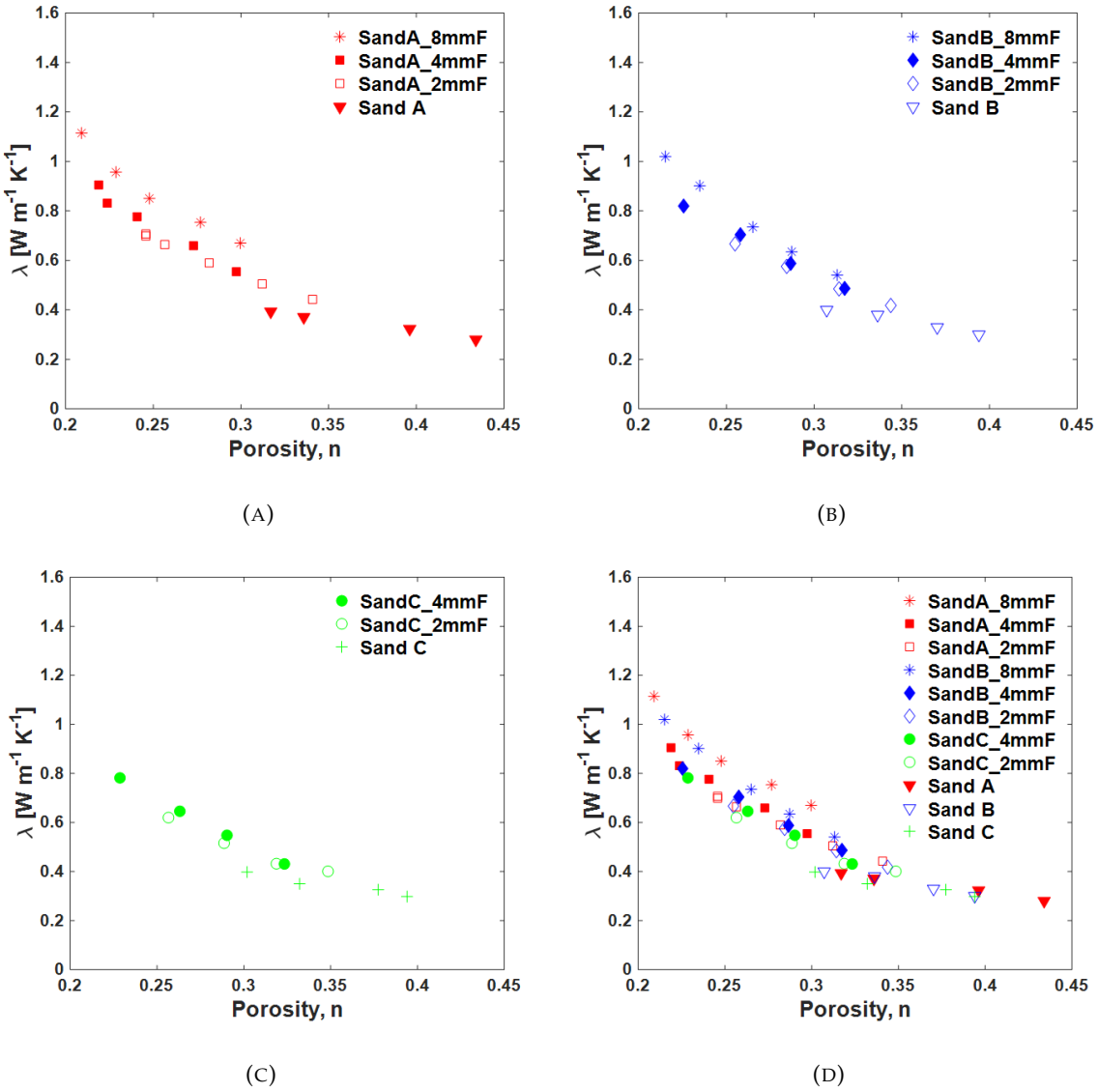

FIGURE 5.3: Thermal conductivity as function of porosity in dry state for original sands and modified sands with stonedust.

The behaviour or the characteristics of a trend of increasing thermal conductivity is quite similar to that of modified fuller sand with bentonite. Because of the graduation and the fine particles filled in the interstitial space that increases the grain to grain conduction path, the thermal conductivity is abruptly increased for all modified fuller sands. Another reason could be the reduction of air voids by the fine particles and the thermal conductivity of air is considerably negligible as compared to that of fine particles. This phenomenon can be observed through SEM observations. Figure 5.7 represents the SEM images obtained for a modified 2mmF of sand A (sandA_2mmF) with stone-dust. In Figure 5.7a, the stone-dust filling the cracks of grains improves the heat conduction path and in Figure 5.7b, the stone-dust filled the gap among the grains to bridge the gap by increasing the contact among the grains. In this case, heat is transmitted through much large contact areas rather than through distinct contact points. It can be said that from the results obtained with bentonite and stone-dust, the adding of fine is important to increase the thermal conductivity of the granular soils regardless of the type of fine content. Though the stone dust consists of higher quartz content (see section 4.5) as compared to bentonite, no remarkable effect is observed due to high quartz content in stone-dust. As explained earlier in Chapter 2, in the dry state the microstructure is a dominant parameter than mineralogy and in this case, the fine particles act as the bridge to improve the quality of contacts and hence improve the thermal conduction between grains. As explained earlier, the mineralogy of the main constituent (sand in this mix) is more attributed to enhance the thermal conductivity of the mixed geomaterials.

With SIC

Figure 5.4 shows the relationship between thermal conductivity and porosity of modified fuller sand with SiC and original sand. The modified fuller sands consist of bentonite instead of stone-dust in this case. It shows that the thermal conductivity increases exponentially with a decrease in porosity. For the 8mm fuller sand, the highest thermal conductivity is achieved at a porosity of 0.22. For the same mix (sandA_8mmF with bentonite), the maximum dry thermal conductivity is 1.12 $W\,m^{-1}\,K^{-1}$ whereas that is 1.33 $W\,m^{-1}\,K^{-1}$ when SiC is added. So, it can be clearly said that this improvement in thermal conduction is entirely due to the mineralogy of SiC. It is worth noting that adding SiC has also a great impact on dry thermal conductivity as it is increased by 30% for the material of the same porosity. The highest dry thermal conductivity value (=1.33 $W\,m^{-1}\,K^{-1}$) for porosity 0.22 attained in this study is also close to that of Fluidized thermal backfill (FTB), liquid cement-sand mixture (Radhakrishna, 1981). This proves that mineralogical composition plays a key role in enhancing thermal conduction if the mineral has very high thermal conductivity. The SiC has high mineral thermal conductivity than quartz mineral. However, this effect on dry thermal conductivity decreases with increasing porosity and the thermal conductivity values converge at a porosity of about 0.35.

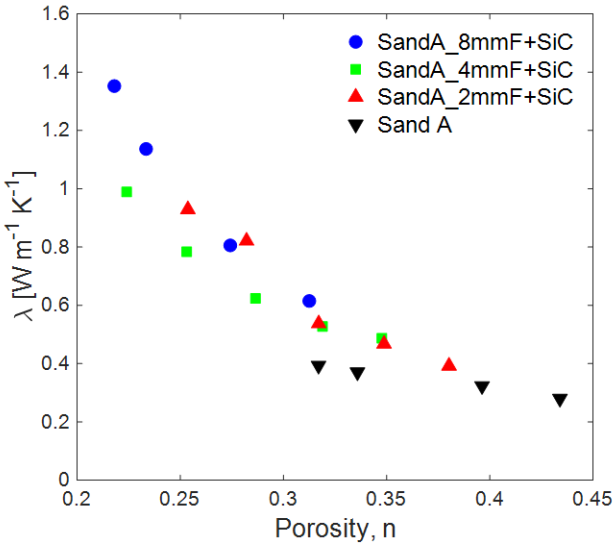

FIGURE 5.4: Thermal conductivity as fuction of porosity in dry state for original sand and modified fuller sand with SiC.

5.2.2 Effect of fine contents on thermal conductivity

In order to know the effect of fine content on the thermal conductivity of dry sand, the different proportion of fine content was added to sand A and the measurement was done. The fine added were bentonite, stone-dust, and kieselguhr. The results shown in Figure 5.5 are from the dense packing for all mixes. The addition of fine particles slightly improve the thermal conductivity in the dry state, but not like in fuller gradation. The stone-dust shows a higher thermal conductivity than others and the content is 30%. At 30% of stone-dust, the optimum thermal conductivity is found to be 0.62 $W\,m^{-1}\,K^{-1}$, which is higher than that of original sand (= 0.39 $W\,m^{-1}\,K^{-1}$). With the increase in fine content, the thermal conductivity increases and reaches optimum value and again starts to decrease. This is typical behaviour of coarse and fine mixtures, which was also noticed by Yun and Santamarina (2007). The optimum content of the fine is different for different fine particles i.e. 30% for stone dust and bentonite and 10% for kieselguhr. The bentonite and stone-dust produce higher dry thermal conductivity than that of kieselguhr, they are used as fine particles in the modified fuller sand.

5.2.3 Effect of saturation on thermal conductivity

Figure 5.6 summaries the experimental results obtained for the thermal conductivity values with respect to the degree of saturation of the original and modified sands for both sand A and B. It shows that full saturation is not achieved for the orginial as well as modified fuller sand. It depends on many factors like soil types, porosity, saturation methods, sample preparation methods, etc. The saturation is reached up to 90 % only because of the saturation method used in this study and the lower porosity. The water is flowing from 1 m height to the specimen which is 10 kPa pore water pressure and that couldn't be enough to replace the entrapped air completely within the soil. However, the saturation reached in this study is in

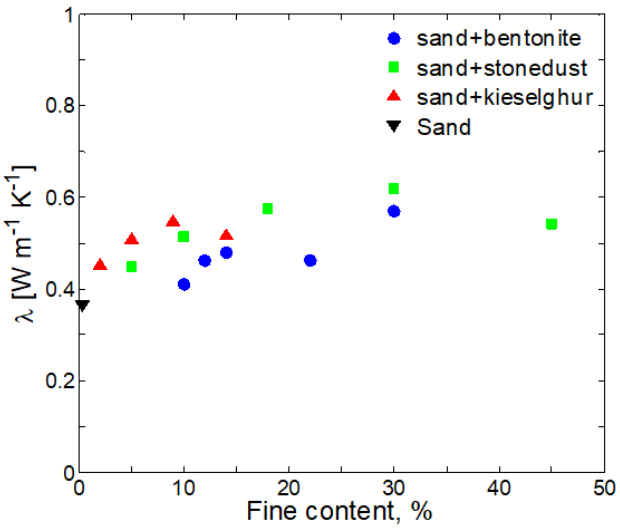

FIGURE 5.5: Thermal conductivity at different fine contents in dry state.

the range of the capillary regime as the range of capillary regime for sand is around 80-100 % and 85-100 % for silt and clay (Dong et al., 2015). In this regime, no further increment of thermal conductivity is found as the pore-water replaces most of the air in the voids.

As expected, the thermal conductivity shows an ascending trend with an increase in the degree of saturation. Moreover, the obtained results follow a general trend of the three saturation regimes. i.e. the pendular regime $S_r \leq 0.2$, characteristics by the substantial variation in thermal conductivity with respect to degree of saturation S_r, the funicular regime S_r = 0.2–0.7, characterized by the mild conduction changes and the capillary regime $S_r \geq$ 0.7, characterized by no significant conduction changes (Shrestha et al., 2019). The thermal conductivity values for the modified fuller sands are higher than that of the original sand across the full range of saturation (0-100 %). The obtained dry thermal conductivity values for the modified 8mmF, 4mmF and 2mmF of sand A are 1.02 $W\,m^{-1}\,K^{-1}$, 0.85 $W\,m^{-1}\,K^{-1}$ and 0.65 $W\,m^{-1}\,K^{-1}$, higher than that (0.365 $W\,m^{-1}\,K^{-1}$) of the original sand A, whereas those for the sand B are 0.96 $W\,m^{-1}\,K^{-1}$, 0.73 $W\,m^{-1}\,K^{-1}$ and 0.51 $W\,m^{-1}\,K^{-1}$ also higher than 0.33 $W\,m^{-1}\,K^{-1}$ of the original sand B. The results show an improvement of 183%, 136% and 80% for 8mmF, 4mmF and 2mmF of sand A, while 191%, 121% and 54% for the 8mmF, 4mmF and 2mmF of sand B in the dry state. Shrestha et al. (2016) also found the improvement of (50– 180) % in the dry state with bentonite. In a similar fashion, the obtained thermal conductivity data for the 8mmF, 4mmF and 2mmF of sand A are 2.54 $W\,m^{-1}\,K^{-1}$, 2.5 $W\,m^{-1}\,K^{-1}$ & 1.5 $W\,m^{-1}\,K^{-1}$, which are comparatively higher than that of the original sand A, 1.2 $W\,m^{-1}\,K^{-1}$ at 10% degree of saturation. On the other hand, at the same 10% degree of saturation, the measured thermal conductivity data for 8mmF, 4mmF and 2mmF of sand B are 1.92 $W\,m^{-1}\,K^{-1}$, 1.75 $W\,m^{-1}\,K^{-1}$ & 1.25 $W\,m^{-1}\,K^{-1}$, which are also higher than that of original sand B (0.7 $W\,m^{-1}\,K^{-1}$). However, it is cleared that sand B and its modified fuller sand have lower thermal conductivity values than sand A due to quartz content and dry density (Shrestha et al., 2019; Shrestha et al., 2018).

During the pendular regime, the thermal conductivity of modified sands increases rapidly

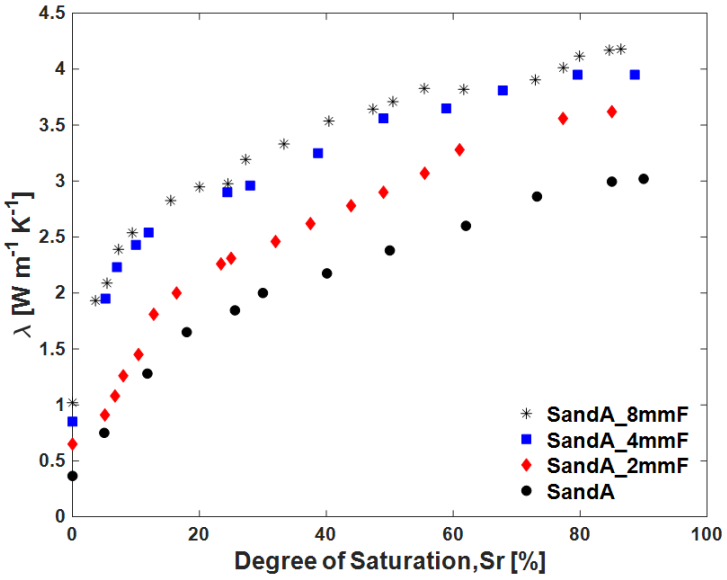

(A)

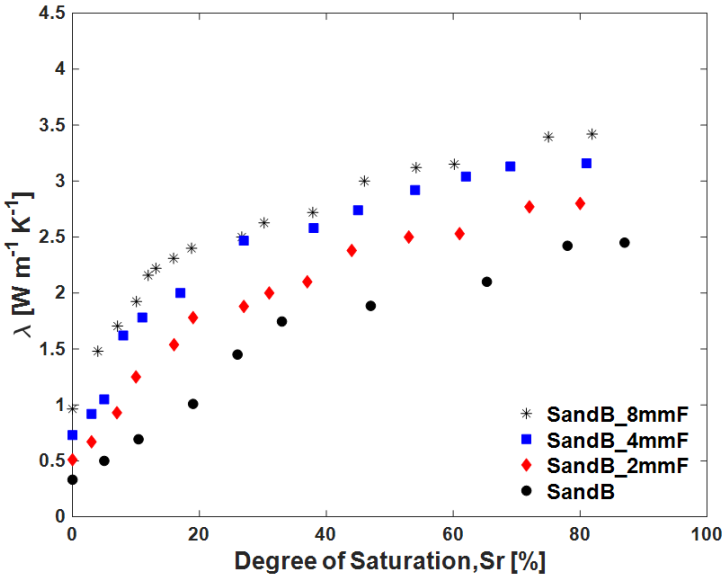

(B)

FIGURE 5.6: Thermal conductivity as function of degree of saturation for modified and original sand A (a) and sand B (b) with stonedust.

than that of original sand as heat is transmitted through the solid phase via the contact points between the grains. Because of the graduation and the fine particles filled in the interstitial space that increases the grain to grain conduction path and the addition of moisture starts to bridge between soil grains. This phenomenon can be observed through SEM observations. Figure 5.7 represents the SEM images obtained for a modified 2mmF of sand A. In Figure 5.7a, the stone dust filling the cracks of grain improve the heat conduction path and in Figure 5.7b, the stone dust filled the gap among the grains to bridge the gap by increasing the contact among the grains. In this case, heat is transmitted through much large contact areas rather than through distinct contact points. The thermal conductivity of the 8mmF and

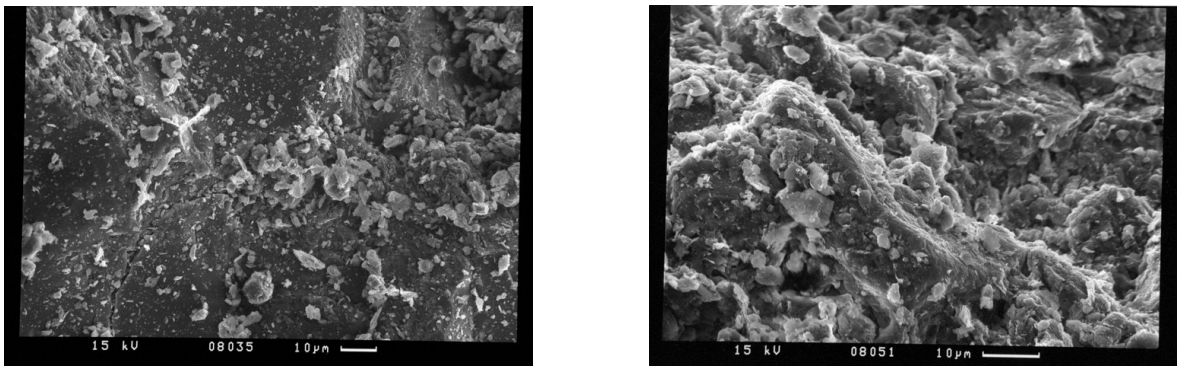

(A) (B)

FIGURE 5.7: SEM images obtained for the modified 2mmF of sand A: (a) stone dust filling the cracks in grain and (b) stone dust filling the pore space between the sand grains.

4mmF has sharply increased while that of the 2mmF has not increased in the range (0–5) % of saturation because the 2mmF has more fine particles than the 4mmF % 8mmF and it needs more water to bridge the soil grains. Lu et al. (2007) also noticed this phenomenon with fine-textured soils. After this regime, the increase in thermal conductivity depends mainly on the replacement of air by water, and as a result, the thermal conductivity increases slowly during the funicular regime. That's why the rate of increment is almost identical for the modified and the original sand. No more conduction changes are observed during the capillary regime because most solid particles are already connected and the addition of water will not increase the thermal conductivity. It is also observed that the thermal conductivity values of sandA_8mmF and sandB_8mmF are slightly higher than that of sandA_4mmF and sandB_4mmFhas at various water content, though 8mmF has remarkably higher dry thermal conductivity than that of 4mmF for both sand A and B. This could be because of dense packing in both fuller gradations and a small amount of water is enough to trigger a change in thermal conductivity in both cases. The thermal conductivity of the original, as well as the modified sand for sand B, are less than that of sand A over the full range of saturation because sand B has comparatively less quartz content than sand A. As explained earlier in Chapter 2, the mineral plays a vital role to enhance the thermal conductivity in the moist state.

5.2.4 Effect of dry density and saturation on thermal conductivity

Figure 5.8 shows the relation between the thermal conductivity and dry density at different degrees of saturation for sand A and B. In the figures, the variation in dry densities represents the densities of modified fuller sands of 8mmF, 4mmF, & 2mmF and sand. These densities are the maximum possible densities that can be attained with conventional compaction for respective modified fuller sand and original sand. The highest dry density (ρ_d = 2.08 g cm^{-3}) was achieved for 8mmF and the dry density is decreased with decreasing maximum particle size of fuller sands. For example, the fuller sandA_4mmF owing maximum

particle size of 4mm has a dry density of 2.04 g cm^{-3}, the dry density of 2mmF owing maximum particle size of 2mm is 1.95 g cm^{-3} and finally, that of sand-A is 1.71 g cm^{-3}. Similarly, for sand-B, the dry densities of sandB_8mmF, sandB_4mmF, sandB_2mmF, and sand-B are 2.08 g cm^{-3}, 2.02 g cm^{-3}, 1.92 g cm^{-3} and 1.71 g cm^{-3}, respectively. As expected, the thermal conductivity increases with an increase in dry density at various water content (or degree of saturation). It is noticed that the change in thermal conductivity is mild at lower (below 2 g cm^{-3}) and higher densities (above 2 g cm^{-3}). However, the thermal conductivity increases drastically from lower to higher densities (1.95 to 2.04 g cm^{-3}). The increment in the thermal conductivity between the saturation degree of 0 and 25% is relatively high than other saturation degrees regardless of dry density. This increment is even very high in the case of higher densities greater than 2.0 g cm^{-3}. The reason behind this increment is that heat is transmitted through the solid phase via the contact points between the grains. The dense density is achieved due to gradation and the fine particles filled in the interstitial space that increases the grain to grain conduction path and the addition of moisture starts to bridge between soil grains which leads to increase the thermal conductivity.

5.2.5 Effect of mineralogy on thermal conductivity

As discussed earlier in chapter 2, the mineralogy also affects the thermal conductivity of soils. From the experimental results obtained in this study, two key findings are noticed regarding the mineralogy effects. The first one is that despite the difference in quartz content in original sand, no significant difference in thermal conductivity is found in the dry state. Figure 5.9 shows the thermal conductivity as a function of porosity in the dry state for all modified and original sand. The conductivity is sharply increased with a decrease in porosity in the case of modified fuller sand, while a gradual increase is noticed in the case of original sand. In both cases, the mineralogy has less influence on the dry thermal conductivity of modified and original sand. Sand A has almost all of the quartz (99% quartz) whereas sand B and sand C have respectively quartz contents of 70% and 80%. In dry soils, the microstructure is more prominent than mineralogy (Johansen, 1975; Farouki, 1981; Yun and Santamarina, 2007; Côté and Konrad, 2009).

But it is also evident that if the highly conductive material is added to soil, the difference in thermal conductivity is somehow noticed. In this study, SiC was added to modified fuller sand A and the thermal conductivity of that mix was measured. The results are shown in Figure 5.10. The effect is more significant at the lowest porosity. For example, the maximum dry thermal conductivity of the sample sandA_8mmF is 1.12 W m^{-1} K^{-1} whereas that is 1.33 W m^{-1} K^{-1} for the same porosity of 0.22 when SiC is added to the same mix. So, it can be clearly said that this improvement in thermal conduction is completely due to the mineralogy of SiC. It is worth noting that adding SiC has also a great impact on dry thermal conductivity as it is increased by 30% for the material of the same porosity. However, this effect on dry thermal conductivity decreases with increasing porosity and the thermal conductivity values converge at a porosity of about 0.35.

The second one is that the mineralogical effect is noticed in unsaturated as well as in the saturated state. Figure 5.11 shows the thermal conductivity measurement of modified fuller

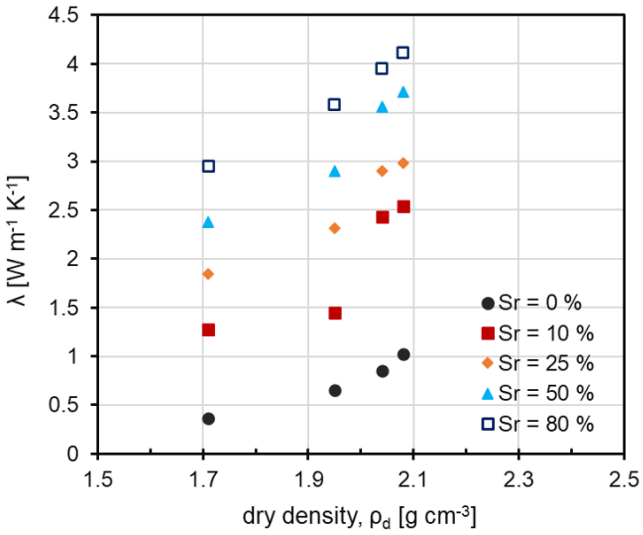

(A)

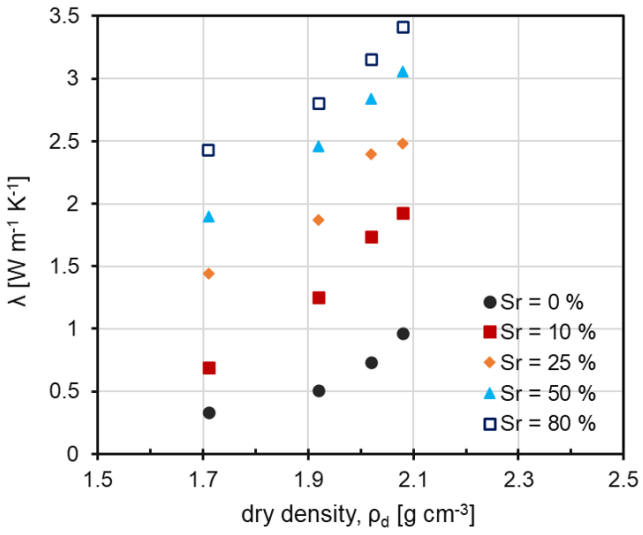

(B)

FIGURE 5.8: Thermal conductivity as function of dry density at different saturation of degree for (a) sand A and (b) sand B.

sand A and B with stone-dust. The thermal conductivity of modified as well as original sand A is remarkably higher than that of sand B fur the full range of degree of saturation. This is due to the mineralogical content of sands. Sand A has higher quart content than sand B (Table 4.1). As explained earlier, quartz is the dominant minerals in the soil as it has a thermal conductivity of 7.7 $W\,m^{-1}\,K^{-1}$. That's why most of the prediction models which consider the effect of minerals and include the thermal conductivity of quartz are more successful than other models. Like Johansen (1975), Côté and Konrad (2005a), Lu et al. (2007), Balland and Arp (2005), and Haigh (2012) are some prediction models which consider the thermal conductivity of minerals.

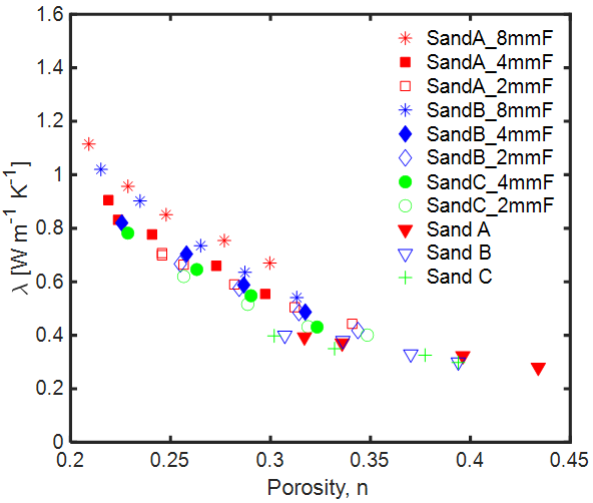

FIGURE 5.9: Thermal conductivity as function of porosity for original sands and modified fuller sands with stonedust.

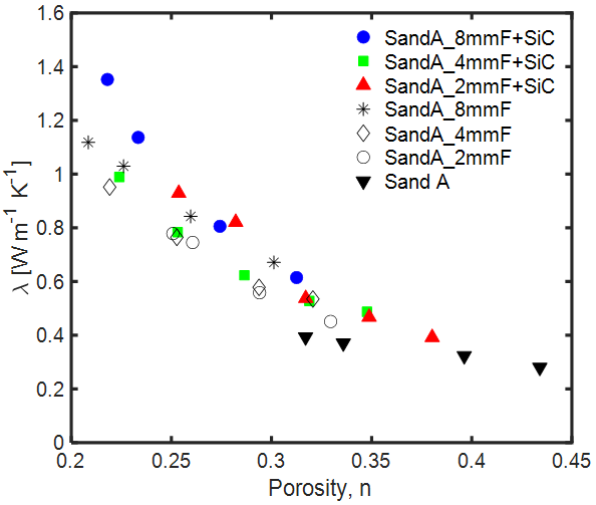

FIGURE 5.10: Thermal conductivity as function of porosity for modified fuller sands with and without SiC.

5.3 Improvement in thermal conductivity

The improvement in thermal conductivity can be discussed in two different conditions; (a) dry state and (b) moist state, because it is noticed from the experimental results that the improvement is higher in the dry state as compared to the moist state.

5.3.1 Dry state

The improvement in the thermal conductivity of modified fuller sands can be distinctively observed from Figures 5.12 & 5.13 with bentonite and stone-dust, respectively in dry condition. The improvement in thermal conductivity (I) is calculated using Equation 5.1 , where the thermal conductivity of original sand is taken as the average measured thermal conductivity of original sands A, B and C.

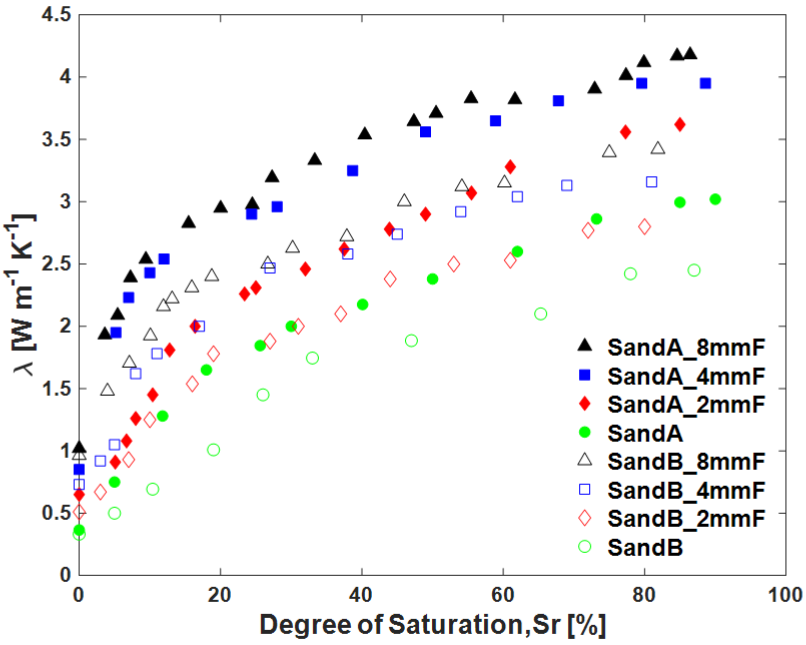

FIGURE 5.11: Thermal conductivity vs degree of saturation for modified fuller sands A and B with stonedust.

$$I = \frac{\lambda_{modified} - \lambda_{original}}{\lambda_{original}} \tag{5.1}$$

where $\lambda_{modified}$ ($W\,m^{-1}\,K^{-1}$) and $\lambda_{original}$ ($W\,m^{-1}\,K^{-1}$) are thermal conductivity of modified fuller sand and original sand, respectively, I (%) is an improvement in thermal conductivity. The average thermal conductivity values are 0.342 $W\,m^{-1}\,K^{-1}$, 0.342 $W\,m^{-1}\,K^{-1}$ and 0.343 $W\,m^{-1}\,K^{-1}$ for sand A, B and C, respectively. The thermal conductivity values are increased by 10- 230% for all modified fuller sands. From the figures 5.12 & 5.13, it is clearly noted that the greatest improvement (about 230%) is found with the 8mmF of sand A & B at their lowest porosity while the lowest improvement is found with 2mmF of sand A & B at their highest porosity. It confirms that the bigger particle sizes enhance thermal conduction better. The thermal conductivity is decreased with a decrease in maximum particle size and consequently, 2mmF has the lowest improvement in thermal conductivity.

According to the denseness of the materials, the improvement in thermal conductivity varies. In the loose state (i.e. maximum porosity), the improvement is less and this keeps increasing with decreasing porosity and it becomes maximum at the lowest porosity (i.e. dense packing). This characteristic is noticed with all modified fuller sand. For the porosities range from 0.2-0,35, the improvements in thermal conductivity for 8mmF, 4mmF and 2mmF of sand A with both bentonite and stone-dust are 90-230 %, 50-170% and 25-120%. The main advantage of adding fine particles is to act as a bridge at contacts to improve the quality and quantity of contacts. In this case, heat is conducted through much large contact areas rather than through distinct contact points. Despite the different types of fine materials, both fine materials contribute in the same way. So, the main important factor is a certain amount

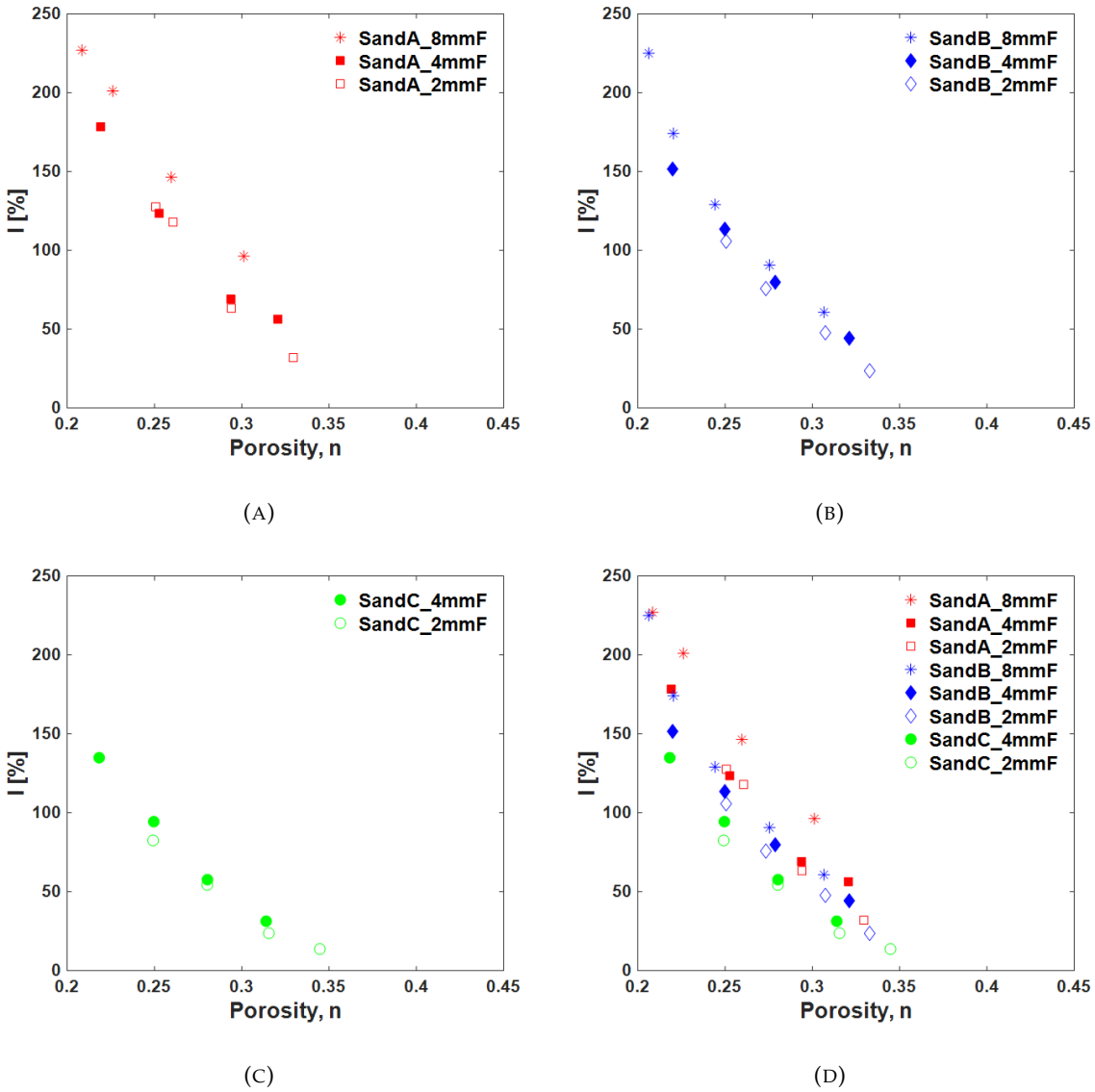

FIGURE 5.12: Improvement in thermal conductivity vs. porosity for modified fuller sands with bentonite.

of fine particles can enhance the thermal conductivity with wide a range of particles by attaining lower porosity (i.e dense packing).

A significant improvement in thermal conductivity is achieved for modified fuller sand of both sand A and B in dry conditions. The maximum dry thermal conductivity of 1.12 $W\,m^{-1}\,K^{-1}$, which is itself 230% increment from the original thermal conductivity, is attained at the lowest porosity (dense packing) for 8mmF modified sand. Even in the loose state for 8mmF, the thermal conductivity is about 0.6 $W\,m^{-1}\,K^{-1}$, still improved by 80% than the thermal conductivity of original sand. (Drefke et al., 2015) also found the improvement in the thermal conductivity in the dry state in the case of coarse-grained liquid soil only as it predominantly consists of well-graded quartz sand. So, the shape and size of the particles and mineral content are the vital factors to affect the thermal conductivity. As stated earlier in chapter 2, the dry thermal conductivity of natural soil is less than 0.5 $W\,m^{-1}\,K^{-1}$. In this study, the dry thermal conductivity of natural sand is significantly enhanced by just

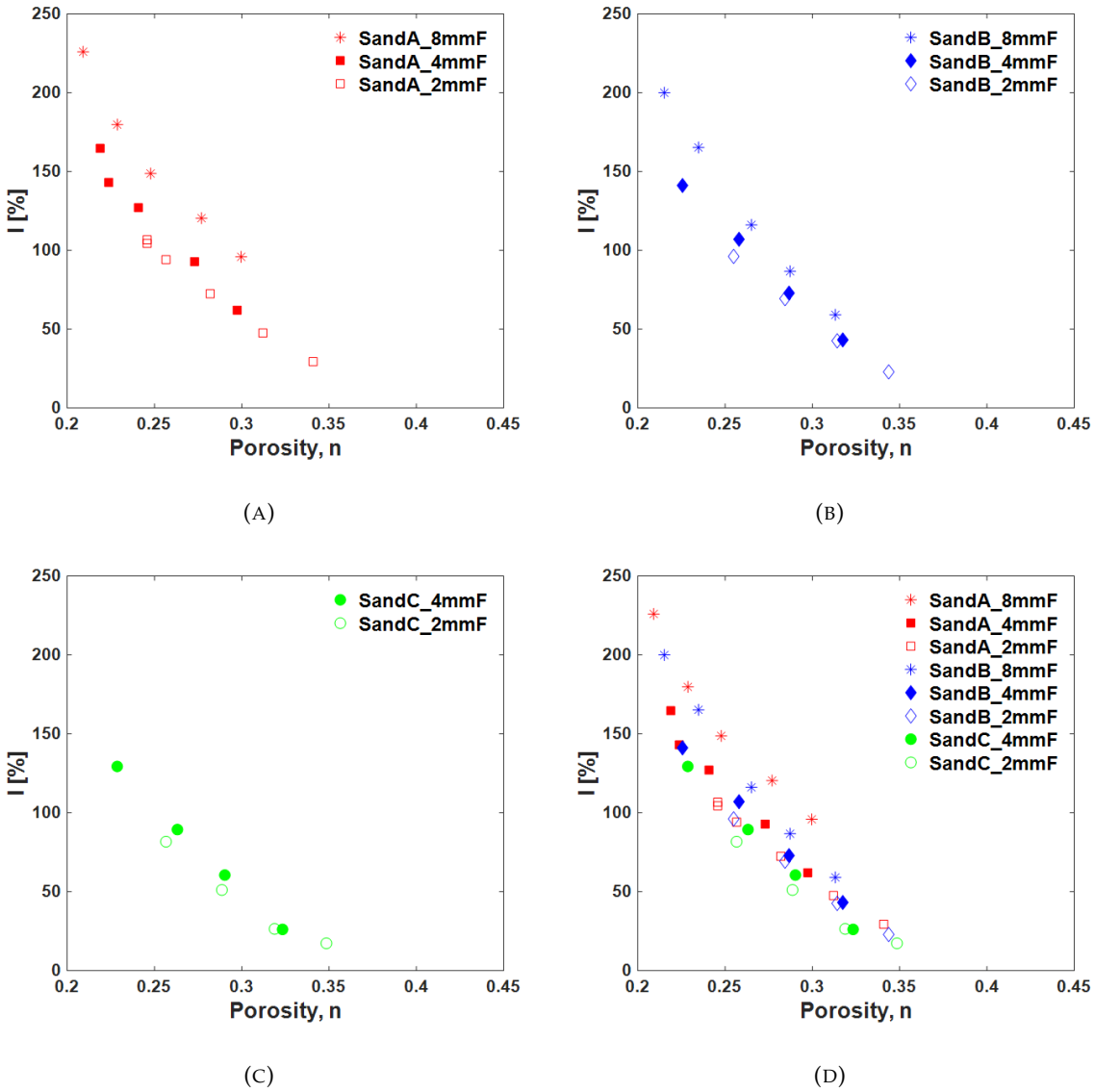

(A) (B)

(C) (D)

FIGURE 5.13: Improvement in thermal conductivity vs. porosity for modified fuller sands with stonedust.

changing gradation and adding fillers, which is the main objective of this study.

5.3.2 Moist state

The thermal conductivity values for both modified sand A and B are found to be higher than that of original sand across the full range of saturation. Figure 5.14 shows the improvement in thermal conductivity over the various degree of saturation for modified fuller sands of A and B. In this case, the improvement is calculated using the same Equation 5.1, where the thermal conductivity of the original sand is taken as the measured thermal conductivity of original sand A and B at the respective degree of saturation. For example, the obtained thermal conductivity data for the 8mmF, 4mmF and 2mmF of sand A are 2.54 $W\,m^{-1}\,K^{-1}$, 2.5 $W\,m^{-1}\,K^{-1}$ & 1.5 $W\,m^{-1}\,K^{-1}$, which are comparatively higher than that of the original sand, 1.2 $W\,m^{-1}\,K^{-1}$ at 10% saturation. It means about 112%, 108% and 25% improvements

are achieved for the 8mmF, 4mmF and 2mmF respectively at 10% saturation. For the full range of saturation, the improvement of (22–80) % for the sandA_2mmF, (35–136)% for the sandA_4mmF and (40–180)% for the sandA_8mmF are achieved. The improvement is highest at the dry state and decreases with an increase in the saturation degree. This observation is due to the filling of air void (λ = 0.0024 $W\,m^{-1}\,K^{-1}$) with the stone dust of dominant quartz content (λ_q = 7.7 $W\,m^{-1}\,K^{-1}$). The improvements of 22%, 35% and 40% are achieved for the 2mmF, 2mmF and 8mmF of sand A, whereas 15%, 30% and 40% are achieved in the 2mmF, 4mmF and 8mmF of sand B, respectively at full saturation. In the same manner, (Drefke et al., 2015) also found the improvement in thermal conductivity in the wet state in the case of both materials; coarse-grained liquid soil and fine-grained backfill material by adding highly heat-conductive additives. So, the shape and size of the particles and mineral content are the vital factors to affect the thermal conductivity. The obtained dry thermal conductivity values for the modified 8mmF, 4mmF and 2mmF of sand A are 1.02 $W\,m^{-1}\,K^{-1}$, 0.85 $W\,m^{-1}\,K^{-1}$ and 0.65 $W\,m^{-1}\,K^{-1}$, higher than that (0.365 $W\,m^{-1}\,K^{-1}$) of the original sand A, whereas those for the sand B are 0.96 $W\,m^{-1}\,K^{-1}$, 0.73 $W\,m^{-1}\,K^{-1}$ and 0.51 $W\,m^{-1}\,K^{-1}$ also higher than a thermal conductivity (0.33 $W\,m^{-1}\,K^{-1}$) of the original sand B. The results show an improvement by 183%, 136% and 80% for 8mmF, 4mmF and 2mmF of sand A, while 191%, 121% and 54% for the 8mmF, 4mmF and 2mmF of sand B in the dry state. This shows a significant improvement in the dry and the lower saturation states and a moderate improvement in the high saturation. In the same manner, there is an improvement of (15–56) % for the 2mmF, (30–121) % for the 4mmF and (40–191) % for the 8mmF in case of sand B. The thermal conductivity of the original, as well as the modified sands for sand B, are less than that of sand A over the full range of saturation because sand B has comparatively less quartz content than sand A.

For the backfill materials used for underground power cables, the problem is the dryness of the materials as it has a very low thermal conductivity in the dry state as compared to the moist state. In this study, the greatest improvement is achieved in a dry state as compared to a moist state, which is a very essential requirement in terms of backfill materials development. This improvement helps underground power cables to carry the current to full capacity and increase the life of the cable by dissipating the heat generated from the cable to the surrounding soil.

5.4 Relation between proctor density, water content and thermal conductivity

Measuring the thermal conductivity at proctor density and various water content is a very essential step while designing the thermal backfills as the backfill materials are compacted in the site using proctor density and optimum water content. The thermal conductivity values were measured at various proctor densities and corresponding moisture contents. The results are shown in Figure 5.15 for modified fuller sands of sand A.

The samples were prepared at different water contents and subjected to the same compaction effort. The density, therefore, varies with water content and showing a maximum

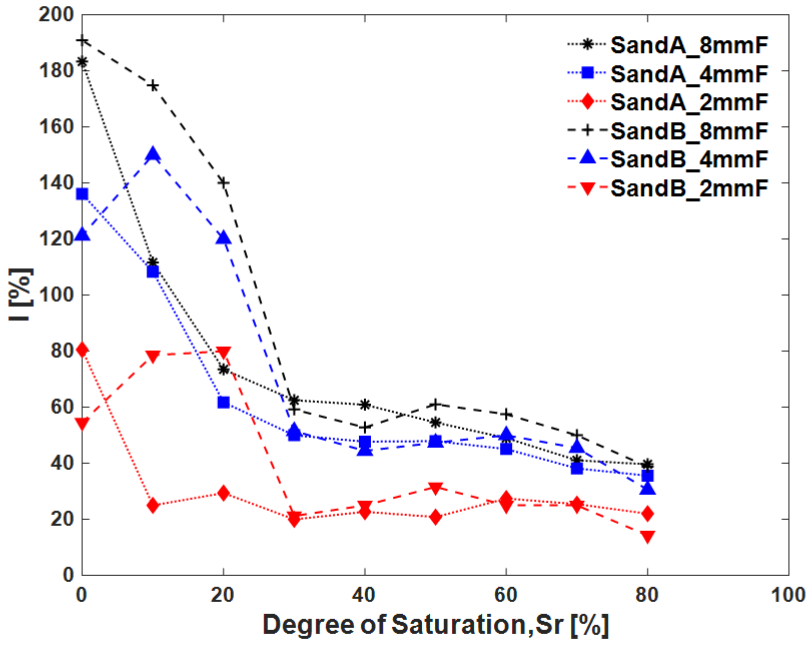

FIGURE 5.14: Improvement in thermal conductivity as function of degree of saturation for modified fuller sands A and B with stonedust.

dry density at the optimum water content. The maximum dry densities of modified fuller sands:sandA_8mmF, sandA_4mmF, and sandA_2mmF are 2.09 g cm^{-3}, 2.01 g cm^{-3} and 1.96 g cm^{-3} at corresponding optimum water contents of 7.0%, 8.2% and 9.5%, respectively while that of original sand A is 1.71 g cm^{-3} at an optimum water content of 11%. The dry densities including peak dry density of sandA_8mmF are higher than that of sandA_4mmF, sandA_2mmF and original sand A. With an increase in maximum particle size of fuller gradation, the dry densities increase for the same water content. It can be said that a wide range of particles with fine materials can produce dense packing (i.e. lowest porosity).

The thermal conductivity of modified sands also varies with density. The highest thermal conductivity value coincides with maximum dry density at optimum water content; 4 W m^{-1} K^{-1} for both 8mmF and 4mmF and 3.4 W m^{-1} K^{-1} for 2mmF of sand A. At the dry side of optimum, the thermal conductivity varies abruptly with water content and dry density. For example, the thermal conductivity of 8mmF of sand A is about 3.63 W m^{-1} K^{-1} at a water content of 4.6% and dry density of 2.05 g cm^{-3}. When the water content is changed from 4,6% to 2.6%, the thermal conductivity is reduced drastically to 1.98 W m^{-1} K^{-1}. However, at the wet side of optimum, the thermal conductivity values don't vary with water content and density since most solid particles are already connected and the addition of water will not increase the thermal conductivity. Adams and Baljet (1968) also noticed the same behaviour for well-graded sand and stone screening. Obviously, for a particular soil, the thermal conductivity depends on both density and moisture content. But, the more influencing factor is moisture content (Johansen, 1975; Farouki, 1981; Côté and Konrad, 2005a; Lu et al., 2007). This is also proved from the results obtained in this study. The thermal conductivity of modified fuller sand and original sand A can be arranged in order of 8mmF >

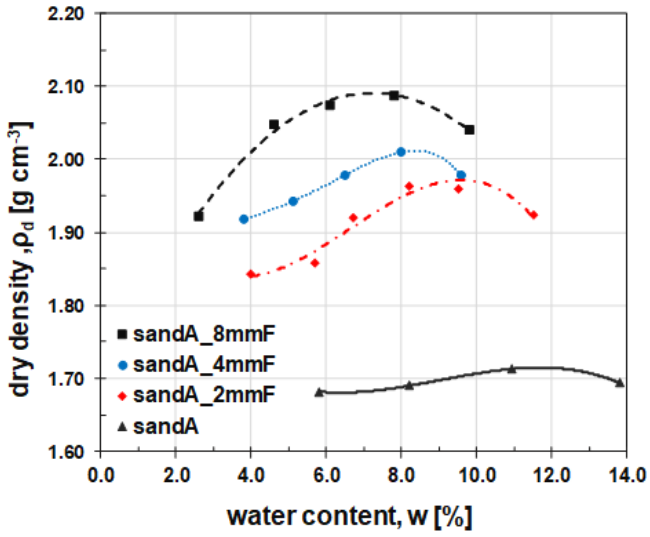

(A)

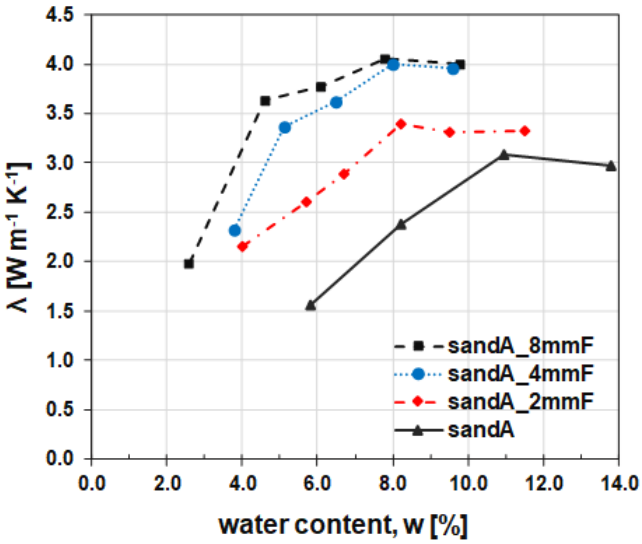

(B)

FIGURE 5.15: Dry density (a) and thermal conductivity (b) at various water content for modified fuller sands and original sand A with stonedust.

4mmF > 2mmF > sand-A. The same observations are also noticed in the Figure 5.6a as shown earlier. However, the thermal conductivity of 8mmF is slightly higher than that of 4mmF at wet side of optimum. The fuller gradation owning maximum particle size (8mmF in this study) attain the lowest porosity and hence produces the highest thermal conductivity than others.

5.5 Comparison of experimental results with prediction models

In this section, all the experimental results obtained are compared to existing theoretical and semi-empirical prediction models. The thermal conductivity prediction models have been

already described in detail in the previous chapter's section 2.6.

5.5.1 Two phase prediction models

As described in section 2.6, several two-phase models for the predicting thermal conductivity of soils exist. Soil exits in either two or three phases. These models are especially for two-phase soils, consist of fluid and continuous solid medium. The state is defined according to the fluid-filled by either air or water. The state is defined as dry when it is filled by air while that is defined as saturated when it is filled by water. In this study, the measured thermal conductivity in the dry state is compared with the most commonly used and popular prediction models; theoretical and semi-empirical prediction models. Most theoretical models have been developed for two-phase soils (Hashin and Shtrikman, 1962; Gori and Corasaniti, 2004; Maxwell, 1954; De Vries, 1963; Yun and Santamarina, 2007; Smith, 1942; Woodside and Messmer, 1961; Kunii and Smith, 1960) while few models for three-phase soils (Mickley, 1951; Tong et al., 2009; Haigh, 2012) have been developed.

Theoretical prediction models

Figure 5.16 presents a comparison of all measured thermal conductivity values of modified and original sands with theoretical models. The theoretical models are computed assuming that the thermal conductivity of quartz and air are $\lambda_{mineral}$ = 7.7 $W\,m^{-1}\,K^{-1}$ and $\lambda_{mineral}$ = 0.024 $W\,m^{-1}\,K^{-1}$ at 20^{o}C. The thermal conductivity of solid particles is calculated by using the geometric mean (GM) equation proposed by Johansen (1975). The thermal conductivity of all samples drops sharply from that of quartz (Figure 5.16). As expected, all measured thermal conductivity values are between Weiner bound (series and parallel flow model) and Hashin and Shtrikman Bound (Hashin and Shtrikman, 1962). The geometric mean yields the values between parallel and series models. The three models series, parallel and GM have been used by many researchers as a basis to develop other theoretical and semi-empirical models. The geometric mean method overestimates the thermal conductivity of all studied samples while cubic cell (Gori and Corasaniti, 2004) underestimates the measured thermal conductivity. The geometric mean method only gives satisfactory results when the ratio of thermal conductivity of solids to that of fluids (either liquid or gas), $\lambda_s/\lambda_f < 15$ (Côté and Konrad, 2005a). In this case, the air being fluid, $\lambda_s/\lambda_f > 100$ leads to an overestimation of thermal conductivity. However, the GM model has a good prediction for saturated cases (Johansen, 1975; Farouki, 1981; Côté and Konrad, 2005a; Balland and Arp, 2005; Lu et al., 2007). Maxwell (1954) model is identical to Hashin and Shtrikman (1962) upper boundary model.

The Volume Fraction (VF) model with fitted parameter 's=-0.25' gives average prediction for all modified fuller sands but not for original sands. Since the VF model considers volumetric fractions and bulk conductivity of each phase, the model can predict the average thermal conductivity of modified fuller sands but without providing any significant meaning of the fitting parameter. On the other hand, the Log model predicts well for original sand but underestimates the thermal conductivity of modified fuller sand. The Log model

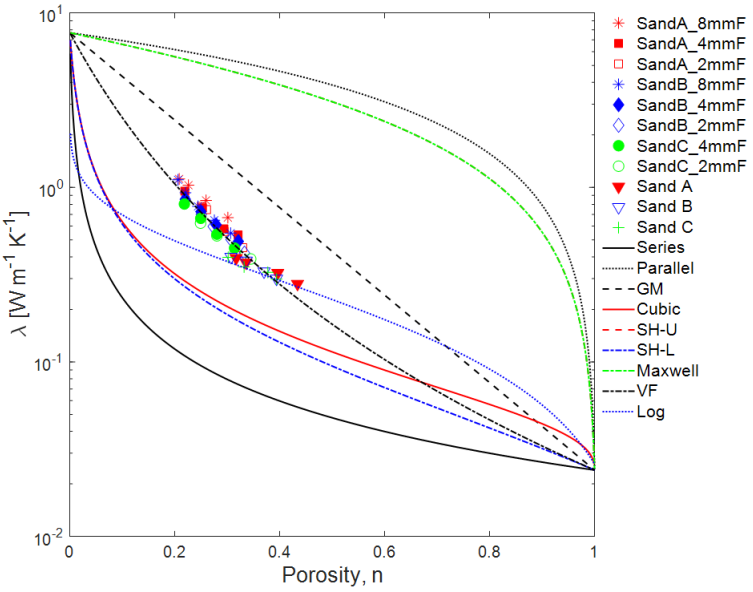

FIGURE 5.16: Comparison of experimental results with theoretical models.

is also fitted with fitting parameters. It is also observed from Figure 5.16 that the theoretical models provides the boundary of thermal conductivity values.

Empirical prediction models

Figure 5.17 shows experimental thermal conductivity values against the porosity with empirical thermal conductivity models. All the models for soils except Balland and Arp (2005) model underestimate experimental thermal conductivities of modified fuller sands. Nevertheless, these models are able to show good agreement with experimental data for original sand. This is probably due to the fact that these models are primarily based on dry density (or porosity) of media and lack considerations of inherent presence of contacts quality and quantity in dry soils. Balland and Arp (2005) overestimates the experiment results of both original and modified sand as the model depends on empirical parameters which govern the thermal conductivity of solid particles. The Balland and Arp (2005) model is based on the mainly dry density of the soils and thermal conductivity of solid soils. If the thermal conductivity of solid soils is considered as 3 $W\,m^{-1}\,K^{-1}$, it will give the same prediction as Johansen (1975) model. In this case, the thermal conductivity of solid soil is calculated using Equation 2.35 taking thermal conductivity of quartz 7.7 $W\,m^{-1}\,K^{-1}$ and 2.0 $W\,m^{-1}\,K^{-1}$ for other minerals. The reason for overestimating thermal conductivity values is taking a higher value of thermal conductivity of soil solids (λ_s = 6.29 $W\,m^{-1}\,K^{-1}$) in this case. However, the Balland and Arp (2005) model cab be referred to as boundary models for thermal conductivity of modified fuller sand.

The comparison between theoretical and experimental results suggest that thermal conductivity models should not only consider volumetric function and bulk conductivity of each constituent but also the inherent presence of contacts in granular materials. On the

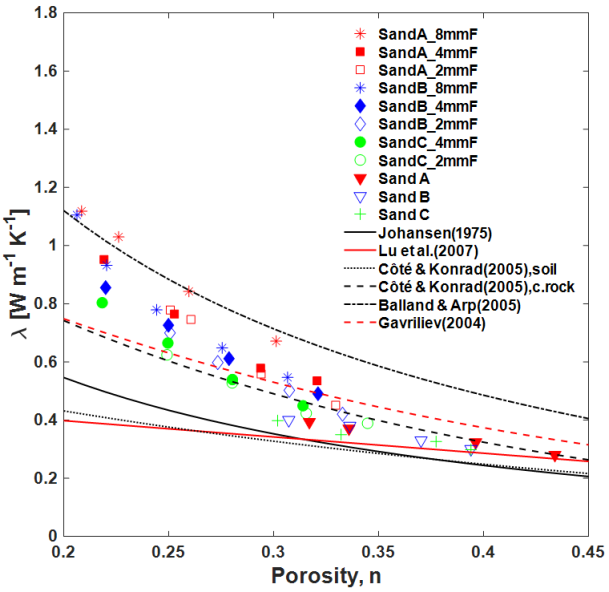

FIGURE 5.17: Comparison of experimental results with semi-empirical models.

other hand, the comparison between empirical and experimental results shows the importance of microstructure effects as well as porosity (dry density). The development of thermal conductivity models in dry soils must identify that interparticle contacts play a decisive role in heat transfer. Most of the models discussed here simplify the problems by including several assumptions associated with the aforementioned factors that affect the thermal conductivity of soils. Consequently, most of the existing methods fail to consider inherent characteristics of particle behaviour contacts, microstructure, etc. That's why an alternative simple method is needed to fulfil this gap. Therefore, an artificial neural network approach has been developed in this study to effectively model the dry thermal conductivity of modified fuller sand.

5.5.2 Theoretical and empirical prediction models over full range of saturation

The measured thermal conductivity values are also compared with semi-empirical prediction models as depicted in Figures 5.18 and 5.19. The thermal conductivity is plotted against the degree of saturation in these figures. The saturated thermal conductivity (λ_{sat}) and solid thermal conductivity (λ_s) were calculated using Equation 2.34 and 2.35, respectively for all semi-empirical prediction models used for the comparison. Since the dry densities and quartz contents of sand A & B and modified fuller sand; sandA_2mmF, sandA_2mmF, sandA_2mmF, sandA_2mmF, sandA_2mmF, sandA_2mmF are different (ref Chapter 3), the prediction models were calculated using these values and the results are presented in Figures 5.18a - 5.18d and 5.19a - 5.19d.

All semi-empirical models show good agreement with natural sands A & B as well as modified sands 2mmF of both sand. But, Haigh (2012) model couldn't predict the effective

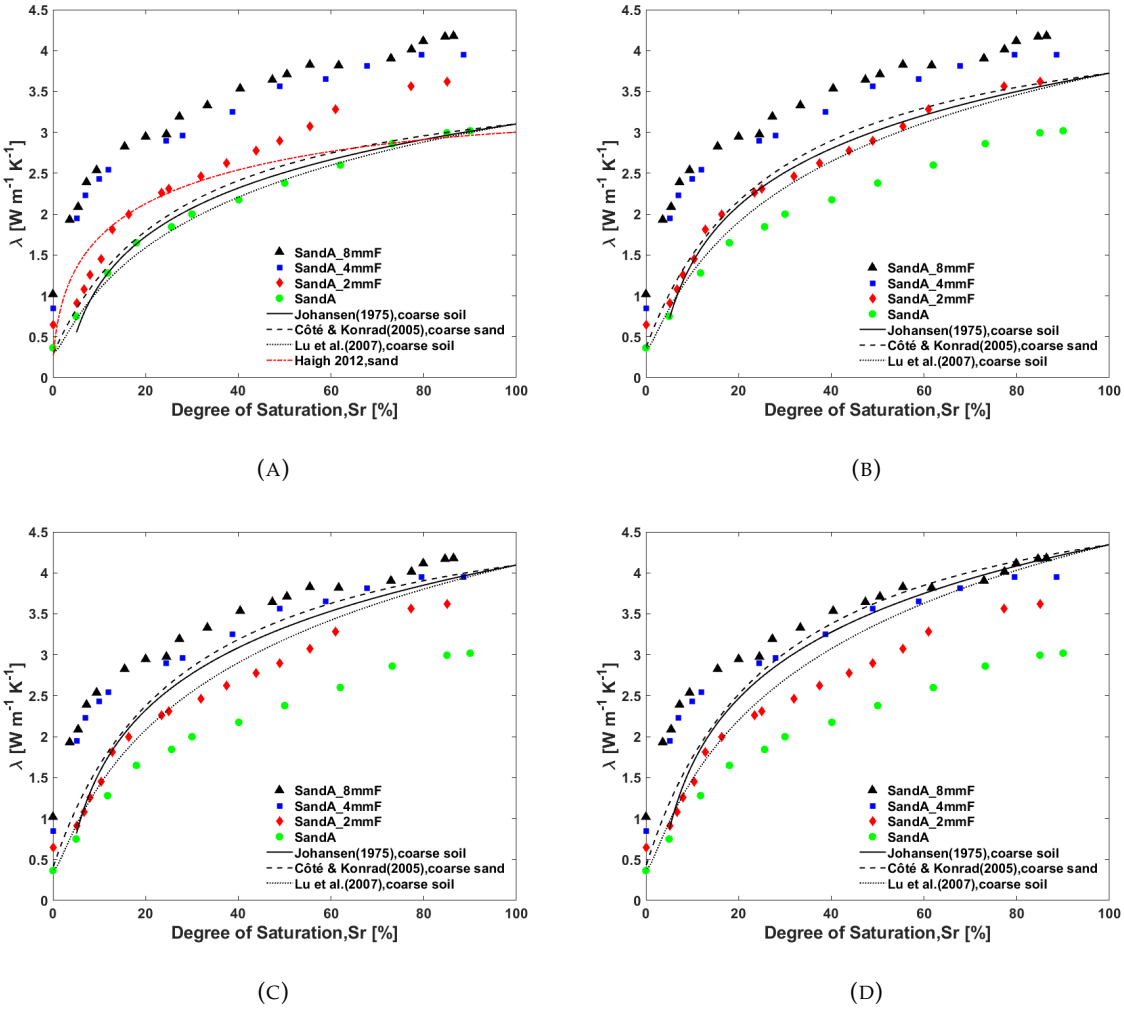

FIGURE 5.18: Comparision of experimental results with semi-empirical models for (a)sand-A, (b)2mmF, (c)4mmF & (d)8mmF.

thermal conductivity for the modified fuller sand (2mmF,4mmF,8mmF) due to higher densities of modified fuller sand. The model produces imaginary values when the dry density is higher than 1.90 g cm^{-3}. As the dry density increases in the order of sand < 2mmF < 4mmF < 8mmF, the thermal conductivity also increases in the same order for the full range of saturation and attain the highest thermal conductivity for 8mmF regardless of the degree of saturation. It implies that the higher the density, the higher the thermal conductivity. The measured and predicted thermal conductivity is also increased with an increase of the degree of saturation and attain maximum thermal conductivity at full saturation. Hence, it is certain that the dry density and saturation affects the thermal conductivity of the soils. All remaining three models (Johansen (1975), Côté and Konrad (2005a), Lu et al. (2007)) underestimate measured thermal conductivity values for modified sand (4mmF and 8mmF) of both sand A and B until 30% of the degree of saturation and then provides the best correlation to the measured thermal conductivity for the remaining degree of saturation. It is evident that these prediction models especially cannot predict for a lower degree of saturation (S_r below 30%). Due to the higher density of the modified sand samples, the small amount of water can facilitate a good conduction path by forming bridges between solid particles and

hence the thermal conductivity increases abruptly than conventional prediction models at a lower degree of saturation. The degree of saturation at which a sharp thermal conductivity increase begins is greater for the 2mmF modified sand than for the 4mmF and 8mmF modified sand. It is due to fact that the 2mmF modified sand has larger surface areas and more water is required before water bridges are formed between solid particles.

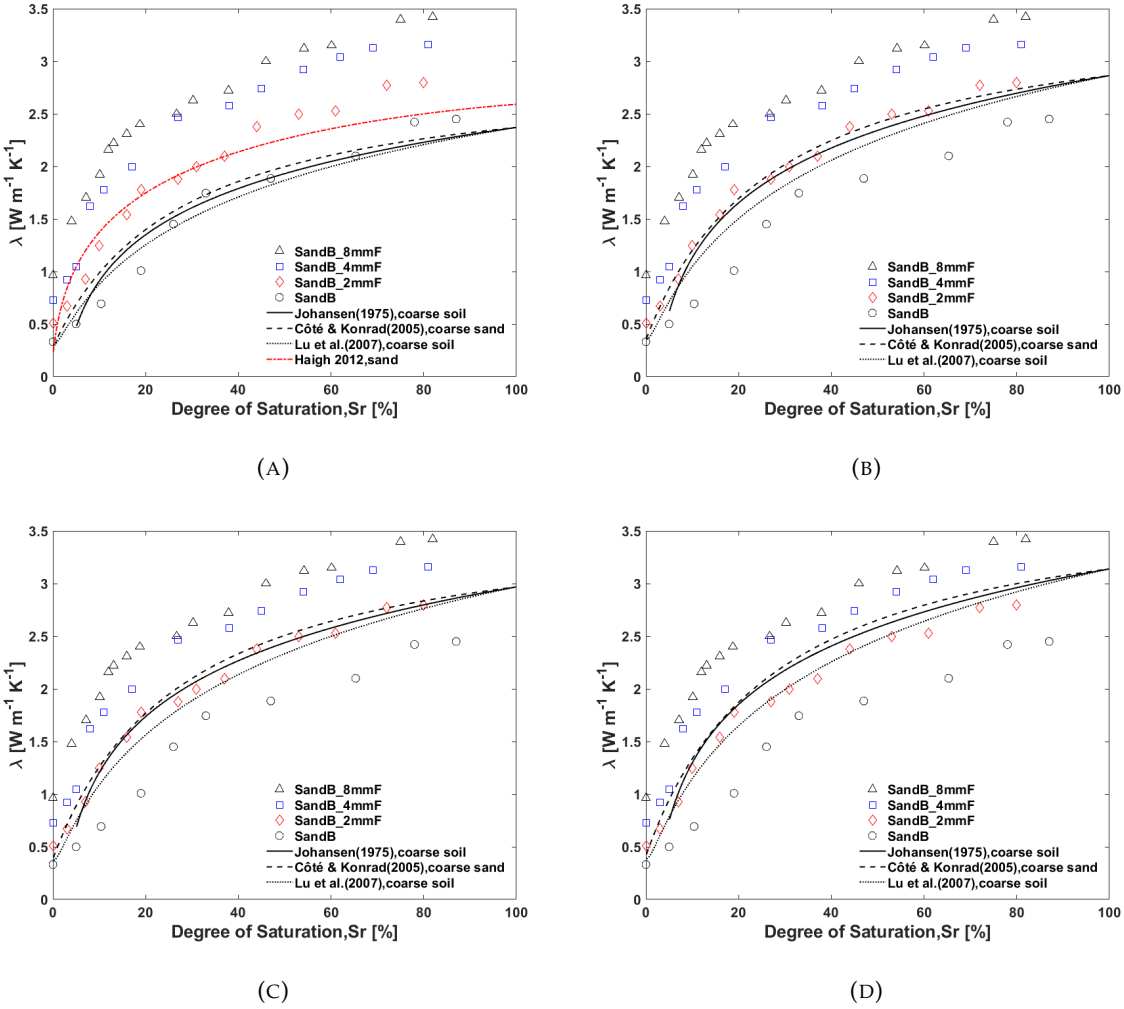

FIGURE 5.19: Comparision of experimental results with semi-empirical models for (a)sand-B, (b)2mmF, (c)4mmF & (d)8mmF.

All three predictions models developed in the past are based on some assumptions to simplify the problems and they are developed for a specific type of soil and boundary conditions. So, these models couldn't predict well in the case of modified fuller sands, especially for the lower side of saturation. This is probably due to the fact that these models lack considerations of the inherent presence of contacts quality and quantity in soils. Therefore, an artificial neural network (ANN) as a simple method is proposed to predict the thermal conductivity of modified sands for the full range of saturation. The development of the ANN model is discussed in detail in the next chapter 6.

5.6 Mechanical test results

The Odometer tests were also performed to investigate the mechanical stability of selected developed materials in this study. The tests were carried out for the modified fuller sands with stone-dust and original sand and the results are shown in Figure 5.20. As expected, there is a reduction in the strength for the modified fuller sands as compared to the strength of the original sand. It is observed that there is less deformation with 8mmF as compared to other fuller gradation mixes since the 8mmF has fewer fine materials by volume. The deformation increases with an increase in the content of fine materials as 8mmF, 4mmF and 2mmF contain 12%, 17% and 25% fine content by volume. It is more clear from the compression index parameter (Table 5.1). The C_c for the sandA is 0.0329 and those for 8mmF, 4mmF & 2mmF are 0.0365, 0.0396 and 0.0465, respectively. The strength decreases with an increase in fine content. The deformation for modified fuller sand is considerably higher at greater stresses, whilst at lower stress, no significant deformations are observed. For example, at 100kPa, the vertical strain for sandA is 1.1%, whereas that for modified fuller sands lies between 1.5 & and 2.2 %.

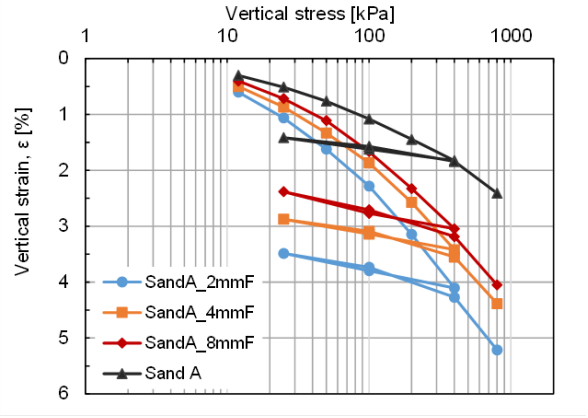

(A)

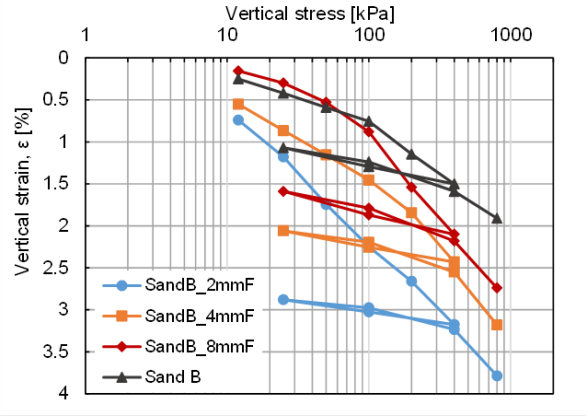

(B)

FIGURE 5.20: Vertical stress vs strain for for modified fuller sands with stone-dust and original sand A (a) and sand B (b).

TABLE 5.1: Odometer parameters for modified fuller and original sands.

Materials	C_c	C_s	C_r
sand-A	0.0329 (400-800 kPa)	0.0058	0.0060
sandA_2mmF	0.0465 (200-800 kPa)	0.0070	0.0088
sandA_4mmF	0.0396 (200-800 kPa)	0.0060	0.0074
sandA_8mmF	0.0365 (200-800 kPa)	0.0070	0.0085
sand-B	0.0217 (100-800 kPa)	0.0060	0.0073
sandB_2mmF	0.0264 (200-800 kPa)	0.0035	0.0042
sandb_4mmF	0.0299 (200-800 kPa)	0.0041	0.0055
sandB_8mmF	0.0272 (100-800 kPa)	0.0056	0.0065

C_c = Compression index; C_s = Swelling index; C_r = Recompression index

The Odometer parameters are presented in Table 5.1. The swelling index properties are almost the same for modified fuller and original sand.

5.7 Summary

This chapter explained almost all the outcomes and discussed them to provide actual insight of the results. Furthermore, it explained the factors affecting the thermal conductivity of the materials and discussed about the current prediction models and its limitation in the estimation of designed geomaterials. These experimental data have been further used to develop ANN models, described in Chapter 6.

Chapter 6

Development of new conductivity models for granular materials by using ANNs

6.1 Introduction

This chapter explains the ANN methodology used to predict the thermal conductivity of designed geomaterials as well as sand based on different input parameters. The proposed ANN models have been validated on new experimental data and performance assessment of proposed ANN models with other existing prediction models have been also made to reinforce the applicability and superiority of the ANN models.

6.2 ANNs model setup

Basically, an ANN consists of layers and neurons that are organized in a certain structure to perform a particular function at a given time. Different ANNs are distinguished from each other in terms of the number of layers, method of determining the weights between the neurons of different layers, a connection between the neurons of the layers, the direction of information flow and the transfer function used to get the output from the neurons (Sinha et al., 2015).

Setting up or constructing the ANN model basically has the following major steps procedure.

1. At first, the data to be used need to be defined and presented to the ANN as a pattern of input data with the desired outcome or target. It is also called pre-processing of data which contains normalization of all input and output data.

2. The data are categorized to be either in the training set, validation and testing set. The ANN only uses the training set in its learning process in developing the model. The validation set is used to test the model for its predictive ability and when to stop the training of the ANN. The testing set is used to assess the performance of the ANN model.

3. The ANN structure is defined by selecting the number of hidden layers to be constructed and the number of neurons for each hidden layer. Starting with 1 hidden layer and 1 neuron.

4. Fourthly, all the ANN parameters are set before starting the training process.

5. Next, the training process is started. The training process involves the computation of the output from the input data and the weights. The Levenberg-Marquardt back-propagation algorithm is used to 'train' the ANN by adjusting its weights to minimize the difference between the current ANN output and the desired output.

6. Finally, an evaluation process has to be conducted to determine if the ANN has 'learned' to solve the task at hand. This evaluation process may involve periodically halting the training process and testing its performance until an acceptable result is obtained. When an acceptable result is obtained, the ANN is then deemed to have been trained and ready to be used. The selection of the best performing ANN model is done based on standard error parameters.

The above steps are also shown in Figure 6.1 in the form of a flow chart which presents the calculation process for the proposed ANN models. As there are no fixed rules in determining the ANN structure or its parameter values, a large number of ANNs may have to be constructed with different structures and parameters with the activation function/s before determining an acceptable model. The trial and error process can be a tedious, laborious and time-consuming method. Determining when the training process needs to be halted is of vital importance in obtaining a good model. If an ANN is overtrained, a curve-fitting problem may occur whereby the ANN starts to fit itself to the training set instead of creating a generalized model. This typically results in poor predictions of the test and validation data set. On the other hand, if the ANN is not trained for long enough, it may settle at a local minimum, rather than the global minimum solution. This typically generates a sub-optimal model. By performing periodic testing of the ANN on the test set and recording both the results of the training and test data set results, the number of iterations that produce the best model can be obtained. All that is needed is to reset the ANN and train the network up to that number of iterations.

As explained earlier, ANN users don't need strong computational knowledge and background as commercial ANN software is available in the market. The use of this software has been the most popular method for developing an ANN model. With the rapid development of computer software, several ANN software which can be used for developing ANN models have been developed in the past decade. Some of them are Neural-Ware Professional, Neural-Shell, Neuro-solution (Neuro-Dimension, Inc., Gainesville, FL), Matlab Neural network toolbox (MathWorks, Inc., Natick, MA), Statistica Neural Networks (StatSoft, Inc., Tulsa, OK) and Neuro-Genetic Optimizer (BioComp Systems, Inc, Bloomington, MN). In this study, the design and training of the networks were performed using the MatLab programming environment (version R2019a) with Neural Networks Toolbox.

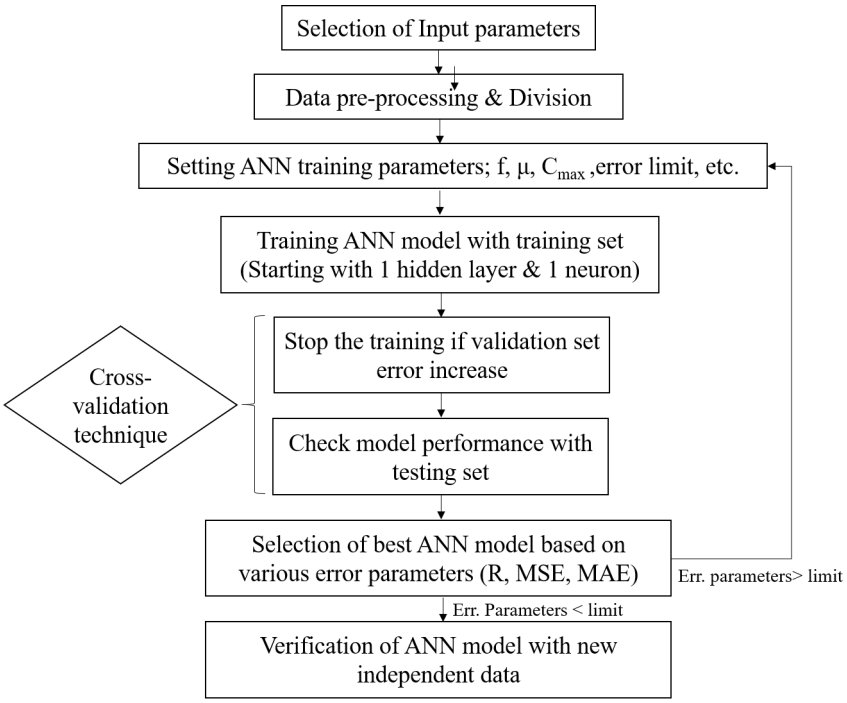

FIGURE 6.1: Flow chart of ANN models calculation procedure.

6.3 Data division and pre-processing

The data used to train the ANN model were obtained from extensive experimental work (chapter 3). Some of the data were also collected from the literature survey, especially the thermal conductivity measurement for original sands. The tested sand samples were prepared with different porosities and various water contents and subjected to thermal conductivity measurement as reported by previous researchers (Yun and Santamarina, 2007; Chen, 2008; Erzin et al., 2008; Tarnawski et al., 2013; Tarnawski et al., 2015; Alrtimi et al., 2016; Zhang et al., 2015; Zhang et al., 2020b; Zhang et al., 2020a). After obtaining the data, the variables were pre-processed by them to a suitable form and to eliminate their dimension before they are applied to the ANN. The input variables are selected on the base of influencing factors on thermal conductivity and the output variable is thermal conductivity. This is explained in the next section when selecting the input parameters of each ANN model. For the convenience of model calculation, both input and output parameters of each model were normalized using equation 6.1 as suggested by earlier researchers to create value that lies between 0 and 1 (Erzin et al., 2008; Zhang et al., 2020b).

$$x_N = \frac{x - x_{min}}{x_{max} - x_{min}} \tag{6.1}$$

where x_n is the normalized value for model calculation, x is the actual input-output value, x_{min} & x_{max} are the minimum and maximum values, respectively.

The data division was done using the cross-validation technique in which the was divided into three sets viz. training set, validation set and testing set. The training set is used

to update the connection weights and the updating process is monitored by the error of validation data. Training the model will stop when the error of validation data in the validation set begins to increase, at which point the model generalization is considered to reach its best stage. Finally, the testing set is used to evaluate the performance of the trained network. In this study, training set, validation set, and testing set are account for 60%, 20%, and 20% of the database in total, respectively.

6.4 Determination of ANN model Architecture

Determining the network architecture is one of the most important and difficult tasks in ANN model development. It requires the selection of the optimum number of hidden layers and the number of neurons in each hidden layer. However, The number of nodes in the input and output layers are decided by the number of input variables and outputs. There is no unified theory for the determination of an optimal ANN architecture (Shahin et al., 2002b). When the neural network has too few hidden neurons, the model complexity is not sufficient to extract the deterministic relationship between the input variables and the outputs. On the other hand, a neural network with more hidden neurons could precisely adjust the training data and fit the noise present in the data, but gave the ANN predictions deprived of physical connotation. More hidden layers can also result in 'over-training' (or lack of generalization) and lead to large 'verification errors'. Therefore, its performance depended largely on the particular training set.

In this study, separate ANN models were developed for dry and moist states respectively since the dry thermal conductivity in the dry and unsaturated states is affected by different factors. Therefore, the input variables are different for each model. Three error indicators as explained earlier were used to compare network usefulness in the prediction of thermal conductivity after training.

6.4.1 ANN architecture for dry materials

As discussed earlier, soil thermal conduction in the dry state is affected by many factors, viz., dry density or porosity, microstructure, a volumetric fraction of each constituent, quartz content, and particle size gradation. In this study, the prediction models based on the artificial neural network were developed independently for modified fuller sand and original sand, which were denoted as ANN-F for modified fuller sand and ANN-S for sand. Furthermore, a generalized model denoted as ANN-G was also developed which accounts for both modified fuller and original sands. Two input parameters (porosity, n & quartz content, q_c) were set for individual models(ANN-F, ANN-S), while three input parameters (n, q_c, & gradation parameters, C_u) were utilized for the generalized model(ANN-G). It should be noted that gradation parameters and quartz content were selected as input parameters for the ANN-G model because these two parameters represent variations in the gradation and the mineralogy, respectively. The fine content (f_c) as additional parameters was added to individual ANN-F model since the proportion of fine content in fuller curve is different by volume. All

these models have one output parameter i.e. dry thermal conductivity (λ_{dry}). The boundaries for input and output parameters of the ANN models are listed in Table 6.1. The input and output parameters of each ANN model were scaled to lie between 0 and 1 by using equation 6.1. As said earlier, the dataset was divided to 60:20:20, the number of the dataset used for training, testing and validation used for different ANN models are presented in Table 6.2.

TABLE 6.1: Boundaries of the input & output paremeter for ANN models.

Model symbol	**Input/Output**	**Min.**	**Max.**
ANN-F	n	0.206	0.361
	q_c [%]	52.5	87.5
	f_c [%]	12.5	25
	λ [$\mathrm{W\,m^{-1}\,K^{-1}}$]	0.389	1.153
ANN-S	n	0.302	0.550
	q_c [%]	70	99
	λ [$\mathrm{W\,m^{-1}\,K^{-1}}$]	0.14	0.40
ANN-G	n	0.206	0.550
	q_c [%]	52.5	99
	C_u	1.15	36.0
	λ [$\mathrm{W\,m^{-1}\,K^{-1}}$]	0.14	1.153
ANNs-F	ρ_d [$\mathrm{g\,cm^{-3}}$]	1.92	2.08
	q_c [%]	71.3	97.5
	S_r [%]	0.0	100
	λ [$\mathrm{W\,m^{-1}\,K^{-1}}$]	0.51	4.239
ANNs-S	ρ_d [$\mathrm{g\,cm^{-3}}$]	1.20	1.80
	q_c [%]	35	100
	S_r [%]	0.0	100
	λ [$\mathrm{W\,m^{-1}\,K^{-1}}$]	0.14	3.37
ANNs-G	ρ_d [$\mathrm{g\,cm^{-3}}$]	1.20	2.08
	q_c [%]	35	100
	S_r [%]	0.0	100
	C_u	1.15	36.0
	λ [$\mathrm{W\,m^{-1}\,K^{-1}}$]	0.14	4.239

6.4.2 ANN architecture for moist materials

Three different ANN models namely ANNs-F, ANNs-S and ANNs-G were developed for modified fuller sand, sand only and combined modified fuller and original sand. The first two are individual models which predict independently for modified fuller sands and original sands whereas the third one is generalised models which accounts for both modified and original sand. As discussed in chapter 2, various factors like dry density, saturation, mineral contents, particle size gradation, etc on thermal conductivity of soils. So, three input parameters (dry density (ρ_d), quartz content (q_c), and degree of saturation S_r) were set

TABLE 6.2: Data division for different ANN models.

Model symbol	**Training**	**Testing**	**Validation**	**train function**
ANN-F	67	23	23	trainlm
ANN-S	46	15	15	trainlm
ANN-G	104	34	34	trainlm
ANNs-F	125	42	42	trainlm
ANNs-S	115	39	39	trainlm
ANNs-G	240	80	80	trainlm

for individual models (ANNs-F, ANNs-S), while four input parameters (ρ_d, S_r, q_c, gradation parameters, C_u) were utilized for the generalized model (ANNs-G). It should be noted that gradation parameters and quartz content were selected as input parameters for the ANNs-G model because these two parameters represent variations in the gradation and the mineralogy, respectively. All these models have one output parameter i.e. effective thermal conductivity of materials over the various degree of saturation. The boundaries for input and output parameters of the ANN models are listed in Table 6.1. The input and output paramters of each ANN model were scaled to lie between 0 and 1 by using equation 6.1. As said earlier , the dataset was divided to 60:20:20, the number of dataset used for training, testing and validation used for different ANN models are presented in Table 6.2.

TABLE 6.3: Artificial Neural Network Paramters.

Paramters	**Value**
Learning rate	0.01 to 0.001
Momentum, mu	0.9
Maximum momentum, mu_max	1e10
Momentum decrease factor, mu_dec	0.8
Momentum increase factor, mu_inc	1.5
Maximum Epoch	1000
Maximum validation fail	30
Performacne goal	1e-5
minimum performance gradient	1e-7

Since it has been shown that a network with one hidden layer can approximate any continuous function (Hornik et al., 1989; Lawrence, 1993), in this study, different neural networks models with one hidden layer and several neurons in the hidden layer were developed. The optimum number of neurons in the hidden layer of each model was determined by varying their number between 1 and 10 with an increment of 1. This resulted in a total of 10 networks for each ANN model besides ANN-S models. ANN-S has hidden neurons between 1 and 20 with the increment of 2, 3 and 5 as shown in Table A.2. Therefore, ANN-S has 8 network models. So, altogether 58 artificial neural network models were

created for dry and moist states, 10 each for ANN-F, ANN-G, ANNs-F, ANNs-S and ANNs-G. All of the networks were feed-forward and the Levenberg-Marquardt back-propagation algorithm was used in the learning process. The Levenberg-Marquardt method, which combines the gradient descent method and the Gaus-Newton optimization method (Levenberg, 1944; Marquardt, 1963) uses the supervised learning technique. In this method, the network weights and bias are initialized randomly at the starting of the training phase and the network is trained by adjusting its weights and bias to minimize the difference between the current ANN ouptput and the desired output. The training function used in the matlab is 'trainlm'. The hyperbolic tangent function was used for all of the hidden and output layers as the activation function. The maximum epochs set for training the networks was 1000. The ANN parameters utilized in training the network are presented in Table 6.3. Since the back-propagation algorithm uses a first-order gradient descent technique to adjust the connection weights, it may get trapped in a local minimum if the initial starting point in the weight space is unfavourable (Shahin et al., 2002b). Consequently, the model that has the optimum momentum term and the learning rate is retrained several times with different initial weights until no further improvement occurs.

6.5 Stop criteria

The criteria to stop the training process is called stopping criteria. It stops the training process when the model has been optimally or sub-optimally trained. As said earlier, the cross-validation technique was used in this study to stop the training. The training is stopped when the validation set error has started to increase. The training is also stopped when the performance goal is reached to the desired limit while using the 'trainlm' function. The 'trainlm' function is a network training function that updates weight and bias values according to Levenberg-Marquardt optimization. The other conditions when the training is stopped are a) when the maximum number of epochs is reached, b) when the momentum exceeds mu_max and c) when the performance gradient falls below min_grad. Despite various stopping conditions, the validation set error and the performance goal are main criteria to stop the training in this study.

6.6 Model optimization (Training)

The performance of the network during the training and testing processes was examined for each network size until no significant improvement occurred. As said earlier, three performance parameters MSE, R and MAE were used to check the performance of the developed ANN models. The values are presented in Appendix A in tabular form. The values of R, MSE and MAE are listed in Tables A.1 to A.6 for respective ANN-F, ANN-S, ANN-G (dry ANN models) and ANNs-F, ANNs-S, ANNs-G (moist ANN models). It can be noted that the individual models (ANN/s-F, ANN/s-S) and the generalized model (ANN/s-G) are quite efficient in estimating thermal conductivity of sand and modified fuller sand in both dry and moist states as their R are very close to unity and MSE are very close to zero. In each subset

(i.e., training data, validation data, and testing data), predicted thermal conductivity values show good agreement with the measured ones, which indicates that the cross-validation technique is effective and feasible for developing these ANN prediction models.

6.6.1 For dry materials

It was found that the best ANN architecture for predicting the thermal conductivity of modified fuller sand in a dry state was constructed from one hidden layer with 6 neurons (bold number in Table A.1) for ANN-F. The R values of training, validation and testing of selected architecture are very close to unity than other architecture and their respective MSE values are the lowest ones. Besides that, another ANN architecture with one hidden layer and 7 neurons was also selected since the R, MSE and MAE are better than other networks. Similarly for the individual models of sand, ANN-S, two ANN structures were selected one hidden layer with 9 neurons and 20 neurons (bold number in Table A.2) providing good performance indices than others. For generalised model ANN-G, two ANN architectures viz. one hidden layer with 6 neurons and 9 neurons (bold number in Table A.3) were selected. All these selected ANN models have used the trainlm function. As said earlier, one hidden layer is sufficient to solve most of the engineering problems. It is observed from Tables A.1-A.3 that one hidden layer with a various number of neurons is good enough to develop the relationship between dry thermal conductivity and influencing factors like porosity, quartz content and gradation. Another noticeable characteristic is that the generalised ANN models (ANN-G) performs better than the individual ANN models (ANN-S) for predicting the thermal conductivity of dry original sand as the performances indices of ANN-G are better than ANN-S. It could be due to the inclusion of gradation parameters in the generalised models. As mentioned earlier, the dry thermal conductivity is greatly influenced by the porosity and structure of the soils.

6.6.2 For moist materials

For predicting the thermal conductivity in the moist state (i.e. over the various degree of saturation), various ANNs as explained earlier were created and their performances indices are listed in Tables A.4-A.6. It is also observed from Tables A.4-A.6, one hidden layer is quite enough to develop ANN models to estimate the thermal conductivity of modified sand and original sand over various ranges of water content since the R-value of training, testing and validation of all proposed structures are very close to unity, while MSE and MAE are also close to zero. Two ANN architectures with one hidden layer with 7 and 9 neurons were selected for the individual model of modified sand (ANNs-F) since the three performances indices R, MSE and MAE of selected structures are better than others (shown bold in Table A.4). However, it is also noticed from Table A.4 that neural networks consist of 3 neurons to 10 neurons show good performance indices values, which ensure that a single hidden layer is able to solve this kind of problem. Similarly, for the original sand (ANNs-S), two ANN structures with one hidden layer with 6 and 9 neurons were selected based on better performances indices (shown bold in Table A.5). In the same manner, two

ANN structures with one hidden layer with 6 and 8 neurons were selected (shown bold in Table A.6. Not only the individual models show good agreement between predicted and measured values, but also the generalised ANN models also show good agreement between predicted and measured thermal conductivity values. The inclusion of gradation parameters in generalised models differentiates the modified fuller sand and original sand. So, the generalised ANN models are also applicable for estimating the thermal conductivity of both modified and original sand. It is also evident that in all subsets (i.e., training data, validation data, testing data), the predicted values agree well with measured values.

6.6.3 Comparison of experimental and predicted thermal conductivity using selected ANN models

From these selected ANN models, a list of weights can be obtained and applied in a spreadsheet to obtain a very accurate tool for predicting the thermal conductivity of geomaterials in dry as well as in the moist case. However, in this study, the thermal conductivities are calculated in MATLAB directly using selected ANN models. The selected ANN models for ANN-F, ANN-S and ANN-G were used to calculate the thermal conductivity of samples used in training, validation and testing for dry cases, while those for ANNs-F, ANNs-S and ANNs-G were used to calculate the thermal conductivity of samples for the moist case.

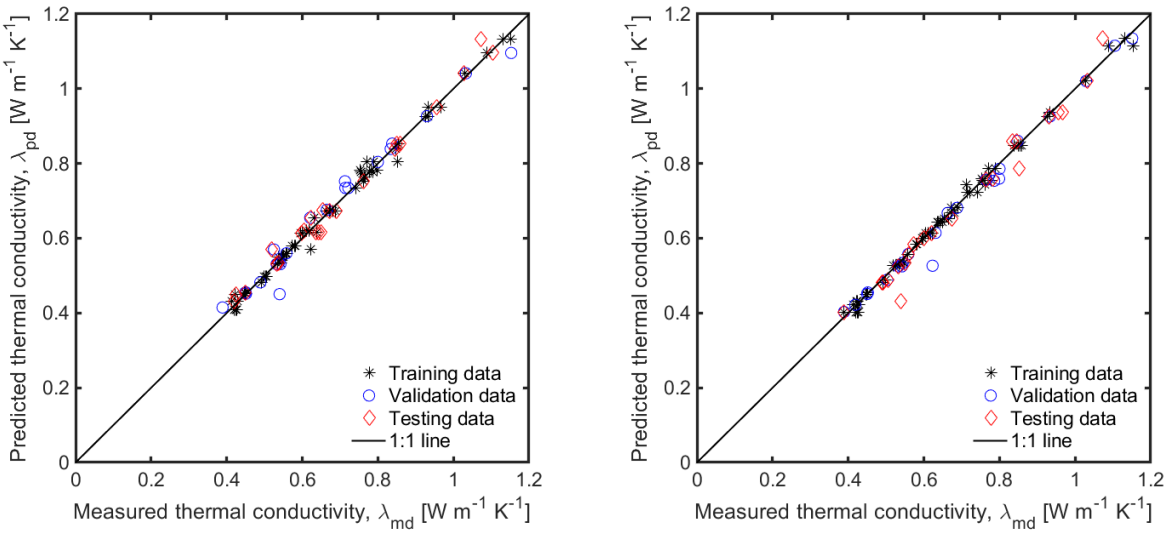

FIGURE 6.2: Comparison of measured and predicted thermal conductivity using ANN-F models: (a) ANNF6L and (b) ANNF7L.

A comparison of experimental results with the results obtained from selected ANN models for training, validation and testing samples are shown in Figures 6.2-6.4 for dry case and 6.5-6.7 for various degrees of saturation. It is observed from these figures that, the predicted thermal conductivity values are quite close to the measured thermal conductivity values for all data including training, validation and testing indicating the high quality of the ANN architectures. The validation and testing data are independent data, which are not used in the training. The performances indices of these independent data also yield satisfactory. In

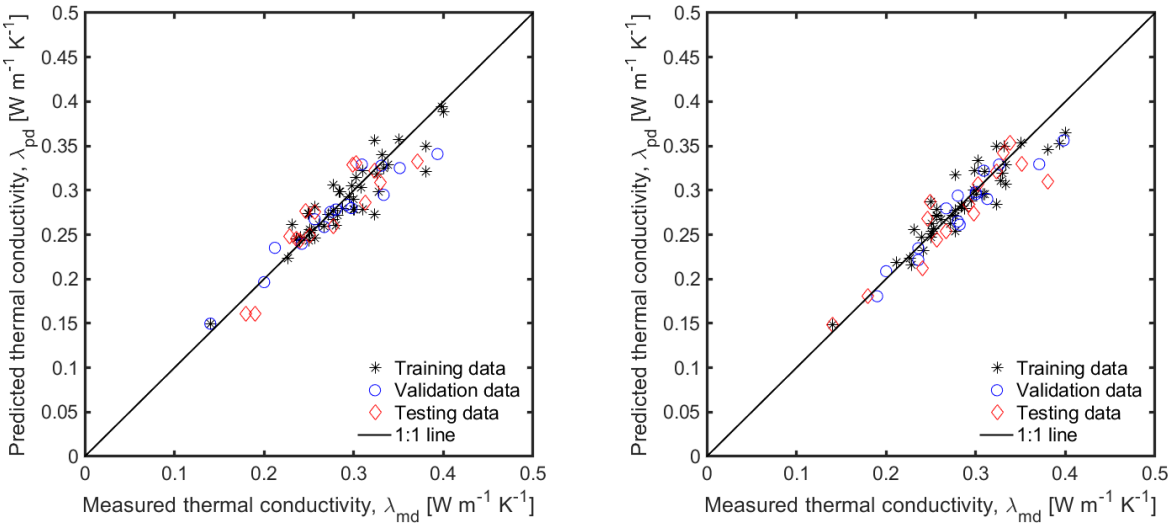

FIGURE 6.3: Comparison of measured and predicted thermal conductivity using ANN-S models: (a) ANNS9L and (b) ANNS20L.

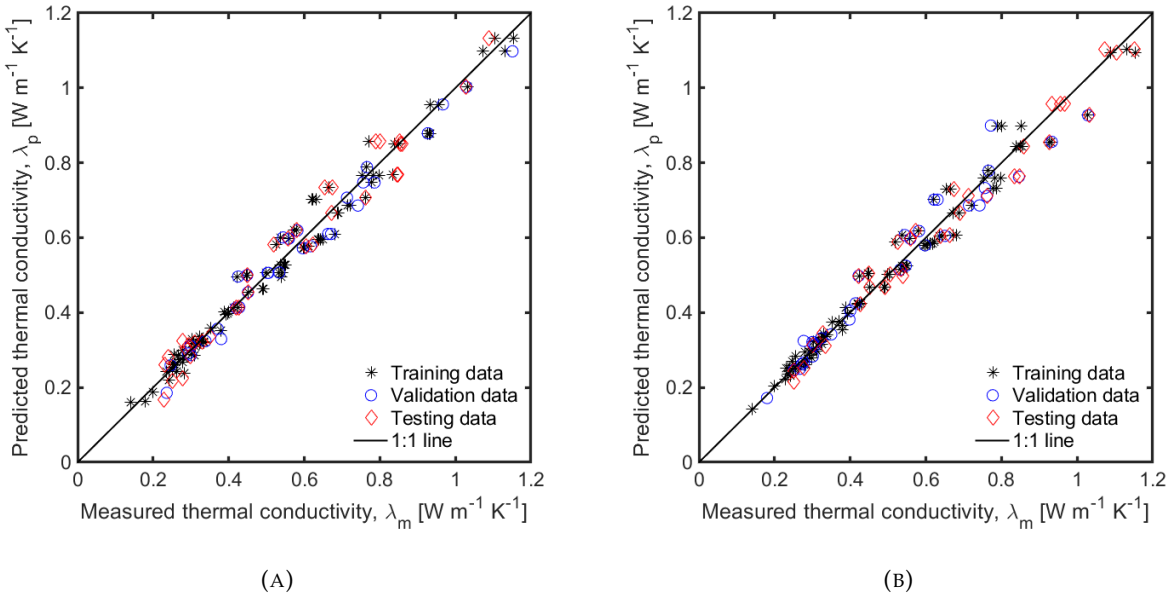

FIGURE 6.4: Comparison of measured and predicted thermal conductivity using ANN-G models: (a) ANNG6L and (b) ANNG9L.

the case of the dry state, the generalised ANN models (ANN-G) performs better than the individual ANN models (ANN-S) for predicting the thermal conductivity of dry original sand as the performances indices of ANN-G are better than that of ANN-S. It could be due to the inclusion of gradation parameters in the generalised models. As discussed earlier in the literature and experimental results, the dry thermal conductivity is more influenced by microstructure and it should be accounted for while developing the prediction models. On the other hand, the individual ANN models as well as generalised ANN models show good agreement between measured and predicted thermal conductivity values for all datasets. The inclusion of gradation parameters for generalised ANN models helps to predict the

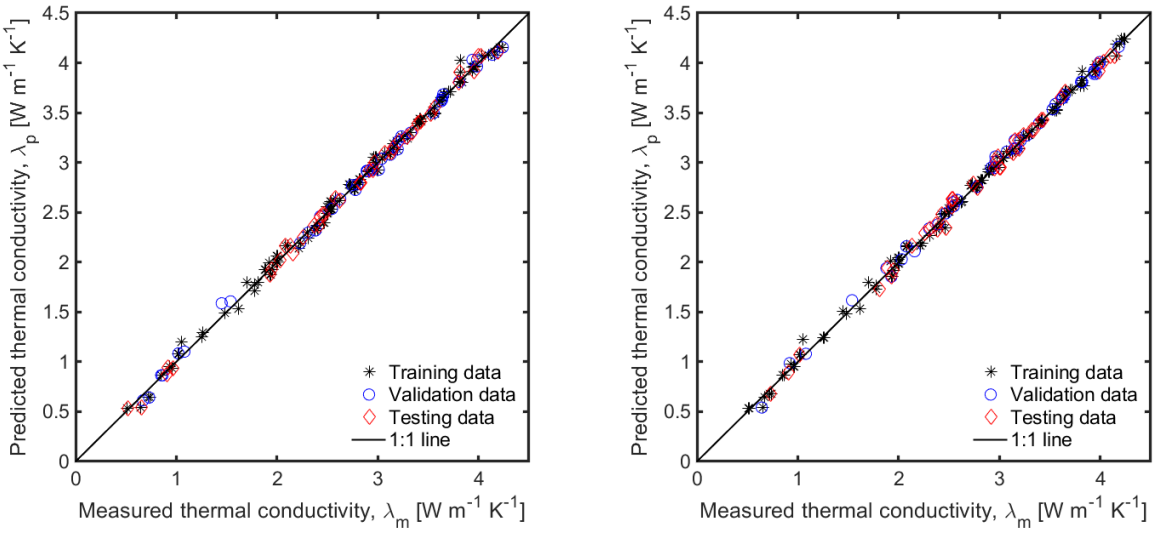

(A) (B)

FIGURE 6.5: Comparison of measured and predicted thermal conductivity using ANNs-F models: (a) ANNs-F7L and (b) ANNs-F9L.

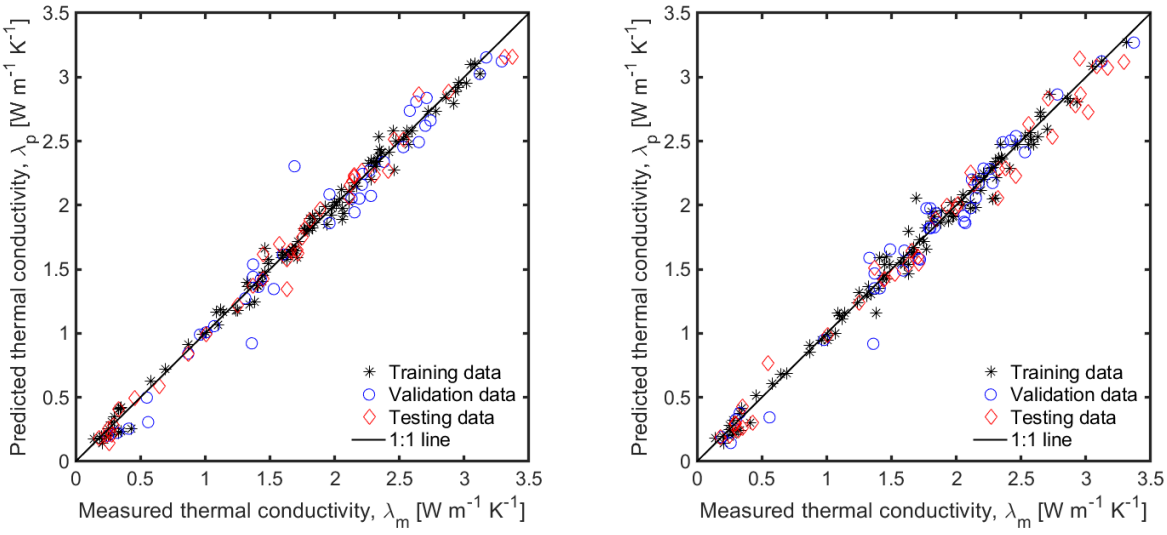

(A) (B)

FIGURE 6.6: Comparison of measured and predicted thermal conductivity using ANNs-S models: (a) ANNs-S6L and (b) ANNs-S9L.

thermal conductivity of both modified fuller sand and original sand.

6.7 Validation of developed ANN models

The validation of developed ANN models was done using independent experimental data. The thermal conductivity data obtained from laboratory measurement for modified fuller sand B and C with stone-dust and three sand used in this study which was not part of the developing the ANN models were selected to check the performance of the developed

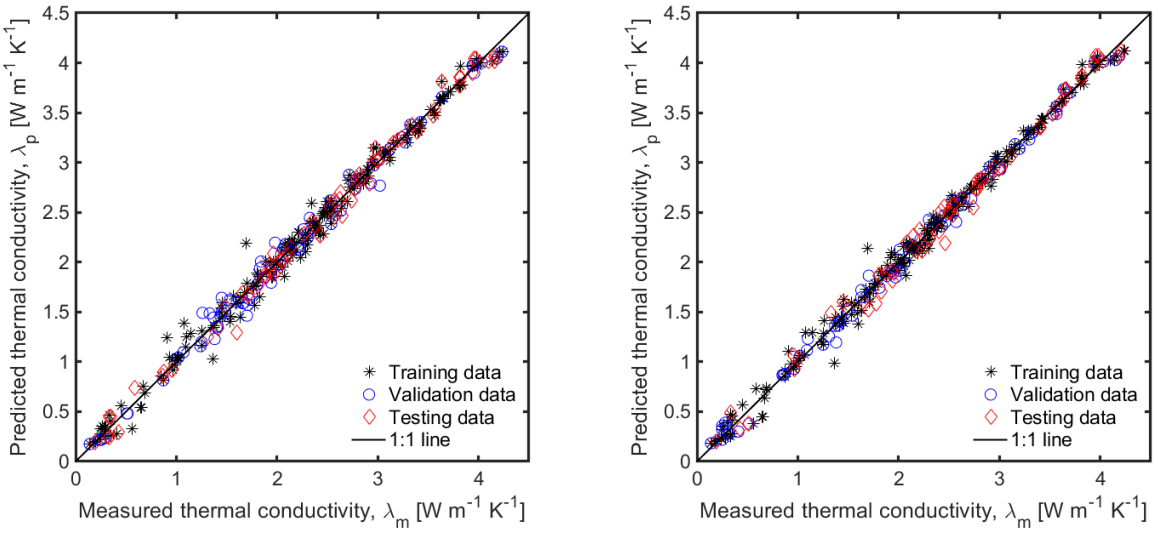

FIGURE 6.7: Comparison of measured and predicted thermal conductivity using ANNs-G models: (a) ANNs-G6L and (b) ANNs-G8L.

ANN models for dry state. On the other hand, the sandB_4mmF and sandA were used for verifying the validity of the ANN models in the full range of saturation. These data are completely independent and were fed into the developed models and their prediction outputs were also compared with the laboratory-measured results. Three error indicators; R, MSE and MAE as explained earlier were employed for further quantitatively checking the reliability of the developed models. The performances indices of all the proposed models are presented in Tables A.7-A.9 and A.10-A.12 of Appendix A for dry ANN models and moist ANN models (individual and generalised), respectively while the selected ANN models' parameters are presented in Table 6.4.

6.7.1 For dry materials

It is observed from the Table A.7-A.9 that the R values are greater than 0.96 and 0.92 for all individual models ANN-F and ANN-S respectively besides ANN-F models with 1 and 10 neurons, while that for generalised model ANN-G is greater than 0.92 excepts the models with 7 neurons. The MSE are also very low and less than 0.0040, 0.00031 and 0.0091 for ANN-F, ANN-S and ANN-G, respectively. This shows that using the single hidden layer is also sufficient to predict the thermal conductivity of modified fuller sand and original sand. The selected ANN-F models ANNF6L and ANNF7L have R values of 0.9867 and 0.9773, MSE of 0.0007 and .0012, and MAE of 0.0227 and 0.0286 indicating superior performance in predicting the thermal conductivity of new independent data of modified and original sand. Similarly, the selected ANN models ANNS9L and ANNS20L for predicting sand only and ANNG6L and ANNG9L for predicting both sand and modified sand show better performances indices value (Table A.8-A.9). The generalised ANN models (ANN-G) are able to perform better than individual models (ANN-S) since their R values are slightly higher than those of individual models (ANN-S).

TABLE 6.4: Performance indices for different ANN models obtained for new experimental data in dry as well as in moist case.

Model symbol	Hidden nodes	Exp. data	R	MSE	MAE
ANNF6L	6	Fuller sands	0.9867	0.0070	0.0227
ANNF7L	7	Fuller sands	0.9773	0.0012	0.0286
ANNS9L	9	Sands	0.9223	0.0003	0.0139
ANNS20L	20	Sands	0.9199	0.0003	0.0153
ANNG6L	6	Fuller/sands	0.9353	0.0043	0.0435
ANNG9L	9	Fuller/sands	0.9594	0.0027	0.0388
ANNs-F7L	7	Fuller sands	0.9971	0.0041	0.0487
ANNs-F9L	9	Fuller sands	0.9962	0.0053	0.0572
ANNs-S6L	6	Sands	0.9676	0.0460	0.1861
ANNs-S9L	9	Sands	0.9141	0.1186	0.2943
ANNs-G6L	6	sandB_4mmF	0.9922	0.0110	0.0721
ANNs-G6L	6	sandA	0.9207	0.1099	0.2573
ANNs-G8L	8	sandB_4mmF	0.9540	0.0635	0.2231
ANNs-G8L	8	sandA	0.9149	0.1175	0.2871
dry case: ANNF,	*ANNS, ANNG;*	*moist case: ANNs-F,*	*ANNs-S,*	*ANNs-G.*	

Figure 6.8 shows a comparison of measured thermal conductivity of independent data with the thermal conductivity obtained from selected individual ANN models for dry modified fuller sands and original sands. The thermal conductivity obtained from selected generalised ANN models are also compared to experimental results and it is presented in the Figure 6.9. As explained earlier, it is clearly seen from these figures that the selected ANN models (ANN-F, ANN-S, ANN-G) show good agreement between measured and predicted values of new experimental data. It is more clear when the predicted and measured thermal conductivity values are plotted against porosity.

Figure 6.10 shows the measured thermal conductivity against the porosity with predicted thermal conductivity obtained from selected individual ANN models (i.e. ANN-F, ANN-S) while Figure 6.11 shows the prediction of experimental data for the generalised model, ANN-G in the dry state. These figures give a more clear picture that how well the ANN models (ANN-F, ANN-S, ANN-G) can predict the measured values of new independent data. With decreasing the porosity, the measured thermal conductivity of modified fuller sand is exponentially increased and the same trend is followed by proposed ANN models. The generalised ANN models can predict measured thermal conductivity in the dry state for both modified and original sand within all given porosity ranges (0.20-0.45). However, the individual models ANN-F and ANN-S predict the thermal conductivity of modified fuller sand for the porosity range (0.20-0.36) and that of sand for the porosity range (0.30-0.45).

6.7.2 For moist materials

On the other hand, the ANN models (ANNs-F, ANNs-S, ANNs-G) developed for the moist state have also shown good agreement between predicted and measured values since the

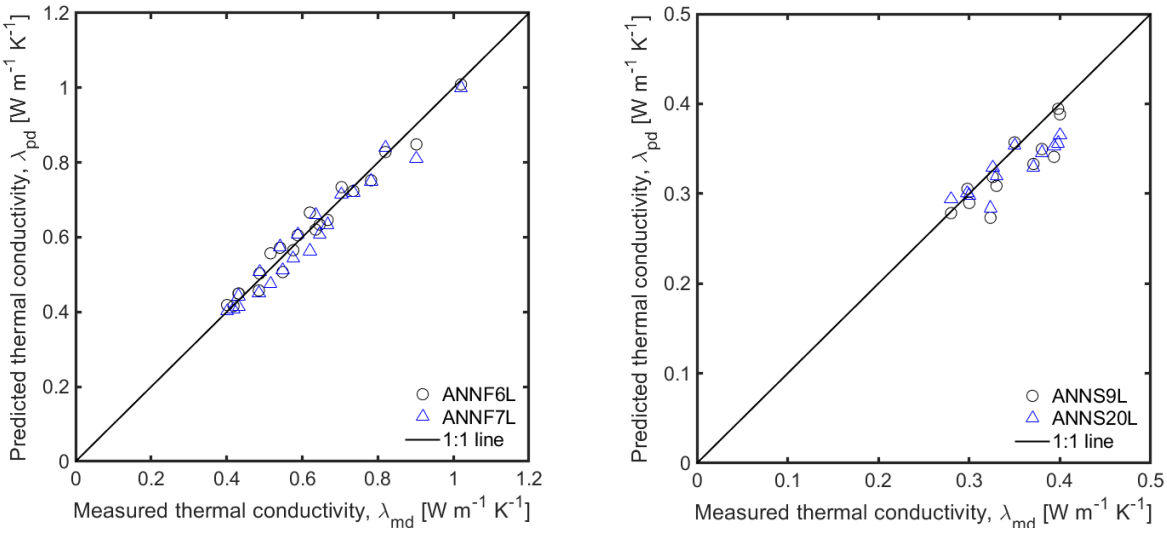

(A) (B)

FIGURE 6.8: Comparison of measured and predicted thermal conductivity using individual models: (a)selected ANN-F and (b)selected ANN-S for independent data.

performances indices R, MSE and MAE are within the acceptable level. The R values of selected individual models ANNs-F are very close to unity i.e. higher than 0.99 showing good agreement between predicted and measured values of modified fuller sands (Table A.10), whereas those of selected ANNs-S (Table A.11) are also higher than 0.91. The generalised models ANNs-G were separately tested with modified fuller sand and original sand as shown in Table A.12. The R values of generalised models ANNs-G are slightly lower than those of individual ANNs-F when predicting the thermal conductivity for modified fuller sand, while the R values of both generalised ANNs-G and individual ANNs-S for estimating sand thermal conductivity are almost the same. This observation shows that the generalized model predicts the thermal conductivity of both modified and original sand in moist cases quite accurately. The selected generalised model ANNs-G6L has R values of 0.9922 and 0.9207 for predicting modified fuller sand (sandB_4mmF) and sand-A respectively, while those for ANNs-G8L are 0.9540 and 0.9149. The MSE and MAE can be obtained from Table A.12. The generalised model (ANNs-G6L) predicts more accurately than the latter one (ANNs-G8L) for both modified and original sand. Another noticeable characteristic is that the performances indices of all ANN models with three and more neurons are satisfactory when predicting new independent data. It confirms the validation of proposed ANN models with new experimental data.

Figure 6.12 shows a comparison of measured thermal conductivity of independent data with the thermal conductivity obtained from selected individual ANN models for modified fuller sands (Fig. 6.12a) and original sands (Fig. 6.12b) in moist case. The individual models ANNs-F7L & ANNs-F9L predict very well for independent data since R is very close to unity, whereas the ANNs-S6L & ANNs-S9L slightly overestimates for the lower degree of saturation. The thermal conductivity obtained from selected generalised ANN models are also compared to measured thermal conductivity values of both modified fuller and original

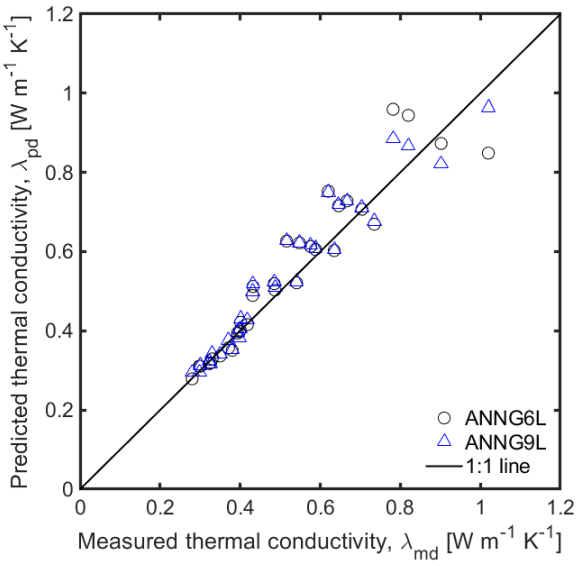

FIGURE 6.9: Comparison of measured and predicted thermal conductivity using generalized model, ANN-G for independent data.

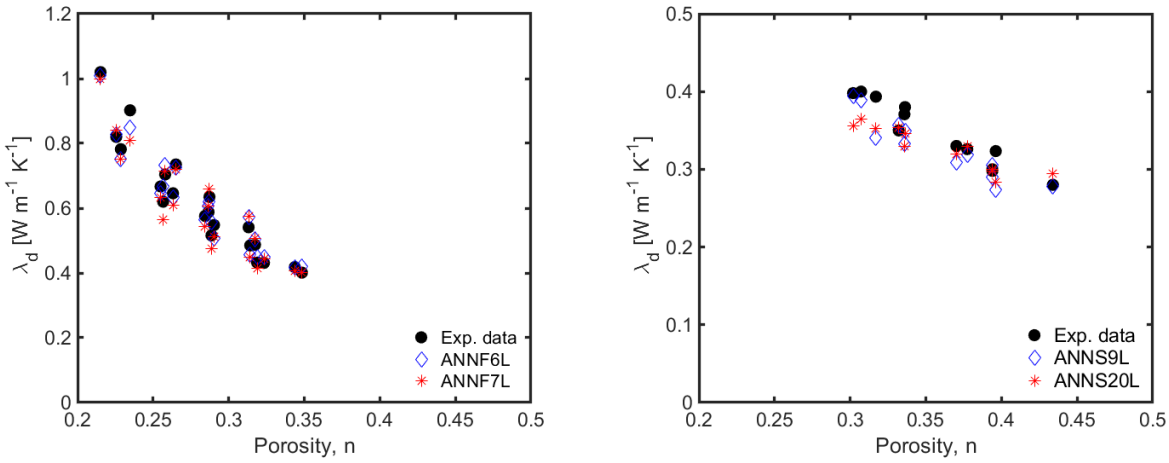

(A) (B)

FIGURE 6.10: Comparison of measured and predicted thermal conductivity using individual models: (a)selected ANN-F and (b)selected ANN-S for independent data.

sand in the moist case and it is presented in Figure 6.13. The generalised models ANNs-G6L & ANNs-G8L estimates very well for modified fuller sand while the models slightly overestimate measured values between 1-2.6 W m^{-1} K^{-1} for sand. It is more clearly observed from Figures 6.14 & 6.15. These figures show the measured and predicted values obtained from selected individual ANN models (ANNs-F & ANNs-S) and generalised model (ANNs-G) plotted against the degree of saturation for modified fuller and original sands. Both selected models ANNs-F7L & ANNS-F9L perfectly match the experimental thermal conductivity of modified fuller sand (sansB_4mmF) across the full range of saturation degrees. However, in the case of individual ANN models for sand, ANNs-S9L slightly overestimates the measured value across the full range of saturation while ANNs-S6L overestimates slightly till

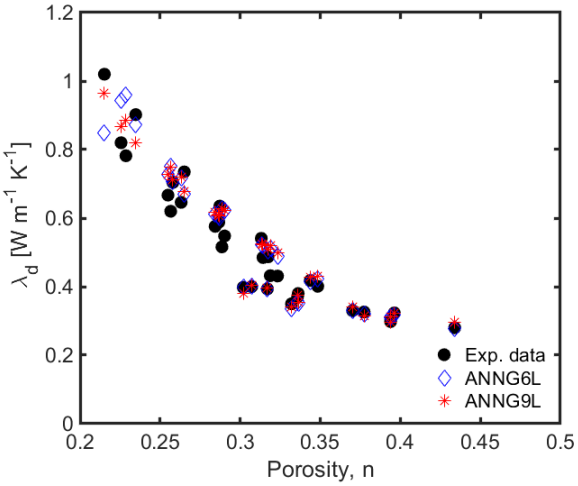

FIGURE 6.11: Comparison of measured and predicted thermal conductivity using generalized model, ANN-G for independent data.

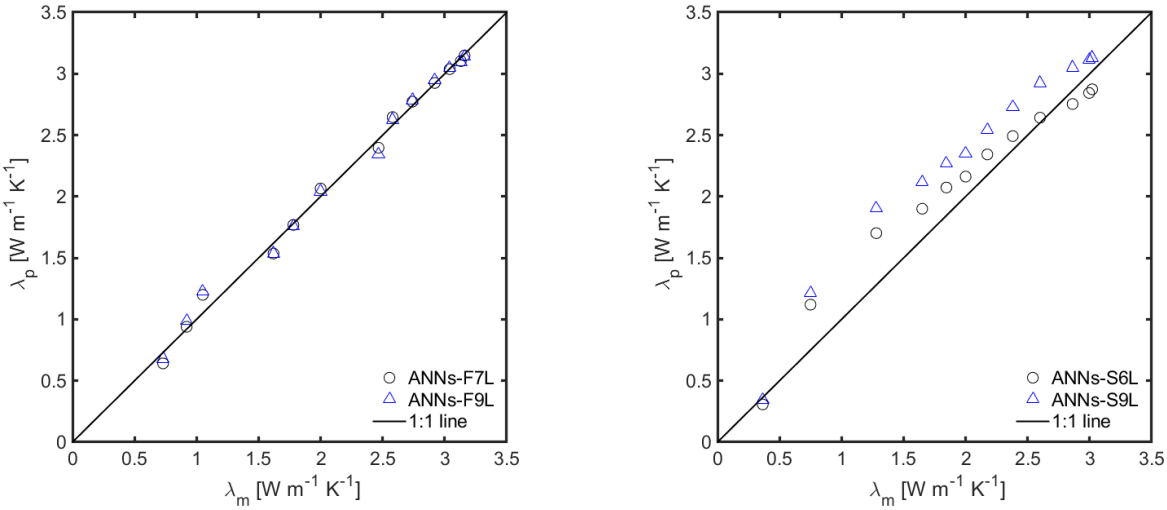

(A) (B)

FIGURE 6.12: Comparison of measured and predicted thermal conductivity using individual models: (a)selected ANNs-F and (b)selected ANNs-S for independent data.

60% degree of saturation and then-after slightly underestimates. This is due to the measured thermal conductivity data used to develop the ANN models have a sharp tendency to increase in the thermal conductivity at lower saturation degrees. It is observed from Figure 6.15, the generalised ANN models are very good to predict the measured thermal conductivity values across the full range of saturation degrees for both modified and original sand. For modified fuller sand, the predicted values obtained from ANNs-G6L agrees very well with measured values, but ANNs-G8L slightly underestimates the measured values over 10% saturation degree. On the other hand, both selected ANNs-G6L and ANNs-G8L overestimate slightly until the degree of saturation of 70% and perfectly match after that. The inclusion of one more parameter in generalised models seem to be good as the ANN models

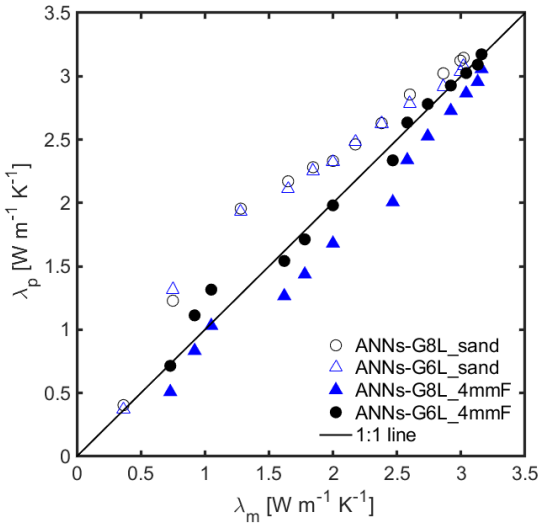

FIGURE 6.13: Comparison of measured and predicted thermal conductivity using generalized model, ANNs-G for independent data

can predict the thermal conductivity for both modified and original sands.

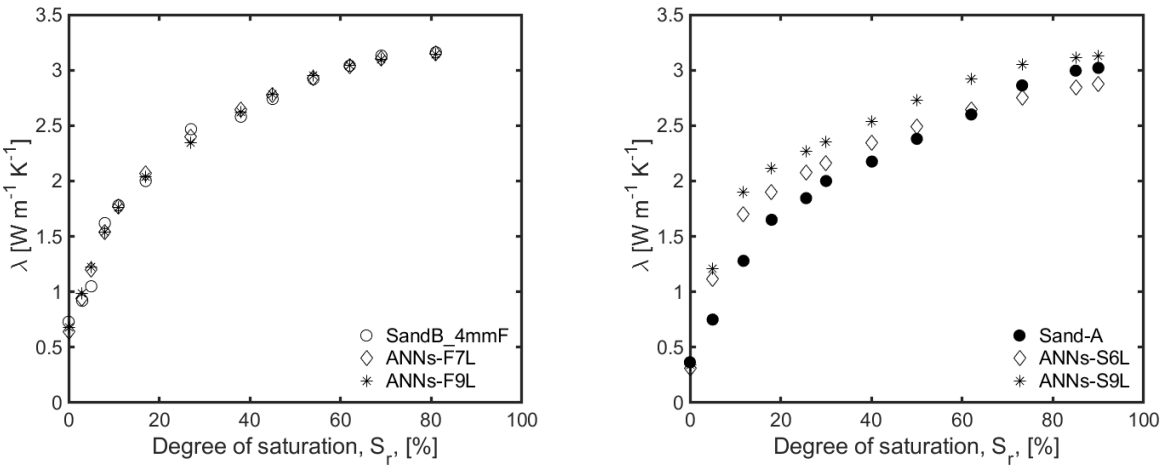

(A) (B)

FIGURE 6.14: Comparison of measured and predicted thermal conductivity using individual models: (a)selected ANNs-F and (b)selected ANNs-S for independent data.

6.8 Performance assessment of proposed ANN models

A comparison of proposed ANN models with existing prediction models was performed in this study in order to reinforce the applicability and superiority of the proposed prediction models.

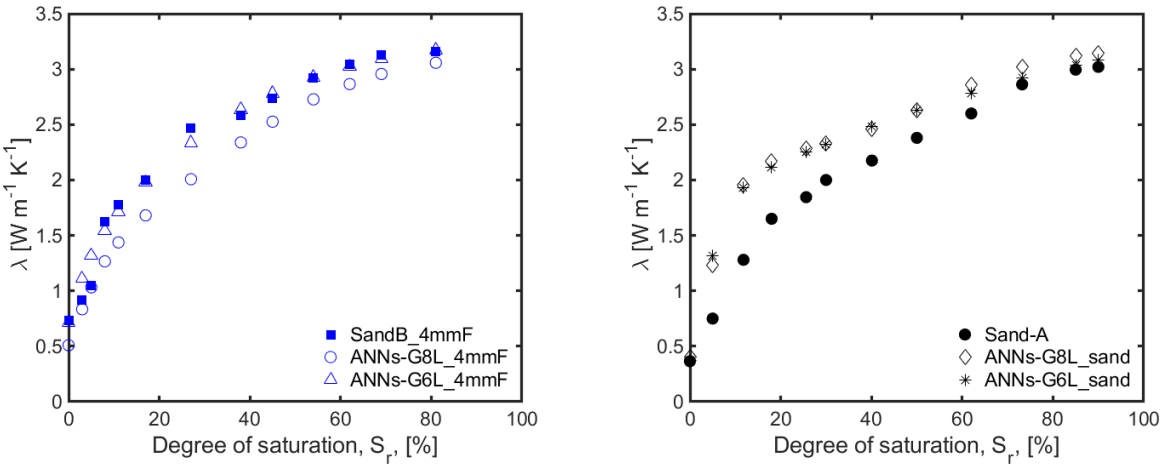

(A) (B)

FIGURE 6.15: Comparison of measured and predicted thermal conductivity using generalised models ANNs-G for (a) modified fuller sand (SandB_4mmF) and (b) sand-A.

6.8.1 For dry ANN models

The most commonly used semi-empirical models proposed by earlier researchers (Johansen, 1975; Côté and Konrad, 2005a; Lu et al., 2007; Balland and Arp, 2005; Gavriliev, 2004) to predict the dry thermal conductivity of the soils were selected as comparison models which are explained in detail in chapter 2. The proposed ANN models, individual (ANN-F & ANN-S) and generalised (ANN-G) ANN models, were deployed for independent measured thermal conductivity data to obtain the predicted value and the results are shown in Figure 6.16.

Figure 6.16a presents the comparison of the predicted thermal conductivity from the ANN-F & ANN-S and semi-empirical models with the independent measured thermal conductivity for modified fuller sand with stone-dust and original sand. It is evident that the proposed individual ANN Models yield much better matching with measured values as compared to those calculated from empirical models since there are two separate ANN models for modified fuller sand and original sand. On the other hand, the predicted thermal conductivity from the ANN-G and empirical are compared with measured values (Figure 6.16b). It is observed from the figure that the ANN-G model predicts well for the measured value of both modified fuller sand and original sand, though few higher measured thermal conductivity values for the porosity between 0.25-0.30 are underestimated by the ANN-G model. The empirical prediction models for sand can predict quite well for original sand besides Balland and Arp (2005) models since the data obtained from this model used the thermal conductivity of solids as 6.29 $W\,m^{-1}\,K^{-1}$ and hence it overestimates the measured values. As explained earlier, if the model use λ_{sL} = 3 $W\,m^{-1}\,K^{-1}$, it can perfectly match for the original sand. However, these prediction models cannot predict well and underestimate the measured values for modified fuller sand. Since these models are not developed for the specific type of soils and boundary conditions, they couldn't predict the measured values

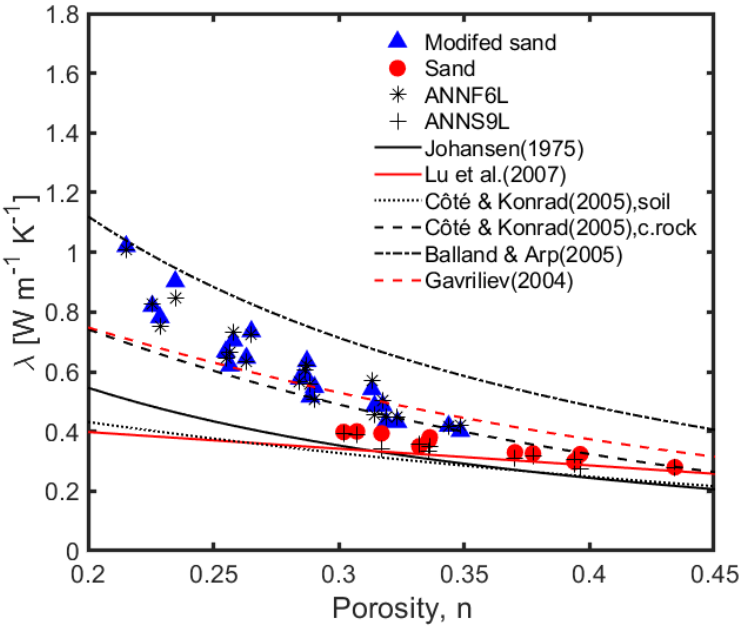

(A)

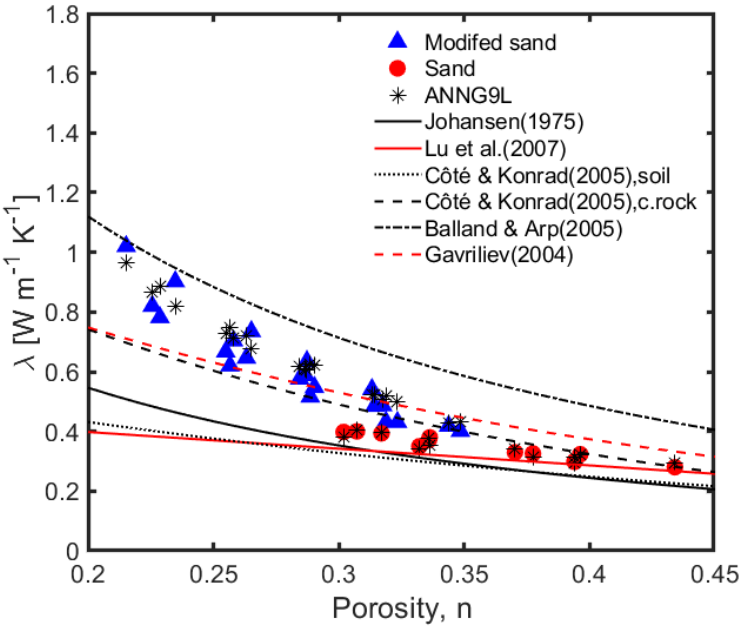

(B)

FIGURE 6.16: Comparison of proposed ANN models and empirical models with measured thermal conductivity value (a)ANN-F & ANN-S (b) ANN-G.

at the porosity below 0.30. It will be more clearly observed from Figure 6.17. The predicted data obtained from ANN models are very close to 1:1 line, while for other prediction models, it is far from 1:1 line when the thermal conductivity is increased below the porosity 0.3. The predicted values obtained from mostly empirical models are below the 1:1 line, underestimating the measured values. On contrary, Balland and Arp (2005) overestimates

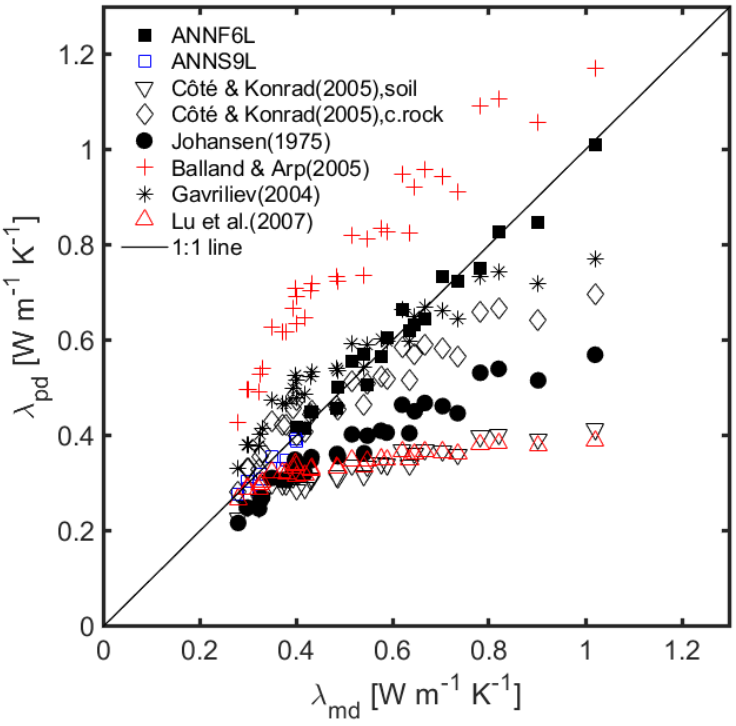

(A)

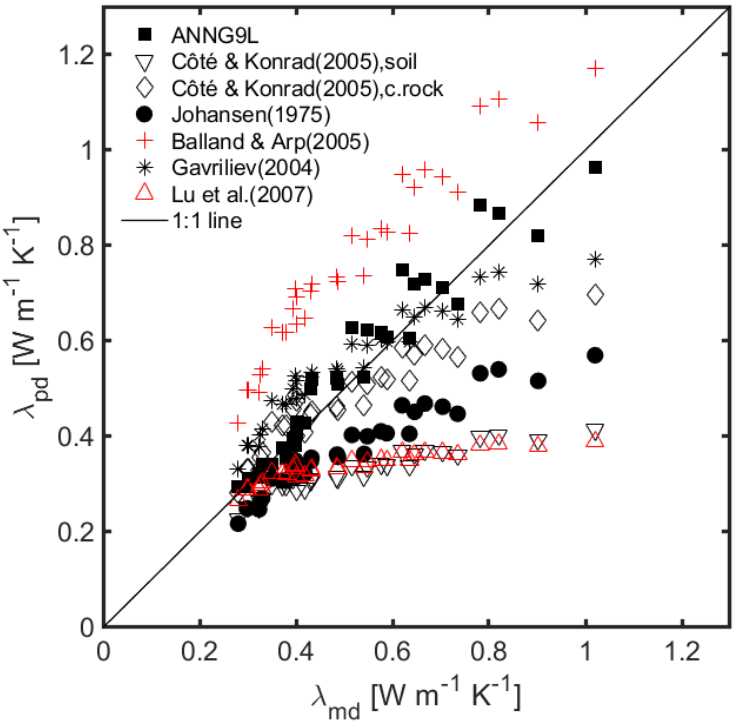

(B)

FIGURE 6.17: Comparison of proposed ANN models and empirical models with measured thermal conductivity value (a)ANN-F & ANN-S (b) ANN-G.

by showing predicted values over the 1:1 line.

6.8.2 For moist ANN models

A comparison of prediction performance between proposed ANN models in the moist case and three semi-empirical (Johansen (1975), Côté and Konrad (2005a), and Lu et al. (2007)) and a theoretical model (Haigh (2012)) has been made for independent experimental data and the results are presented in Figures 6.18 & 6.19.

The details about these prediction models are explained in Chapter 2. In these figures, the thermal conductivity is plotted against the degree of saturation. It is evident that the proposed ANN models yield much better matching with measured values as compared to those calculated from empirical models in the case of modified fuller sand. The predicted results of all three semi-empirical prediction models model have an obvious characteristic of underestimation. However, in the case of sand, all four prediction models provide a good fit to the experimental data (Figs. 6.18b & 6.19b). In addition, the predicted results of the individual and generalised ANN models are acceptable when the degree of saturation of the sandy soils are over 30%, whereas, below this value, the models slightly overestimate the measured values. This is due to that the measured thermal conductivity data used to develop the ANN models have a sharp tendency to increase in the thermal conductivity at lower saturation degrees. It is also evident from Figure 6.20a that the ANN models slightly overestimate the measured values when the thermal conductivity values of the sands are between 0.80 $\mathrm{W\,m^{-1}\,K^{-1}}$ and 2.0 $\mathrm{W\,m^{-1}\,K^{-1}}$ and for the rest, the selected ANN models provide the best matching to new measured data. In contrast, the ANN models possess a superior prediction performance than the three empirical models in the case of modified fuller sand. It is also observed from the Figure 6.20b that the predicted values obtained from the ANN models are almost on the 1:1 line indicating a perfect prediction of the measured values while the semi-empirical prediction models underestimate the measured values. Haigh (2012) model does not appear in Figures 6.18a & 6.19a because the model highly overestimates measured thermal conductivity values of the modified fuller sand due to higher dry density ($\rho_d = 2.04\mathrm{g\,cm^{-3}}$). At this dry density, the saturated thermal conductivity is 9.62 $\mathrm{W\,m^{-1}\,K^{-1}}$ which is not possible in the case of sandy soil. This is the limitation of Haigh (2012) model, which is only valid for the sandy soils with a dry density below 1.90 $\mathrm{g\,cm^{-3}}$. It is also evident that the ANN models (ANNs-G, ANNs-S) are very close to Haigh (2012) model when predicting for the sand.

Statistical analysis was conducted to quantitatively assess the accuracy of the proposed ANN models and prediction models in calculating the thermal conductivity of soils. Three performances indices R, MSE and MAE as shown in Equations 3.22, 3.23 and 3.24, were employed here to determine the prediction accuracy of each model. The statistical analysis results of each prediction model in both dry and moist states are summarized in Table 6.5. In the case of the dry condition, the analysis attests that the generalized model (ANN-G) provides the best matching to the measured data of the modified fuller sand and original sand because it possesses the lowest MSE value and highest R-value. Individual models (ANN-F, ANN-S) also exert a good performance when predicting for modified fuller sand

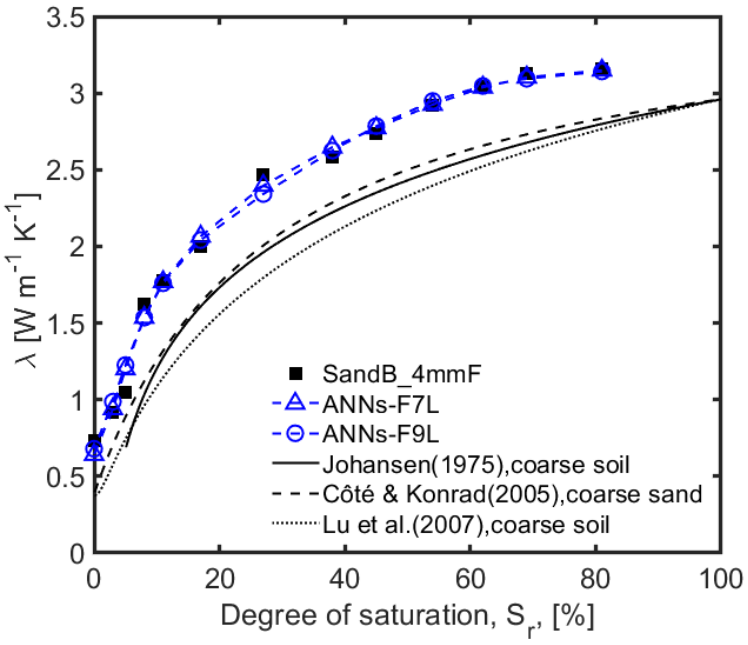

(A)

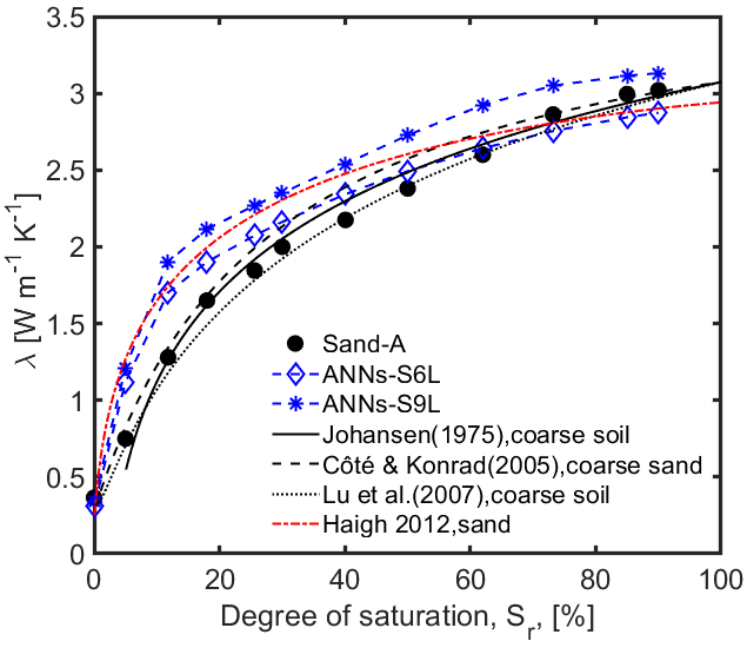

(B)

FIGURE 6.18: Comparison of proposed individual ANN models and semi-empirical models with measured thermal conductivity values for (a) modified fuller sand (SandB_4mmF) and (b) sand-A.

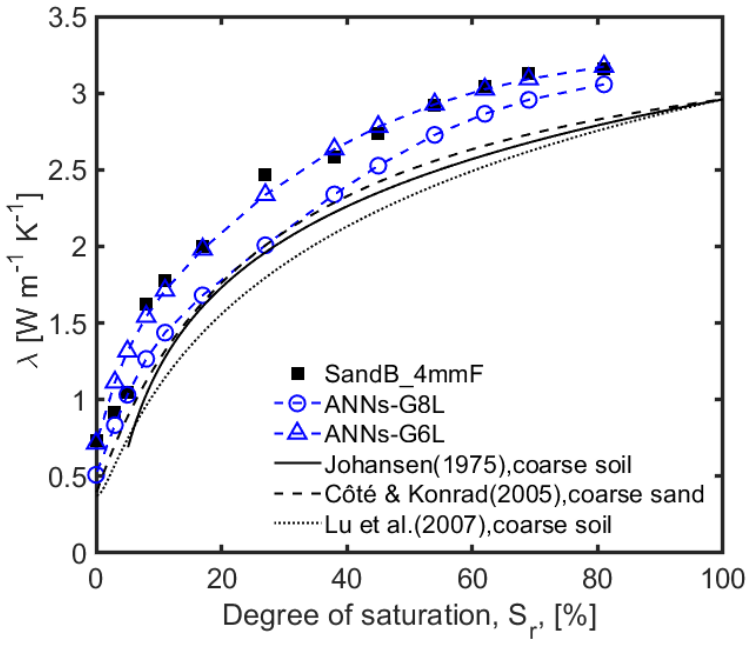

(A)

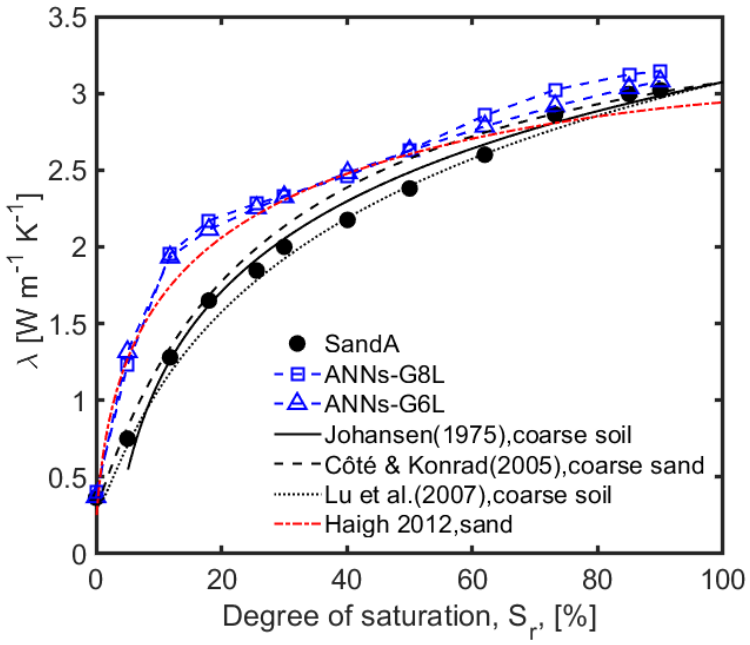

(B)

FIGURE 6.19: Comparison of proposed generalised ANN models and semi-empirical models with measured thermal conductivity values for (a) modified fuller sand (SandB_4mmF) and (b) sand-A.

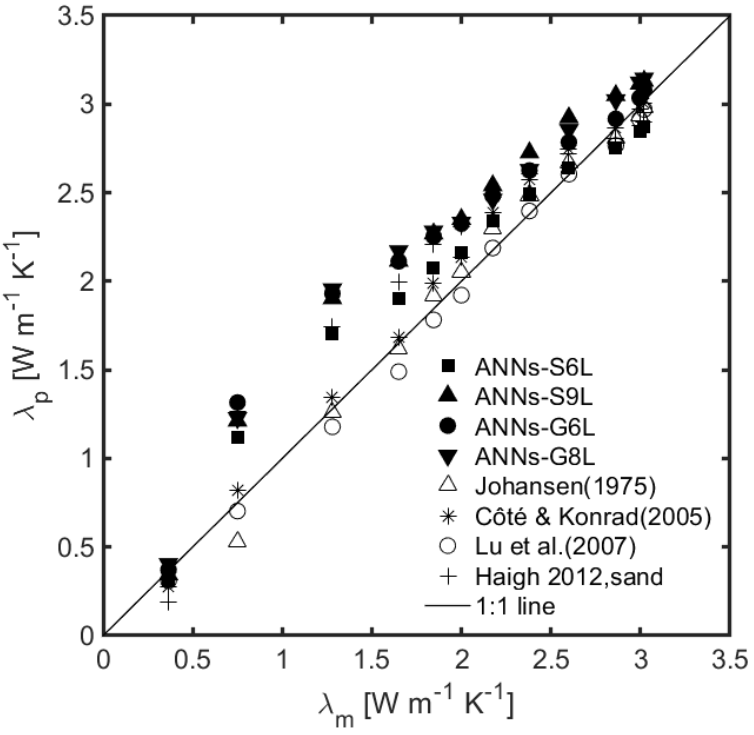

(A)

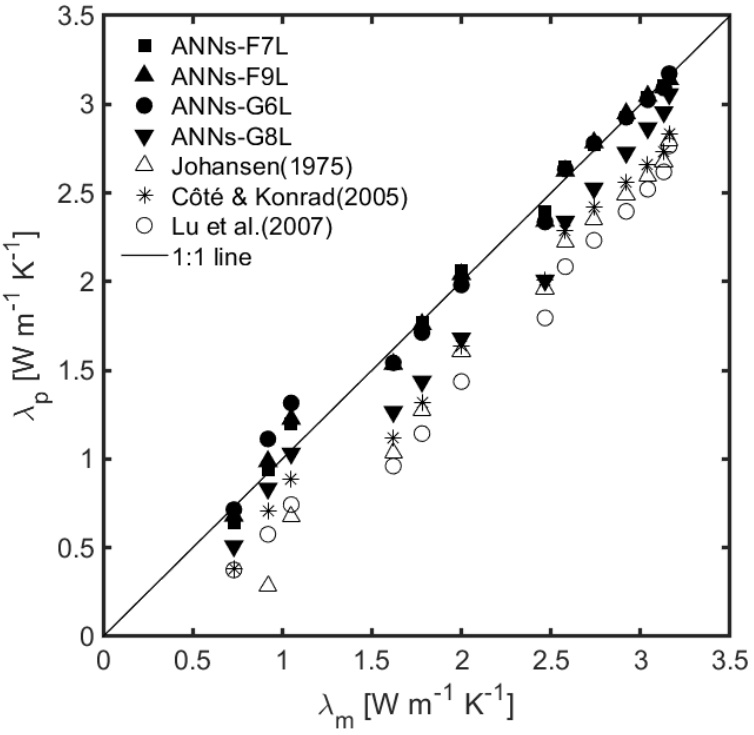

(B)

FIGURE 6.20: Comparison of proposed ANN models and empirical models with measured thermal conductivity value for (a)sand (b) modified fuller sand.

and original sand separately. It is certain that Gavriliev (2004) and Côté and Konrad (2005a) model for crushed rocks performs best in six empirical models, while predicted results of other empirical models are unacceptable since their MSE values are too high (> 0.040 W/K m).

TABLE 6.5: Performance indices of proposed ANN models and prediction models in predicting thermal conductivity of modified fuller and original sands in dry and moist case.

Model symbol	**State**	**Materials**	**R**	**MSE**	**MAE**
ANN-F6L	dry	modified fuller sand	0.9867	0.0007	0.0227
ANN-S9L		sand	0.9223	0.0003	0.0139
ANN-G9L		both sands	0.9594	0.0027	0.0388
Johansen (1975)		both sands	-	0.0480	0.0185
Lu et al. (2007)		both sands	-	0.0906	0.2422
Côté and Konrad (2005a)		both sands	-	0.0893	0.2512
Côté and Konrad (2005a)		both sands	0.7662	0.0174	0.0968
Balland and Arp (2005)		both sands	-	0.0570	0.2314
Gavriliev (2004)		both sands	0.8655	0.0106	0.0800
ANNs-F7L	moist	sandB_4mmF	0.9971	0.0041	0.0487
ANNs-F9L		sandB_4mmF	0.9962	0.0053	0.0572
ANNs-G6L		sandB_4mmF	0.9922	0.0110	0.0721
ANNs-G8L		sandB_4mmF	0.9540	0.0635	0.2231
Johansen (1975)		sandB_4mmF	0.7951	0.2129	0.4534
Côté and Konrad (2005a)		sandB_4mmF	0.9005	0.1335	0.3537
Lu et al. (2007)		sandB_4mmF	0.7928	0.2622	0.4989
ANNs-S6L		sandA	0.9676	0.0460	0.1861
ANNs-S9L		sandA	0.9141	0.1186	0.2943
ANNs-G6L		sandA	0.9207	0.1099	0.2573
ANNs-G8L		sandA	0.9149	0.1175	0.2871
Johansen (1975)		sandA	0.9910	0.0087	0.0762
Côté and Konrad (2005a)		sandA	0.9901	0.0135	0.0941
Lu et al. (2007)		sandA	0.9957	0.0058	0.0638
Haigh (2012)		sandA	0.9342	0.0870	0.2592

In the case of the moist state, the generalised model (ANNs-G) shows the best agreement predicting the measured thermal conductivity of both modified and original sand than other prediction models as it has the highest R-value and the lowest MSE value. Individual model ANNs-F provides the best matching to measured data of modified fuller sand than other models. However, the other three models besides Haigh (2012) model show a good performance than individual model ANNs-S when predicting for sand only. It means the existing prediction models are still the best prediction models when used for natural soils as they are developed specifically for that kind of material. Nevertheless, they couldn't provide the best matching for the measured value of designed materials in this study.

In summary, the generalized ANN models (ANN-G, ANNs-G) can be used to predict the thermal conductivity of modified fuller sand as well as original sand in both dry and moist

conditions, whereas the individual ANN models (ANN-F, ANN-S, ANNs-F, ANNs-S) can predict the thermal conductivity of modified and original sands separately.

6.9 Summary

In this chapter, the separate ANN models for the dry and moist states were established. For both models, individual and generalised ANN models were developed according to geomaterials. Individual ANN models were applied to specific geomaterials (original sand and modified fuller sand separately in this study) while generalised ANN models were applied to both materials. The developed models are also verified with independent experimental data and produced satisfactory results. The performance assessment of proposed ANN models with existing empirical, theoretical models was also done and it was found to be better than the latter.

Chapter 7

Applications of new materials design for embedded cables

7.1 Introduction

This chapter deals with the thermal simulation of a single cable using Finite Method software (Comsol multiphysics) to observe the heat dissipation characteristics around the underground cable with original and modified backfill materials.

7.2 Background

The performance and efficiency of underground high voltage cable depend on the thermal conductivity of the medium where it is placed. The thermal energy (heat) generated by the cable should be dissipated from the cable for safe operation and durability of the cable by maintaining the safe operating temperature of the cable. The current carrying capacity (or the ampacity) of the cable is proportional to the amount of maximum operating temperature of a cable, which is a function of the damage that the insulation of cable can suffer as a consequence of high operating temperature. Thus, the cable may lead to failure. The remedial cost of removing and replacing damaged cable and poor backfills are very high. In order to avoid this problem, the thermal conductivity of the medium where the cable is placed should have higher thermal conductivity than that of the surrounding soil. As explained earlier in chapter 2, the thermal conductivity is moisture dependent and very dry soils are usually characterized by low thermal conductivity due to interstitial air in the pores. A saturated soil has a higher thermal conductivity than a dry one. Therefore, particular attention has been given to heat transfer of the underground cables set in dry soils. It has not been taken into consideration the presence of humidity in the soil. These types of soil can determine a certain kind of condition such as thermal stress experienced by electric cables, which lead to a decrease in cable lifetime.

In order to study the thermal field in these circumstances, numerical simulation is done to calculate the steady-state and transient temperature distribution in underground high voltage power cables. The transient conditions are assumed to be caused by short-circuit conditions which result in several circuit breaker reclosure cycles. The analysis is the result of an energy balance, which includes the cable and surrounding earth. The numerical

simulation predicts the radial temperature distribution as a function of time with backfill materials. Numerical analysis is a design tool, which can be used to predict possible cable arrangement geometries, and operating conditions, which will lead to safe material temperatures under steady-state, and transient conditions. The numerical simulation also saves time as compared to physical modelling done in the laboratory.

In this study, the model was set up using Comsol Multiphysics (FEM software) in order to study and analysis of the phenomena of heat transfer with original and modified soils where a single cable was installed.

7.3 2D Simulation

7.3.1 Model setup

Figure 7.1 shows the geometry of the model with mesh generation, which consists of single cable, directly buried in the trench at 1.3m depth. The trench has a width of 0.5m and depth of 1.5m, while the size of the model, which represents surrounding soil, is 6m in width and 5m in height. The trench was first filled with sand and then with modified sand for the simulation. The trench is assumed to be in the dry state which is the worst-case scenario of the high voltage buried cables. Therefore, no moisture movement is considered in the simulation. Mechanical and thermal conductivity measurement was done on the proposed material. The results of the experimental testing are used in the numerical model to predict the behaviour of backfill material under various boundary conditions. The properties of the material, used in this simulation, are presented in Table 7.1.

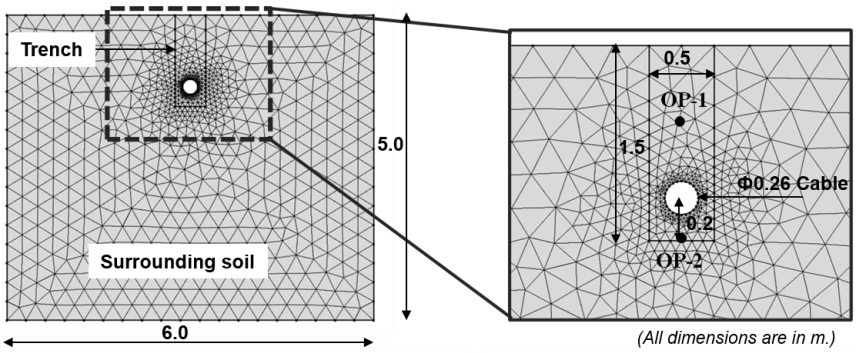

FIGURE 7.1: Geometry of model setup with mesh generation, after Shrestha et al. (2016).

The geometry was simulated in a 2-D environment, while the influence of air thermal conductivity was taken into consideration. Each material was assumed to be homogeneous with constant thermal conductivity and specific heat. The cable temperature was fixed at 90^{o}C, the maximum temperature the underground power cable can reach. The initial cable temperature distribution is assumed to be the steady-state values, which exist when the cable is operated without current fluctuations. At the boundary between the trench and surrounding soil, continuity of heat flux and temperature was assumed. The soil surface and other three sides were represented as an isothermal boundary at the temperature of

20^oC and 15^oC respectively. The transient heat transfer equation was solved numerically for 200 hrs using the Comsol Multiphysics software.

7.3.2 Results and discussions

Figure 7.2 show the outputs of the simulation showing the temperature distribution for 24 hrs, 72 hrs and 120 hrs respectively with unmodified sand (left) and modified sand (right).

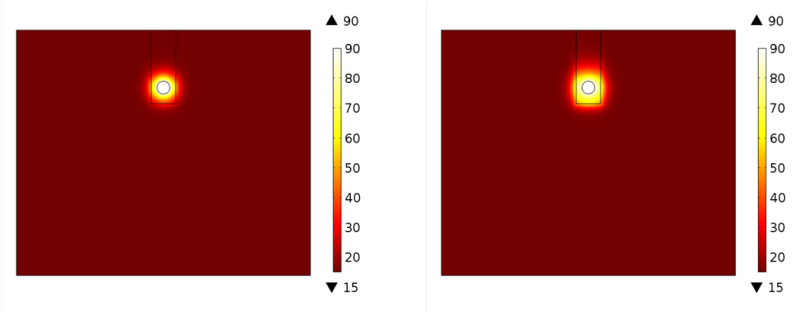

(A)

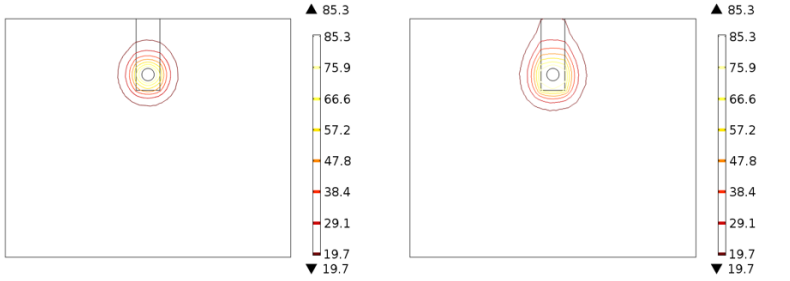

(B)

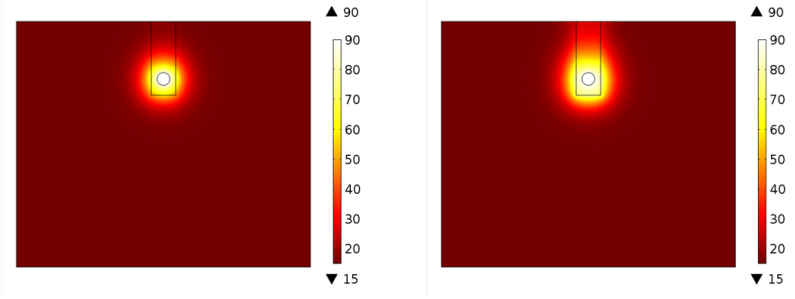

(C)

FIGURE 7.2: Temperature distribution around the underground cable with sand (left) and modified sand (right) at (a)24 hrs (b) 72 hrs (c) 120 hrs, after Shrestha et al. (2016).

The heat generated from the cable is dissipated away in a faster manner in the presence of modified fuller sand as compared to the original sand. It is due to the higher thermal conductivity of the modified fuller sand. Because of the lower thermal conductivity of the sand, the heat is generated in the cable faster than it dissipates away and a dry buffer zone is created around the cable which leads the cable temperature beyond its safe limit. Consequently, it leads to cable failure. At 120 hours, it is noticed that heat is accumulated around

TABLE 7.1: Thermal properties of simulated geometry.

Material	**thermal conductivity**	**Density**	**Heat capacity at constant pressure**
Unit	$W\,m^{-1}\,K^{-1}$	$kg\,m^{-3}$	$J\,kg^{-1}\,K^{-1}$
Soil	0.18	1450	900
Sand	0.36	1650	800
Modifiedsand	1.0	2000	800

the vicinity of the cables in case of original sand, whereas heat is dissipating away from the cables in case of modified fuller sand. Even at 24 hours, the heat is started to dissipate in case of modified fuller sand from the vicinity of the cable, but in the case of original sand, the dry buffer zone around the cable is started to create which will in long term affects the current capacity of the power cables. The results clearly indicate that the large improvement in heat dissipation for the modified soils which helps to prevent the cable overheated and thus prevent the cable failure and extend their life.

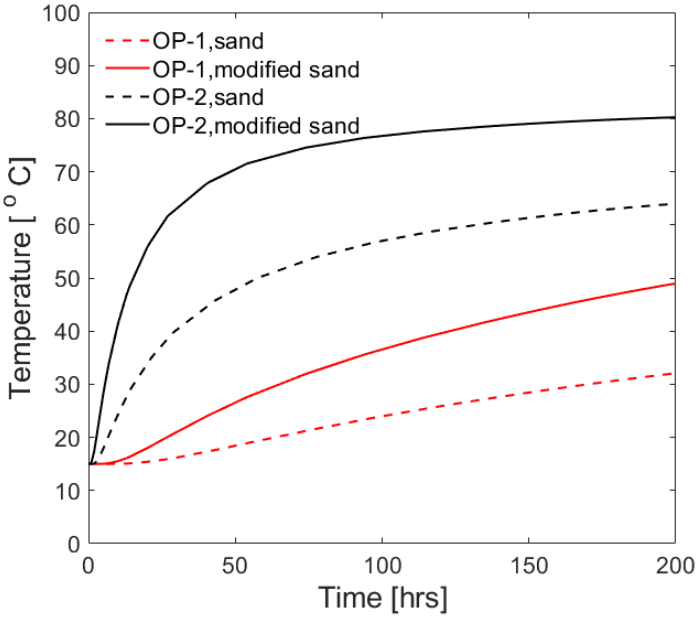

FIGURE 7.3: Temperature versus time at two observation points for original and modified sand, after Shrestha et al. (2016).

Two observation points OP-1 & OP-2 were plotted at depth of 0.5m & 1.5m respectively as shown in Figure 7.1 to observe the temperature rise characteristics within the selected period of 200hrs. Figure 7.3 shows temperature increment with respect to time at two selected points for unmodified and modified sand. The heat dissipations in the case of modified sand are faster as compared to unmodified sand in both observation points. At OP-2, there is an abrupt change in temperature in the beginning and 63^{o}C is reached in just 30 hrs for modified sand, whereas 200 hrs are needed to reach the same temperature for unmodified sand. Thereafter the temperature increases steadily after 50 hrs and 100 hrs for modified and unmodified sand respectively. The temperature is gradually increasing at OP-1 and

reaches to 50^{o}C and 32^{o}C for modified and unmodified sand respectively in 200 hrs. This behaviour can be also verified with a big-box experiment simulating a single underground cable. However, this is not the scope of this study.

7.4 Summary

A simple 2-D thermal simulation of a single underground cable was successfully done using Finite method software (Comsol mutliphysics) and the results show great improvement in heat dissipation away from the cable in case of modified fuller sand as compared to original sand due to its higher thermal conductivity.

Chapter 8

Conclusions and Recommendations

8.1 Conclusions

The efficiency and performance of geo-energy applications like underground high voltage power cables, heat storage facilities, nuclear waste disposal facilities, etc. depend on the thermal conductivity of the soil where they are built. Especially, the underground high voltage power cables need backfill materials with high thermal conductivity because of their influences on the designs, performances and economics of underground cables. The thermal conductivity itself is dependent of several factors such as porosity, moisture content, soil fabrics, mineralogy, temperature, etc. In this regard, the variation and correlation of these factors on thermal conductivity was analysed theoretically and experimentally in order to design the composite granular materials with high thermal conductivity. As the thermal conductivity is mostly moisture dependent, the thermal conductivity is drastically reduced with a decrease in moisture and attains very low thermal conductivity in a dry state. So, the main focus was made in a dry state while developing the backfill materials as it is the worst scenario in the case of the underground high voltage power cables. The extensive experimental investigations that include materials selection, detailed planning of experimental procedure, use of the right equipment were performed to obtain the desired goal of this study. The granular materials with high thermal conductivity were developed and the effect of various factors on its thermal conductivity was investigated.

In this study, the original sand was modified by changing its gradation into fuller curve gradation and adding fine particles as fillers. This modification shows a strong effect on increasing the thermal conductivity of sand for dry conditions as well as various moisture content. Comparing the thermal conductivity of modified sand with that of original sand shows improvement up to 230% in the dry case. In the case of the dry state, the filler types don't make any difference on thermal conductivity since the improvement achieved for the dry case remains the same. The highest thermal conductivity achieved for 8mmF fuller sand was 1.12 $\mathrm{W\,m^{-1}\,K^{-1}}$ at lowest porosity and for the same material, the thermal conductivity was 0.6 $\mathrm{W\,m^{-1}\,K^{-1}}$ at loose state, i.e. 90% improvement. According to the denseness of the materials, the improvement in the thrermal conductivity varies. Hence, the improvement in thermal conductivity for 8mmF, 4mmF and 2mmF are in the range of 90-230%, 50-170%, 25-120%. These thermal conductivity data of developed materials are significantly higher than that of the original sand. Even in this study, the highest thermal conductivity for the sand

is 0.4 $W\,m^{-1}\,K^{-1}$. Therefore, even in the worst-case scenario of underground high voltage cables, these developed materials could provide a better alternative since the major problems of the backfill used in this application is the dryness of the materials and the thermal conductivity of soils, in this case, is below 0.5 $W\,m^{-1}\,K^{-1}$.

These developed materials were also tested across the various moisture content. As expected, the thermal conductivity of the modified sands and the original sand increased with increasing moisture content. However, the modified sand increased rapidly in the range of 0–20% saturation than the original sand. An improvement of 80–136% was achieved for the modified sand A whereas (54–120)% for the modified sand B in the dry state. A significant improvement was noticed in the dry and lower saturation, whereas, a considerable improvement was observed in the higher saturation. For the full range of saturation, the improvement of (22–80)% for the 2mmF, (35–135)% for 4mmF and (40–180)% for 8mmF are achieved with sand A. Even with sand B, the improvement of (15-191) % was achieved despite having low quartz content than sand A. The improvement is highest at the dry state and decreases with an increase in the moisture content. This characteristic is a very essential requirement in terms of backfill materials development. The improvement achieved helps underground power cables to carry the current to full capacity and increase the cable life. Therefore, the developed material could be a better alternative where high thermal conductivity is needed even at a low saturation value.

The work presented in this study also confirms previous findings such as the decrease in thermal conductivity with an increase in soil porosity, the increase in thermal conductivity with the increase in moisture content, the impact of high quartz content on the thermal conductivity, the particle size distribution influence on the dry thermal conductivity, an improvement of quality of contacts due to addition of fine particles which in turn enhances thermal conduction. The filler types don't make any difference in dry thermal conductivity. The use of bentonite and stone-dust produced the same results despite different characteristics. However, in the case of moisture, the stone-dust was better due to the highly swelling and impermeable characteristics of bentonite. The mineral has also a strong impact on the thermal conductivity in the case of saturation and unsaturation case. However, in the case of the dry state, no significant influence could be noticed unless using highly conductive materials like SiC.

The experiment results were compared with existing prediction models and observed that the existing empirical prediction models are unable to capture the increment of the thermal conductivity and underestimate the measured thermal conductivity. The thermal conductivity increases with decreasing void volume and increasing the filler content due to an increase in the amount of contact area through which heat transfer can take place in granular matter. This study shows that effective thermal conductivity of dry granular matrix with filler and voids not only depends upon total void volume (porosity) but it is influenced by contact conductance, local particle and volume shape and the heat conduction path. These parameters are not considered in semi-empirical modelling. Most of the existing prediction models simplify the problem by including several assumptions associated with the aforementioned factors that affect the thermal conductivity. Therefore, a reasonable agreement

could not be obtained with existing semi-empirical models while comparing with experimental results. The new prediction models for developed materials are developed on the basis of artificial neural network (ANN) technology.

An Artificial neural network as an alternative simple method was selected to predict the thermal conductivity of modified fuller sands as well as original sand. The developed artificial neural network (ANN) was capable of demonstrating its usefulness for the estimation of the effective parameters. An individual and generalised ANN models were developed for the dry and moist states and they were confirmed to describe the measured data as well. The individual ANN models are only suitable for modified and original sand, whereas the generalised ANN model is applicable to both sand. The individual ANN models are suggested to be used for predicting thermal conductivity when the gradation parameters of targeted soils are not clear, whilst the generalized ANN model is preferable when the gradation parameters are known. The proposed ANN models have been verified and compared with existing prediction models to reinforce their superiority and applicability using independent data. All the developed ANN models show good agreement with experimental results as their R is very close to 1 and MSE and MAE are also very low. The cross-validation technique used in this study is also useful to develop the ANN models. A single hidden layer with multiple neurons is capable to predict the thermal conductivity of modified and original sand in dry as well as the moist state. The ANN models proposed in this study are only valid for the types of geomaterials discussed in this research. The applicability of the proposed models to other types of geomaterials should be checked in future studies.

The output of thermal simulation done in this study for underground cable clearly indicate that the large improvement in heat dissipation for the modified soils helps to prevent the cable overheated and thus extend the cable life.

8.2 Recommendations for future work

In this research, the composite granular materials with enhanced thermal conductivity were developed by analysing various influencing factors and incorporating those factors while designing geomaterials and ANN models were also established for the prediction of thermal conductivity of developed geomaterials. However, some recommendations for future work on the improvement and extension of the present work are discussed below.

- The multi-purpose test including thermal conductivity and water potential measurement can be done to obtain the water characteristics curve and thermal conductivity curve of the same condition.
- Thermal stability test can be done for further validation of the use of the materials.
- A big box experiment can be performed to simulate the underground power cables in order to know the suitability and applicability of developed materials.

- Study of moisture variation across the length/depth of the sample depending on the size of the sample and its effect on the thermal conductivity of the different types of soils using the vertical thermal needle probe.
- Possibility of extension and validation of such improved method for fine-textured soils such as silty clay.
- Assessment of the use of high conductive materials to improve further.
- ANN models can be expanded to other types of materials with more experimental data to include all the available boundary conditions. ANN models developed here are limited to some specific boundary conditions.
- More experimental data are needed to build a good database so that generalised ANN models consisting of more factors can be developed with a wide range of boundary conditions.
- ANN models with multi-layer and GA technologies for the prediction of thermal conductivity of soils so that ANN can even solve complex problems.

Appendix A

ANN models' performance indices

A.1 Performances indices of different ANN models for Training, Validation & Testing data

The performance indices (R, MSE, MAE) of the network are calculated for the training, validation and testing data for each proposed network size. The values of R, MSE and MAE are listed in Tables A.1 to A.6 for respective ANN-F, ANN-S, ANN-G (dry ANN models) and ANNs-F, ANNs-S, ANNs-G (moist ANN models). The ANN networks for different conditions and materials are selected as per best performances indices and the selected ANN networks are highlighted in bold letters in each Table.

A.2 Performances indices of different ANN models for new experimental data

The performances indices of all the developed models are presented in Tables A.7-A.9 for dry ANN models and A.10-A.12 moist ANN models (individual and generalised). These indices check the validity of proposed ANN models by predicting the thermal conductivity of new experimental (independent) data. The data has not been used while developing the ANN models. The selected ANN models show good agreement with experimental data.

TABLE A.1: Performance indices for different ANN-F models.

Model symbol	**Hidden nodes**	**Data**	**R**	**MSE**	**MAE**
ANN-F	1	Training	0.9725	0.0018	0.0350
		Validation	0.9438	0.0055	0.0536
		Testing	0.9628	0.0026	0.0443
ANN-F	2	Training	0.9875	0.0010	0.0198
		Validation	0.9864	0.0012	0.0260
		Testing	0.9702	0.0015	0.0292
ANN-F	3	Training	0.9924	0.0006	0.0175
		Validation	0.9851	0.0008	0.0174
		Testing	0.9750	0.0022	0.0319
ANN-F	4	Training	0.9978	0.0002	0.0094
		Validation	0.9956	0.0003	0.0121
		Testing	0.9700	0.0013	0.0200
ANN-F	5	Training	0.9943	0.0004	0.0143
		Validation	0.9887	0.0007	0.0174
		Testing	0.9938	0.0005	0.0157
ANN-F	**6**	Training	**0.9968**	**0.0002**	**0.0101**
		Validation	**0.9900**	**0.0008**	**0.0198**
		Testing	**0.9931**	**0.0005**	**0.0173**
ANN-F	**7**	Training	**0.9980**	**0.0004**	**0.0085**
		Validation	**0.9932**	**0.0006**	**0.0153**
		Testing	**0.9856**	**0.0011**	**0.0215**
ANN-F	8	Training	0.9971	0.0002	0.0080
		Validation	0.9922	0.0008	0.0211
		Testing	0.9863	0.0008	0.0189
ANN-F	9	Training	0.9961	0.0003	0.0118
		Validation	0.9876	0.0008	0.0185
		Testing	0.9904	0.0007	0.0160
ANN-F	10	Training	0.9963	0.0003	0.0108
		Validation	0.9838	0.0007	0.0183
		Testing	0.9808	0.0007	0.0191

TABLE A.2: Performance indices for different ANN-S models.

Model symbol	**Hidden nodes**	**Data**	**R**	**MSE**	**MAE**
ANN-S	1	Training	0.8894	0.00062	0.0214
		Validation	0.7710	0.00100	0.0279
		Testing	0.6218	0.00057	0.0206
ANN-S	3	Training	0.9072	0.00042	0.0175
		Validation	0.9187	0.00045	0.0194
		Testing	0.9047	0.00068	0.0232
ANN-S	5	Training	0.9140	0.00055	0.0181
		Validation	0.8328	0.00074	0.0200
		Testing	0.7469	0.00043	0.0169
ANN-S	7	Training	0.9600	0.00025	0.0120
		Validation	0.8317	0.00050	0.0181
		Testing	0.8628	0.00063	0.0195
ANN-S	**9**	Training	**0.9184**	**0.00037**	**0.0143**
		Validation	**0.9412**	**0.00044**	**0.0152**
		Testing	**0.8988**	**0.00051**	**0.0197**
ANN-S	12	Training	0.9253	0.00031	0.0129
		Validation	0.9571	0.00038	0.0151
		Testing	0.8617	0.00056	0.0184
ANN-S	15	Training	0.8722	0.00054	0.0193
		Validation	0.9288	0.00045	0.0192
		Testing	0.9373	0.00044	0.0145
ANN-S	**20**	Training	**0.9232**	**0.00034**	**0.0102**
		Validation	**0.9362**	**0.00037**	**0.0150**
		Testing	**0.9149**	**0.00063**	**0.0184**

TABLE A.3: Performance indices for different ANN-G models.

Model symbol	**Hidden nodes**	**Data**	**R**	**MSE**	**MAE**
ANN-G	1	Training	0.9724	0.0030	0.0384
		Validation	0.9658	0.0046	0.0475
		Testing	0.9503	0.0048	0.0478
ANN-G	2	Training	0.9856	0.0018	0.0293
		Validation	0.9615	0.0034	0.0468
		Testing	0.9815	0.0017	0.0302
ANN-G	3	Training	0.9716	0.0030	0.0384
		Validation	0.9745	0.0036	0.0413
		Testing	0.9644	0.0039	0.0445
ANN-G	4	Training	0.9849	0.0016	0.0306
		Validation	0.9757	0.0017	0.0354
		Testing	0.9806	0.0034	0.0446
ANN-G	5	Training	0.9888	0.0012	0.0259
		Validation	0.9815	0.0026	0.0372
		Testing	0.9717	0.0027	0.0412
ANN-G	**6**	Training	**0.9894**	**0.0012**	**0.0271**
		Validation	**0.9880**	**0.0012**	**0.0288**
		Testing	**0.9854**	**0.0018**	**0.0351**
ANN-G	7	Training	0.9930	0.0008	0.0219
		Validation	0.9928	0.0008	0.0190
		Testing	0.9837	0.0016	0.0309
ANN-G	8	Training	0.9878	0.0013	0.0287
		Validation	0.9937	0.0009	0.0237
		Testing	0.9850	0.0015	0.0313
ANN-G	**9**	Training	**0.9870**	**0.0013**	**0.0266**
		Validation	**0.9761**	**0.0023**	**0.0361**
		Testing	**0.9860**	**0.0019**	**0.0351**
ANN-G	10	Training	0.9848	0.0018	0.0340
		Validation	0.9798	0.0013	0.0291
		Testing	0.9844	0.0020	0.0365

TABLE A.4: Performance indices for different ANNs-F models.

Model symbol	**Hidden nodes**	**Data**	**R**	**MSE**	**MAE**
ANNs-F	1	Training	0.9407	0.1042	0.2646
		Validation	0.9609	0.0662	0.2103
		Testing	0.9436	0.0841	0.2417
ANNs-F	2	Training	0.9918	0.0149	0.1001
		Validation	0.9876	0.0159	0.1056
		Testing	0.9925	0.0132	0.0906
ANNs-F	3	Training	0.9968	0.0054	0.0554
		Validation	0.9967	0.0060	0.0568
		Testing	0.9962	0.0064	0.0603
ANNs-F	4	Training	0.9977	0.0038	0.0469
		Validation	0.9966	0.0061	0.0574
		Testing	0.9974	0.0051	0.0569
ANNs-F	5	Training	0.9978	0.0037	0.0478
		Validation	0.9973	0.0068	0.0703
		Testing	0.9969	0.0041	0.0523
ANNs-F	6	Training	0.9982	0.0024	0.0396
		Validation	0.9982	0.0024	0.0396
		Testing	0.9982	0.0040	0.0536
ANNs-F	**7**	Training	**0.9984**	**0.0026**	**0.0389**
		Validation	**0.9988**	**0.0023**	**0.0376**
		Testing	**0.9989**	**0.0020**	**0.0350**
ANNs-F	8	Training	0.9990	0.0016	0.0325
		Validation	0.9983	0.0036	0.0477
		Testing	0.9978	0.0036	0.0425
ANNs-F	**9**	Training	**0.9990**	**0.0019**	**0.0328**
		Validation	**0.9988**	**0.0019**	**0.0338**
		Testing	**0.9979**	**0.0028**	**0.0449**
ANNs-F	10	Training	0.9992	0.0014	0.0280
		Validation	0.9976	0.0032	0.0412
		Testing	0.9981	0.0037	0.0412

TABLE A.5: Performance indices for different ANNs-S models.

Model symbol	**Hidden nodes**	**Data**	**R**	**MSE**	**MAE**
ANNs-S	1	Training	0.8987	0.1427	0.3043
		Validation	0.9215	0.1167	0.2500
		Testing	0.7767	0.1961	0.3483
ANNs-S	2	Training	0.9715	0.0389	0.1556
		Validation	0.9776	0.0365	0.1316
		Testing	0.9417	0.0609	0.2020
ANNs-S	3	Training	0.9874	0.0173	0.1025
		Validation	0.9843	0.0282	0.1344
		Testing	0.9731	0.0235	0.1173
ANNs-S	4	Training	0.9872	0.0177	0.1033
		Validation	0.9912	0.0150	0.0954
		Testing	0.9752	0.0232	0.1290
ANNs-S	5	Training	0.9918	0.0114	0.0752
		Validation	0.9828	0.0212	0.1196
		Testing	0.9856	0.0202	0.1108
ANNs-S	**6**	Training	**0.9964**	**0.0046**	**0.0522**
		Validation	**0.9813**	**0.0269**	**0.1145**
		Testing	**0.9940**	**0.0091**	**0.0706**
ANNs-S	7	Training	0.9910	0.0106	0.0737
		Validation	0.9917	0.0156	0.1020
		Testing	0.9894	0.0144	0.0973
ANNs-S	8	Training	0.9938	0.0102	0.0763
		Validation	0.9816	0.0149	0.0957
		Testing	0.9895	0.0113	0.0845
ANNs-S	**9**	Training	**0.9947**	**0.0070**	**0.0603**
		Validation	**0.9827**	**0.0183**	**0.1048**
		Testing	**0.9919**	**0.0148**	**0.0943**
ANNs-S	10	Training	0.9949	0.0070	0.0605
		Validation	0.9820	0.0237	0.12162
		Testing	0.9860	0.0207	0.1168

TABLE A.6: Performance indices for different ANNs-G models.

Model symbol	**Hidden nodes**	**Data**	**R**	**MSE**	**MAE**
ANNs-G	1	Training	0.9143	0.1770	0.3351
		Validation	0.8944	0.1875	0.3329
		Testing	0.9323	0.1521	0.3294
ANNs-G	2	Training	0.9829	0.0355	0.1429
		Validation	0.9710	0.0496	0.1641
		Testing	0.9841	0.0394	0.1450
ANNs-G	3	Training	0.9889	0.0219	0.1154
		Validation	0.9908	0.0231	0.1182
		Testing	0.9877	0.0266	0.1267
ANNs-G	4	Training	0.9942	0.0118	0.0834
		Validation	0.9955	0.0115	0.0805
		Testing	0.9907	0.0185	0.1016
ANNs-G	5	Training	0.9962	0.0082	0.0697
		Validation	0.9925	0.0162	0.0950
		Testing	0.9945	0.0110	0.0725
ANNs-G	**6**	Training	**0.9957**	**0.0091**	**0.0684**
		Validation	**0.9953**	**0.0092**	**0.0745**
		Testing	**0.9968**	**0.0071**	**0.0653**
ANNs-G	7	Training	0.9965	0.0071	0.0614
		Validation	0.9969	0.0073	0.0684
		Testing	0.9959	0.0089	0.0723
ANNs-G	**8**	Training	**0.9966**	**0.0069**	**0.0593**
		Validation	**0.9978**	**0.0054**	**0.0588**
		Testing	**0.9957**	**0.0079**	**0.0703**
ANNs-G	9	Training	0.9978	0.0046	0.0483
		Validation	0.9960	0.0082	0.0618
		Testing	0.9963	0.0088	0.0720
ANNs-G	10	Training	0.9976	0.0053	0.0493
		Validation	0.9963	0.0081	0.0687
		Testing	0.9937	0.0112	0.0796

TABLE A.7: Performance indices for different ANN-F models obtained for new experimental data.

Model symbol	Hidden nodes	R	MSE	MAE
ANNF1L	1	0.9270	0.0037	0.0489
ANNF2L	2	0.9746	0.0013	0.0297
ANNF3L	3	0.9796	0.0011	0.0279
ANNF4L	4	0.9817	0.0009	0.0277
ANNF5L	5	0.9755	0.0013	0.0270
ANNF6L	6	0.9867	0.0007	0.0227
ANNF7L	7	0.9773	0.0012	0.0286
ANNF8L	8	0.9695	0.0016	0.0327
ANNF9L	9	0.9842	0.0026	0.0404
ANNF10L	10	0.9198	0.0040	0.0364

TABLE A.8: Performance indices for different ANN-S models obtained for new experimental data.

Model symbol	Hidden nodes	R	MSE	MAE
ANNS1L	1	0.96384	0.00027	0.0152
ANNS3L	3	0.93850	0.00025	0.0132
ANNS5L	5	0.93385	0.00024	0.0137
ANNS7L	7	0.93325	0.00023	0.0130
ANNS9L	9	0.92226	0.00027	0.0139
ANNS12L	12	0.93181	0.00023	0.0121
ANNS15L	15	0.92694	0.00027	0.0144
ANNS20L	20	0.91993	0.00031	0.0153

TABLE A.9: Performance indices for different ANN-G models obtained for new experimental data.

Model symbol	Hidden nodes	R	MSE	MAE
ANNG1L	1	0.9709	0.0020	0.0325
ANNG2L	2	0.9624	0.0025	0.0354
ANNG3L	3	0.9749	0.0017	0.0316
ANNG4L	4	0.9503	0.0033	0.0438
ANNG5L	5	0.9438	0.0037	0.0474
ANNG6L	6	0.9353	0.0043	0.0435
ANNG7L	7	0.8567	0.0091	0.0576
ANNG8L	8	0.9224	0.0051	0.0476
ANNG9L	9	0.9594	0.0027	0.0388
ANNG10L	10	0.9482	0.0035	0.0445

TABLE A.10: Performance indices for different ANNs-F models obtained for independent data.

Model symbol	Hidden nodes	R	MSE	MAE
ANNs-F1L	1	0.9462	0.0740	0.2260
ANNs-F2L	2	0.9879	0.0170	0.1125
ANNs-F3L	3	0.9950	0.0071	0.0653
ANNs-F4L	4	0.9966	0.0049	0.0463
ANNs-F5L	5	0.9962	0.0054	0.0558
ANNs-F6L	6	0.9972	0.0039	0.0488
ANNs-F7L	7	0.9971	0.0041	0.0487
ANNs-F8L	8	0.9965	0.0050	0.0517
ANNs-F9L	9	0.9962	0.0053	0.0572
ANNs-F10L	10	0.9950	0.0071	0.0551

TABLE A.11: Performance indices for different ANNs-S models obtained for new experimental data.

Model symbol	Hidden nodes	R	MSE	MAE
ANNs-S1L	1	0.8867	0.1543	0.315
ANNs-S2L	2	0.8882	0.1523	0.3007
ANNs-S3L	3	0.9398	0.0842	0.2273
ANNs-S4L	4	0.9318	0.0951	0.2323
ANNs-S5L	5	0.9022	0.1342	0.3074
ANNS6L	6	0.9676	0.0460	0.1861
ANNs-S7L	7	0.9100	0.1241	0.3028
ANNs-S8L	8	0.9225	0.1075	0.2838
ANNs-S9L	9	0.9141	0.1186	0.2943
ANNs-S10L	10	0.8188	0.2377	0.3621

TABLE A.12: Performance indices for different ANNs-G models obtained for new experimental data.

Model symbol	Hidden nodes	Exp. data	R	MSE	MAE
ANNs-G1L	1	sandB_4mmF	0.9344	0.0896	0.2426
ANNs-G1L	1	sandA	0.7853	0.2766	0.4777
ANNs-G2L	2	sandB_4mmF	0.9798	0.0283	0.1419
ANNs-G2L	2	sandA	0.8805	0.1621	0.3866
ANNs-G3L	3	sandB_4mmF	0.9814	0.0260	0.1347
ANNs-G3L	3	sandA	0.9376	0.0873	0.2236
ANNs-G4L	4	sandB_4mmF	0.9778	0.0310	0.1445
ANNs-G4L	4	sandA	0.9385	0.0861	0.2176
ANNs-G5L	5	sandB_4mmF	0.9923	0.0108	0.0707
ANNs-G5L	5	sandA	0.9257	0.1032	0.2571
ANNs-G6L	6	sandB_4mmF	0.9922	0.0110	0.0721
ANNs-G6L	6	sandA	0.9207	0.1099	0.2573
ANNs-G7L	7	sandB_4mmF	0.9863	0.0192	0.1159
ANNs-G7L	7	sandA	0.9170	0.1147	0.2941
ANNs-G8L	8	sandB_4mmF	0.9540	0.0635	0.2231
ANNs-G8L	8	sandA	0.9149	0.1175	0.2871
ANNs-G9L	9	sandB_4mmF	0.9920	0.0112	0.0827
ANNs-G9L	9	sandA	0.9275	0.1008	0.2480
ANNs-G10L	10	sandB_4mmF	0.9852	0.0207	0.1305
ANNs-G10L	10	sandA	0.9253	0.1038	0.2710

Bibliography

Abu-Hamdeh, N. H. and R. C. Reeder (2000). "Soil thermal conductivity: Effects of density, moisture, salt concentration and organic matter". In: *Soil Science Socieity of American Journal* 64, pp. 1285–1290.

Abuel-Naga, H. M., D. T. Bergado, and A. Bouazza (2008). "Thermal conductivity evolution of saturated clay under consolidation process". In: *International Journal of Geomechanics* 8.2, pp. 114–122.

Adams, J. I. and A. F. Baljet (1968). "Thermal behaviour of cable backfill materials". In: *IEEE Transaction on Power Apparatus and Systems* 87.4, pp. 1149–1161.

Afa, J. T. (2010). "Subsoil temperature and underground cable distribution in Port Harcourt City". In: *Journal of Applied Sceince Engineering Technology* 2.6, pp. 527–531.

Akrouch, G. A., M. Sanchez, and J. L. Briaud (2015). "Effect of the unsaturted soil condition on the thermal efficiency of energy piles". In: *IFCEE*, pp. 1618–1627.

Alrtimi, A., M. Rouainia, and S. K. Haigh (2016). "Thermal conductivity of a sandy soil". In: *Applied Thermal Engineering* 106, pp. 551–560.

Alrtimi, A. A. (2008). "Experimental investigation of thermal conductivity of soils and borehole grouting materials". In: *PhD thesis. School of Civil Engineering and Geosciences, Newcastle University, UK.*

Amari, S. I., N. Murata, K. R. Muller, M. Finke, and H. H. Yang (1993). "Asympotic statistical theory of overtraining and cross-validation". In: *IEEE Transactions on Neural Networks* 8.5, pp. 985–996.

Anders, G. J. and H. S. Radhakrishna (1988). "Power cable thermal analysis with consideration of heat and moisture transfer in the soil". In: *IEEE Transactions on Power Delivery* 3.4, pp. 1280–1288.

ApalooBara, K. K., A. A. Salami, M. K. Kodjo, A. Guenoukpati, S. O. Djandja, and K. Bedja (2019). "Estimation of soils electrical resisitivity using artificial neural network approach". In: *American Journal of Applied Sciences* 16.2, pp. 43–58.

ASTM D 5334 - 08 (2008). *Standard test method for determination of thermal conductivity of soil and soft rock by thermal needle probe procedure*. ASTM International, West Conshohocken, Pennsylvania, USA.

Attoh-Okine, N. O. (1999). "Analysis of learning rate and momnetum term in back-propagation neural network algorithm trained to predict pavement performance". In: *Advance in Engineering Software* 30, pp. 291–302.

Azoff, E. M. (1994). "Neural Network Time series Forcasting of financial markets". In: *John Wiley & Sons, England*.

Balland, V. and P. A. Arp (2005). "Modelling soil thermal conductivities over a wide range of conditions". In: *Journal of Environmental Engineering Science* 4.6, pp. 549–558.

Banimahd, M., S. S. Yasrobi, and P. K. Woodward (2005). "Artificial neural network for stress strain behavior of sandy soils: Knowledge based verification". In: *Computer and Geotechnics* 32, pp. 377–386.

Baziar, M. H. and N. Nilipour (2003). "Evaluation of liquefaction potential using neural networks and CPT results". In: *Soil Dynamics and Earthquake Engineering* 23, pp. 631–636.

Benning, R. M., T. M. Becker, and A. Delgado (2001). "Initial studies of predicting flow fields with an ANN hybrid". In: *Advances in Engineering Software* 32, pp. 895–901.

Berke, L. and P. Hajela (1991). "Application of neural networks in structural optimization". In: *NATO/AGARD Advanced Study Institute* 23.2, pp. 731–745.

Bian, H., S. Liu, G. Cai, and L. Tian (2015). "Artificial neural network models for predicting soil electrical resisitivity". In: *Journal of Intelligent and Fuzzy Systems* 29.5, pp. 1751–1759.

Bowden, G. J., H. R. Maier, and G. C. Dandy (2002). "Optimal division of data for neural network models in water resources applications". In: *Water Resources Research* 38.2, pp. 201–211.

Braddock, R.D., M. L. Kremer, and L. Sanzogni (1998). "Feed-forward artificial neural network model for forecasting rainfall run-off". In: *Journal of Hydrologic Engineering* 9, pp. 419–432.

Cavalieria, S., P. Maccarrone, and R. Pintoa (2003). "Parametric vs neural network models for the estimation of prouduction costs: A case study in the automotive industry". In: *International Jouranal of Proudcution Economics* 11.5, pp. 497–507.

Chauhan, S., W. Ruehaak, H. Anbergen, A. Kabdenov, M. Freise, T. Wille, and I. Sass (2016a). "Phase segmentation of X-ray computer tomography rock images using machine learning techniques: an accuracy and performance study". In: *Solid Earth* 7, pp. 1125–1139.

Chauhan, S., W. Ruehaak, F. Khan, F. Enzmann, P. Mielke, M. Kersten, and I. Sass (2016b). "Processing of rock core microtomography images: Using seven different machine learning algorithms". In: *Computer & Geosciences* 86, pp. 120–128.

Chayjan, R. A., G. A. Montazer, T. T. Hashjin, M. H. Khoshtaghaza, and B. Ghobadian (2007). "Using neural networks to predict thermal conductivity of food as a function of moisture content, temperature and apparent porosity". In: *International Journal of Agriculture & Biology* 9, pp. 816–820.

Chen, S. X. (2008). "Thermal conductivity of sands". In: *Heat Mass Transfer* 44.1241.

Chester, D. L. (1990). "Why two hidden layers are better than one". In: *International Joint Conference on Neural Networks* 1, pp. 265–268.

Choo, J., J. H. Lee, Y. S. Kim, and T. S. Yun (2012). "Stress-dependent thermal conductivity evolution of granular materials". In: *Geocongress, ASCE*, pp. 4486–4494.

Cortes, D. D., A. I. Martin, T. S. Yun, F. M. Francisca, J. C. Santamarina, and C. Ruppel (2009). "Thermal conductivity of hydrate-bearing sediments". In: *Journal of Geophysical Research* 114.

Côté, J. and J. M. Konrad (2005a). "A generalized thermal conductivity model for soils and construction materials". In: *Canadian Geotechinical Journal* 42, pp. 443–458.

Côté, J. and J. M. Konrad (2005b). "Thermal conductivity of basecourse materials". In: *Canadian Geotechinical Journal* 42, pp. 61–78.

Côté, J. and J. M. Konrad (2009). "Assessment of strucure effects on the thermal conductivtiy of two-phase geomaterials". In: *International Journal of Heat and Mass Transfer* 52, pp. 796–804.

De León, F. and G. J. Anders (2008). "Effects of backfilling on cable amapacity analyzed with the finite element method". In: *IEEE Transactions on Power Delivery* 23.2, pp. 537–543.

De Vries, D. A. (1963). "Physics of plant environment". In: *W.R. Van Wijk (eds.), Thermal properties of soils* 00, pp. 210–235.

Denton, J. W., L. Sayeed, N. D. Perkins, and A. H. Moorman (1995). "Neural networks to classify employees for tax purpose". In: *Accounting, Management and Information Technologies* 5.2, pp. 123–138.

Dong, Y., J. S. McCartney, and N. Lu (2015). "Critical review of thermal conductivity models for unsaturated soils". In: *Geotechnical and Geological Engineering* 33.2, pp. 207–221.

Drefke, C., J. Stegner, J. Dietrich, and I. Sass (2015). "Influence of the Hydraulic Properties of Unconsolidated Rocks and Backfill Materials on the Change of the Thermophysical Characteristics by Heat Transfer". In: *World Geothermal Congress, Melbourne*.

Erzin, Y., B. H. Rao, A. Patel, S. D. Gumaste, and D. N. Singh (2010). "Artificial neural network models for predicting electrical resisitivity of soils from their thermal resistivity". In: *International Journal of Thermal Sceinces* 49.1, pp. 118–130.

Erzin, Y., B. H. Rao, and D. N. Singh (2008). "Artificial neural network models for predicting soil thermal resistivity". In: *International Journal of Thermal Sceinces* 47.10, pp. 1347–1358.

Fahlman, S. E. and C. Lebiere (1990). "The cascade-correlation learning architecture". In: *Advances in Neural Information Processing Systems 2, D. S. Touretzky, ed., Morgan Kaufmann, San Mateo, Californian*, pp. 524–532.

Farouki, O. T. (1981). "Thermal properties of soils". In: *CRREL Monograph 81-1, US Army Corps of Engineers, Cold Regions Research and Engineering Laboratory, Hanover, N.H., United States* 00.

Fausett, L. V. (1994). "Fundamentals neural networks: Architecture, algorithms, and applications". In: *Fundamentals neural networks,Prentice-Hall, Englewood Cliffs, N.J.*

Fayala, F., H. Alibi, S. Benltoufa, and A. Jemni (2008). "Neural network for prediciting thermal conductivity of knit materials". In: *Journal of Engineed Fibers and Fabrics* 3.4, pp. 53–60.

Feng, Y. T., K. Han, C. F. Lin, and D. R. J. Owen (2008). "Discrete thermal element modeling of heat conduction in particle system:basic formulations". In: *Journal of Computer Physics* 227, pp. 5072–5089.

Fisha, K. E., J. H. Barnes, and M. W. Aiken (1995). "A new methodology for Industrial market segmentation". In: *Industrial Marketing Managment* 24, pp. 431–438.

Flood, I. and N. Kartam (1994). "Neural networks in civil engineering I: Principles and understanding". In: *Journal of Computing in Civil Engineering* 8.2, pp. 131–148.

Fuller, W. B. and S. E. Thomson (1907). "Power cable thermal analysis with consideration of heat and moisture transfer in the soil". In: *Trans. ASCE* 59.2, pp. 67–143.

Gavriliev, R. I. (2004). "Thermal properties of soils and surface covers". In: *Thermal Analysis, Construction, and Monitoring Methods for Frozen Ground. Ed. by D. C. Esch. American Society of Civil Engineers, Reston, Virginia, USA*, pp. 277–294.

Ghaboussi, J. and D. E. Sidarta (1998). "New nested adaptive neural networks for constitutive modeling". In: *Computers and Geotechnics* 22.1, pp. 29–52.

Globus, A. M. and S. K. Rozenshtok (1989). "Nonisothermal internal moisture exchange in an incompletely saturated porous medium with alkaline interstitail solution". In: *Sov. Soil Science (in translation)* 21, pp. 111–115.

Goh, A. T. C. (1995). "Seismic liquefaction potential assessed by neural networks". In: *Journal of Geotechnical & Geoenvironmental Engineering, ASCE* 120, pp. 1467–1480.

Gontarski, C. A., P. R. Rodrigues, M. Mori, and L. F. Prenem (2000). "Simulation of an industrial wastewater treatment plant using artificial neural networks". In: *Computers and Chemical engineering* 24, pp. 1719–1723.

Gori, F. and S. Corasaniti (2004). "Theoretical prediction of the thermal conductivity and temperature variation inside Mars soil analogues". In: *Planet Space Science* 52, pp. 91–99.

Gouda, O. E. (1986). "Formation of the dried out zone around under-ground cables loaded by peak loadings". In: *Modeling, Simulation & Control, ASME Press.* 7.3, pp. 35–46.

Grabarczyk, M. and P. Furmanski (2013). "Predicting the effective thermal conductivity of dry granular media using artificial neural networks". In: *Journal of Power Technologies* 93.2, pp. 59–66.

Guyon, E., L. Oger, and T. J. Plona (1987). "Transport properties in sintered porous media composed of two particle size". In: *Journal of Applied Physics* 20, pp. 1637–1644.

Habibagahi, G. and A. Bamdad (2003). "A neural network framework for mechanical behaviour of unsaturated soils". In: *Canadian Geotechnical Journal* 40.3, pp. 684–693.

Haigh, S. K. (2012). "Thermal conductivity of sands". In: *Géotechnique* 62.7, pp. 617–625.

Hailemariam, H., D. Shrestha, K. Sembdner, F. Wuttke, and N. Wagner (2015). "Effect of hydro-mechanical changes on the relationship between thermal conductivity and dielectric permittivity of soils". In: *Proceedings of the 2nd EAGEWorkshop on Geomechanics and Energy: The Ground as Energy Source and Storage.Celle, Germany: European Association of Geoscientists and Engineers EAGE*, pp. 110–114.

Hailemariam, H., D. Shrestha, and F. Wuttke (2016a). "Analysis of cement-based thermal energy storages considering natural convection". In: *Proceedings of the 1st International Conference on Energy Geotechnics ICEGT 2016, Kiel, Germany*, pp. 277–284.

Hailemariam, H., D. Shrestha, and F. Wuttke (2016b). "CTE analysis of saturated cement-based sensible heat storage materials". In: *Proceedings of the 1st International Conference on Energy Geotechnics ICEGT 2016, Kiel, Germany*, pp. 299–304.

Hailemariam, H., D. Shrestha, and F. Wuttke (2016c). "Steady state vs transient thermal conductivity of soils". In: *Proceedings of the 1st International Conference on Energy Geotechnics ICEGT 2016. Ed. by F. Wuttke, S. Bauer, and M. Sánchez. Kiel, Germany: Taylor & Francis Group, Balkema CRC Press*, pp. 389–396.

Hailemariam, H., D. Shrestha, F. Wuttke, and N. Wagner (2017). "Thermal and dielectric behaviour of fine-grained soils". In: *Environmental Geotechnics* 4.2, pp. 79–93.

Hailemariam, H. and F. Wuttke (2018). "Temperature dependency of the thermal conductivity of porous heat storage media". In: *Heat and Mass Transfer* 54.4, pp. 1031–1051.

Hardy, M. (1992). "Xray diffraction measurement of the quartz content of clay and silt fractions in soils". In: *Clay Miner* 27.1, pp. 47–55.

Hashin, Z. and S. Shtrikman (1962). "A Variational approach to the theory of the effective magnetic permeability of multiphase materials". In: *Journal of Applied Physics* 33.10, pp. 3125–3131.

Haykin, S. (1999). "Neural network; a comprehensive foundation". In: *Prentice Hall, New Jersey, USA*.

HechtNielsen, R. (1989). "Theory of the back-propagation neural network". In: *Proceedings of the International Joint Conference on Neural Networks, Washington DC*, pp. 593–605.

Hiraiwa, Y. and T. Kasubuchi (2000). "Temperature dependence of thermal conductivity of soil over a wide ragne of temperature (5-75C)". In: *Europerian Journal Soil Science* 51.2, pp. 211–218.

Holger, R. M. and C. D. Graeme (1996). "The use of artificial neural networks for the prediction of water quality parameters". In: *Water Resources Research* 32.4, pp. 1013–1022.

Holger, R. M. and C. D. Graeme (1999). "Empirical comparision of various methods for training feed-forward neural networks for salinity forecasting". In: *Water Resources Research* 35.8, pp. 2591–2596.

Horai, K. I. and G. Simmons (1969). "Thermal conductivity of rock-forming minerals". In: *Earth Planet Science Letter* 6.5, pp. 359–368.

Hornik, K., M. Stinchcombe, and H. White (1989). "Multilayer feed forward networks are universal approximators". In: *Neural Networks* 2, pp. 359–366.

Hush, D. R. and B. G. Horne (1993). "Progress in supervised neural networks". In: *IEEE SP Magazine* 10.1, pp. 8–39.

Hussain, A. M. and M. Rahman (1999). "Using neural networks to predict thermal conductivity of food as a function of moisture content, temperature and apparent porosity". In: *Journal of Food Properties* 2, pp. 121–138.

IEEE 442 (1981). *IEEE guide for soil thermal resistivity measurements*. Institute of Electrical and Electronics Engineers, New York, USA.

Jason, K. and N. Wilson (2018). "Prediction of the factor of safety of a slope using artificial neural networks". In: *International Journal of Computer Science and Information Security* 16.11, pp. 9–17.

Johansen, O. (1975). "Thermal conductivity of soils". In: *PhD thesis* 00, pp. 210–235.

Karahn, M. and O. Kalenderli (2011). "Heat transfer-engineering applications". In: *V. Vikhrenko(eds.), Coupled Electrical and Thermal Analysis of Power Cables using finite element method*, pp. 205–230.

Karkir, M., B. Garnier, and A. Boudenne (2011). "Numerical and experimental study of the thermo physical properties of spheres composite materials". In: *High Temp High Pressures* 40.1, pp. 61–84.

Karnin, E. D. (1993). "A simple procedure for pruning back-propagation trained neural networks". In: *IEEE Transactions on Neural Networks* 1.2, pp. 239–242.

Kavli, T. (1993). "ASMOD An algorithm for adaptive spline modeling of observation data". In: *International Journal of Control* 58.4, pp. 947–967.

Kersten, M. S. (1949). "Thermal properties of soils". In: *Bulletin 28, Engineering Experiment Station, University of Minnesota, Minneapolis, USA*.

Kim, C. Y., G. J. Bae, G. J. Hong, C. H. Park, H. K. Moonb, and H. S. Shin (2001). "Neural network based prediction of ground surface settlements due to tunnelling". In: *Computers and Geotechnics* 28, pp. 517–547.

Kim, P. (2017). "MATLAB Deep Learning: with machine learning, neural networks and artificial intelligence". In: *Apress, first edition*.

Kingston, G. B., H. R. Maier, and M. F. Lambert (2008). "Bayesian model selection applied to artificial neural networks used for water resources modeling". In: *Water Resources Research* 44.W04419. URL: doi:10.1029/2007WR006155.

Kocjancic, R. and J. Zupan (2000). "Modeling of the river flow rate: The influence of the training set selection". In: *Chemometric and Intelligent Laboratory Systems* 54, pp. 21–34.

Kumlutas, D. and I. Tavman (2006). "A numerical and experimental study on thermal conductivity of particle filled polymer composites". In: *Journal of Thermoplast Compos* 19, pp. 441–455.

Kunii, D. and J. M. Smith (1960). "Heat trasfer characteristics of porous rocks". In: *American Institue of Chemical Engineers Journal* 6.1, pp. 71–78.

Lawrence, J. (1993). "Introuduction to neural networks: Design, Theory, and Applications". In: *California Scientific Software, 6th Edition, Neveda City*.

Lee, S. C. (2003). "Prediction of conrete strength using neural networks". In: *Engineering Structures* 25, pp. 849–857.

Lee, S. C., S. K. Park, and B. H. Lee (2001). "Development of the approximate analytical model for the sub-girder system using neural networks". In: *Computers and Structures* 79, pp. 1013–1025.

Lee, T. L. and D. S. Jeng (2002). "Application of artificial neural networks in tide-forcasting". In: *Ocean Engineering* 29.9, pp. 1003–1022.

Lee, T. L., C. P. Tsai, D. S. Jeng, and R. J. Shieh (2002). "Neural networks for the prediction and supplment of tidal record in Taichung Harbor,Taiwan". In: *Advances in Engineering Software* 33, pp. 329–338.

Levenberg, K. (1944). "A method for the solution of certain non-linear problems in least squares". In: *Quarterly of Applied Mathematics* 2.2, pp. 164–168.

Low, J. F., F. A. Loveridge, and W. Powrie (2013). "Measuring soil thermal properties for use in energy foundation design". In: *Proceedings of the 18th International Conference on Soil Mechanics and Geotechnical Engineering. Paris, France*.

Lu, S., T. Ren, Y. Gong, and R. Horton (2007). "An improved model for predicting soil thermal conductivity from water content at room temperature". In: *Soil Science Soceity of America Journal* 71.1, pp. 8–14.

Maier, H. R. and G. C. Dandy (2000). "Neural networks for the prediction and forecasting of water resources variables: A review of modeling issues and applications". In: *Environmental Modeling & Software* 15, pp. 101–124.

Mansour, M. Y., M. Dicleli, J. Y. Lee, and J. Zhang (2004). "Predicting the shear strength of reinforced conrete beam using artificial neural networks". In: *Engineering Structures* 26.6, pp. 781–799.

Marquardt, D. W. (1963). "An algorithm for least-square estimation of nonlinear parameters". In: *Journal of the society for Industrial & Applied Mathematics* 11.2, pp. 431–441.

Masters, T. (1993). "Practical Neural Network Recipes in C++". In: *Academic Press Inc. San Diego, CA,USA* 6.

Maxwell, J. C. (1954). "A treatise on electricity and magnetism". In: *third edition, Dover, New York*.

McGuinness, T., P. Hemmingway, and M. Long (2014). "Design and development of a low-cost divided bar apparatus". In: *Geotechnical Testing Journal* 37.2, pp. 230–241.

Mickley, A. S. (1951). "The thermal conductivity of moist soil". In: *American Institue of Electrical Engineers Transactions* 70, pp. 1789–1797.

Midttomme, K. and E. Roaldset (1998). "The effect of grain size on thermal conductivity of quartz sands and silts". In: *Petrolium Geoscience* 4, pp. 165–172.

Minsky, M. and S. A. Papert (1969). "Perceptrons". In: *MIT Press, Cambridge, MA, USA*.

Mishra, P. N., S. Surendra, V. K. Gadi, R. A. Joseph, and D. N. Arnepalli (2017). "Generalized approach for determination of thermal conductivity of buffer materials". In: *Journal of Hazardous, Toxic and Radioactive Waste* 21.4.

Mitchell, J. K. and T. C. Kao (1978). "Measurement of soil thermal resistivity". In: *Journal of the Geotechnical Engineering Division* 104, pp. 1307–1320.

Mitchell, J. K., J. C. McMillan, S. L. Green, and R. C. Sisson (1981). "Field tesging of Cable backfill sysetems". In: *Proceedings of the Symposium on Underground Cable Thermal backfill, Toronto*, pp. 19–33.

Mitchell, J. K. and K. Soga (2005). "Fundamentals of Soil Behaviour". In: *John Wiley & Sons, New York*.

Momose, T., I. Sakaguchi, and T. Kasubuchi (2008). "Development of an apparatus for measuring one-dimensional steady-state heat flux of soil under reduced air pressure". In: *European Journal of Soil Science* 59.5, pp. 982–989.

Mozan, M. A., M. A. El-Kady, and A. A. Mazi (1997). "Advanced thermal analysis of underground power cables". In: *Record of the Fifth International Middle East Power Conference MEPCON'97, Alexandria*, pp. 506–510.

Naidu, A. D. and D. N. Singh (2004). "A generalized procedure for determining thermal resistivity of soils," in: *Internatiional Journal of Thermal Sciences* 43, pp. 43–51.

Najjar, Y. M. and I. A. Basheer (1996). "Utilizing computational neural networks for evaluating the permeability of compacted clay liners". In: *Geotech Geology Engineering* 14, p. 193.

Nasirian, A., D.D. Cortes, and S. Dai (2015). "The physical nature of thermal conduction in dry granular media". In: *Géotechnique Letters* 5, pp. 1–5.

Nawari, N. O., R. Liang, and J. Nusairat (1999). "Artificial intelligence techniques for the design and analysis of deep foundations". In: *Electronic Journal of Geotechnical Engineering*. URL: http://geotech.civeng.okstate.edu/ejge/ppr9909.

Nejad, F. P., M. B. Jaksa, M. Kakhi, and B. A. McCabe (2009). "Prediction of pile settlement using artificial neural networks based on Standard Penetration Test data". In: *Journal of Geotechnical and Geo envrionmental Engineering* 36.7, pp. 1125–1133.

NeuralWare (1997). "NeuralWorks Predict Release 2.1". In: *NeuralWare Inc., Pittsburgh*.

Noborio, K. and K. J. McInnes (1993). "Thermal conductivity of salt affected soils". In: *Soil Science Socieity of American Journal* 57, pp. 329–334.

Peters-Lidard, C. D., E. Blackburn, X. Liang, and E. F. Wood (1998). "The effect of soil thermal conductivity parameterization on surface energy fluxes and temperatures". In: *Journal of the Atmospheric Sciences* 55.7, pp. 1209–1224.

Radhakrishna, H. S. (1981). "Fluidized cable backfills". In: *Proceedings of the Symposium on Underground Cable Thermal Backfill, Toronto, Canada*, pp. 34–53.

Radhakrishna, H. S., F. Y. Chu, and S. A. Boggs (1980). "Thermal instability and its prediction in cable backfill soils". In: *IEEE Transactions on Power Apparatus and Systems* 99.3, pp. 856–867.

Rahman, M. S. and J. Wang (2002). "Fuzzy neural network models for liquefaction prediction". In: *Soil Dynamics and Earthquake Engineering* 22, pp. 685–694.

Rao, M. V. B. B. Gangadhara and D. N. Singh (1999). "A generalized relationship to estimate thermal resistivity of soils". In: *Canadian Geotechinical Journal* 36, pp. 767–773.

Ray, C. and K. K. Klindworth (2000). "Neural networks for agrichemical vulnerability assessment of rural private wells". In: *Journal of Hydrologic Engineering* 5.2, pp. 162–171.

Rizvi, Z. H., D. Shrestha, A. S. Sattari, and F. Wuttke (2018). "Numerical modelling of effective thermal conductivity for modified geomaterial using lattice element method". In: *Heat Mass Transfer* 54, pp. 483–499. URL: https://doi.org/10.1007/s00231-017-2140-2.

Rooyen, M. Van and H. F. Winterkorn (1959). "Structural and textural influences on thermal conductivity of soils". In: *Anuual meeting 38th Washington, DC, 5-9 Jan, 1959*, pp. 576–621.

Rumelhart, D. E., G. E. Hinton, and R. J. Williams (1986). "Learning internal representation by error propagation". In: *Parallel distributed processing, D. E. Rumelhart and J. L. McClelland, eds., MIT Press, Cambridge, Mass* 1.8.

Sablani, S. S., O. D. Baik, and M. Marcotte (2002). "Neural networks for prediciting thermal conductivity of bakery products". In: *Journal of Food Science* 52, pp. 299–304.

Sablani, S. S. and M. S. Rahman (2003). "Using neural networks to predict thermal conductivity of food as a function of moisture content, temperature and apparent porosity". In: *Food Research International* 36.6, pp. 617–623.

Salchenberger, L. M., E. M. Cinar, and N. A. Lash (1992). "Neural networks: A new tool for predicting thrift failures". In: *Decision Science* 23, pp. 899–916.

Sandiford, P. (1981). "Cable backfill materials state-of-the-art". In: *Proceedings of the Symposium on Underground Cable Thermal backfill, Toronto*, pp. 3–9.

Santamarina, J. C., K. A. Klein, and M. Fam (2001). "Soils and Waves Particulate Materials Behavior". In: *Characterization and Process Monitoring, Wiley, New York*.

Sarbu, I. and C. Sebarchievici (2014). "General review of ground source heat pump systems for heating and cooling of buildingsl". In: *Energy Build* 70, pp. 441–454.

Sass, I. and J. Stegner (2012). "Coupled measurements of thermophysical and hydraulical properties of unsaturated and unconsolidated rocks". In: *Proceedings of the 37th Workshop on Geothermal Reservoir Engineering. Stanford University, Stanford, California, USA*.

Scott, D. J., P. V. Coveney, J. A. Kilner, J. C. H. Rossiny, and N. M. N. Alford (2007). "Prediction of the functional properties of ceramic materials from composition using artificial neural networks". In: *Journal of the European Ceramic Society* 27.16, pp. 4425–4435.

Shahin, M. A., M. B. Jaksa, and H. R. Maier (2001). "Artificial neural netrwork applications in geotechnical engineering". In: *Australian Geomechanics* 36.1, pp. 49–62.

Shahin, M. A., M. B. Jaksa, and H. R. Maier (2002a). "Artificial neural network based settlement prediction formula for shallow foundations on granular soils". In: *Australian Geomechanics* 45.

Shahin, M. A., H. R. Maier, and M. B. Jaksa (2002b). "Predicting settlements of shallow foundations using artificial neural networks". In: *Journal of Geotech and Geoenvironmnet Engergy, ASCE* 128.9, pp. 785–793.

Shahin, M. A., H. R. Maier, and M. B. Jaska (2004). "Data division for developing neural networks applied to geotechnical engineering". In: *Journal of Computing in Civil Engineering, ASCE* 18.2, pp. 105–114.

Shamy, U. E., O. D. Leon, and R. Wells (2013). "Discrete thermal element study on effect of shear-induced anisotropy on thermal conductivity of granular soils". In: *International Journal of Geomechanic* 13.1, pp. 57–64.

Shih, Y. (1994). "Neuralyst". In: *Neuralyst User's Guide, Cheshire Engineering Corporatiion, USA*.

Shrestha, D., H. Hailemariam, and F. Wuttke (2016). "Enhancement of soil thermal conductivity in dry condition". In: *Energy Geotechnics-Proceedings of the 1st International Conference on Energy Geotechnics, ICEGT 2016*. URL: https://doi.org/10.1201/b21938-64.

Shrestha, D., Z. H. Rizvi, and F. Wuttke (2018). "Effective thermal conductivity of modified geomaterials". In: *UNSAT2018: The 7th International Conference on Unsaturated Soils, Honkong*.

Shrestha, D., Z. H. Rizvi, and F. Wuttke (2019). "Effective thermal conductivity of unsaturated granular geocomposite using lattice element method". In: *Heat Mass Transfer* 55, pp. 1671–1683. URL: https://doi.org/10.1007/s00231-018-02544-3.

Shrestha, D. and F. Wuttke (2020). "Predicting the effective thermal conductivity of geomaterials using artificial neural networks". In: *Proceedings of the 2nd International Conference on Energy Geotechnics (ICEGT2020), 10 - 13 April 2022, La Jolla, CA, USA*.

Singh, R., R. S. Bhoopal, and S. Kumar (2011). "Prediction of effective thermal conductivity of moist porous materials using artificial neural network apporach". In: *Building and Environment* 46.2, pp. 2603–2608.

Singh, T. N., S. Sinha, and V. Singh (2007). "Predicition of thermal conductivity of rock through physico-mechanical properties". In: *Buidling and Envrionment* 42.1, pp. 146–155.

Sinha, S., V. Singh, and M. P. Jakhanwal (2015). "Rainfall runoff modelling of Punpun river Basin using ANN: A case study". In: *International Journal of Researcg in Engineering and Social Sciences* 5.5, pp. 32–49.

Smith, W. O. (1942). "The thermal conductivtiy of dry soil". In: *Soil Science* 53, pp. 425–459.

Smits, K. M., T. Sakaki, S. E. Howington, J. F. Peters, and T. H. Illangasekare (2013). "Temperature dependence of thermal properties of sands across a wide range of tempearaures (30-70C)". In: *Vadose Zone Journal* 12.1.

Stegner, J., D. Nguyen, R. Seehaus, and I. Sass (2011). "Development of a thermal conductivity and diffusivity meter for unconsolidated rocks". In: *Proceedings of the 18. Tagung für Ingeniergeologie. Berlin, Germany*.

Stone, M. (1974). "Cross-validatory choice and assessment of statistical predictions". In: *Journal of Royal Statistical Society* B36, pp. 111–147.

Tarnawski, V. R., M. L. McCombie, T. Momose, I. Sukaguchi, and W. H. Leong (2013). "Thermal conductivity of standard sands. Part III. Full range of saturation". In: *International Journal of Thermophysics* 34, pp. 1130–1147.

Tarnawski, V. R., T. Momose, and W. H. Leong (2009). "Assessing the impact of quartz content on the prediction of soil thermal conductivity". In: *Géotechnique* 59.4, pp. 331–338. URL: https://doi.org/10.1680/geot.2009.59.4.331.

Tarnawski, V. R., T. Momose, M. L. McCombie, and W. H. Leong (2015). "Canadian Field Soils III. Thermal conductivity Data and Modeling". In: *International Journal of Thermophysics* 36, pp. 119–156.

Tokar, S. A. and P. A. Johnson (1999). "Rainfall-runoff modeling using artificial neural networks". In: *Journal of Hydrologic Engineering* 4.3, pp. 232–239.

Tong, F., L. Jing, and R. W. Zimmerman (2009). "An effective thermal conductivity model of geological porous medium for coupled thermo-hydro-mechanical systems with multiphase flow". In: *International Journal of Rock Mechanics and Mineral Science* 46.8, pp. 1358–1369.

Twomey, J. M. and A. E. Smith (1997). "Validation and verification". In: *Artificial neural networks for civil engineers: Fundamentals and applications, N. Kartam, I. Flood, and J. H. Garrett, eds., ASCE, New York*, pp. 44–64.

Usowicz, B., J. Lipiec, and A. Ferrero (2006). "Prediction of soil thermal conductivity based on penetration resistance and water content or air-filled porosity". In: *International Journal of Heat and Mass Transfer* 49.25, pp. 5010–5017.

Venuleo, S., L. Laloui, D. Terzis, T. Huekel, and M. Hassan (2015). "Effect of microbially induced calcite precipitation on soil thermal conductivity". In: *Géotechnique Letters* 00, pp. 1–6.

Waite, W. F., J. C. Santamarina, and D. D. Cortes et al. (2009). "Thermal conductivity of hydrate-bearing sediments". In: *Journal of Geophysical Research* 114.

Wang, J. and M. S. Rahman (1999). "A neural network model for liquefaction-induced horizontal ground displacement". In: *Soil Dynamics and Earthquake Engineering* 18, pp. 555–568.

Woodside, W. and J. M. Messmer (1961). "Thermal conductivtiy of porous media". In: *Journal of Applied Physics* 32.9, pp. 1688–1706.

Woodward, N. R., J. M. Tinjum, and R. Wu (2013). "Water migration impacts on thermal resistivity testing procedures". In: *Geotechnical Testing Journal* 36.6, pp. 948–955.

Xu, Y., G. Ray, and B. Abdel-Magidn (2006). "Thermal behavior of singlewalled carbon nanotube polymer-matrix composites". In: *Compos Part A* 37, pp. 114–121.

Yao, J., H. Oh, W. J. Likos, and J. M. Tinjum (Nov. 2014). "Three laboratory methods for measuring thermal resisitivity dryout curves of coarse-grained soils". In: *Geotechnical Testing Journal* 37.6, pp. 1056–1067.

Yoon, Y., T. Guimaraes, and G. Swales (1990). "Integrating artificial neural networks with rule-based expert systems". In: *Decision Support Systems* 11.5, pp. 497–507.

Yun, T. S. and J. C. Santamarina (2007). "Fundamental study of thermal conduction in dry soils". In: *Granual Matter* 10.3, pp. 197–207.

Zhang, N., X. Yu, A. Pradhan, and A. J. Puppala (2015). "Thermal conductivity of quartz sands by thermo TDR probe and model prediction". In: *Journal of Materials in Civil Engineering, ASCE*.

Zhang, N., X. Yu, A. Pradhan, and A. J. Puppala (2017). "A new generalized soil thermal conductivity model for sand kaolin clay mixtures using thermo time domain reflectometry probe test". In: *Acta Geotechnica* 12, pp. 739–752. URL: https://doi.org/10.1007/s11440-016-0506-0.

Zhang, N., H. Zou, L. Zhang, A. J. Puppala, and S. Liu adn G. Cai (2020a). "A unified soil thermal conductivity model based on artificial neural network". In: *International Journal of Thermal Sciences* 155.2, pp. 43–58.

Zhang, Q. and J. S. Stephen (1999). "Forecasting raw-water qulality paramters for the North Saskatchewan River by neural network modeling". In: *Water Research* 31.9, pp. 2340–2350.

Zhang, T., C. Wang, S. Liu, N. Zhang, and T. Zhang (2020b). "Assesment of soil thermal conduction using artificial neural network". In: *Cold Regions Science and Technology* 169.

Zhou, J. H., A. B. Yu, and Y. W. Zhang (2007). "A boundary element method for evaluation of effective thermal conductivity of packed beds". In: *Journal of Heat and Transfer* 129, pp. 363–371.

Soil thermal conductivity has an important role in geo-energy applications such as high voltage buried power cables, oil and gas pipelines, shallow geo-energy storage systems and heat transfer modelling. Hence, improvement of thermal conductivity of geomaterials is important in many engineering applications. In this thesis, an extensive experimental investigation was performed to enhance the thermal conductivity of geomaterials by modifying particle size distribution into fuller curve gradation, and by adding fine particles in an appropriate ratio as fillers. A significant improvement in the thermal conductivity was achieved with the newly developed geomaterials.

An adaptive model based on artificial neural networks (ANNs) was developed to generalize the different conditions and soil types for estimating the thermal conductivity of geomaterials. After a corresponding training phase of the model based on the experimental data, the ANN model was able to predict the thermal conductivity of the independent experimental data very well. In perspective, the model can be supplemented with data of further soil types and conditions, so that a comprehensive representation of the saturation-dependent thermal conductivity of any materials can be prepared. The numerical ‚black box' model developed in this way can generalize the relationships between different materials for later added amounts of data and soil types. In addition to the model development, a detailed validation was carried out using different geomaterials and boundary conditions to reinforce the applicability and superiority of the prediction models.

ISSN: 2365-7162